DEVELOPMENT AND CHARACTERIZATION OF FeAl BASED COMPOSITES

Ph.D. THESIS

by

RAVI KANT

DEPARTMENT OF METALLURGICAL AND MATERIALS ENGINEERING
INDIAN INSTITUTE OF TECHNOLOGY ROORKEE
ROORKEE – 247667, INDIA

MAY, 2015

DEVELOPMENT AND CHARACTERIZATION OF FeAl BASED COMPOSITES

A THESIS

Submitted in partial fulfilment of the requirements for the award of the degree of

DOCTOR OF PHILOSOPHY

in

METALLURGICAL AND MATERIALS ENGINEERING

by

RAVI KANT

DEPARTMENT OF METALLURGICAL AND MATERIALS ENGINEERING
INDIAN INSTITUTE OF TECHNOLOGY ROORKEE
ROORKEE – 247667, INDIA

MAY, 2015

INDIAN INSTITUTE OF TECHNOLOGY ROORKEE
ROORKEE

CANDIDATE'S DECLARATION

I hereby certify that the work which is being presented in the thesis, entitled **"Development and Characterization of FeAl based Composites"** in partial fulfilment of the requirements for the award of the degree of Doctor of Philosophy and submitted in the Department of Metallurgical and Materials Engineering, Indian Institute of Technology Roorkee, Roorkee is an authentic record of my own work carried out during the period from October, 2010 to May, 2015 under the supervision of **Dr. Ujjwal Prakash**, Associate Professor and **Dr. Vijaya Agarwala**, Professor, Department of Metallurgical and Materials Engineering, Indian Institute of Technology Roorkee, Roorkee.

The matter presented in this thesis has not been submitted by me for the award of any other degree of this or any other institute.

(**RAVI KANT**)

This is to certify that the above statement made by the candidate is correct to the best of our knowledge.

(Ujjwal Prakash)
Supervisor

(Vijaya Agarwala)
Supervisor

Date:

Abstract

Iron aluminides are promising structural materials for industrial applications relative to typical steels and other engineering alloys due to its low density, low material costs, high melting point and excellent high-temperature oxidation resistance. Poor room temperature ductility and drop in the strength of iron aluminides above 550^{o}C limits their role as structural materials. There has been considerable effort devoted to the improvement of mechanical properties by refining microstructure and by the introduction of a fine dispersion of second phase particles.

Addition of carbon to the Fe–16wt.% Al alloy results in improvement in strength, machinability, creep resistance and resistance to environmental embrittlement. Carbon additions of 0.03 wt.% or more result in precipitation of $Fe_3AlC_{0.5}$ phase in these alloys, which imparts significant dispersion strengthening and leads to improvement in creep resistance. Though $Fe_3AlC_{0.5}$ (k-carbide) is a hard and brittle phase its presence in the alloys matrix does not affect the ductility of these alloys. This is because interstitial carbon competes with hydrogen for interstitial sites thus reducing the mobility of hydrogen atoms leading to brittle embrittlement. This susceptibility to embrittlement in moist environments is a major cause for poor room temperature ductility and machinability.

Carbon additions to B2 FeAl based alloys having more than 20%Al results in the precipitation of soft graphite. The increase in the carbon content from 0.27%C to 1.1%C, results in the decrease in the poor creep rate, strength and stress rupture life. This may be attributed to the precipitation of soft graphite phase against the hard $Fe_3AlC_{0.5}$ carbide. The precipitation of graphite to limited extent also causes poor wear resistance of FeAl based alloy.

A stronger carbide forming element has been proposed to avoid the graphite precipitation and improvement in the mechanical properties of FeAl based alloys. In the present research work attempts are made to develop FeAl based iron aluminides containing carbon. Transition metals like Ti, Zr are stronger carbide forming elements and avoid the graphite precipitation in FeAl based alloy. In the present work Ti/Zr additions resulted in the formation of alloy carbides which improved mechanical properties at room as well as elevated temperatures. The wear resistance of FeAl based alloys containing carbon have also improved due to Ti/Zr additions.

The whole research work has been presented in eight chapters in the thesis.

Chapter 1 represents the introduction about the intermetallics compounds and the difference in their mechanical and physical properties from the conventional alloys and metals. A brief introduction about the iron aluminides has also been reported in this section.

Chapter 2 presents a critical review of the available literature on iron aluminides, their different types depending upon the content of aluminium. The chapter represents the effect of carbon additions on microstructure and mechanical properties of iron aluminides.

Chapter 3 consists of formulation of problem, objectives of present work based on literature review and planning of experimental works.

Chapter 4 consists of the experimental procedures employed for present work. Details of various instruments used to study the mechanical properties, thermal properties and wear bevaiour has been described. Various heat treatments given to specimens of various alloys are described in details in this study.

Chapter 5 deals with characterization of microstructural and mechanical properties as well as the thermal properties of FeAl based alloys containing carbon on Ti addition.

Chapter 6 describes the wear behaviour of FeAl based alloys containing carbon on Ti additions. The effect of applied loads and sliding speeds has been investigated and correlate with microstructures observed.

Chapter 7 deals with the comparative studies of FeAl based alloys containing carbon on Ti/Zr additions in terms of microstructural and mechanical properties. Also the wear behaviour of these alloys has been studied**.**

Chapter 8 describes the future directions in which these studies can be extended.

Acknowledgement

Every success which is a result of hard efforts never tastes that good if each and every one who participated in it is not acknowledged. First and foremost, I would like to express my gratitude and acknowledgement to almighty God who has given me enthusiasm and passion toward research work. My sincere thanks go to Dr. Ujjwal Prakash and Dr. Vijaya Agarwala, Department of Metallurgical and Materials Engineering, Indian Institute of Technology Roorkee, my thesis supervisors for giving me the wonderful opportunity of doing research under them. Their enthusiasm on the problem and encouragement throughout the course of this work is very much appreciable. They have always been available for discussion and guided me to accomplish the objective of this study; they have been an inspiring and driving force during the course of this work. Without their timely help, intellectual input, constructive criticism and painstaking efforts, it would not have been possible for me to complete this thesis in the present form.

I would also like to thank Dr. S. K. Nath, Professor & Head and Dr. Vikram Dabhade, IIT Roorkee, Department of Metallurgical and Materials Engineering for their valuable suggestions.

The alloys used in this investigation were prepared at DMRL, Hyderabad, India. I am great thankful to Dr. V.V. Satyaprasad, Sc. 'F' and Mr. Shiv Kumar Khapale Sc. 'C' of the organization as also the keen interest they took in this study.

I also wish to thank the whole staff of the Department of Metallurgical and Materials Engineering, Indian Institute of Technology Roorkee, in particular Mr. Rajinder K. Sharma, Mr. Naresh Sharma, Mr. Pradeep Kumar, Mr. R. K. Sharma, Mr. Shakti Gupta, Mr. S. M. Giri. Many thanks go to Mr. S. K. Saini, Mr. Shiv Kumar and Mr. Vaibhav Bajpayi of Institute Instrumentation Centre, IIT Roorkee for helping me in doing XRD, SEM and EDS work.

I am indebted to Mr. Ashish Selokar for his friendship and support without whom this thesis manuscript would not have been in the same format; in fact he has helped a lot. The discussions and interactions with the colleagues have been very fruitful. Many thank goes to Ph.D. fellows and friends, Mr. Abhishek Kumar, Mr. Dharmendra singh, Mr. Sanjay Rathore, Mr. Paritosh Dubey, Mr Vipin Sharma, Mr. Debesh Mishra, Tilak, Kaushal, Prabhat, Vaneeta,

Preeti, Nidhi, Monu, R. Sunil, Deepak, Sankulp, Sanjeev, Ravinder, Sandan, Brijkishor and Ramkishor.

The author expresses his deepest esteem to his parents, Mr. Raj Paul and Mrs. Nirmala Devi always wanted me to become successful in all my endeavors and it is their blessings that took me this far. I am also grateful to my sister Aruna, jiju Manoj, brother Arvind and bhabhi Veena for their support. You're waited for many years to see this moment. Thank you for all sacrifices that you're made. Without you I would never be where I am now. The support I have got from my fiancée Falki during the last year cannot be expressed in words. I know it was not easy. You will be always with me in memories. Thanks for giving me strength and the spark of hope when everything looked hopeless.

I also like to thank everyone who supported me for completing this work successfully and I express my apology that I could not mention everyone individually.

(Ravi Kant)

Contents

List of Figures

List of Tables

List of Publications

In International Journals:

1. ***Ravi Kant,*** *Ashish Selokar, Vijaya Agarwala1, and U. Prakash,* "The Influence of carbon additions on microstructure and mechanical properties of Fe-22.0Al-5.0Ti alloy" Advanced Materials Research, 1043, 17-21(2014)

2. ***Ravi Kant,*** *U. Prakash, Vijaya Agarwala, V.V. Satya Prasad* "Wear behavior of FeAl based alloys containing titanium and carbon", Intermetallics, 61, 21-26 (2015)

3. ***Ravi Kant,*** *U. Prakash, Vijaya Agarwala, V.V. Satya Prasad* "Effect of carbon and titanium additions on mechanical properties of B2 FeAl"**,** Trans. Ind. Int. Met. (2015) accepted for publication.

4. ***Ravi Kant****, Ujjwal Prakash, Vijaya Agarwala, "*Effect of alloying additions on structure and mechanical properties of B2 FeAl alloys containing high carbon" communicated.

5. ***Ravi Kant,*** *U. Prakash, Vijaya Agarwala, V.V. Satya Prasad,* "FeAl based intermetallic matrix composites through melt route", to be communicated.

In conferences/seminars:

1. ***Ravi Kant,*** *U. Prakash, V. Agarwala,* Characterization of Iron-aluminide Alloys Reinforced with Titanium Carbide, presented in National seminar on "Microstructure-2011: Microstructure Across Length scales and Material Properties" organized by Deptt. of Metallurgical and Material Engg.IIT Roorkee, Roorkee. Nov. 4-5, 2011

2. ***Ravi Kant,*** *U. Prakash, Vijaya Agarwala,* Effect of Titanium on FeAl intermetallic alloy containing carbon, presented in International Symposium "International Symposium for Research Scholars (ISRS-2012)" during December 2012 organised by Deptt. of Metallurical and Materials engg. IIT Madras, Chennai. Dec 13^{th}-15^{th} 2012.

3. ***Ravi Kant,*** *U. Prakash, Vijaya Agarwala, R. G. Baligidad,* Microstructure and Mechanical properties of *in-situ* FeAl (B2) based alloys with strengthening nano/micron carbides, presented in National conference "Recent Trends in Materials Engg. (RTME-2013)" organized by Mechanical Engineering Society, BRCM College of Engg. & Tech., Bahal. Oct 4^{th} -5^{th} 2013.

4. ***Ravi Kant,*** *U. Prakash, Vijaya Agarwala, R. G. Baligidad,* Formation of Iron aluminide-carbides nano/micro hybrid composites, presented in International

conference "International Conference on Interdisciplanary areas with Chemical Sciences (ICIACS-2013)" organized by Deptt. of Chemistry Panjab University Chandigarh. 30th Oct-01st Nov, 2013.

5. ***Ravi Kant,*** *Ashish Selokar, Vijaya Agarwala, U. Prakash,* "The influence of carbon addition on microstructure and mechanical properties of Fe-22.0Al-5.0Ti alloy", submitted in international conference **"**International Conference on Engineering and Innovative Materials (ICEIM 2014)" held in Kuala Lumpur, Malaysia during September 4-5, 2014.

Chapter 1
Introduction

This chapter deals with the brief discussion about the intermetallic compounds and their various industrial applications. The chapter describes how these compounds are different from the other materials. The various physical and mechanical properties of intermetallic compounds are discussed and the challenges to improvement in these properties.

1.1. General considerations

1.1.1 Brief information of intermetallics

Intermetallic compounds are expected to be most important material for various industries because they have remarkable properties, such as good mechanical qualities, thermoelectric, superconducting and magnetic properties [Westbrook and Fleischer 1995]. These compounds will be useful in future for developing smart materials and systems ranging from micro- to nano- lengths in the 21th century. This study mainly deals with the mechanical properties of intermetallic compounds. Intermetallic compounds are being considered as potential materials high temperature applications and much effort has been devoted to promote the development in last decade. Intermetallics consist of an ordered arrangement of mixed atoms of metal-metal or metal-semimetal types [Morris 2005]. The bonding between the different atomic species is partially metallic and partially ionic (or covalent) nature. In some metal-metal intermetallic compounds, the atomic size differences are responsible for an ordered arrangement, notably for Laves phases. The presence of strong bonding between the atomic species causes to higher elastic moduli of the materials.

Intermetallics based on transition metal aluminides with ordered structure have been proposed as structural materials for elevated applications. The developments of such compounds, which have the advantages of low density and high operating temperatures, have been focused on the aluminides of iron, nickel and titanium. Though these materials possess excellent properties at elevated temperatures, their utilization is limited due to their decrease in the strength at high temperature and poor ductility due to susceptibility to environmental effects.

1.1.2 Comparison between intermetallic and conventional alloys

Intermetallic compounds are hard and brittle due to difference in the structural arrangements of their constituents. They are differentiated from the conventional alloys as follows [Porter 1981; Foster 1938; Liu 1990; Cahn 1996].

i) In conventional alloys, constituent two or more elements are randomly oriented to from the solid solution. They exhibit same crystal structure as that of predominant element with certain changes in the lattice parameters that may occur due to addition of alloying elements. On the other hand, intermetallic compounds consist of base material in which certain percentages of foreign elements have been introduced. They might have completely different structure than that of original pure elements.

ii) The bonding between the atoms in conventional alloys is purely metallic while intermetallic compounds have partly covalent or ionic in nature, thus leading to stiffness and strength. Alternatively, the metallic bonding may be possible but the atoms of the individual constituent occupy the particular positions in the crystal lattice structure. This preferred orientation of atoms in the crystal structure causes ordering in the lattice thereby leading to loss in ductility. This ordered crystallographic structure lasts only at below certain critical temperature known as critical ordering temperature (T_c) and is based on simple stoichiometry in the formula. In most of the intermetallic compounds, this ordering temperature is close to the melting point of the material. When these conditions do not meet, the crystal lattice loses its order.

iii) The ordered structure of intermetallic compounds lead to much lower self diffusion coefficient than that of conventional alloys having disordered structure. The self diffusion coefficients of intermetallic compounds can be several orders of magnitude smaller than that of conventional alloys at a particular temperature.

1.2 Mechanical behavior of intermetallics

Intermetallics possess an ordered arrangement of mixed atoms species of different elements. The existence of strong bonding among atoms leads to higher elastic moduli. The ordered superlattice structure of intermetallics needs larger shear displacement required to deform plastically leading to brittleness. The desirable mechanical properties of intermetallics from brittle to ductile are shown graphically in Fig. 1.1. The variety of mechanical properties uprises from the nature of chemical bonding. As Pauling [Burdett 1997] has pointed out, using the modified concept of chemical bonding to provide a common point of view for inter-material interactions.

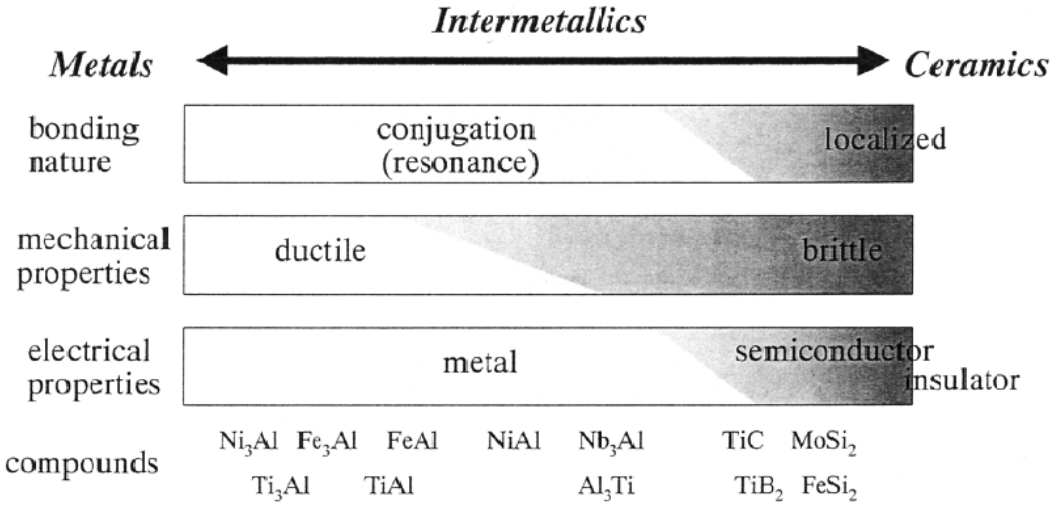

Fig. 1.1: Relationship between nature of bonding and properties of intermetallics [Cantor 2003].

The mechanical properties of intermetallics are more complex than disordered alloys and metals. The factors influencing the mechanical behavior of intermetallics are shown in Fig. 1.2. Intermetallics have characteristics pair of dislocations, called superpartial dislocation pairs. An anti-phase boundary (APB), usually a defect, is formed between the partials dislocations. These dislocations cannot move independently and APB energy is an important parameter in determining the plastic deformability of alloys. This movement (resistance to dislocation motion) is proportional to the APB energy. For example, NiAl is extreme brittle due to high APB energy originating from bond characteristics than FeAl irrespective of same crystal structure. Further, the dislocation motion in intermetallics is also influenced by dispersoids and point defects (anti-site atoms, vacancies and solute atoms) [Schaefer 1999, Kogachi 1997].

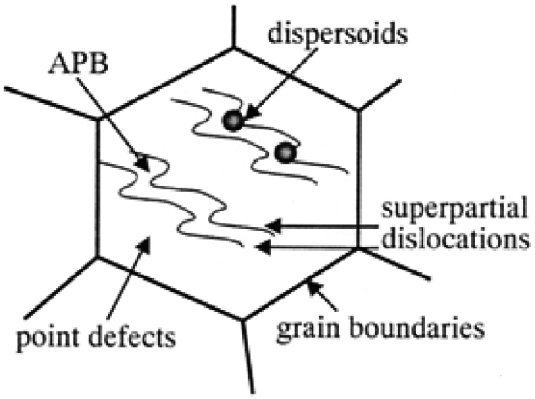

Fig. 1.2: Influential factors on the mechanical behaviour of intermetallics [Cantor 2003].

1.3 Transition metal aluminides

Aluminides contain sufficient amount of aluminium which forms a protective alumina layer on the surface of the alloy. They exhibit relatively high melting point, low density, good thermal conductivity and high temperature strength. Thus, these materials are investigated for structural material for elevated temperature applications. Table 1.1 presents the list of various aluminides of transition metals with their characteristic properties. It is pointed out that the different aluminides have relatively low densities and, for the most of them, the melting point coincidence with the ordering temperature.

Table 1.1: General properties of various intermetallic compounds [Liu 1990].

Intermetallic	Critical ordering temperature (^oC)	Melting point (^oC)	Density (g/cm^3)	Young's modulus (GPa)
Ni_3Al	*1390*	1390	7.50	179
NiAl	1640	1640	5.86	294
Ti_3Al	1100	1600	4.2	145
TiAl	*1460*	1460	3.91	176
$TiAl_3$	1350	1350	3.4	--
Fe_3Al	540	1540	6.72	141
	760	1540	--	--
FeAl	1250	1250	5.56	261

1.3.1 Nickel aluminides

Nickel aluminides have received considerable attention as a potential structural alloy. Ni_3Al acts as a strengthening phase in most superalloys [Dey 1993]. Because of its high melting temperature, low density, good thermal conductivity and excellent oxidation resistance NiAl has emerged as a possible high temperature structural material. It has several advantages over superalloys [Dey & Sekhar 1997]. As is the case with other alumindies, NiAl and Ni_3Al have certain drawbacks, the most important being the poor ductility at ambient temperature and lack of good high temperature creep resistance. Several efforts have been made to overcome the problem of room temperature brittleness in Ni_3Al and NiAl through modification of slip systems, use of single crystals, grain refinement and addition of microalloying with boron [Lahrman 1991; Field 1991]. In the case of Ni_3Al, single crystals have been found to be ductile [Pope and Ezz 1984]. The level of research effort in the case of Ni_3Al has been substantially more than in case of other aluminides and commercialization of Ni_3Al alloys for selected

applications should occur very soon. NiAl has one of the promising materials for casting turbine blades [Matsushita 2008]. The problem of lack of ductility in NiAl has been addressed [Noebe 1993]. It has been demonstrated that this intermetallic compound shows large ductility under certain conditions of impurity and imperfection content, heat treatment and surface perfection [Levit 1996]. In the past decade several alloying additions to NiAl have been attempted to improve its ductility [Darolie 1992]. Intermetallics can be fabricated both by conventional melting and casting route as well as the powder metallurgy route.

1.3.2 Titanium aluminides

Titanium aluminides have been investigated over past few decade due to their lower densities and higher specific modulus (Table 1.1) [Gupta 2014]. Titanium aluminides of industrial importance are mainly γ (TiAl) based aluminides (γ aluminides) and α2 (Ti_3Al) based aluminides (α2 aluminides). The strength retention in the α2 aluminides is up to a temperature of 700^{o}C whereas γ aluminides retain strength up to 900^{o}C due to their respective crystal structure and lattice parameters. Among these two, γ titanium aluminides are more attractive due to relatively lower density and better high temperature properties. The most important γ Ti-aluminides are the two phase alloys based on TiAl and Ti_3Al with aluminum content ranging from 36 to 50 at.% [Gupta 2012].

Application of γ titanium aluminides are envisaged as turbine blades, turbine rotor discs, fins, pressure vessels for satellites, nozzle fins and automobile rotor discs [Tetsui 2002, Gupta 2010]. In fact, Mitsubishi is already using γ titanium aluminide turbocharger rotors in commercial automobiles since 1999 [Tetsui 2002, Huang 1994]. The alloy has also received tremendous attention from aeronautics as well [Saeed-Akbari 2013; Mosecker 2013]. Extensive work on development and characterization of gamma aluminides is being carried out worldwide [Tetsui 2002, Huang 1994] to achieve better combination of properties. The inherent brittle nature of aluminides has necessitated development of new alloys and processing routes to achieve the required form and shapes. Alloy developments have been focused mainly on binary alloy of Ti 44–50Al (at.%) having maximum ductility (up to 2 %). Small additions of B, C, Cr, V, Mn has been studied to further improve the ductility of the alloy [Huang 1994, Wu 2006] and through thermo mechanical treatments (TMT) [Agarwala 2005]. Efforts have also been made towards improvements in oxidation resistance at elevated temperature [Zhao 2003, Pather 2003] through alloy additions of Nb, W and Mo (as low as 1–2 at.%) [Teng 2007, Shih 1991].

1.3.3 Iron aluminides

The relatively low materials costs and high-temperature corrosion resistance are the most attractive aspects of Fe–Al alloys. The corrosion resistance of Fe–Al alloys in several environments depends basically on the content of Al. In Fe-Al based alloys having disordered structure have not yet been considered for high temperature applications because of insufficient strength. Fe–Al alloys based on the iron aluminides Fe_3Al and FeAl having ordered structure belong to the widely studied Fe–Al alloys for structural material for high temperature and functional applications [Umakoshi 1980; Baker 1987; Liu 1989; Crimp 1986; Baker 1988; Pang 1998]. Based on the composition of Al, iron-aluminium alloys can be classified with respect to their atomic ordering in the following way depending upon the content of aluminium, b.c.c. disordered ferritic Fe(Al) alloys, DO_3-ordered Fe_3Al alloys and B2-ordered FeAl alloys. Iron aluminides having B2 structure shows lower density and better corrosion and oxidation resistance than Fe_3Al having DO_3 structure. The detailed study of about these structures are given in chapter 2.

1.3.3.1 Attempts at applications of iron aluminides

The properties like low density, excellent oxidation and sulfidation resistance of FeAl alloys made the promising material for applications in the petrochemical industry and possibly in coal conversion plants or in conventional power plants in particular in steam turbines [Deevi 1996, Itoi 2010]. The potential applications of iron aluminides are as below.

i) One of the major applications of iron aluminide is used for hot gas filters. The gas filters are produced by sintering powders using proprietary process and are employed to filter the particulate from the gas furnished during the coal gasification process which has high sulphur content.

ii) Used as a heating elements in the form of wire in ovens, toasters and dryers. The high resistivity which remains constant up to 1000^oC and oxidation resistance of iron aluminide made the materials suitable for the same.

iii) Regenerator disks in which iron aluminide is utilized as heat exchanger in the gas turbine engine. The foil required is manufactured primarily by warm rolling followed by the cold rolling in last few passes.

iv) Used as a shielding material for avoiding the excessive oxidation of the tube in power plants. This is prepared by using bending the warm-rolled sheet.

v) A thin sheet of FeAl based alloys is used in the microheaters.

vi) In automobile industry, FeAl based alloys are used as piston valves manufactured by casting route. Exhaust valves in car engine and disk brakes are potentially be used as wear resistance applications. However, the performance improvement of the engine over the currently used materials has still been required to show the results.

1.3.3.2 Properties of iron aluminides

i) Lower density than that of various stainless steels and offer better strength to weight ratio [Deevi 1997].
ii) Excellent corrosion resistance in many liquid environments [Deevi 1996].
iii) Good oxidation resistance temperatures up to 1473K [Liu 1997].
iv) Higher resistance to sulfidation and carburizing atmosphere as well in molten carbonate and nitrates atmosphere than that of aluminides of other transition metals.
v) High electrical resistivity that increases with rise in temperature.
vi) Lower thermal conductivities than that of Ni-based alloys and their thermal expansion coefficient is similar to that of stainless steels [George 1994].

Iron aluminides show higher strength with anomalous temperature dependence [Stoloff 1964, Hanada 1981, Stein 2003] in comparison to conventional iron alloys. Problems are the low deformability and toughness at room temperature and the strength decrease above about 500^{o}C [Morris 1994]. Alloying additions such as Zr, Nb, Cr, Ti, C and B are effective in improving the creep resistance of FeAl alloys through precipitation hardening or solid solution hardening [Munroe 1996, Titran 1984, Maziasz 1996].

One of the major problems experienced is the brittleness of Fe-Al based alloys where sufficient strength is attained. Poor ductility is often accompanied with an insufficient number of slip systems for large-scale plasticity, or with the difficulty of activating a sufficient number of slip systems even though in principle these exist. For example, in the case of FeAl where slip occurs at room temperature essentially by dislocation glide on (111) {110} systems [Umakoshi and Yamaguchi 1980]. In case of poor ductility of the alloy, the failure is mainly occurs by a mixed intergranular/cleavage mode despite the availability of a considerable number of slip systems [Baker and Gaydosh 1987]. It has been reported that poor ductility for this alloy may be partially caused by grain boundary embrittlement, which may be an environmental effect [Liu 1989] that may be perhaps opposed by careful additions to the alloy [Crimp and Vedula 1986]. Another possible way to try to increase strength and ductility is to refinement in the

microstructure [Strothers 1988], i.e. to reduce the grain size or to incorporate particles distribution. Baker et al [Baker 1988] have reported that mixing of yttria particles into an FeAl alloy by using mechanical alloying techniques results dispersion strengthened material with fine grain size showed sufficient improvement in strength and ductility.

The susceptibility of iron aluminides to hydrogen embrittlement is the major cause of the low ductility at room temperature. Carbon addition to Fe-Al alloys is found to be suitable for the reduction in the environmental embrittlement. It also results in improvement in the strength due to carbide formation in Fe_3Al based alloys. In Fe-40Al-0.6C alloy, the presence of grain boundary carbides does not appear to be detrimental to ductility. In fact, the presence of carbides may increase the ductility of the alloy by providing modified path at carbide/matrix interfaces that act as hydrogen traps [Pang and Kumar 1998]. Iron aluminides also show anomalous dependence of yield strength on temperature. The mechanical behavior is improved by alloying with foreign elements thermomechanical treatments and reduction in aluminium content. For example, addition of boron, zirconium and molybdenum to Fe_3Al and FeAl result improvement in the ductility and toughness which enable them to used a potential material for heat exchanger which works at service temperature between 700 and 800^{o}C. Mechanical properties of iron aluminides can be enhanced by control of microstructure, alloying and addition of second phase particles.

1.3.3.3 Compatibility of reinforcement with iron aluminides matrix

The potential drawback of loss in the strength of iron aluminides at high temperature can be overcome by inclusion of the reinforcement. The essential requirement for reinforcement material for iron aluminides are: i) high strength at elevated temperatures, ii) high modulus, iii) close match in the coefficient of thermal expansion (CTE) and iv) chemical compatibility with the matrix. The stability of the composite materials mainly depends upon the two factors i.e. coefficient of thermal expansion compatibility and chemical compatibility. The chemical compatibility of the materials is identified on the basis of thermodynamic considerations by evaluating the CTE and mechanical compatibility of the matrix. But, it is impossible for reinforcement materials to satisfy all the factors discussed above.

Chapter 2
Literature survey

This chapter contains the detailed information about the iron aluminides. The chapter describes the various types of iron aluminides and their structure depending upon the content of aluminium. The aluminium content affects the basic ordering structure which leading to modification in mechanical properties of iron aluminides. The mechanical, physical and thermal properties of iron aluminides are further modified by addition of alloying elements, altering the microstructure and thermomechanical treatments.

2.1 Introduction

Iron aluminides such as DO_3 type Fe_3Al and B2 type FeAl because of their high strength/density ratio, remarkable corrosion resistance and low raw material cost have attracted great attention as potential structural materials in industrial applications [Stoloff 1998]. Iron aluminides based on Fe_3Al and FeAl has been focused to improve the strength for high temperature applications. This could be achieved by dispersion of fine and stable [Gaydosh 1989; Ray 1983; Morris 1990; Morris 1990; Schniebel 1997] second phase through thermo-mechanical processing by powder metallurgy route. In the last ten years, the emphasis to prepare carbon containing the Fe-Al alloys by ingot metallurgy route has been reported. In Fe-Al alloys, carbon is important alloying element and influenced the mechanical properties to greater extent. Carbon addition has been reported to improve the weldability [Mckamey 1996]. It has also found to improve the machinability of these intermetallics alloys [Ray 1983; Morris 1990; Morris 1990]. On the other hand, carbide particles help in inhibiting the grain coarsening at high temperature exposure [Mckamey 1996; Baligidad 1996a; Baligidad 1998b; Baligidad 1997a; Vedula 1996]. FeAl alloys (37-50 at.%Al) containing upto 0.28at.% C also showed similar observations. Further addition of carbon leads to precipitation of graphite. Fe-Al based alloys and they are classified as below.

2.1.1 Disordered *α*-phase alloys

The ferritic iron-aluminium steel is principally based on the binary Fe-Al phase diagram shown in Fig. 2.1. Al has very little solublity in f.c.c Fe and dissolution of nearly 1.5% A1 is enough to inhibit the formation of the γ phase. However, Al is highly soluble in b.c.c. iron (Fe) up to a solubility limit of~ 34% [Prescott 1992]. The addition of Al would bring solidus temperature from 1538^{o}C for pure Fe to~1200^{o}C at 34% Al.

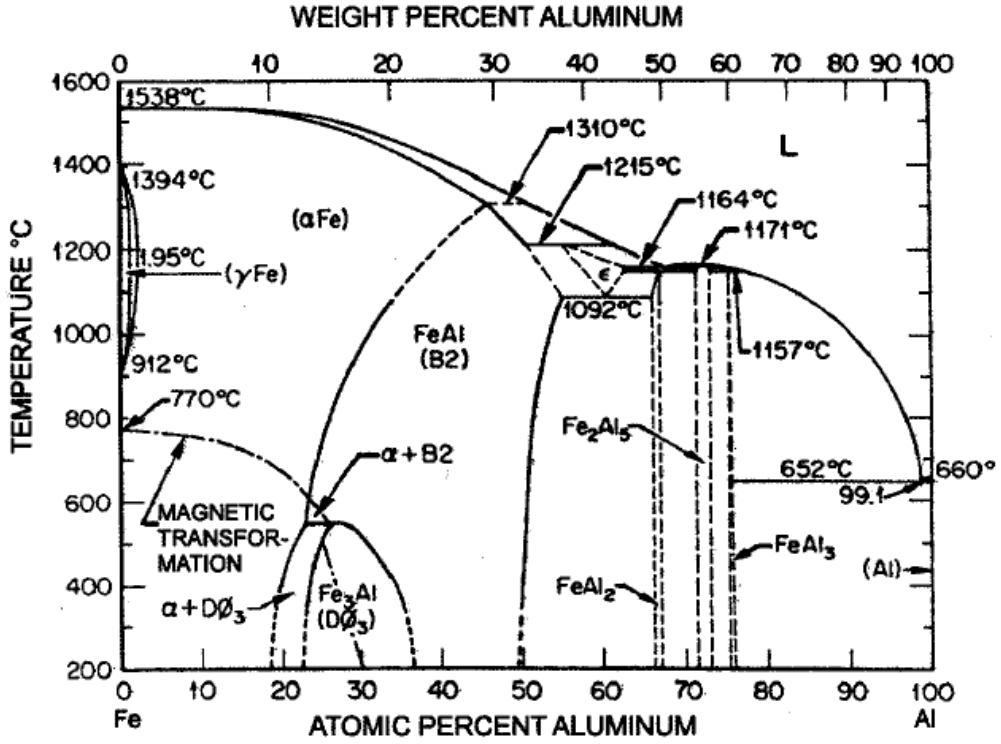

Fig 2.1: Fe-Al binary phase diagram [Frommeyer 1999]

From iron (Fe) rich side, three types of lattice structures are present which are derived from b.c.c. structure. One of them is dis-ordered A2 lattice structure which forms due to the solid solution of iron-aluminium up to about 20 at.% Al at room and high temperatures (Fig. 2.2).

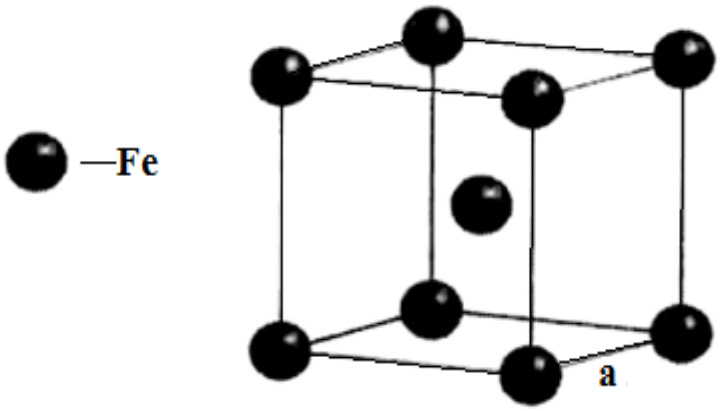

Fig 2.2: BCC Lattice Structure (Disorderd A2) [Frommeyer 1999].

A very few studied have been reported with lower aluminium content, i.e. disordered α-phase alloys, has been limited. The disordered matrix of alloy exhibited high ductility. The

wrought alloy showed significantly higher strength (600 MPa) than that reported for binary Fe-16at%Al with similar elongation. Alloys of this composition offer similar properties than the intermetallic composition both in mechanical and magnetic properties. In fact, the mechanical properties of disordered α-phase are likely to offer an alternate to the poor room temperature ductility encountered in the intermetallic composition with reasonably high strength. The yield strength of pure iron-aluminium solid solution is increasing with increasing aluminium content because aluminium is a strong solid solution strengthener of iron. The magnetic properties also offer a compromise between the decreasing saturation induction and the increasing permeability and resistivity with increasing aluminium content [Syahrila 2002].

The iron-aluminum light weight steel (α-phase) containing~17at.%Al shows a reduction in density**.** The density, determined by different methods, such as X-ray diffraction (theoretical density, lattice constants), levitation and pycnometric measurements vs Al content for different iron-aluminium alloys is shown in Fig. 2.3. At 6 wt.%Al, the steel reduces its density from 7.8 to 7.25 g/cm^3, and at 8.5 wt.%Al, the density reaches 7 g/cm^3, respectively. This reduction in density is more than 10 percent [Frommeyer 1999].

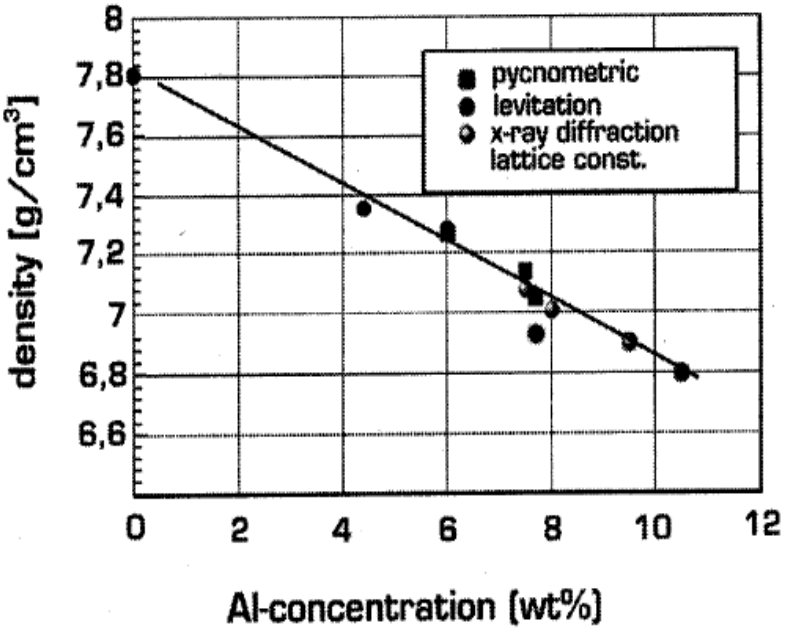

Fig 2.3: Variation of density of disordered α-phase with Al concentration [Frommeyer 1999]

Earlier studies revealed that Fe-A1 alloys can be cold worked which containing up to 6% A1 content while hot working can be extended up to 12% A1. Nearly 8% Al addition is considered to be enough for Fe-Al based alloys to have good oxidation resistance at high temperature. Thus, such alloys face problems during fabrication. In order to reduce levels of

embrittlement these alloys must be prepared under protected environment such as vacuum conditions or inert atmosphere. Oxygen, as a special case, must be avoided or oxide films may be developed in as-cast structure of the alloy. The embrittlement may also be occurs due to deoxidation with carbon because of carbide formation [Prescott 1992]. Due to poor thermal conductivity and high thermal expansion coefficient, large thermal stresses are developed which may increase intercrystalline fracture during working.

2.1.2 Fe_3Al based alloys

Fe_3Al based iron aluminide exhibits ordered DO_3 structure (Fig. 2.4), and is stable in 23-36 at.% Al in temperature ranging from room temperature to 550°C. For temperature well above 550°C, DO_3 converts in to an imperfectly ordered B2 structure, which ultimately transforms to a disordered solid solution [Prakash 1991]. Fe_3Al having ordered structure is one of the few intermetallics which can be transformed into disordered (with respect to DO_3 structure) by suitable heat treatment. This phenomenon has its own advantage and disadvantage. It is useful for scientific studies of the influence of ordering on mechanical behavior, while on the other hand there is decrease in the creep and tensile strengths on transferring the ordering structure. This disordering takes place at low temperature, approx. 550°C called critical transition temperature (Tc).

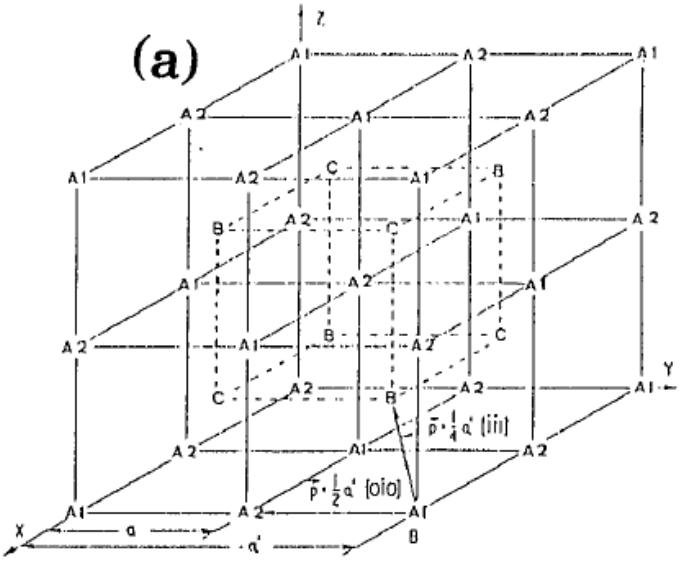

Fig 2.4: Unit cell and APB vectors for the (a) DO_3 A, Al, A2 and C are Fe sites. B represents Al sites [Prakash 1991].

This temperature becomes the limitation for Fe_3Al based alloys to use as structural material for high temperature applications. But, this critical temperature can be raised

considerably by addition of different alloying elements such as molybdenum or silicon, among other solutes. Currently, some of the major problems like poor creep resistance at elevated temperatures, low impact resistance and ductility at room temperatures [Prakash 1991] that sustain to delay commercialization of these alloys. The ordered DO_3 superlattice structure contains 16 atoms (12 Fe and 4 Al atoms) per unit cell (Fig 2.4) is present in the concentration range from 23-36 at.% Al. Iron aluminides (Fe_3Al) exhibit order-disorder transformations and large fractions of defects can be vary with composition and temperature. In ordering transformations, small ordered nuclei are formed which finally grow until the entire crystal is transferred in to ordered array, forming in an anti-phase domain structure. This has further been characterized by transmission electron microscopy (TEM). Depending upon the structure of ordered alloys, the anti-phase boundaries are classified into different categories [Martinez 2006].

In ordered DO_3 structure, two types of anti-phase boundaries are formed; APB1 that is characterized by A2 to DO_3 transformation, with a fault vector $a_0/4$ <111> (where a_0 is the lattice parameter of the DO_3 unit cell) and APB2 (or DO_3-type APB) related to the B2/DO_3 transformation, with a fault vector $a_0/2$ <100>as shown in Fig. 2.5 **[**Martinez 2006].

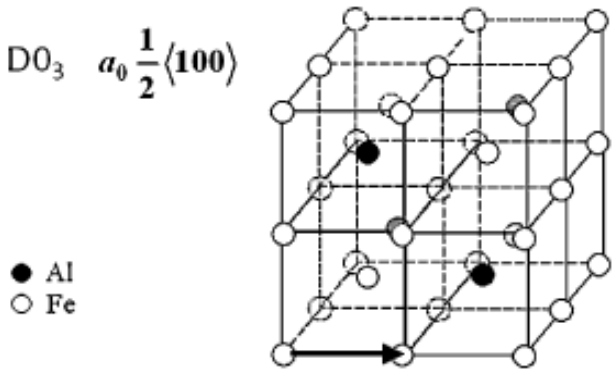

Fig 2.5: Ordered DO_3 phase showing displacement vectors [Martinez 2006].

The section of Fe-Al phase diagram, in the locality of 25 at.%Al, shown in Fig. 2.6 . Fe_3Al alloy with DO_3 structure falls in the range with Al content from approx. 22-30 at.% Al, but two-phase regions exist on either side. It is noted in the diagram must be considered for two-phase A2+B2 and A2+DO_3 regions while deciding the heat treatment programme for alloys. These two different regions have been reported to alter mechanical properties due to age hardening. It has been noted that for alloys for which the Al content varies 20-25 at.% Al and temperature lies in the range of approx. 300-550^oC, it is likely to preserve a stable two-phase

A2+DO_3 ordered microstructure corresponding to nickel-base super alloys. This temperature range of stability of the mixture of two-phases can be expanded by addition of Si with range of 1-3% [Mckamey 1996].

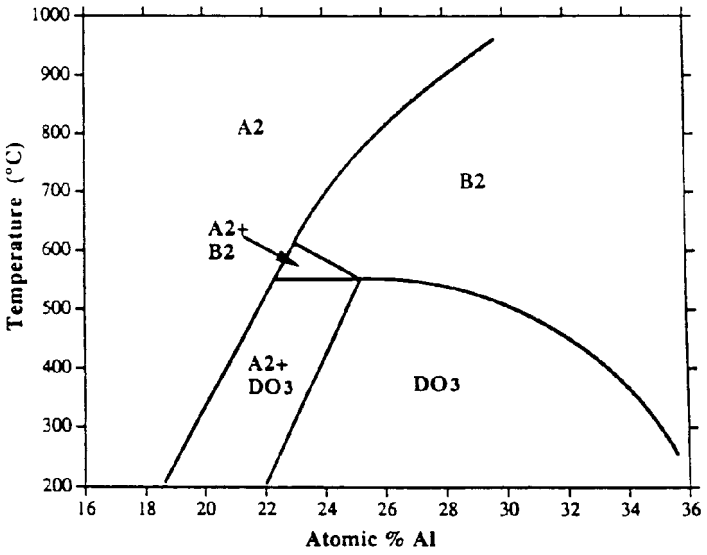

Fig 2.6: Phase diagram in locality of Fe-25 at.% Al [Mckamey 1996]

The relatively low density and lower material cost of iron aluminides than stainless steel lead to an interesting material. These advantages with their excellent sulfidation and oxidation resistances have led to consider iron aluminides as better structural material for high temperature structural applications [Syahrila 2002]. The study of corrosion resistance of Fe-Al alloys was first reported in 1930s and seems to be excellent. But detailed studies of mechanical behaviour were first reported by Cahn and his co-workers in early 1960s. The work involved the study of creep behaviour of Fe_3Al alloy above and below the critical ordering temperature (T_c) i.e. 550^{o}C. This also included the influence of long-range order on mechanical twinning and yielding. However, the abrupt fall in strength above 600°C and poor ductility at room temperature has been major drawbacks to consider this material for structural applications.

The improvement in the room temperature ductility of Fe_3Al based alloys have been done by employing various methods. It is also find that even single-crystal FeAl showed environmental embrittlement which causes poor ductility. For example, the alloy having highly elongated microstructure with minimum transverse grain boundaries has been found less tendency to hydrogen diffusion and hence shows highest ductility. In contrast to this, the increased recrystallization as a result of higher-temperature annealing enhanced the number of transverse grain boundaries, caused the increment in inward hydrogen diffusion. This resulted in reduction ductility of the alloy. Alloying with suitable elements resulted in more stable and

reproducible improvement in ductility. The elements such as Ti, Si, Mg, V, Cr, Mo and Ni were considered for solid-solution strengthening and C, Cu, B, Ta and Zr were added for precipitation strengthening. In general, the inclusion of alloying elements either for solid-solution strengthening or precipitation strengthening to increase the high-temperature tensile strength and creep resistance resulted in low room-temperature tensile elongations. It was observed that the chromium seem to be an effective alloying addition to increase the ductility of iron aluminides having higher aluminium contents. The combination of adding various alloying elements led to the optimization of properties of iron aluminides [Hausild 2009; Suwas 1996; Suwas1997].

2.1.3 FeAl based alloys

FeAl based iron aluminide exhibits ordered B2 structure in the composition range 36-50 at.%Al and stable up to the melting temperature [Liu 1993]. FeAl based alloys possess interesting properties such as low density, low cost, good wear resistance and outstanding corrosion resistance at high temperature with some advantages over Fe_3Al based alloys. These properties make this material suitable for a wide variety of structural applications at high temperature. In addition, it possesses high electrical resistivity and would be able to show ferromagnetic under certain conditions [Alexander 1998; Kumar 1998]. The unique characteristic of FeAl (B2 structure) is that it generates large number of thermal vacancies and goes on increasing with increase in Al concentration [Wurschum 1996, Xiao1995, Kogachi 1997].

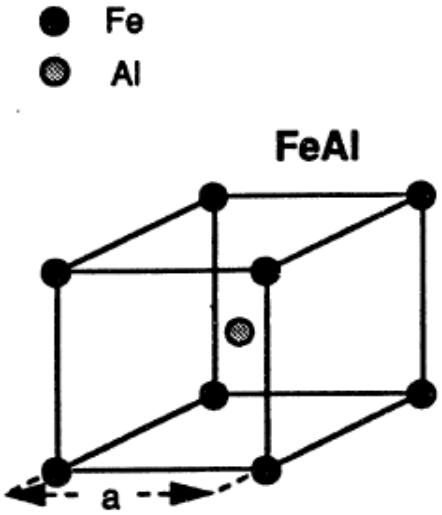

Fig 2.7: Ordered B2 lattice structure [Morris 1990]

Both Fe_3Al and FeAl ordered structures exist over a wide range of composition at room temperature. However, Fe_3Al experiences a change from order to disorder structure at temperatures near 540ºC, which is function of Al content. Above 550ºC, Fe_3Al structure changes to an imperfectly ordered B2 structure, which finally transforms to a disordered solid solution. On the other hand, FeAl does not undergo any transformation and retains ordered structure up to its melting point. With increasing Al content i.e. (36-50 at.%Al), the B2 superlattice structure is present in the iron aluminides as shown in Fig 2.7. The melting points of Fe_3Al and FeAl are 1520ºC and 1250ºC, respectively. The density values of these alloys are 6.72 and 5.56 g cm^{-3} respectively [Wasilkowska 2004].

An ordered alloy comprises of different types of anti-phase boundaries (APB) which depend on their structure. In B2 ordered alloys, there exist only one type of anti-phase boundary, the B2-type APB (or APB1) i.e. formed in A2 to B2 ordering transformation and that has a fault vector a/2(111) as shown in Fig. 2.8 (where 'a' is the lattice parameter of the B2 unit cell) [Martinez 2006].

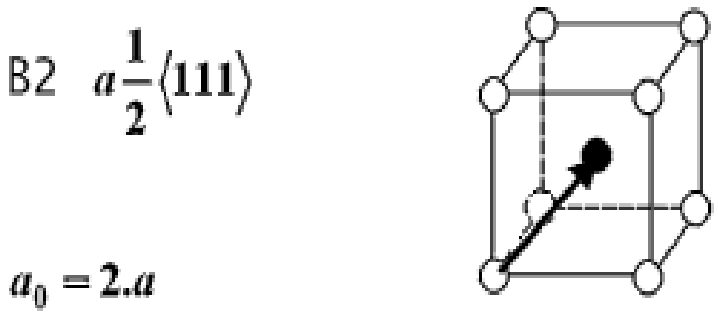

Fig 2.8: Ordered B2 phase showing displacement vectors [Martinez 2006]

Iron aluminides based on FeAl has lower density than Fe_3Al based alloys and as much as 30 to 40%, compared to steels and other commercial iron-based alloys. These alloys also exhibit poor ductility at room-temperature. The main reason of poor ductility of FeAl-based alloys is due to the fact that they are highly reactive to hydrogen present in the environmental [Liu 1989]. A unique feature of FeAl is that it produces a huge number of thermal vacancies determine by cooling rate and heat treatment temperature. The number of vacancies increases with increasing Al content [Kogachi 1997; Pike 1994; Wurschum 1996; Xiao 1995; Collins 1996; Yang 1998] and their concentration greatly affects the mechanical properties (strength, ductility and creep resistance).

In recent years, the improvement in the ductility of the alloys is achieved by considerable efforts such as kinds of thermo mechanical treatments or by suitable alloying additions [Bahadur 1995]. The yield strength and ductility of FeAl based alloys at ambient temperature are dependent on heat treatments and followed by cooling rate to room temperature. This is closely related with the tendency of FeAl to retain a large number of vacancies even after fairly slow cooling rate. Though, iron aluminides have high yield strength at ambient temperatures but they shows the low strength and creep resistance at higher temperatures. This fall in the strength may be attributed to the open B2 structure, which increases diffusion-controlled creep at temperatures higher than about 0.4 on the homologous temperature scale. Both, the strength and ductility of FeAl alloys (B2) is also strongly temperature dependent. Thus, annealing for long duration at low temperature i.e. 400^{o}C seems to cause a significant reduction in yield strength and hardness.

The poor ductility of B2 based alloy is primarily due to the environmental embrittlement which produced by hydrogen present in the moisture contained in air at room temperature. It is termed as hydrogen embrittlement because it occurs due to reaction between H_2O vapor and Al and produces nascent hydrogen which absorbed at crack tips and leads to brittle fracture. It is also observed in the single crystals and the degree of embrittlement is dependent on both grain size and stoichiometry. A very small amount of moisture is enough to cause embrittlement of FeAl (<10 p.p.m. for Fe-36 at.% Al) [Pang 1998].

The strength of the binary alloy has been significantly increased on the addition of alloying elements. The alloying with elements such as Ti, Mg, Cr and Co moderately improved the creep resistance of FeAl based alloys because of solid solution hardening. On the other hand Hf, Zr, Nb, B and Ta have been successfully added to improve the creep strength of B2 FeAl through precipitation hardening [Mendiratta 1987; Vedula 1987; Maziasz 1996]. It was observed that creep resistance of Fe-40Al based alloys also found to be effectively improved with addition of oxide dispersion strengthening (ODS) through Y_2O_3 powder [Wolski 1996; Morris-Munoz 1999].

Another approach to improve the strength limitations is to addition of carbide reinforcements, such as ZrC, SiC, TiC or TiB_2 particulates in the alloy. The shape, size, spatial distribution and the volume fraction of the reinforcement significantly affect the mechanical behaviour of FeAl based alloy. Thus, it is assumable that a microstructure with homogenous distribution of carbides or borides in FeAl matrix led to increase in ductility and strength at room temperatures. The addition of boron (B) has been tried to improve the ductility of FeAl-

based alloys. The environment has also significant effect of the ductility of FeAl alloys. In FeAl based (36.5at.% Al) alloy, it was demonstrated that the tensile ductility found to be increased (2.2 to 17.6%) when the test was conducted in different environmental conditions i.e. changed from air to dry oxygen.

It was observed that the results were not similar for the 40at.% Al alloy. This might be due to in 36.5 at% Al alloy failed due to transgranular cleavage in air and changed in to brittle grain-boundary fracture in 40at.%Al. When the same testing was conducing in oxygen environment, the mode of fracture for the Fe-36.5 at.% Al alloy switched from transgranular failure in air to intergranular in oxygen. In case of Fe-40 at.% Al alloy, the fracture mode did not change on changing the condition from air to oxygen. This shows that Fe-40 at.% Al alloy exhibits are relatively weaker grain boundaries, and cause brittleness due to intergranular fracture at room temperature. The boron addition upto 300 ppm (by weight) resulted in the in ductility of Fe-40 at.% Al alloy in oxygen environment. These results indicate that boron addition (B) strengthens the grain boundaries but is not helpful in reducing the environmental effect in Fe-40 at. % Al alloy [Russel 2003, Liu 1990, Baker 1997, Cohron 1998, Lejcek 2003].

The Al content in binary FeAl alloys decides their mechanical properties. The tensile ductility of Fe-Al alloys at room temperature decrease with the increase of Al content, while the yield strength increases with the increase of Al content up to 40 at.% Al. Further, the mechanical properties of Fe-at.40%Al are strongly influenced by the temperature. Like B2 Cu-Zn system, there exists a ductile-to-brittle transition temperature range and the yield strength of Fe-at.40%Al (both polycrystalline and single crystal material) shows positive temperature dependence. Several theories based on dislocation decomposition and dislocation reactions have been proposed to explain the increase in the yield stress with increase in temperature.

2.2 Classification of Fe-Al based alloys on carbon additions

In Fig. 2.9, the ternary phase diagram of Fe-Al-C is shown [Palm 1995]. Carbon has very limited solubility in (<0.2at%C) in FeAl based alloys and thus resulted in precipitation of perovskite type $Fe_3AlC_{0.5}$ phase (K-phase) in Fig. 2.9.

In Fe-Al alloys, most of the carbon is taken by $Fe_3AlC_{0.5}$ carbide phase. The amount of carbide depends upon the content of carbon and their fraction increases with increasing in carbon content. The alloy matrix has three phase namely α–phase, Fe_3Al or FeAl with crystal structure i.e. A2, $D0_3$ of B2 respectively depending upon the concentration of Al. The Al however, is present in both the phases. In Fe-(15-23 at.%) Al alloy containing 6 at.%C or more,

the carbide becomes the major phase [Jung 1989; Sanders 1997; Wunnicke-Sanders 1993; Sanders 1997]. Similar observation is observed in Fe-(23-33at.%) Al alloy. Further, it may be noted that at high (37at.% or more) Al-contents, formation of graphite may occur (Fig. 2.9). These alloys are classified below depending on the Al-content but it must be noted that the state of the order (B2 or $D0_3$) present in the matrix also depends on the heat treatment.

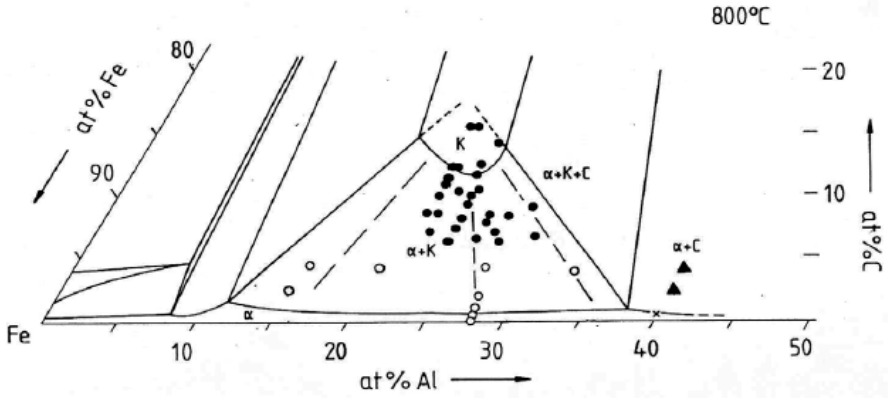

Fig 2.9: Showing isothermal ternary phase diagram of Fe-Al-C at 800°C [Palm 1995]

2.2.1 α–phase with $Fe_3AlC_{0.5}$ carbide phase

The addition of 4at.% C to Fe-15at.%Al was processed by air induction melting (AIM) followed by electroslag melting (ESR). The microstructure exhibited the uniform distribution of precipitates obtained after heat treatment and thermo-mechanical processing. In these alloys perovskite carbide, $Fe_3AlC_{0.5}$ is primary phase accompanied by α–phase [Baligidad 1998a; Satya Prasad 2014; Khaple 2010]. The microhardness of Fe-15at%Al alloy was found to enhance with increasing carbon content. This suggests that rule of mixture for two phases is followed by these alloys. Further, the Vickers hardness of these alloys was found to decrease with increase in the temperature from 500 VHN at room temperature to 50 VHN at 1173K. The compressive flow stress also found to decrease 1200 MPa at 673K to 25 MPa at 1173K. The carbon addition accomplished with improvement in the tensile elongation from 8 to 16%. Fe-15at%Al containing 1.6at%C and 4at%C produced by ESR were shown to better strength and elongation than those reported, cast vacuum induction melting (VIM) ingots containing similar Al content in the temperature ranging from room temperature to 1073K. A sharp drop in the strength with improved elongation was observed at 873K or above. With increase in the strain rate, fracture strain was observed in compression tests leading to conclusion that these alloys may be sensible to embrittlement. A brittle to ductile transition (BDTT) in 4-point bend test (> 5% strain) on increasing temperature was reported [Sanders 1997]. This was found to increase

from 873 to 1273K with increase in volume fraction $Fe_3AlC_{0.5}$ phase 50 to 100%. Thus from above studies, it may be concluded that these alloys with carbides as matrix phase [Sanders 1997; Sanders1997] were very brittle and were tested only in bend tests or compression testing.

2.2.2 Fe_3Al alloys with $Fe_3AlC_{0.5}$ carbide phase

Fe_3Al based alloys has been noticeable due to their low density, high strength to weight ratio, low cost, excellent oxidation and sulfidation resistance [Liu 1990; Tortorelli 1998; Kai 1997; Prakash 1991]. But drop in the strength above 600^{o}C and low room temperature ductility has limited their possible applications [Liu 1990; Stoloff 1998]. McKamey et al [McKamey 1991] has been reported the salient characteristics of these materials. Most of reported literature on iron aluminides is only related to low carbon content (<0.01 wt.%C). Carbon addition is known to embrittle these alloys [Stoloff 1998; Kerr 1986], therefore, literature is salient about carbon addition. In contrast to this, iron aluminides synthesized by an electroslag-remelting process (ESR) were found to show improvement in the strength on the addition of carbon as an alloying element [Baligidad 1996a; Baligidad 1996b; Baligidad 1994; Baligidad 1997a; Baligidad 1997b]. This improvement in the strength was primarily due to solid solution strengthening by interstitial carbon at low concentrations and $Fe_3AlC_{0.5}$ carbide precipitation at high carbon concentrations. It has also been reported that carbon addition to these alloys were shown to exhibit a reduction in susceptibility to embrittlement [Baligidad 1997b]. This may be attributed due to providing carbide matrix interfaces that act as hydrogen traps. The improved strength was attributed to significant fraction of $Fe_3AlC_{0.5}$ and volume increases with increase in concentration of carbon. In carbon free alloys with comparable Al-contents, the alloys showed the similar behavior [Morris 1995] with rapid fall in the strength above 873K.

The carbon addition to these alloys resulted improvement in the strength which led to have better creep resistance [Baligidad 1996a]. The carbon containing alloys exhibited a lower creep rate and improved rupture life over the binary alloys [Baligidad 1996b]. On the other hand, carbon addition resulted decrease in the charpy impact energy of these alloys due to precipitation of $Fe_3AlC_{0.5}$ carbides. The increase in the carbon addition up to 4at.%C in Fe_3Al based alloys showed the formation of Fe_3Al-$Fe_3AlC_{0.5}$ duplex structure. This complex structure contributed to improvement in the creep resistance and the strength [Baligidad 1997b]. Subsequently, Fe-33at%Al-4at%C alloy showed a similar structure which exhibited similar properties [Baligidad 1997b]. The compressive creep behavior of Fe-28at%Al-2at%C revealed the improvement in the creep strength without significantly influencing the stress exponent.

It was important to find out that the $Fe_3AlC_{0.5}$ carbide precipitates exhibit rapid coarsening at elevated temperatures. This effect may be more pronounced at lower carbon contents where the precipitates are finer. Further, it may be pointed out that the morphology of $Fe_3AlC_{0.5}$ carbide may be dependent on the carbon content. This limits the improvement in high temperature strength of Fe_3Al based alloys. The mechanical properties of Fe_3Al based alloys are significantly improved by carbon addition, but its influence on high-temperature oxidation has to be examined. In Fe_3Al alloys containing $Fe_3AlC_{0.5}$ alloys, $Fe_3AlC_{0.5}$ is more prone to oxidation than matrix Fe_3Al [Rao 2002]. Thus, the addition of carbon to Fe_3Al alloys resulted decrease in oxidation resistance.

In Fe-Al-C compositions with carbide matrix and Fe_3Al as the minor phase have been investigated. These alloys contain 23-30at.%Al and 6-16at.%C and exhibit similar to those reported [Jung 1989; Wunnicke-Sanders 1993] for alloys containing α+$Fe_3AlC_{0.5}$ phases with α-phase as the minor considered in the previous section.

2.2.3 FeAl alloys with $Fe_3AlC_{0.5}$ carbide and graphite phases

Recently, it has been reported that carbon addition to Fe_3Al based alloys leads to improvement in the strength, machinability, creep resistance and resistant to environment embrittelement [Baligidad 1997a; Baligidad 1997b; Baligidad 1998b]. These properties were improved primarily due to presence of $Fe_3AlC_{0.5}$ carbides. The same concept was applied to FeAl based alloys and few works on the carbon containing FeAl alloys has been reported [Baligidad 2005]. Presently, the addition of carbon seems to improve the mechanical properties of FeAl alloys [Pang 1998; Radhakrishna 2001]. The solidification behavior of FeAl based alloys containing carbon alloys is quite complicated. Carbon has limited solid solubility to FeAl based alloys and precipitates either as graphite or as carbide of $Fe_3AlC_{0.5}$ type with a perovskite structure (k-phase), depending on composition [Radhakrishna 2001]. The FeAl based alloys containing carbon was produced by using air induction melting (AIM) followed by electroslag melting [Radhakrishna 2001]. The addition of carbon up to (1.0at.% C) in Fe-38at.%Al accompanied with the precipitation of $Fe_3AlC_{0.5}$ carbides. Further addition of carbon to higher level (5.0at.% C) leads to the formation of soft graphite phase [Radhakrishna 2001].

The Fe-40at.%Al with 0.6at.%C addition was produced by vacuum induction melting (VIM) and extruded at 1273K. The microstructure of the alloy contained significant amount of $Fe_3AlC_{0.5}$ carbides which were stable up to 1173K. Some graphite precipitates were also observed in the alloy. The ductility of alloy was not determined by the presence of carbide

precipitate at the grain boundaries. The annealing caused improved in the ductility of the alloy. This may be due to decrease in the vacancy concentration and to some extent by the precipitation of interstitial carbon as carbide. It was also found to decrease in the strength of the alloy from 521 to 316 MPa. The carbon addition upto 0.6at%C to Fe-40at%Al alloy also resulted improvement in the impact toughness as compared to binary Fe-40at%Al alloy [Pang 2000].

On heating up to 1173K, the $Fe_3AlC_{0.5}$ carbide got dissolve in the matrix. Thus, a continuous film of graphite would form on the grain boundaries of the alloy rendering to the brittleness. This may definitely effect the mechanical properties of FeAl based alloys. This would seem like to be globular graphite particles participating in a reaction involving supersaturated liquid phase. U. Prakash et al has reported effect of carbon addition (1.8 and 3.5at.%C) on the tensile behavior of Fe-40at%Al melted by vacuum induction melting (VIM) [Prakash 2001]. At lower carbon addition i.e. 1.8at.%C, both graphite as well as $Fe_3AlC_{0.5}$ carbide were seen in the alloy while only graphite precipitates were observed in the alloy containing 3.5at%C. This graphite precipitation resulted decrease in the yield strength of Fe-40at.%Al alloy from 398 to 358 MPa on increasing the carbon content from 1.8 to 3.5 at.%C.

2.3 Iron aluminides containing carbon on quaternary additions

The binary Fe-Al based alloys need to improve the ductility at room temperature and fall in the strength above 873K. The presence of second phase particles to Fe-Al matrix has been recommended for number of reasons. The presence of the carbides leads to improvement in the ductility at room temperature besides the precipitation strengthening effect [Baligidad 1997b; Sen 2001]. The presence of these carbide particles [Sen 2001; Parvathavarthini 2002] is responsible for improvement in the machinability of iron aluminides. The studies also revealed the beneficial effect of hard carbide particles in the Fe–Al matrix helps in the increasing of tribological (friction) properties such as erosion and wear resistance [Alman 2001]. The Laves phase precipitation in Fe–Al alloys as a result of additional alloying element is also proposed because of its strengthening effect [Sauthoff 1995; Sauthoff 2000; Prakash 2001].

The different alloying additions such as Zr, Ti, Cr, Mo, Si, Ni and Nb have been used to enhance the mechanical properties of Fe_3Al or FeAl alloys [McKamey 1989; Diehm 1987; McKamey 1988; Mendiratta 1993; Mendritta 1985; Dobes 2013; Pandey 2002]. Cr addition results significantly improvement in ductility at room temperature of iron aluminides. This may be due to reducing environmental embrittlement and enhancing cleavage strength. Addition of

Ti, Si and Mo alloying elements resulted in significant increase in the strength at temperatures up to 973K. This increment was primarily due to solid solution strengthening mechanisms and precipitation. Recently, it has been reported that carbon addition plays a significant role in Fe_3Al-based alloys. Baligidad et al has shown that the effect of addition of quaternary alloying elements such as Mn, Ti, Ni and Cr on the microstructure and mechanical properties of Fe_3Al based alloys which contain high carbon content (1.0 wt.%C). The alloying with Cr, Ni and Mn elements to Fe_3Al alloys containing carbon resulted two-phase structures of $Fe_3AlC_{0.5}$ in Fe_3Al matrix. Both $Fe_3AlC_{0.5}$ and Fe_3Al phases have limited solubility for Cr, Ni and Mn. The room temperature tensile strength Fe_3Al based alloys have no significant effect on alloying addition such as Cr, Ti and Mn. Ti has also considerable amount of solubility in Fe_3Al and $Fe_3AlC_{0.5}$ phases in Fe-Al-C alloying having high carbon content. The microstructure mainly composed of primary TiC with dendritic small TiC particle and secondary elongated $Fe_3AlC_{0.5}$ carbides. The creep resistance and high temperature tensile strength of Fe-Al-C system containing Ti and Mn have inferior to ternary Fe_3Al based alloys with comparable Al and C contents. No explanations for these observations were offered. The Zr addition to Fe-Al-C system showed ZrC particles in the grains in addition to ternary intermetallics phase Fe_6Al_6Zr as well as unidentified Fe-Al-Zr phase containing 23at.%Zr at the grain boundaries [Kratochvil 2012]. The precipitates of ZrC were most equiaxed. In the Nb containing Fe_3Al based alloy the NbC formed as small carbides within the grains as well as at the grain boundaries. All the carbides were very stable up to 1373K and did not have any effect on their morphology and distribution.

The addition of alloying element in carbon containing alloys limits the role of carbon present in the iron aluminides. These alloying elements such as Ti, Zr, Cr etc. primarily served as carbide formers instead of alloying to iron aluminides containing carbon. Alloying with these elements resulted in the formation of alloy carbides in significant reduction of volume fraction of other phases [Chaudhary 2015]. Alloy carbides such as TiC can enhance the hardness, creep resistance and wear resistance of iron aluminides and also TiC reinforced Fe_3Al based composites have been produced by pulse discharge sintering, pressureless and melt-infiltration [Ko 2002; Ko 1999; Subramanian 1997c; Subramanian 1996]. The in situ Ti_3Al-TiAl based composite reinforced with TiC particles was prepared with laser melting Ni-Al-Ti-C powder [Chen 2005]. The composite showed high hardness and improved wear resistance attributed to high hardness and thermal stability of TiC, in addition with strong atomic bonding with nickel aluminides. Zhang et al [Zhang 2011] has also reported that the presence of TiC hard particles increased the wear resistance of Fe-28Al-5Cr in the ambient temperature.

As reported earlier, at Al-content of 37at.% or more, the graphite precipitation occurs in Fe-Al-C (1.0 at.%C or more) based alloys. Here the carbide former elements such as Ti, Zr, Cr and Nb may play an important role by forming the respective alloy carbides. The graphite formation in FeAl based alloys can be prevented by appropriate alloying element additions. FeAl alloys containing carbon which may from the corresponding carbides with alloying additions such as Ti, Zr, Cr, V etc. The addition of Ti resulted successfully addition of carbon to FeAl based alloys. Alloy exhibited the formation of alloy carbide i.e. TiC in addition to $Fe_3AlC_{0.5}$. No graphite precipitation was observed in FeAl alloys containing carbon on Ti addition.

2.4 Mechanical properties of iron aluminides reinforced with second phase

Iron aluminides has one of the major drawback is to show low ductility due to grain boundary failure or their brittleness fracture. The inclusion of second phase to the matrix results uniformly distribution of stress concentrations. The homogeneous distribution of second phase particles causes obstacles to the dislocation motion. The fine distribution of particles would result in the reduction of local stress concentration by reducing the mean free path of the dislocation. On the other hand, the fine particles also used to improve the strength of the material. The dispersoid particles must be stables at high temperature; only then the improved strength and ductility are to be maintained for high temperature applications. Only stable particles are able to avoid the particle and grain growth during the hot working conditions.

Both Fe_3Al and FeAl based alloys shows steep decline in the strength above 550^{o}C [Morris 2001; Morris 1998; Schneider 2004]. The strengthening can be achieved by solid solution hardening, ternary alloying addition that causes atomic ordering to higher temperatures and introducing precipitates hardening [Morris 1998; Schneider 2004]. Many studies have provided valuable information about the strengthening of the iron aluminides. For example, the addition of Mo is useful in solid solution hardening and strengthening by particles such as yttrium oxides [Morris 1998], niobium carbides (NbC) [McKamey 1992], titanium carbide (TiC) [Gao 2005] and zirconium carbides (ZrC) [Kratochvil 2012].

Titanium carbide (TiC) found to be suitable reinforcement with intermetallics due to its high temperature and wear resistance properties which combine with the engineering properties of intermetallics. They have been recommended as potential materials for high temperature applications and in oxidative and corrosive conditions where commercial WC/Co cermets may fail.

2.5 Effect of carbon addition to iron aluminides

2.5.1 Hydrogen effects in iron aluminides

Cast ingots of high carbon alloys were readily machinabale using water based coolants by conventional turning on the lathe [Baligidad 1994]. This contrasts with very poor machinability due to surface cracking reported for low carbon compositions [Stoloff and Liu 1994]. The surface cracking is to be due to susceptibility of iron aluminides to hydrogen embrittlement. This embrittlement may be considered as primarily reason for low room temperature ductility. The moisture present in the atmosphere is the most common source of hydrogen which found to react with aluminium in these alloys to produce atomic hydrogen.

The presence of uniform distributed carbide precipitates which may be act as hydrogen traps were cited to explain the improved machinability in carbon containing alloys. These observations together with limited improvement in ductility obtained after coating the tensile samples in oil or after changing the grain size as well as grain orientation led to the concentration that carbon containing alloys exhibit a reduced susceptibility to environmental embrittelement [Baligidad 1997a; Baligidad 1996a].

Improved machinability has been reported in Fe-40at%Al-3.5at%C alloy where carbon is present as graphite [Prakash 2001]. The improvement in machinability was demonstrated for a number of Fe_3Al/FeAl based alloys and did not depend on types (Perovskite/alloy carbide or graphite) of second phase present but was thought to be related to lower mobility of hydrogen in the alloys on account of blocking of interstitial sites by carbon. Despite the improved machinability, the alloy still exhibited hydrogen embrittlement during subsequent tensile tests.

Effect of carbon addition on hydrogen permeation on Fe_3Al and FeAl has recently been reported [Zhang 2006; Prakash 2007] the hydrogen solubility in Fe-28at%Al alloy is unchanged on addition of 4at%C indicating that the amount of hydrogen reversibly trapped is the same in Fe-28at%Al and Fe-28at%Al-4at%C alloy. The hydrogen mobility decreased by a factor of two on addition of carbon. This may significantly reduce susceptibility to hydrogen induced cracking and explain the improved machinability of carbon containing alloys. The reduction in mobility on carbon addition was also observed in Fe-40Al alloy [Prakash 2007]. The hydrogen solubility also increases on adding carbon to Fe-40Al where carbon is present as graphite. Both these factors may lead to improved resistance to hydrogen embrittlement and hence improved machinability.

2.5.2 Corrosion and oxidation resistance of iron aluminides

In the last five years, oxidation, sufidation, hot and aqueous corrosion studies have been reported for Fe-Al alloys containing carbon. Oxidation studies carried out 973K to 1273K indicate that oxidation becomes a problem at (15at% or less) Al-contents [Singh 2004; Rao 2002]. This is probably due to significant depletion of α-matrix of aluminium because of the formation of perovskite carbide which has a higher Al-content. At higher Al contents carbon addition does not seem to significantly change the oxidation upto 1373K. However, the carbide may exhibit a higher rate of oxide growth [Rao 2003; Rao 2005]. An overview on the oxidation of Fe-Al-C alloy containing carbon has been published [Rao 2004].

Hot corrosion studies on Fe-25at%Al and Fe-28at%Al-4at%C has been reported at 1100, 1225 and 1330K have been reported [Das 2003]. The alloys were coated with sodium sulfate prior to exposure in the oxygen. The carbon containing alloy exhibited lower corrosion kinetics. Long term sulphidation of a range of alloy (15 to 28at%Al and upto 4at%Al) have been carried out at 1073K in a SO_2+O_2 environment. No significant effect of C or Al-content was observed on sulfidation behavior. This sulfidation rates were much lower than the 310 stainless steel [Rao 2003].

One of the major drawbacks of carbon addition is that the resistance to electrochemical corrosion and passivity deteriorate with increasing the carbon content. This was attributed to preferential attack on the carbide in aqueous sulfuric acid medium [Rao 2002]. Ce addition of ~1at% has been reported to refine the carbide size and lead to lower corrosion rate [Nigam 2006; Sriram 2006]. However, these were still higher than mild steel with low (0.05wt%) carbon content. Zr addition in Fe_3Al-based alloys has been synthesized for high temperature applications also show excellent resistance up to 900-1000°C [Hotar 2012].

2.5.3 Machinability of iron aluminides

Iron aluminides having ordered DO_3/B2 structures show embrittlement due to hydrogen susceptibility [Stoloff 1994]. The long-range ordering of the structure should be considered the main reason for the intrinsic embrittlement of a two-component B2 FeAl phase [Kupka 2011]. The hydrogen is easily available from atmospheric moisture which reacts with aluminium in the alloys and produce nascent hydrogen by chemical reaction: $2Al + 3H_2O = Al_2O_3 + 6H$. This hydrogen may be primary cause for poor ductility as well as machinability of iron aluminides. Carbon additions from 0.3 to 4.2 at% to iron aluminides (Fe_3Al based) lead to precipitation of $Fe_3AlC_{0.5}$ carbide phase. It was proposed that the carbide precipitates may act

as tarps for hydrogen thus minimizing the susceptibility of iron aluminides to hydrogen embrittlement [Baligidad 1997a]. On the other hand an Fe-40at%Al-0.6at%C alloy, machined using electro-discharge machining (EDM), has been reported to exhibit increased ductility with increasing strain rate during tensile tests [Pang 1998].

The carbon addition ranging from 0.1 to 1.0 wt% to iron aluminides improves the machinability without showing any crack on the surface. This improvement shows no dependency on the types of second phase present (graphite or carbides). The carbon addition may be blocked the interstitial sites on account to reduction in the susceptibility of hydrogen embrittlement in these alloys.

2.5.4 Wear properties of iron aluminides on carbon addition

The microstructure and sliding wear of Fe_3Al-$Fe_3AlC_{0.5}$ composites have been studied [Yang 2004; Yang 2005]. The alloys were prepared by combustion synthesis and not by ingot metallurgy. Alloy with carbide content of 60wt% was found to exhibit the best wear resistance. But later studies reveal that the $Fe_3AlC_{0.5}$ in Fe_3Al alloys got deformed under high applied load [Itoi 2010]. This deformation of carbides can be overcome by the presence of alloy carbides like TiC and ZrC [Itoi 2010]. The wear resistance of Fe_3Al based alloys were significantly increased by the presence of these alloys carbides. The *in-situ* formed carbides were found to be more compatible with matrix resulting strong bonding between them.

2.6 Types of reinforcements

A hard phase having high elastic modulus can be incorporated in iron aluminide matrix by a number of methods. The second phase must be chemically stable and compatible with the matrix. A number of compatible reinforcements were identified for iron aluminides [Misra 1990]. From thermodynamic considerations alone Al_2O_3 was considered to be the most stable reinforcement in iron aluminide matrices. A number of carbides, borides and oxides were also identified as potential reinforcements. As described in later sections borides and carbides have been found to be more effective while oxides have been of very limited use.

The choice of reinforcement is also determined by its availability as well the form in which it is available (for example powders, fibres, whiskers and laminates). As iron aluminides are being developed due to their low cost as the cost of reinforcement may also be an important consideration. A further requirement is the compatibility between thermal expansion between the reinforcement and the matrix as these may undergo several thermal cycles. Kumar and Bao

[1994] have compiled coefficient of thermal expansion (CTE) data for a number of ceramic reinforcements. Most ceramics have a lower (50% or less) CTE than those reported for iron aluminides (~$20x10^{-6}$/K). Dimensional mismatch between due to difference in CTE between the matrix and reinforcement has to be accommodated by plastic deformation of the matrix as the ceramic is too brittle to deform plastically. Iron aluminides exhibit limited room temperature ductility. However significant improvements may be achieved by careful composition and process control. Lu et al (1991) have argued that below a critical reinforcement size matrix cracking due to CTE mismatch may be suppressed in Intermetallic matrix composites.

Significant number of routes relies on precipitation or eutectic formation. Methods used for processing of intermetallic matrix composites based on iron aluminides depend on the reinforcement and the form (eg. Fibre or particulate) in which it is desired. A vast majority of iron aluminide composites are particulate reinforced. These can be prepared by both melt as well as powder processing routes. Melt as well as mechanical alloying/reaction synthesis routes rely on in-situ formation of the reinforcement particles. Particulate reinforcements can also be added in powder processing. Finally displacement reaction with Fe_2O_3 particulates has been used to achieve oxide dispersion in an iron aluminide matrix.

2.6.1 Fibre reinforced composites

The literature on fibre reinforced iron aluminide composites is very limited. Nourbakhsh and Margolin [1991] have reported processing of continuous fibre (Al_2O_3 and Al_2O_3-20wt% ZrO_2) Fe_3Al based composites by pressure casting. Fibres of 20 μm were used to produce composite discs 52mm in diameter and 12mm thickness or rods measuring 13mm in diameter and 150mm in length with fibre volume fractions of up to 0.6. The matrix composition was Fe-28at% Al-2at%Cr-1at%Ti. Chromium was added to improve the ductility of the alloy and Ti was added to improve wettability of molten alloy with the fibres. ZrO_2 from fibres was dissolved in the melt and precipitated as Fe_2AlZr at the end of solidification due to limited solubility of Zr in iron aluminide. Growth in alumina fibre grain size was observed due to high melting temperature of the alloy requiring high (1923K) processing temperature. A high density of dislocations was observed at the matrix fibre interface and was attributed to the difference in CTE of matrix and fibre. No properties of the composites were reported. This may be partly attributed to the fact that study included TiAl and Ni_3Al based intermetallics and these

may have been followed up in subsequent investigations. Fibre reinforcement resulted in a two fold increase in modulus and a five fold increase in strength of Ni_3Al based composites.

Continuous fibre composites with Fe-40at%Al matrix with 10 μm diameter Al_2O_3 fibres with 10 volume% of fibres have been investigated [Inoue 1998; Inoue, Suganama and Nihara 2000]. Elemental powders of Fe and Al along with powders of Si and B were mixed in a ball mill in ethanol. The fibres were dipped in the slurry unidirectionally. These were then removed and stacked in a mold. The slurry was poured between the fibre layers. These performs were dried and then hot pressed at 1373 K for 0.5 hours in a vacuum of 10^{-4} Torr at 30 MPa with the direction of fibre normal to that of pressing. The temperature was chosen to prevent grain growth in fibres expected at higher temperatures. Reactive sintering occurs during pressing as the elemental powders of Fe and Al react to form the iron aluminide. Reaction synthesis of iron alumindes has been described in detail by Rabin and Wright [1991]. Aluminium oxide particles (1-2 vol%) are formed during processing. These were dispersed along the grain boundaries and led to a fine (15 μm) grain size iron aluminide matrix. Boron was added to improve fracture toughness by reducing susceptibility to environmental embrittlement of the iron aluminide and also to increase grain boundary cohesion while Si was added for strengthening. Both these additions were shown to significantly increase the flexural strength of the composites. The fracture strength of the composites also increased significantly due to the presence of continuous fibres. As expected the alloys exhibited susceptibility to environmental embrittlement.

Iron aluminides have been processed by pressure assisted reactive infiltration of molten Al into perform of steel fibres [Lapin 2000; Tieberghein 2002]. Fibre performs of volume fractions of 40% and 80% (corresponding closely to FeAl and Fe_3Al stoichiometry) were prepared from steel wool. After homogenization for five hours at 1273K intermediate reaction products were eliminated but a non uniform residual porosity distribution remained and this was attributed to a nonuniform distribution of steel fibres used. Also the thickness produced was only 6mm. The method can also be used for preparing an iron aluminde composite with steel mesh reinforcement.

2.6.2 Composites reinforced with particulates/precipitates

2.6.2.1 Oxide reinforced composites

Powder processing of composites is the most common route used for oxide reinforced composites. Schniebel and Deevi [2003] used prealloyed powders of Fe-40at%Al along with

30wt%ZrO_2 (<45μm) or 15vol%Al_2O_3 (<38μm) powders to prepare composites using liquid phase sintering. ZrO_2 was found to be unsuitable for liquid phase sintering because of thermodynamic instability with the molten matrix. The alumina powders could not be wetted by the intermetallic and equal amount (here 15vol%) of TiC powder was then added to improve wettability. Here it is worth recalling that Ti was added by Nourbakhsh and Margolin [1991] to improve wettability of Fe-40t%Al with alumina fibres.

2.6.2.2 Boride reinforced composites

Doucakis and Kumar [1999] has investigated stability of Ti, Zr, Nb or Ta borides in cast Fe_3Al alloys containing a large (10 vol%) of diborides. TiB_2 and ZrB_2 were shown highly resistant to coarsening. Nb and Ta additions lead to formation of multiple phases. Krein et al [2007] have reported strengthening of Fe_3Al-based alloys by borides without significant loss in ductility in VIM ingots. Ti, Hf or Zr (~0.5at%) additions to alloys containing 1at%B led to formation their diborides and improvement in creep properties [Gupta 2010]. V and W do not form borides but solid solution strengthening was observed. Elongations of up to 150% at 1173K have been reported by Malek et al [2002] in VIM cast and worked Fe-30at%Al-5at%Cr alloy modified by TiB_2. It has also been observed that B activated the sintering process and in consequence increases the densification thus improved the mechanical properties [Karwan-Baczewska 2001].

Bordeau [1987] has reported P/M processing of Fe_3Al alloys with TiB_2 dispersoids with tensile elongations of 11% with yield strength approaching 1000MPa. The Fe_3Al-2wt%TiB_2 powder was produced by rapid solidification rate process and consolidated into plates. The alloy exhibited grain growth at temperatures up to 1273K and a fine dispersion of TiB_2 retained in the alloy. Morris and Morris [1991] have reported properties of rapidly solidified Fe-35at%Al-0.2-5mol%ZrB_2 alloy ribbons prepared by melt spinning. Though the presence of ZrB_2 resulted in improvement in strength and even improved ductility in alloys with low (up to 0.2mol%) dispersoid content, the distribution of dispersoids was non-uniform and with most of them being in intercellular regions. Rapid solidification leads to finer (submicron) dispersoid size.

Fe_3Al based composites containing up to 25vol% prepared from mechanical alloying of elemental powders followed by pulse discharge sintering [Park 2006]. Tensile strength of 400-900MPa and elongations of 4-12% were obtained. Presence of pores may adversely affect mechanical properties. Obara, Kudoh and Matsuura [2008] have reported properties of FeAl-

TiB_2 composites prepared from reactive synthesis of Fe, Ti, Al and B powders using a pseudo HIP process. Use of pressure during synthesis leads to reduction in porosity and improvement in ductility. Preheating of powders in vacuum helps in reducing the pore volume fraction as well as the TiB_2 dispersoid size. However a coarse (1-7 μm) dispersoid size was obtained.

Thus composites containing borides have been prepared by ingot and powder processing routes. A number of stable refractory metal diborides have been used to strengthen iron aluminides. These are resistant to coarsening and also prevent grain coarsening. Their addition does not lead to significant deterioration in ductility. A possible explanation may be that presence of boron may lead to improved ductility in iron alumindes or steel [Karwan-Baczewska 2001]. It may also improve resistance to environmental embrittlement [Stoloff and Liu, 1994].

However, additions of TiB_2 or ZrB_2 powders to prealloyed iron aluminide powders have not proved very successful due to limited solubility of borides in iron aluminides. This leads to debonding at boride/aluminide interfaces even in compositions processed by liquid phase sintering thus limiting their potential as structural materials [Schniebel 1999, Subramanian 1997c, Schniebel 1997].

2.6.2.3 Carbide reinforced composites

These constitute the most investigated of iron aluminide composites and also the most promising of the composites. Their low cost is an obvious advantage: most low cost sources of iron (such as steel scrap) contain carbon. Unlike iron boride which dissolves in the iron aluminide matrix at elevated temperatures [Krein 2007], Fe-Al-C system contains a stable $Fe_3AlC0_{.5}$ carbide which has a preovskite structure [Palm and Inden 1995]. This carbide is stable in alloys with low Al-contents (<37at%Al). At higher Al-contents (Fig. 2.9) graphite is more stable and thus only Fe_3Al based alloys can be strengthened by the perovskite carbide. Alloy carbides such as TiC and WC can be used in FeAl as well as Fe_3Al based composites.

2.6.3 Composites containing other dispersoids

Morris et al [2004] have examined creep of Fe_3Al alloys and have concluded that highest creep resistance is obtained in dispersion strengthened alloys. These alloys exhibit values of stress exponents between 5 and 10. Alloys containing various dispersoids including those discussed in previous sections were analysed. The alloys containing dispersoids such as Laves phases or Mo_3Al are too brittle to be of practical use [Falat 2005, Eumann 2004].

Similarly alloys strengthened by Fe-Zr intermetallic exhibit very high good creep properties when tested in compression but the room temperature ductility could be measured only by three point bend test [Morris 2007, Morris 2006]. Thus further optimization of alloy properties is needed. Recently carbon nanotubes have also been used to strengthen iron aluminides but the work is only preliminary and further evaluation is required [Pang 2010].

2.7 Preparation of iron aluminide based composites

2.7.1 Composites prepared by reaction synthesis

Inoue et al [1998] have also studied Al_2O_3 powder (0.4 μm) additions of up to 0.2 volume fraction to Fe-40at%Al. The results were similar to those for fibre reinforced composites. Also flexural strength of composites increases while fracture toughness decreases with increasing volume fraction of dispersoids. However the flexural fracture strength for fibre reinforced composites was more than that of the particulate composite due to load bearing by the fibres.

Wright, Anderson and Wright [1998] have studied Fe-28at%Al-5at%Cr dispersed with 2.5vol% Al_2O_3 prepared by reaction synthesis from elemental Fe, Al and Cr powders. The alumina in the alloy was formed during synthesis. Careful control of extrusion parameters and heat treatment schedule led to secondary recrystallization with coarse final grain size of 25mm. Oxide in the alloy formed during reaction synthesis yielded significant improvement in creep life and minimum creep rate. It was argued that alumina particles of finer than 50nm or coarser than 500nm were not effective in pinning of dislocations during creep. This is also supported by findings of Peng et al [2006] that nano alumina (<100 nm) was ineffective in strengthening the Fe-28at%Al alloy processed by reaction synthesis of elemental Fe and Al powders mixed with 16 vol% nano alumina. Here the problem was compounded by severe agglomeration of alumina powders.

Reaction synthesis of elemental powders mixed with 10wt%Al_2O_3 (~16 vol%) powder (1μm) was carried out using consolidation by Ceracon process [Rabin et al 1992]. The powders pre-reacted prior to consolidation yield more homogeneous performs than those prepared by in situ reaction during consolidation. Also reaction processed material exhibited higher strength than that obtained from prealloyed powders because of finer microstructures obtained in reaction synthesis route.

2.7.2 Composites formed by in-situ displacement reactions

Alumina can be formed by displacement of Fe from Fe_2O_3 by Al. This principle has been used to form iron aluminide composites strengthened by alumina. Fe-40at%Al powder was mixed with fine (1-5 μm) Fe_2O_3 powder by Subramanian et al [1998a]. By varying the powder ratios two composites Fe-32at%Al with 7 vol% Al_2O_3 and Fe-20at%Al with 20 vol% Al_2O_3 were produced. This was accomplished by hot pressing the powders at 1573K. Though the strength increased substantially fracture toughness was lowered by presence of alumina.

Fe_2O_3 powder may be mixed with elemental Al and Fe instead of prealloyed powder [Khodaei 2008]. Ball milling of powder mix led to mechanical alloying. A nanocrystalline Fe_3Al-30vol%Al_2O_3 mix was obtained. Rafiei et al [2010] have used this elemental processing route with TiO_2 powder instead of Fe_2O_3 powder. Here TiO_2 is reduced by Al and an $(Fe, Ti)_3Al$ mix with Al_2O_3 was obtained. Displacement reactions can be used for producing intermetallic matrix composites (IMC) directly from haematite by milling the iron ore and Al powder in appropriate proportions in a ball mill [Oleszak and Krasnovski, 2001]. Processing of composite powders produced after the displacement reactions has received very limited attention.

2.7.3 Composites prepared by mechanical alloying

Oxide dispersion strengthened (ODS) alloys have been produced by mechanical alloying of elemental Fe and Al powders. FeAl based composites wherein the oxide was produced in situ [Wolski 1996]. A stable dispersion of $FeAl_2O_4$ oxide (15nm) in a refined FeAl matrix was obtained using a low temperature (1323K) for sintering to prevent coarsening of microstructure. A large (~15vol%) volume of oxide was obtained by using starting materials with high oxygen content. Mechanical alloying (MA) route yielded stronger alloys than similar composition processed by reaction synthesis route though the alloys showed poor ductility.

Most of the studies on oxide dispersion strengthened (ODS) alloys have used prealloyed FeAl-based powder with a dispersion of 1-2 vol% of yttria to achieve significant strengthening. The main limitation appears to be low tensile elongation (1%) in these alloys. Also yttria may be prone to coarsening due to reaction with the FeAl matrix to form spinel Y-Al-Fe oxides [Morris and Gunther, 1996]. Schniebel et al [1992] have processed Fe-40at%Al alloy with dispersion of 2vol% of yttria (50 nm). Though yields after mechanical alloying were low (no process control agent appears to have been used) hot isostatic pressing of MA powders resulted in attractive creep properties. A high creep exponent of 25 was obtained. Morris and co-

workers have reported a series of studies on Fe-40at%Al-1vol% yttria ODS processed by extrusion/rolling. Though a uniform dispersion of second phase particles [Karwan-Baczewska 2013] was obtained the MA alloy exhibited fine as well as coarse (50 to 200nm) particles [Morris and Gunther 1996]. A later study [Garcia 2003] reported on coarsening of yttria, even when recrystallization of matrix does not occur, by diffusion of yttria through the matrix. Microstructural coarsening can occur both by particle coarsening and by grain growth at elevated temperatures. In an analysis of strengthening mechanisms in the alloy the authors [Munoz-Morris 2002] concluded that grain size plays a limited role due to the high strength of the matrix. However, fine yttria dispersoids contribute strongly to the strength by pinning the grain boundaries. Optimization of composition and processing conditions led to improved room temperature ductility (up to 4%). The material showed excellent creep properties, claimed to be best for a comparable iron aluminide [Morris 2008].

2.7.4 Composites produced using melt route

Most of the work reported so far is on alloyed processed using melt route. Melting of iron aluminides is generally carried out in controlled atmosphere. However carbon containing alloys have been processed by a route comprising air induction melting (AIM) followed by electroslag remelting (ESR) [Baligidad 1994, Baligidad 1996] or even by air induction melting under slag cover [Baligidad 2010, Baligidad 1998a]. Use of slag cover leads to lower sulphur content in the alloy. Electroslag remelted alloys also have lower inclusion content as well as finer precipitate and inclusion size.

Presence of carbon was found to be essential for processing of these alloys in air as alloys with low (<0.06wt%) carbon alloys exhibited cracking during forging [Baligidad 1996b]. Further the high carbon alloys exhibited excellent machinability and could be turned on a lathe. Both these factors were attributed to a reduced susceptibility to hydrogen due to the presence of carbon in the alloys [Baligidad 1996a; 1996b; 1996c and 1997b]. This was initially believed to be due to trapment of hydrogen by carbides. It was later shown that the improved machinability is exhibited in both Fe_3Al and FeAl based alloys containing carbon [Prakash and Sauthoff 2001]. The alloys were machinable irrespective of whether the alloy contained peroskite carbide, alloy carbides or graphite. This led the authors to conclude that it is the interstitial carbon which is responsible for reduced susceptibility to hydrogen embrittlement. It was argued that presence of interstitial carbon leads to increased blocking of interstitial sites and thus slows hydrogen diffusion through the iron aluminide lattice. This in turn can lead to reduced

susceptibility to hydrogen embrittlement. It must be emphasized that the alloys remain susceptible to hydrogen embrittlement as evidenced by increase in tensile ductility when tested in vacuum [Sauthoff and Prakash 2001]. Prakash et al [2007] and Parvathavarthini et al [2002] have later shown that presence of carbon reduces the permeability and diffusivity of carbon in both Fe_3Al as well as FeAl alloys. This may lead to reduced susceptibility to hydrogen embrittlement.

The improved machinability in these alloys is a technological breakthrough as intermetallics generally exhibit poor machinability and this can greatly increase processing costs. Further the use of electrslag remelting leads to improved room temperature ductility when compared to those reported for induction melted [Prakash and Sauthoff 2001, Zhu 2002] alloys.

2.8 Fe_3Al based composites

Solubility of carbon in Fe_3Al alloys is very limited (<0.05wt%) and most of the carbon is present as carbide precipitates. If no strong carbide former (such as Ti, Cr, W, Mo) is added the carbide present is $Fe_3AlC_{0.5}$ perovskite carbide. Thus the matrix structure comprises of Fe_3Al matrix and the $Fe_3AlC_{0.5}$ perovskite carbide precipitates. Thus both the matrix and the precipitate have similar Fe and Al contents and mostly carbon diffusion is required for formation of the carbide. Further in the perovskite carbide a carbon atom locks up ~8 metal atoms. A rough calculation reveals that the carbide present is about twice that of cementite present in steels with comparable carbon contents. The carbide volume fraction increases with carbon content and at 1.1wt%C there is about 40 vol% carbide in the alloy [Baligidad 1998b]. For this reason the alloys reported here are limited to those with 1.1wt%C. At higher Al-contents the perovskite carbide is the primary phase [Sanders 1997a; Sanders 1997b]. These alloys are very brittle and of little practical use.

The peroskite carbides are stable at elevated temperatures and significantly improve tensile and creep properties of Fe_3Al based alloys [Baligidad 1997a; Baligidad 1996a; 1997a]. The alloys with perovskite carbides exhibit good workability [Baligidad 1996a]. However this also leads to recrystallization of microstructure. Thus the creep and stress rupture properties deteriorate when compared to cast alloys with coarser microstructure. For this reason it is recommended that the cast composites should not be hot worked if creep resistance is the primary requirement. At 1.1wt%Al the structure comprises of ~40 vol% of perovskite carbide with alternate lamellae of aluminide matrix and perovskite carbide [Baligidad 1998a, Baligidad

1998c]. The duplex Fe_3Al-$Fe_3AlC_{0.5}$ structure leads to a large improvement in creep and stress rupture properties [Baligidad 1997b]. The strength deteriorates above 923K as the matrix may lose strength at higher temperatures.

The carbide morphology (globular or platelike) depends on the carbon content. Alloys with Fe_3Al-$Fe_3AlC_{0.5}$ eutectic structure have been reported by Schnieder et al (2005). As already discussed, at about 1.1wt%C the alloy exhibits alternate plates of aluminde and carbide [Baligidad 1997a; Baligidad 1997b; Baligidad 1997c]. This is typical of a Fe_3Al-$Fe_3AlC_{0.5}$ eutectic. These are also the alloys with best creep resistance.

The alloy properties are critically dependant on carbide volume fraction [Baligidad 1998b; Baligidad 1999, Prakash 2008]. In particular, hardness and creep resistance increase with increasing carbide content. Addition of strong carbide formers such as Ti, Cr and Mo leads to formation of alloy carbides. This results in a reduction in carbide volume fraction [Prakash and Sauthoff 2001]. It appears that the perovskite carbide is a better choice than alloy carbides for Fe_3Al based alloys as it leads to alloys with larger volume fraction of carbides for a given carbon-content. Compositions with alloy carbides also exhibit low room temperature ductility [Prakash and Sauthoff 2001; Falat 2005].

Schnieder et al [2005] have argued that the perovskite carbide is prone to coarsening at elevated temperatures and this may limit its effectiveness for strengthening at elevated temperatures. The heat treatment given to the alloys was homogenisation at 1473K for 24 hours. The application temperature of alloys is up to 973K as the matrix strength may start decreasing rapidly with temperature and the precipitate coarsening is unlikely to be a major factor.

No improvement in mechanical properties could be achieved by making quaternary additions of Ni, Mn, Cr and Ti to carbon containing Fe_3Al-based alloys [Baligidad and Radhakrishna 2000]. On Mo addition the alloy became too brittle to be machined and only compression tests could be carried out [Baligidad 2001]. This further supports the observation that such alloying additions to carbon containing Fe_3Al-based alloys are unnecessary or indeed harmful.

Ball on disc wear tests have showed that the presence of pervoskite carbides significantly reduce coffecient of friction and wear rate in Fe_3Al-based alloys [Zhu 2002]. However at elevated temperatures (573K and 773K) the wear properties were found to be degraded on carbon addition.

2.9 FeAl based composites

At Al-contents higher than 37at%Al the graphite phase becomes stable and thus FeAl based compositions contain graphite. This leads to loss in strength and creep properties [Radhakrishna 2001, Prakash and Sauthoff 2001]. A possible solution may be to use small additions (0.27wt%) of carbon to avoid graphite formation [Radhakrishna 2005]. However the limitation is that the amount of carbides that can form is limited and this may limit the benefits from dispersion strengthening. Sundar and Deevi [2003] have reported structure and properties of Fe24wt%Al alloys containing 0.05 to 2 wt%C. Addition of carbon resulted in increase in tensile strength and creep properties without affecting the ductility. The creep properties were better than those reported for several commercial Fe and Ni based alloys. Also the room temperature fracture mode changed from intergranular to transgranular cleavage. This was attributed to improved resistance to hydrogen embrittlement on adding carbon. Similarly Pang and Kumar [1998] have reported that fracture is delayed in Fe-40at%Al alloy containing 0.6at%C. This was also attributed to improved resistance to hydrogen embrittlement due to trapment hydrogen by carbides. However as was later shown, hydrogen trapment is unlikely by carbides but its mobility is reduced in presence of carbon [Prakash 2007] which may lead to a reduced susceptibility to hydrogen embrittlement.

To prevent graphite formation the FeAl-based intermetallics may be alloyed with strong carbide formers such as Ti, Cr or Mo. These are important substitutional alloying additions for iron aluminides [Prakash 1991]. In presence of carbon these additions form alloy carbides and their role is essentially to provide dispersion strengthening. Very few FeAl-based alloys strengthened by alloy carbides have been processed by melt route. Zhang, Sundar and Deevi [2004] have reported properties of FeAl-based Fe-40at%Al alloy with 0.5at%Ti and 0.2at%C prepared by arc melting followed by extrusion. The addition of carbon led to improvement in minimum creep rate. However the alloys showed a very low creep strain of about 0.3%. This was attributed to formation of grain boundary cracks in the material.

2.10 Morphology and size dependency of particles

One of the most important aspects characterizing particle containing materials is their good creep strength at intermediate and high temperatures and it is widely accepted that this is due to the attractive dislocation-particle interactions that pins dislocations and inhibits their movement in the matrix. The consequence is that dispersion-strengthened materials exhibit much lower creep rates together with high values of stress exponents and activation energies

compared to those measured from particle-free materials. To rationalize the creep behaviour of dispersion-strengthened alloys different approaches are used. It can be postulated that the size and morphology of second phase particles influence the mechanical properties of the materials. Non-equilibrium processing including chill block melt spinning, atomization, mechanical alloying and physical vapour deposition has been used to produce nano and microcrystalline materials including laminates [Tsakiropoulos 2004; Shao 2000].

2.10.1 Coarse (micron) size reinforcement particles

For FeAl matrices, WC, TiC, ZrB_2, and TiB_2 are suitable choices [Schneibel 1997; Subramanian 1996; Subramanian 1997b; Schneibei 1997; Subramanian 1997c]. In all these cases, the ceramic particulates are thermodynamically stable with respect to the matrix, even when it is in the liquid state. For ceramic volume fractions ranging from about 30 to 60 vol. %, liquid phase sintering above the melting point of FeAl is a suitable processing technique [Schneibel 1997]. The improvement of high-temperature creep resistance by casting in large volume fractions of second phase particles of a variety of phases such as carbides, borides, and various complex intermetallic phases [Risanti 2011; Eumann 2004; Palm 2004; Falat 2005; Schneider 2005; Krein 2007]. While these studies have been successful in achieving good strength, from room temperature up to very high temperatures, the ductility at low temperatures becomes very small, which can probably be related to the coarse networks of brittle phases present after casting. The hard carbide particles in the Fe–Al matrix are also responsible for an improvement of tribological (friction) properties such as wear and erosion resistance [Alman 2001].

2.10.2 Nano size reinforcement particles

Nanocrystalline materials are potentially attractive for many applications since the reduction of the grain size to the nanometer scale can improve their physical and mechanical properties [Gleiter 1992; Suryanarayana 1992; Roy 2009]. For example, Krasnowski et al have demonstrated that the nanocrystalline FeAl intermetallic produced by mechanical alloying followed by hot-pressing consolidation possesses relatively high microhardness [Krasnowski 2007]. Rapid solidification by melt spinning method has been employed to obtained the very fine grain size in Ni-Al-X (X=Fe, Mn, Cr and Si) [Morales 2002] or steel [Lesch 2007]. Further, the refinement of second phase particles has received much less attention, but can be equally interesting for bringing about changes to mechanical behaviour of the alloys. Severe

plastic deformation has been extensively investigated over the past decade or so, generally with the objective of refining the grain size of the material investigated. Various studies of severe plastic deformation carried out on precipitation and dispersion hardening alloys [Gutierrez-Urrutia 2005; Gutierrez-Urrutia 2007; Muñoz-Morris 2011] have shown that finer precipitates are often broken by such deformation into very fine fragments, and particle shape or size as well as the inherent mechanical properties of the second phase may be important in determining behavior. Fe–50Al–30%TiC and Fe–40Al–50%TiC nanocomposites prepared by mechanical alloying and hot-pressing consolidation show high microhardness values of 12.6 and 15.7 GPa, respectively [Krasnowski 2002; Krasnowski 2007]. The microhardness of the Fe–40Al–50%TiC composite produced by liquid-phase reaction is 9.2 GPa [Schneibel 1997].

2.11 Wear behaviour of iron aluminides

Iron aluminides such as DO_3 type Fe_3Al and B2 type FeAl because of their high strength/density ratio, remarkable corrosion resistance and low raw material cost have attracted great attention as potential structural materials in industrial applications [Stoloff 1998]. A lot of research efforts have been studied mainly on mechanical and physical properties and corrosion resistance. At the same time, high elastic modulus, the high hardness, and high work hardening ability of iron aluminides make them a suitable structural material for a variety of anti-wear applications [Alman 2001; Maupin 1993; Yang 2004; Guan 2004; Kim 1998]. Their excellent properties, however, suggest that they will be also promising as tribo-materials to be used in aggressive conditions. The iron–aluminides are particularly promising candidate for oxidizing and sulfidizing environments because of their excellent resistance to environmental degradation [Welsch 1996]. Taking into account these advantages of the intermetallic alloys, various studies based on their application to tribology have been performed [Zhu 2002; Guan 2002; Pauschitz 2008]. It has been found that Fe–Al alloys showed good wear properties and the wear resistance was significantly improved by the addition of high amount of carbon [Yang 2005]. Kim et al. [Kim 1998] studied the room temperature dry sliding wear behavior of iron aluminides of various composition ratios. They investigated that the wear rate of the aluminides increased with the increase in sliding speed and applied load and the wear resistance decreased with the increase in aluminum contents. Hawk et al. [Hawk 1995] and Maupin et al. [Maupin 1993] reported that the addition of Ti to Fe_3Al was very effective in improving the anti-abrasive properties. It is especially important from the practical point of view to clarify the effects of applied load, sliding speed and temperature on the tribological properties such as wear rate and the coefficient of friction. Only these are the main works concerning the

tribology of Fe–Al alloys as far as the authors know and more extensive works are highly desired for applying these alloys in the tribological fields.

The high strength, hardness and work hardening ability also make them be able to perform well in a variety of wear environments, such as wear and oxidation resistant parts in steelmaking industry [Krasnowski 2007; Liu 1998; Yang 2004; Mosbah 2005]. Furthermore, these materials are competitive with most conventional ferrous alloys in terms of economic cost of raw materials, because they compose primarily of abundant and inexpensive elements i.e. iron and aluminum. Thus, iron aluminides have been considered for a variety of wear applications [Ji 2007; D'Angelo 2009; Subramanian 1997b; Tu 1998; Alman 2001]. However, low room temperature ductility and poor creep resistance limits the industrial applications of iron aluminides [Deevi 1996]. Some studies have indicated that coating structural materials with iron aluminides using thermal spraying would not only solve the problems met in the fabrication of them into useful shapes, but also allow the effective use of their environment and corrosion resistant features [Xiao 2006; Liu 1998; Senderowski 2010; Musalek 2010]. However, the oxidation of the feedstock materials occurs during the conventional thermal spraying in which the feedstock undergoes a fully or partially melting state [Senderowski 2010; Musalek 2010], which would change the compositions and microstructure of the feedstock and consequently degrade the properties of the deposits.

It has been reported that the addition of Ti to Fe_3Al was found to reduce both the coefficient of friction and wear rate significantly [Guan 2004; Maupin 1993]. The effects of B2 or DO_3 structures on wear behavior of Fe_3Al have been studied under dry-sliding and wet abrasive wear conditions [Tu 1997] and the wear rate of the aluminides found to be increased with an increase in applied load and sliding speed [Sharma 2004; Kim 1998]. The wear resistance of the material is improved by either introduction of hard phase particles or coating on the material [Chen 2003; Pant 2005; Kambakas 2006]. Fe_3Al alloys prepared by mechanical alloying with subsequent plasma activated sintering resulting fine microstructure and precipitation of hard $Fe_3AlC_{0.5}$ and owing in enhancement of wear resistance and hardness of the alloy [Wang 2010]. Tribological properties of Fe_3Al–$Fe_3AlC_{0.5}$ composites under dry-sliding at ambient condition were studied, and results showed that the composite with 60 wt.% had the best tribological properties [Yang 2005].

Yang et al. [Yang 2004] compared the dry sliding wear behavior of FeAl containing a small volume fraction of $Fe_3AlC_{0.5}$ flakes, which were tens of microns long, by oscillating disks of the material of interest against a AISI52100 bearing steel ball at a variety of loads at room

temperature in air with 56% relative humidity. They found that the FeAl showed lower wear rates at all loads examined. They suggested that oxide layer formation contributed to the reduced wear rate and that the wear mechanism changed from micro fracturing to surface fatigue as the sliding speed was increased [Yang 2004]. Zhu et al. [Guan 2002] also examined the effects of carbon on the wear of extruded Fe-40Al, also using ball (alumina) on disk wear tests, but at several temperatures, i.e. room temperature, 573K and 773K. For the room temperature tests, they compared the wear rates to that of an unspecified cast iron. In this case, X-ray diffraction was used to show that the carbon was present as graphite and not as $Fe_3AlC_{0.5}$. They showed that at room temperature the wear rates of the Fe-40Al decreased with the addition of 0.5 and 1 wt.% C, but that there was a much more dramatic decrease when 2 wt.% C was present even though the hardness decreased with increasing amounts of carbon. Even though the 2 wt.% C addition decreased the wear rates of Fe-40Al, the wear rate was still greater than that of the cast iron at room temperature. The wear rate of the undoped Fe-40Al decreased with increasing temperature up to 773 K, while that of the 1 wt.% C alloy showed an increase at 573 K (but not at 773 K) and that of the 2 wt.% C alloy showed large increases at both 573 K and 773 K. The result was that carbon additions decreased the wear rate at room temperature, which the authors attributed to the observed decrease in friction from the lubricating effect of the graphite. However, the wear rate increased at the higher temperatures, even though the carbon additions had little effect on the tensile properties as a function of temperature. This effect is likely because carbon needs water vapor in order to provide low friction [Guan 2002] and such water vapor would not be present at high temperature.

However, low tensile ductility and brittle fracture are the major disadvantages hindering their industrial applications [Liu 1989; McKamey 1990]. Thus, FeAl intermetallic matrix composites containing secondary reinforcing phase were proposed recently for high temperature structural applications [Subramanian 1998; Chen 2003; Krasnowski 2002; Subramanian 1997; Chen 2004]. Among the reinforcing phases, TiC ceramic particles are expected to be an excellent reinforcement due to their outstanding combination of high hardness (20–32 GPa), low density (4.93 g cm^{-3}) and excellent high temperature stability (3065^{o}C) [Maerky 1996] As reported by Chen and Wang, [Chen 2003; Chen 2004] both the mixed metallic–covalent atomic bonds of the FeAl intermetallic alloy and the high hardness of TiC could result in excellent abrasive and adhesive wear resistance of an FeAl/TiC composite during contacting with a sliding metallic counterpart. Although some studies have been carried out to utilize TiC as reinforcement in iron aluminides, for example TiC reinforced iron aluminide matrix composites produced by melt infiltration processing, [Subramanian 1997] hot

pressing consolidation [Krasnowski 2002] and laser cladding, [Chen 2003; Chen 2004] few attempts have been so far made on TiC reinforced FeAl intermetallic matrix composite bulk parts by selective laser melting (SLM).

Studies have been carried out to investigate the influence of the addition of carbon, or secondary hard particles such as WC, TiB_2 and TiC on the wear performance of bulk iron aluminide material [Guan 2002; Alman 2001]. Addition of TiC hard particle can enhance dramatically hardness and high-temperature creep resistance of Fe_3Al intermetallics, and are also expected to improve wear resistance, and also TiC reinforced Fe_3Al intermetallic composites have been produced by hot-pressing, pressureless melt-infiltration and pulse discharge sintering [Ko 2002; Subramanian 1996; Subramanian 1997; Ko 1999]. Some investigations have demonstrated that ceramic particles can enhance wear resistance of aluminium alloy matrix composites [Jasim 1987; Kanth 1990; Roy 1992]. However, in applications related to wear, loads are compressive in nature, therefore, tensile ductility is not as critical a mechanical property parameter as hardness, strength, and work hardening ability [Sharma 2007]. Consequently, Fe_3Al alloy have also been considered the material for a series of anti-wear applications to substitute for conventional wear resistance cobalt-based alloys and iron-based alloys containing chromium and manganese [Yang 2004]. FeAl intermetallics, produced by combustion synthesis, exhibit better dry-sliding wear resistance than AISI 52100 steel [Yang 2004].

The wear behavior of both $D0_3$-type Fe_3Al and B2-type FeAl alloys has been investigated, and known that their differences in wear resistance are insignificant [Kim 1998; Maupin 1993; Sharma 2007]. The abrasive wear resistance of Fe_3Al alloy is comparable to that of the AISI1060 carbon steel and the SUS304 stainless steel [Blickensderfer 1988; Tylczak 1978]. As mentioned above, Fe_3Al based composites reinforced by hard particles seem to exhibit good wear resistance [Yang 2004; Alan 2001]. However, the studies on the wear properties of the Fe_3Al composites have been scarce.

Intermetallic composites with hard particle reinforcements are also attractive for wear applications in severe, i.e. chemically aggressive, environments. In chemically aggressive environments, the utilization of alloyed binders for composites carbide, instead of pure metallic ones, may mitigate damage during wear [Wang 2010]. For these situations, alloys based on aluminide compounds maybe desirable, as many of these compounds form an impervious and protective oxide layer when exposed to oxidizing, sulfidizing and carburizing environments [Welsch 1996]. Further, the high hardness, strength, and work hardening ability of these

compounds allow them to perform well in a variety of other wear environments, such pure abrasion [Zum Gahr 1987]. Based partly on this combination of attractive properties, it has been recognized that aluminide-based alloys could serve as alternative material for wear applications. Multiphase materials and composites are often used in situations where abrasive wear resistance is important. These materials typically consist of a matrix containing one to several reinforcing phases, usually in the form of particles, whiskers, fibers or fabric weaves. In the majority of cases, the reinforcing phase possesses a higher hardness, strength, or elastic modulus than the matrix, although it has been shown that the fracture toughness of brittle matrix composites with a ductile reinforcement can be increased, thereby improving the wear resistance of the composite [Zum Gahr 1987; Axe´n 1993]. Ideally, a composite combines the best of the individual component properties and suppresses the worst [Axe´n 1994]. Thus, a material with relatively poor wear resistance can be improved with the addition of a suitable reinforcing phase.

Iron aluminides with carbide have been prepared by a variety of methods including melting and casting, powder processing (hot pressing, sintering) [Baligidad 1998b; Sundar 1998; Deevi 1997; Subramanian 1998; Krasnowski 2002]. Melting methods include air induction melting (AIM), vacuum induction melting (VIM), vacuum arc remelting (VAR) and electroslag remelting (ESR). These need above 1500◦C external temperature. Powder processing route utilizes atomized, carbonyl or rapidly solidified pre alloyed powder as starting materials and alloying is carried out either by mechanical alloying or reaction synthesis or by consolidation through hot pressing. This process also involves many processing steps and considerable expense.

Mosbah et al [Mosbah 2005] studied the abrasive wear of Fe-40Al containing WC using pin-on-drum wear tests, while Jozwiak and Karczewski [Józwiak 2009] examined the abrasive wear of Fe-50Al containing Al_2O_3 particles using pin-on-disc wear tests. However, in both cases there were no comparable tests on binary FeAl and so the effects of the ceramic additions are unclear. By the addition of hard phase particles such as $Fe_3AlC_{0.5}$, TiC, Al_2O_3, TiB_2 and so on [Yang 2005; Krasnowski 2002; Gao 2006; Sun 2001; Kok 2007; Herbert 2008; Herbert 2006], the hardness of the Fe_3Al or other alloys was significantly improved, as was the wear resistance. High wear resistance of particulate-reinforced Fe_3Al intermetallic matrix composites is attributed to the ceramic particle protecting the metal matrix from wear [Kok 2007; Jasim 1987]. However, the improvement in hardness was generally accompanied by a reduction of toughness.

Chapter 3
Formulation of Problem

This chapter describes the formulation of the problem and gap in the reported literature on B2 iron aluminides. Carbon addition to B2 iron aluminides has been unsuccessful in the past due to precipitation of graphite. This may be avoided by adding carbide forming elements. Structure and properties of these carbon containing FeAl alloys is investigated.

3.1. Introduction

Iron aluminides because of their excellent oxidation resistance, high strength to weight ratio, low density and low material costs are promising material for high temperature applications. It is seen from the literature that iron aluminides suffer serious setback due to limited room temperature ductility and degradation in the strength above 550^{o}C. The susceptibility of iron aluminides to hydrogen embrittlement is the major cause of the low ductility at room temperature. Carbon addition to Fe-Al alloys is found to be suitable for the reduction in the environmental embrittlement. It also results in improvement in the strength due to carbide formation in Fe_3Al based alloys. Among iron aluminides, FeAl based alloys have advantage as structural material in high temperature application due to high oxidation and corrosion resistance, low density (due to high Al-content) and phase stability. But, in FeAl based alloys, the carbon addition causes graphite precipitation. The graphite precipitation in FeAl based alloys limits their role in high temperature applications due to the fall in strength.

3.2. Addition of carbon

It is now realized that carbon addition far from being harmful may in fact be beneficial for iron aluminides. This realization has come only in the last decade. The carbon containing alloys are still being developed. These alloys cover a large composition range and exhibit a variety of microstructures depending upon the concentration of Al. It is important to evaluate the influence of carbon addition and understand the mechanisms leading to improvement in the mechanical properties. It is observed that Al-content, type of carbide, carbide volume fraction, distribution and the process conditions all influence the alloy properties.

Addition of carbon to iron aluminides leads to a significant reduction in processing costs. The presence of small amount of carbon (>0.2at %) in the alloy allows use of low cost processing techniques such as arc melting for casting. Steel scrap is the cheapest sources of iron

containing carbon. These have been used as source materials for melting carbon containing alloys. This may significantly reduce the overall production costs. The development of low cost melting procedures such as air induction melting which employ cheaper raw materials such as steel scrap and commercial purity aluminium significantly reduces production costs for carbon containing alloys. Iron aluminides containing carbon have definite cost advantage and may be cheaper than the competing stainless steels and superalloys for applications where toughness is not a critical requirement.

It also significantly improves machinability by reducing mobility of hydrogen for higher carbon alloys. Because of the limited solubility (<0.1wt.% C) in these alloys most the carbon is present as perovskite type $Fe_3AlC_{0.5}$ phase referred to as k-phase. The presence of uniformly distributed carbide precipitates which may be act as hydrogen traps were cited to explain the improved machanability in carbon containing alloys. On the other hand, fine carbides help in inhibiting grain growth during hot working and further elevated temperature exposure. This contrasts with very poor machanibility due to surface cracking reported for low carbon compositions. In iron aluminides containing higher aluminium (>20wt% Al), carbon addition leads to precipitation of soft graphite thus reducing the strength.

3.3. Addition of quaternary alloying in Fe-Al-C

At Al-contents of~ 20wt% or more, graphite formation occurs in Fe-Al-C alloys and here the carbide formers may play an important role. The formation of graphite can be prevented at these Al-levels by appropriate alloying elements. The addition of quaternary carbide formers such as Ti, Zr etc. lead to precipitation of respective alloy carbides and avoid the graphite precipitation. The additional advantage of these alloying elements results in the formation of TiC and ZrC with no graphite flakes. The carbides are stable and compatible with iron aluminides even at elevated temperature.

3.4. Development of (B2) FeAl based alloys containing carbon

The addition of transition alloying elements such as Ti, Zr etc. in FeAl alloys containing carbon imply the precipitation of alloy carbides TiC and ZrC respectively. No graphite was observed in FeAl alloys containing carbon on Ti and Zr additions. The carbides present have been identified to be TiC and ZrC depending upon the carbide former. Ti addition may lead to formation of TiC in addition with $Fe_3AlC_{0.5.}$ A complex microstructure comprising of uneven distribution of TiC and $Fe_3AlC_{0.5}$ in FeAl matrix was observed in Ti containing FeAl. This was

attributed to a eutectic reaction between the two phases. The Zr containing alloys FeAl based alloy, in addition to ZrC in the grain also showed precipitation of ternary intermetallic Laves phase $Zr(FeAl)_2$.

3.5. Objectives of the research work

1) To avoid the graphite precipitation in FeAl based alloys by adding of suitable carbide former elements such as Ti and Zr

2) To evaluate change in the microstructural features of FeAl based alloys on additions of different alloying elements.

3) Identifications of different phases using different characterization techniques such as XRD, FESEM and TEM.

4) To optimize the alloy compositions for improved mechanical properties.

5) To enhance the mechanical properties of FeAl based at high temperature above 550^{o}C through alloying additions without affecting the room temperature ductility.

6) To study the thermal expansion behavior of FeAl based alloys due to different reinforcing second phase particles.

7) Wear behaviour of FeAl based alloys has to be studied and correlate with the mechanical properties and microstructural features.

3.6. Planning of experimental work

The experimental details formulated are given in the form of flow chart (Fig. 3.1). FeAl based alloys containing carbon were produced by arc melting in argon atmosphere at Defense Metallurgical Research Laboratory (DMRL), Hyderabad. The samples were heat treated at 1000^{o}C for 24 h to homogenize and then furnace cooled. The samples for metallographical examination, mechanical testing and dry sliding testing were machined. The various compositions with different alloying additions were developed to correlate their microstructure, distribution of different carbides and mechanical properties. The specimens were characterized by using different techniques like optical microscope, X–ray diffraction, field emission scanning electron microscope (FESEM) equipped with EDAX and transmission electron

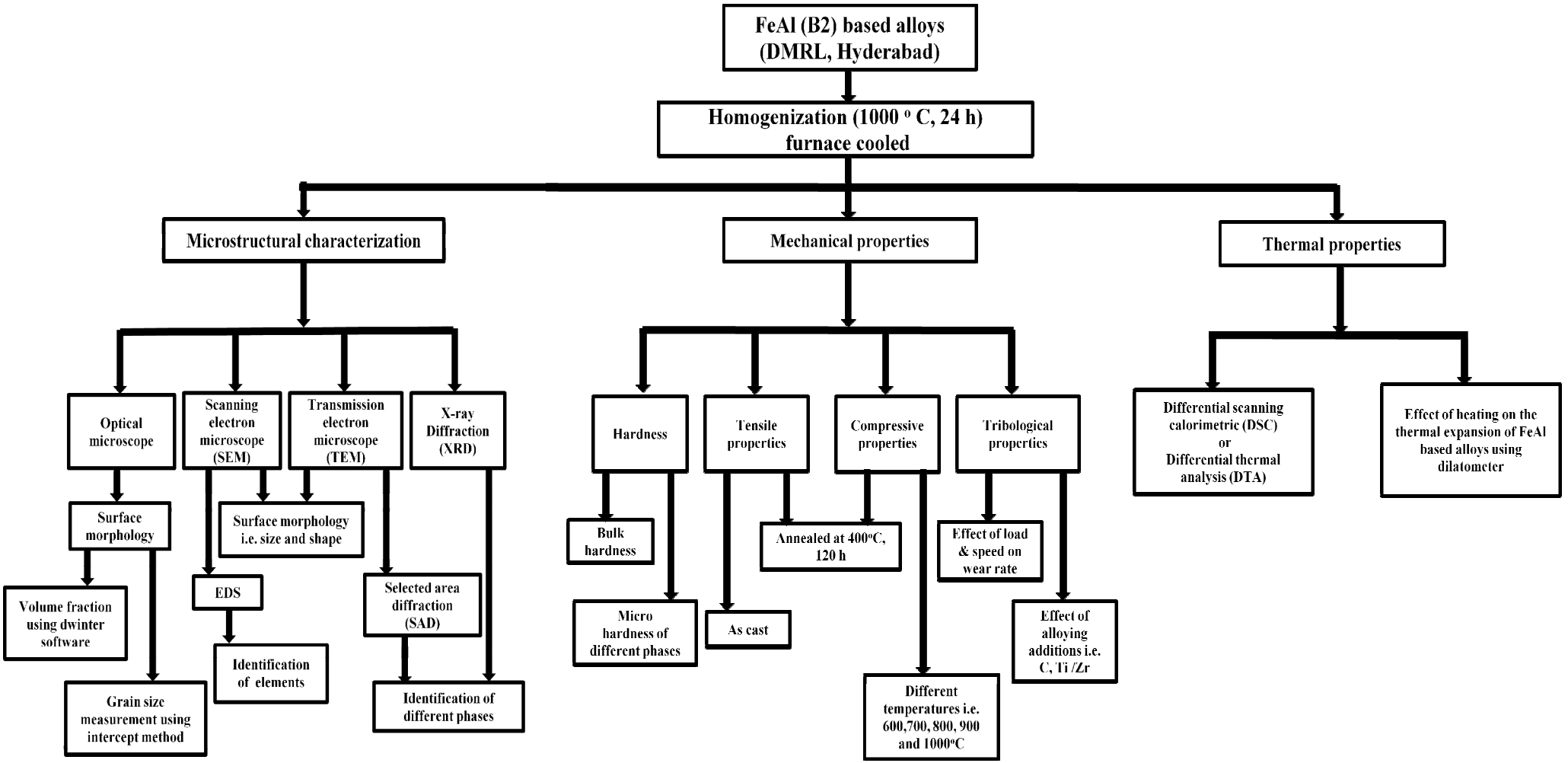

Fig. 3.1: Flow chart showing the design of experimental details.

microscope (TEM). The volume fraction of different carbides particles were also analyzed using Dwinter material plus software equipped with optical microscope.

The strength and hardness of various alloys at room and elevated temperatures have been measured. The dry sliding wear behavior of FeAl based alloys has also been investigated. The effects of various carbides and their distribution in the FeAl matrix on wear rate have been studied and correlate analyzing the wear tracks mechanisms. To assess the thermal stability of various carbide particles at high temperatures, the hardness of samples annealed at 900^{o}C for different timings and then water quenched were measured. The coefficient of thermal expansion of FeAl based alloys have also been determined to study the effect of different carbides using dilatometer.

Chapter 4
Experimental procedure

This chapter presents the experimental techniques and procedures employed for characterization and testing of the alloys. The procedures for analyzing the wear behaviour are also discussed.

4.1 Material selection

Table 4.1 shows the nominal compositions of various alloy investigated. These FeAl based alloys were prepared by arc melting in argon atmosphere, produce pancakes of 75 mm diameter and 10 mm thick at DMRL, Hyderabad. Form the pancakes, these samples were homogenized at 1000^{o}C for 24 h and then furnace cooled. After homogenization, these specimens were characterized by employing various characterization techniques. Al content of the alloys was carefully chosen to ensure a B2 structure with a low level of Al as ductility of B2 alloys decreases with increasing Al content. The Ti (or Zr) to carbon ratio was chosen to ensure that Ti added to more than enough to lock up the carbon added so that graphite does not form.

Table 4.1: Nominal composition of different alloy investigated.

	Compositions (wt. %)			
S. No.	**Al**	**C**	**Ti/Zr**	**Fe**
1	22.0	0.1	---	Balance
2	22.0	1.0	---	Balance
3	22.0	0.1	1.0 (Ti)	Balance
4	22.0	0.1	5.0 (Ti)	Balance
5	22.0	1.0	5.0 (Ti)	Balance
6	22.0	1.5	5.0 (Ti)	Balance
7	22.0	1.0	5.0 (Zr)	Balance

4.2 Microstructural analysis

4.2.1 Optical microscopy

The specimens for optical microscope were cold mounted with acrylic moulding powder, and then mechanically polished with emery paper down to 1500 grit and then with

alumina powder with 0.5 μm size. The specimens were etched with etchant composed of 33% HNO_3 + 33% CH_3COOH + 33% H_2O +1% HF by volume. The microstructure was observed using Leica DMI 5000M optical microscope equipped with digital imaging via computer system. The microscope was also equipped with Dewinter material plus software for measurement of the volume fraction of different carbides.

4.2.2 Field emission scanning electron microscope (FESEM)

The Field emission scanning electron microscope (FESEM) is one of the most versatile instruments (Fig. 4.1) available for the examination and analysis of the microstructure, morphology and chemical composition of second phase particles in the alloys. Field Emission Scanning Electron Microscope (FEI Quanta 200F, Made in Czech Republic) fitted with EDS Genesis software attachment to identify inclusions and elemental compositions of matrix and second phase particles was used in the present work. The samples used for analysis were prepared similarly as in prepared in the optical microscope. The worn out surface of specimens of different alloys after wear testing were also analyzed to understand the phenomenon of wear mechanism.

Fig. 4.1: Field emission scanning electron microscope (FESEM) equipped with EDS analyzer.

4.2.2.1 Energy dispersive spectroscopy (EDS) analysis

The elemental compositions of phases present were determined using EDS analysis. The EDS genesis software indicates the elemental compositions (weight %) present at point/area of interest. FE-SEM/EDS analysis of the specimens is reported in Chapter 5 and 7 of the present study.

4.2.3 Transmission electron microscope (TEM)

Transmission electron microscope (TEM) was used to characterize crystal structure and microstructure of the phases present in the samples of the alloy. The prepared samples were observed under 200 kV FEI TECNAI G2 (TEM) shown in Fig 4.2.

Fig. 4.2: TECNAI G2 Transmission electron microscope (TEM).

4.2.3.1 Sample preparation

Thin foils of 1.0mm thickness from the bulk specimens were cut using diamond cutter and cooling lubricant. While polishing the specimens, the care was taken not to bend the specimens. The specimens were subsequently ground with emery paper to less than 100 µm thickness. Then, the thin foils were punched to 3mm diameter discs with a punch. Struers twin jet polisher was used to conduct the electropolishing. The solution used for the electropolishing was composed of 20% perchloric acid and 80% methanol. Liquid nitrogen was added to

methanol to lower the temperature of the electrolyte. The polishing was performed at constant potential of 15 V with solution at -20^{o}C. The specimens were washed using methanol and then put into distilled water and collected into the mould.

4.2.3.2 Selected area electron diffraction (SAD) pattern

Selected area electron diffraction (SAD) is one of the most reliable methods to identify the unknown carbides. The proposed carbides were selected by using area aperture of the beam and corresponding diffraction was obtained. The indexing of the diffraction pattern confirmed the crystal structure of the carbide particles. Diffraction pattern from the matrix was also taken.

4.3 X-ray diffraction (XRD)

Small pieces of dimension 5x5x4 mm^3 (4 mm in thickness) were cut from as-cast and heat treated specimens and polished with upto 1500 grit emery paper followed by cloth polishing to minimize the distortion in the X-ray diffraction pattern. The polished specimen were subjected to X-ray diffraction using Model D8-Advance Bruker-axe, diffractometer (Fig. 4.3) fitted with goniometer with Cu-K_α radiation (λ_{Cu}=1.54 nm) and used to identify the different phases. The vertical θ-θ goniometer has range 0°-360° (2θ). The detector moves around the sample and measures the intensity and position of peaks which satisfy Bragg's law. An Expert High Score software which has inbuilt inorganic JCPDS (Joint Committee on Powder Diffraction Standards) was used to index the peaks of various phases present in the pattern.

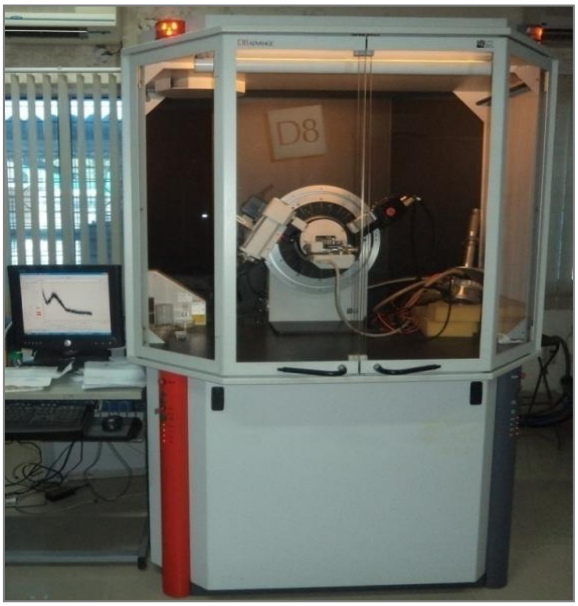

Fig. 4.3: D8-Advance Bruker-axe X-ray diffractometer.

4.4. Mechanical properties

4.4.1. Hardness measurements

4.4.1.1 Bulk hardness

A section from each specimen was cut and then polished by using different emery paper down to 1500 grit and then with alumina powder of 0.5 µm size. The bulk hardness was measured by using FEI-VM50PC Vickers hardness tester and performed according to ASTM E-92-82 procedures on the polished samples. The Vickers hardness tester working on the principle is as shown in Fig. 4.4. The hardness value (HV) is determined by the ratio F/A. Where, F is normal applied force and A is surface area formed after indentation. The surface area is determined by using the relation.

$$A = d^2/2 \sin(136^o/2) \approx d^2/1.8544$$

$$HV = F/A = 1.8544*F/d^2$$

Where 'F' in kgf and 'd' is the average length of diagonal in mm

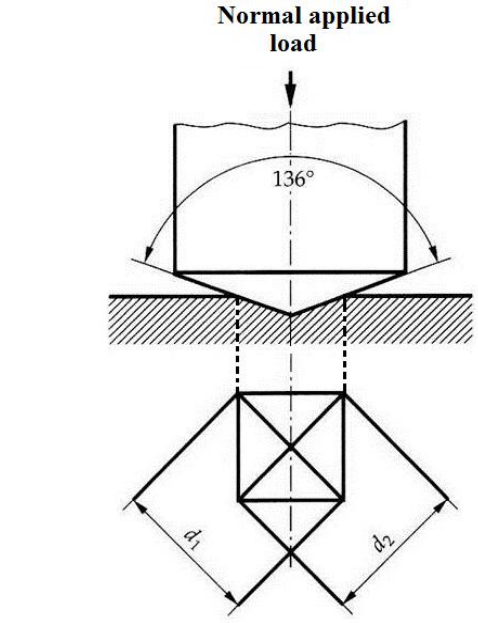

Fig.4.4: Schematic diagram of Vickers hardness principle.

The test was conducted with load of 10kgf and dwell time of 15 sec. Four measurements were taken on each specimen at different spots at a distance of 10 mm and results are presented with average value.

4.4.1.2 Microhardness

For obtaining microhardness of the specimens, the same procedure was followed to polish the samples. The micro hardness of the specimens was measured by using micro hardness Tester (VHM-002 Walter UHL, Germany) using 25 grams of load applied for a dwell time of 15 sec (Fig. 4.5). Each reported value of the microhardness is the average value of five measurements.

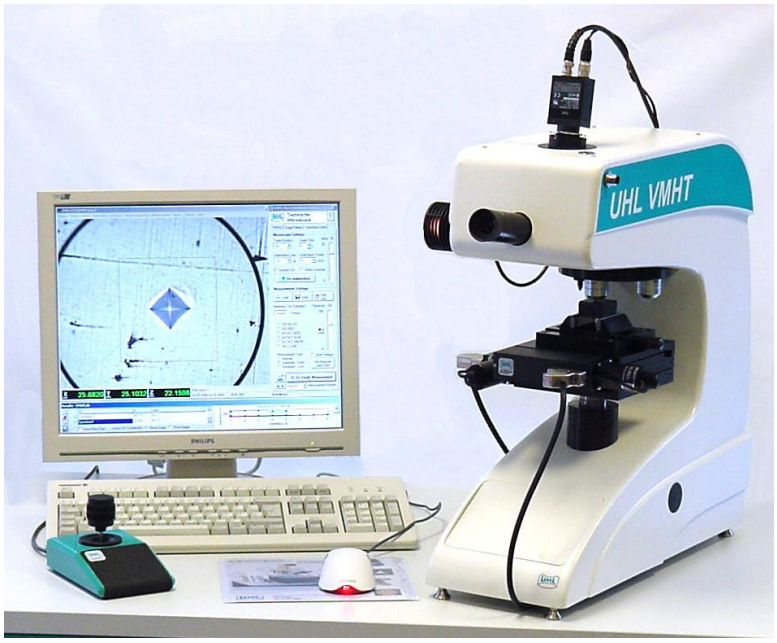

Fig. 4.5: Microhardness tester used for hardness of various phases.

4.4.2. Tensile test

Standard flat tensile specimens with a gauge section 13x3x3 mm were prepared using electro discharge machined as per ASTM E8M-03 specifications. The gauge length of specimens was 13 mm and width and thickness were 3 mm (Fig. 4.6). The as-cast tensile specimens of FeAl-based alloy were usually provided homogenization treatment at 1000^{o}C for 24 hrs followed by furnace cooling to room temperature. The surface of specimen was ground to remove the oxide layer. The tensile tests were carried out on heat treated samples using a computer controlled Hounsfield H25K tensile testing machine with a crosshead speed of 1 mm/min at room temperature. The yield strength and elongation to failure in uniaxial tension of heat treated specimens were obtained. The yield stress has been calculated by adopting 0.2 percent off set proof stress method.

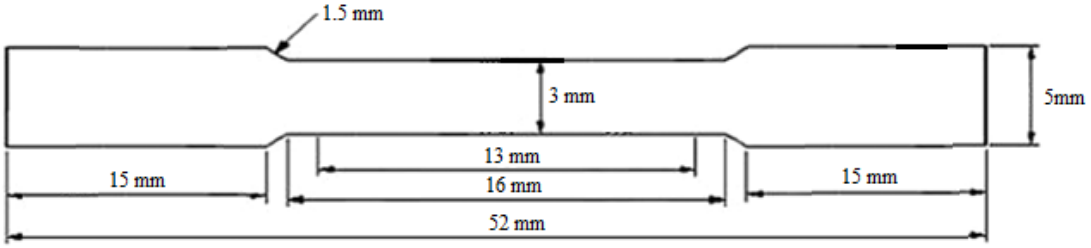

Fig. 4.6: Schematic diagram of flat tensile specimens (in mm).

4.4.3. Compressive test

4.4.3.1 Compression testing at room temperature

The cylindrical specimens of dimension 6mm diameter and 9mm length (Fig. 4.7) for the compression test were also prepared by using the electro discharge machine. The as-cast specimens of FeAl-based alloys were provided homogenization treatment at 1000^{o}C for 24 hrs followed by furnace cooling to room temperature. The surface of specimen was ground to remove the oxide layer. The compression tests were performed using a computer controlled Hounsfield H75K tensile testing machine with cross head speed 1 mm/min at room temperature. The stress strain data of the specimens were obtained and then plotted to find out the strength of various alloys.

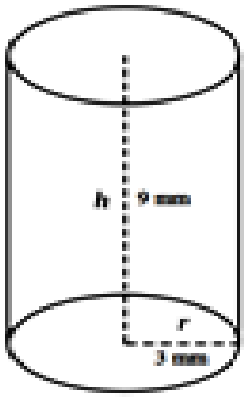

Fig. 4.7: Schematic diagram of compression specimens (in mm).

4.4.3.2 Compression testing at elevated temperature

For high temperature compression test, the specimens of same dimensions (Fig. 4.7) were subjected to deformation by using dynamic testing machine Gleeble 3800 thermomechanical simulator at a strain rate 10^{-3} s^{-1} and at test temperatures of 873, 923, 973 and 1073K. The specimens were subjected to 50% reduction.

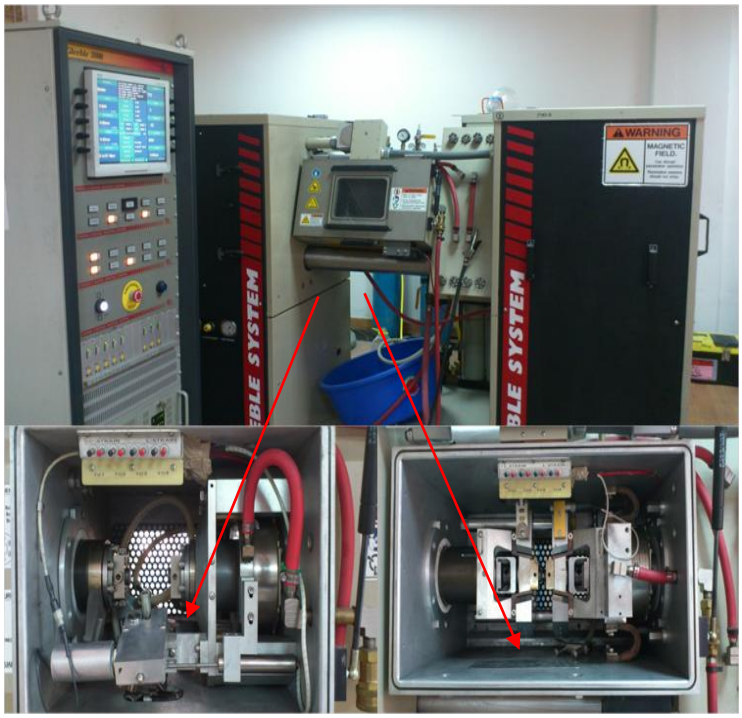

Fig. 4.8: Gleeble3800 thermomechanical simulator.

The 35200 resistance spot welding machine shown in Fig 4.9 is used to join thermocouple wires to the test specimens. It consists of a controller and an integrated welding jig. Holding the specimen and feeding the thermocouple wire is the function of the jig. The controller is used to set the voltage for welding. Thermocouples wires are used to ensure the temperature of the samples and record the change in the dimensions of the samples during testing. The sample is heated by direct resistance heating in the simulator.

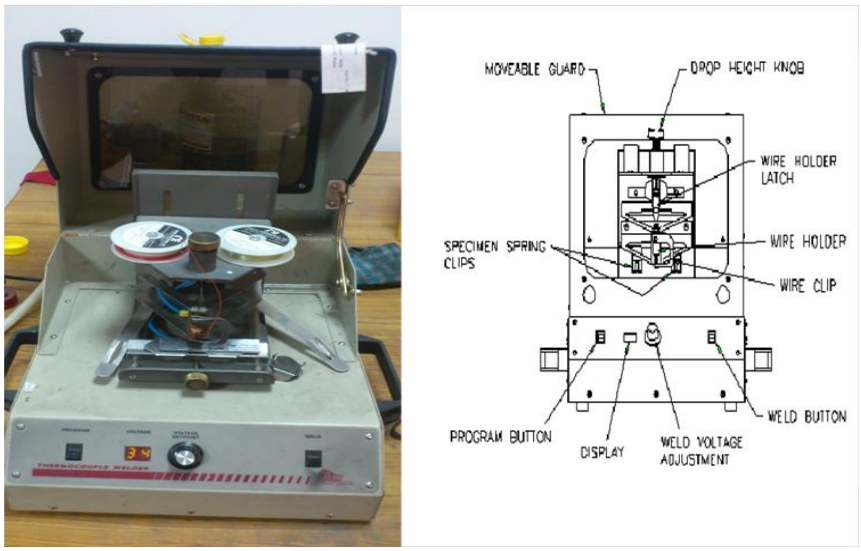

Fig. 4.9: Thermocouple welding machine (35200 model).

4.5. Sliding wear test

The dry sliding wear tests were carried out using a ball-on-disc wear testing machine. The schematic diagram for ball-on-disc is shown in Fig.4.10. The disc samples of different specimens with size of 12x12x5 mm^3 were used. The surface roughness of polished and wear surfaces were carried out by using surface profiler (Mytutoyo SJ-400, Japan). The surface of specimen was polished to roughness of 0.5 µm. SiC balls (6mm dia, hardness 25-28 GPa) were used as the counter material. The tests were conducted at different sliding speeds (0.1, 0.21 and 0.31m/s) with total sliding distance of 120m and 252m under the different loads (5, 10 and 20N). The ball was slid into position above the sample and the disc was rotated at 500 rotations per minute (RPM). The sliding distance was calculated by position of the ball and the RPM of the disc. The wear rate was evaluated by dividing the volume of the wear scar by the load and the sliding distance. The data acquired are the average values taken at three different experiments. The friction force was measured using a loading cell. The wear rate was calculated by dividing the volume of wear scar by the sliding distance. The morphologies of worn surfaces of all the samples were studied by using field emission scanning electron microscopy (FESEM) to understand the wear mechanism. The wear scars were cut vertically by using slow speed diamond saw and transverse view of the wear scars was also examined under FESEM.

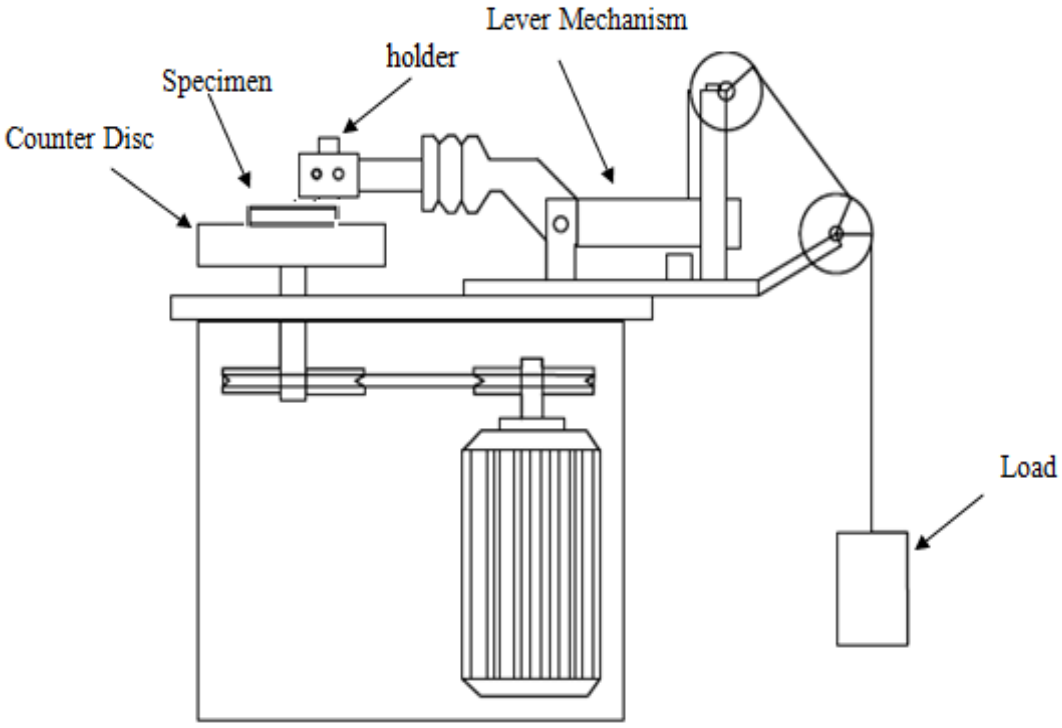

Fig. 4.10: Schematic diagram of ball-on-disc wear test.

4.6. Surface profiler

To measure the surface roughness of polished specimens of different alloys, the surface profiler was used as shown in Fig. 4.11. The surface roughness values of the polished and wear specimens were measured using Surface Roughness Tester (Mitutoyo SJ-400, Japan). An average of 5 reading of the value of surface roughness (R_a) is taken at different positions. The Ra values were obtained by using centre line average method. The surface roughness values are presented in chapters 6 and 7 of the present study.

The same instrument was used to measure the width and depth of the wear tracks of different specimens to find out the volume loss during the wear test. Three different readings were performed from the different locations of the wear tracks to give the average values of the parameters.

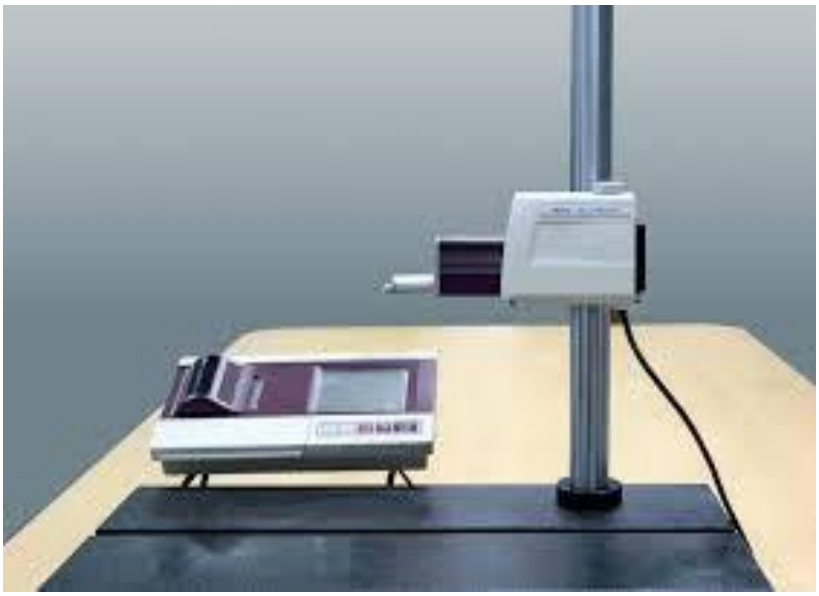

Fig. 4.11: Surface profiler (Mytutoyo SJ-400, Japan) used for surface roughness of the specimens.

4.7 Hot forging

A bar of dimension 10 mm × 10 mm × 70 mm was cut from each specimen and then heat treated to 1200^{o}C in a furnace. The samples were heated in a furnace and held for half an hour after the temperature reached. The hot forging was performed by using a friction screw forging press at 1000 MPa. The sample was subjected to impose with three blows and reduced the height 3 mm initially which led to increase in the width and length ~2 mm. The sample was

quickly rotated perpendicularly and the procedure repeated as discussed earlier. This would lead the sample with square cross section of slightly reduced size.

4.8 Thermal properties

4.8.1 Thermo gravimetric analysis

Thermo gravimetric analysis (TGA) is an analytical technique used to determine thermal stability of the materials and the fraction of volatile component in them by monitoring the weight change that occurs during heating of the specimen. The TGA records mass variations from the decomposition, dehydration and oxidation of samples as the function of time/temperature. The oxidation temperature is basically a thermal stability measurement of a material, in air, pure or less defective samples is always associated higher oxidation temperature.

Fig. 4.12: A photograph of thermo gravimetric analysis (TGA) system used in the present study.

In the present study, thermo gravimetric measurements were carried out using a Perkin-Elmer (Pyris Diamond) instrument (Fig 4.12) from room temperature to 1400^{o}C. The feedstock

materials used for specimen were heated in air with a heating rate of 10^{o}/min. The weight of samples was taken as about 20 mg in each case. The TGA results were used to identify the decomposition temperature of feedstock materials. The TGA results also gave information about phase transformation in the materials in term of weight loss about oxidation of the alloys.

4.8.2 Thermal expansion using dilatometer

LINSIES L 75 dilatometer was used to study the coefficient of thermal expansion (CTE) of the materials (Fig. 4.13). In the present investigation cylindrical specimens of dimension 6 mm diameter and 9 mm length was used and placed the sample in a chamber. The samples were heated with heating rate 5^{o}C/min from room temperature to 1000^{o}C and corresponding change in the dimensions were obtained to find out CTE of the alloys.

Fig. 4.13: LINSEIS L 75 Dilatometer used for coefficient of thermal expansion.

Chapter 5
Effect of carbon and titanium additions on microstructure and mechanical behaviour of FeAl alloy

This chapter deals with the results of addition of carbon to FeAl based alloys and their effect on the microstructure and mechanical properties. Carbon is an important alloying addition in iron aluminides due to precipitation of $Fe_3AlC_{0.5}$ carbide. But, the graphite precipitation at high Al levels (>20wt%) limits the role of carbon addition in FeAl based alloys. Graphite formation can be prevented by formation of strong carbide formers like Ti and Zr. The present study reports the effect of titanium (Ti) addition to carbon containing alloys.

5.1 Microstructural characterizations and phase analysis

5.1.1 Optical

Table 5.1 shows the nominal compositions of various alloy investigated in the present chapter. The Alloy-1 exhibited very fine precipitates along grain boundaries (Fig. 5.1a). In Alloy-2, the particles became coarse and found to be distributed inside and along the grain of the alloy. A few graphite precipitates as a dark grain boundary phase were also observed (Fig. 5.1b). The amount of graphite formed was lower than the carbide phase. Graphite formation has also been reported for alloys with high (1.3%) carbon content [Radhakrishna 2001].

Table 5.1: Nominal composition of different alloy investigated.

	Compositions (wt. %)			
Alloys	**Al**	**C**	**Ti**	**Fe**
1	22.0	0.1	---	Balance
2	22.0	1.0	---	Balance
3	22.0	0.1	1.0	Balance
4	22.0	1.0	5.0	Balance
5	22.0	1.5	5.0	Balance

In order to strengthen FeAl based alloys containing high carbon content, a stronger carbide former element such as titanium (Ti) was introduced. Keeping the carbon content used in the above alloys, the different Ti contents corresponding to TiC formation were introduced. Alloy-3 consists of two types of carbide dispersions at the grain boundaries and in the grains interior. The carbides in Alloy-3 were too fine (Fig. 5.1c) to be identified by XRD.

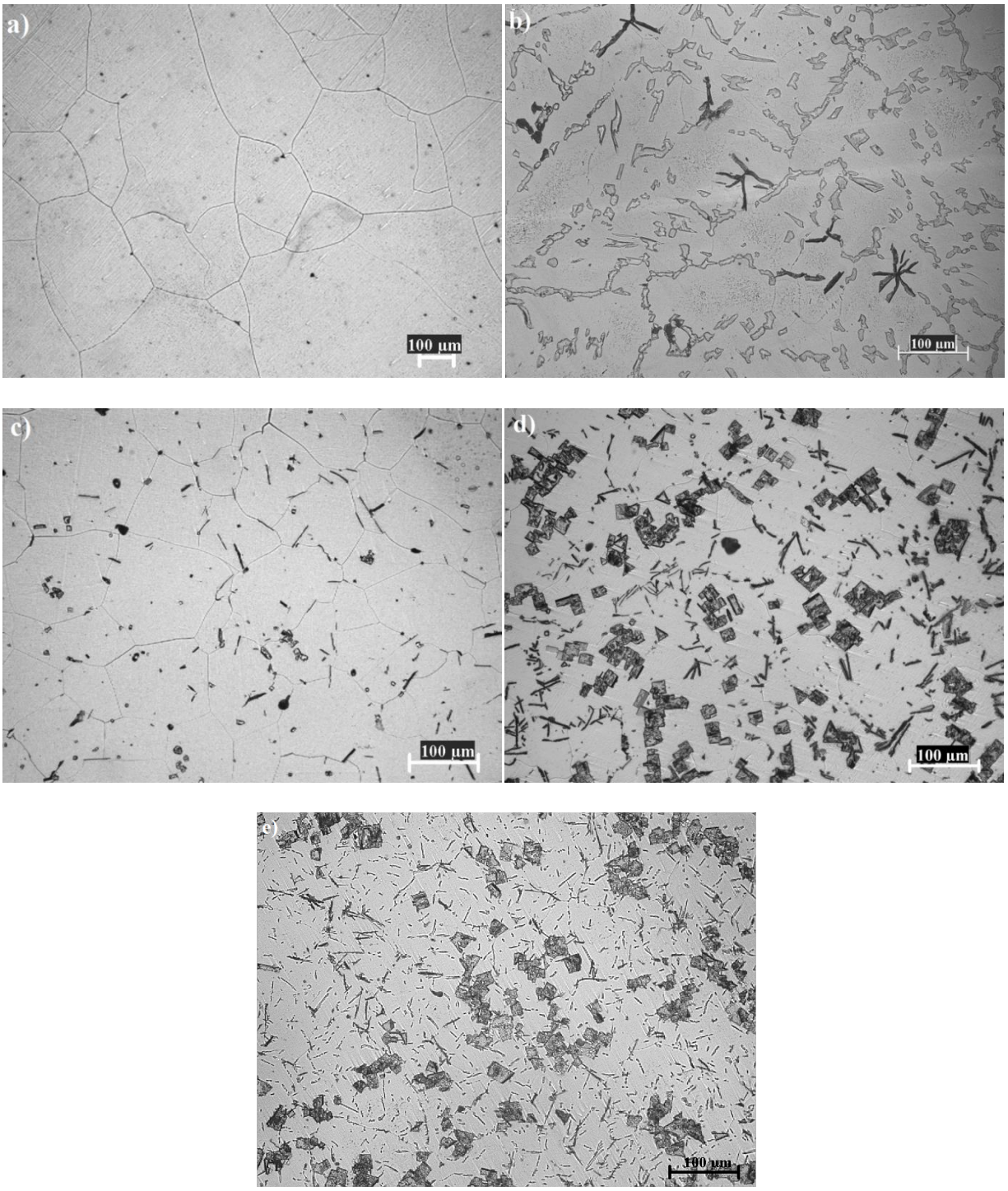

Fig. 5.1: Optical micrographs of alloy samples, (a) Alloy-1 with fine $Fe_3AlC_{0.5}$, (b) Alloy-2 with $Fe_3AlC_{0.5}$ and graphite, (c) Alloy-3 with uniform fine distribution of TiC and $Fe_3AlC_{0.5}$, (d) Alloy-4 and (e) Alloy-5 showing blocky TiC precipitates and elongated $Fe_3AlC_{0.5}$ precipitates within the FeAl matrix.

EDS (Figs. 5.2 and 5.3) confirmed two types of carbides in Alloy-3 (Fig. 5.1c), one with blocky (TiC) and the other with elongated morphology ($Fe_3AlC_{0.5}$). Similarly, in Alloy-4

and Alloy-5 with higher carbon and Ti contents, exhibited two types of carbides (Fig. 5.1d and 5.1e), one with blocky (TiC) and the other with elongated morphology ($Fe_3AlC_{0.5}$). XRD and EDS of both alloys confirmed the presence of both types (TiC) and the other with elongated morphology ($Fe_3AlC_{0.5}$). XRD and EDS of both alloys confirmed the presence of both types of carbides as shown in Figs. 5.2 and 5.3. The volume fraction of different phases observed in the alloys was measured by using Dwintre software equipped with optical microscope as listed in Table 5.2.

The alloy compositions were chosen appropriately to anticipate the formation of TiC. The Ti-content was chosen such that the Ti:C ratios used for Alloy-3 and Alloy-4 were more than that for TiC. In Alloy-5, carbon content was little more but has no significant effect on the microstructure of FeAl based alloy. The titanium carbide, TiC is more stable and may have prevented formation of graphite in Ti containing alloys. TiC-type (MC) carbide with large free negative energy of formation and high melting point may precipitate as primary phase from the liquid [Ko 1999]. Ti has large tendency to absorb the carbon from the liquid and form TiC carbides. With decrease in temperature, $Fe_3AlC_{0.5}$ precipitates form following solidification [Palm 1995]. Thus, these precipitates form by solid state reaction. At high Ti content (Alloy-4), volume fraction of $Fe_3AlC_{0.5}$ precipitates seems to be lower than that of TiC. But, with increase in the carbon content, the volume fraction of $Fe_3AlC_{0.5}$ carbides increases. No graphite formation was observed on Ti additions. The addition of Ti to FeAl alloys also resulted in decrease in the grains size. Similar grain refinement by Ti addition has been reported by Sikka et al in FeAl [Sikka 1998].

5.1.2 Scanning electron microscope equipped with EDS

The SEM micrograph of Alloy-1 shows the fine carbides along the grain boundaries as shown in Fig. 5.3a. The EDS analysis confirmed the particles were rich in Al and Fe. The pattern observed corresponds to grey particles were rich in Al and Fe and confirms the presence of $Fe_3AlC_{0.5}$ in Alloy-2. No peak for Al and Fe were observed in dark particles. In Alloy-3, two phases were observed in the microstructure as shown in Fig 5.1c. The peak positions corresponding to blocky particle is rich in Ti and that of elongated one is rich in Fe, Al and Ti. This suggests that very small amount Ti may also be present in the elongated particles. The EDS spectrum obtained from the matrix also reveals that small amount of Ti also present in the matrix. Thus, it suggests that large amount of Ti was used in the formation of TiC carbide. Similar observations were also obtained in Alloy-4 and Alloy-5.

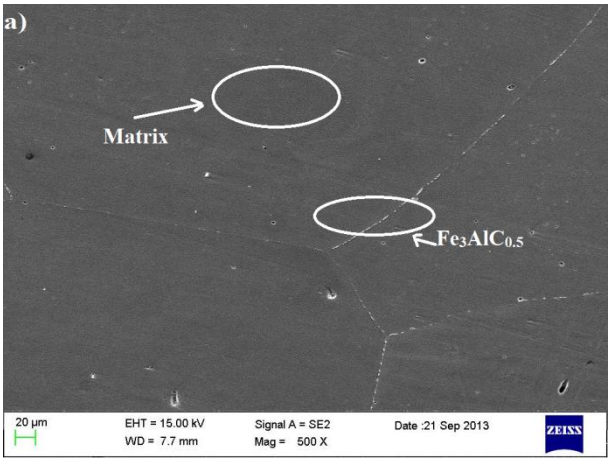
a)
Matrix
$Fe_3AlC_{0.5}$
20 µm
EHT = 15.00 kV
WD = 7.7 mm
Signal A = SE2
Mag = 500 X
Date :21 Sep 2013
ZEISS

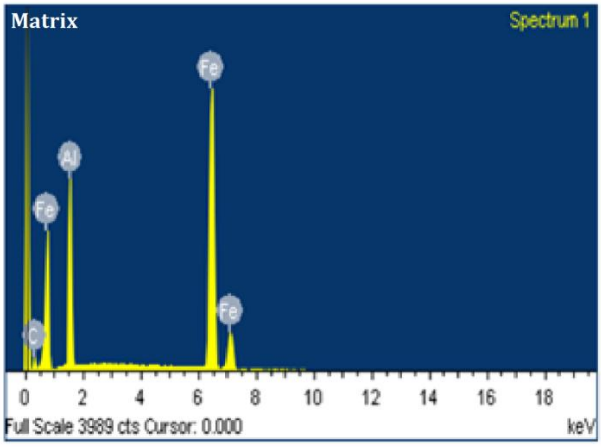
Matrix
Spectrum 1
Fe
Al
Fe
C
Fe
0 2 4 6 8 10 12 14 16 18
Full Scale 3989 cts Cursor: 0.000
keV

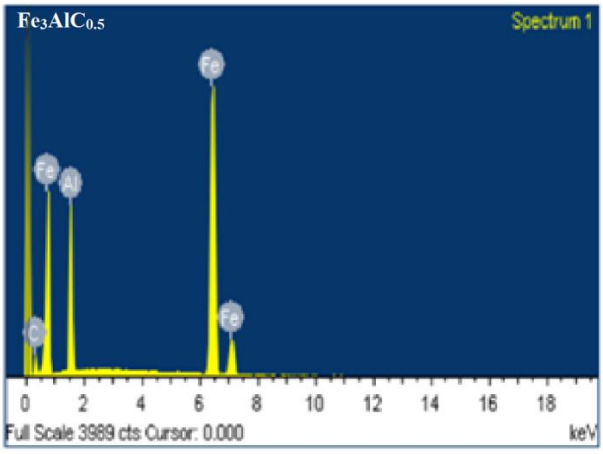
$Fe_3AlC_{0.5}$
Spectrum 1
Fe
Fe
Al
C
Fe
0 2 4 6 8 10 12 14 16 18
Full Scale 3989 cts Cursor: 0.000
keV

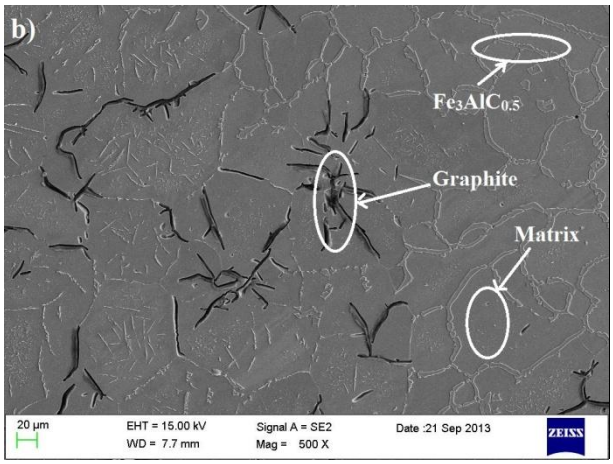
b)
$Fe_3AlC_{0.5}$
Graphite
Matrix
20 µm
EHT = 15.00 kV
WD = 7.7 mm
Signal A = SE2
Mag = 500 X
Date :21 Sep 2013
ZEISS

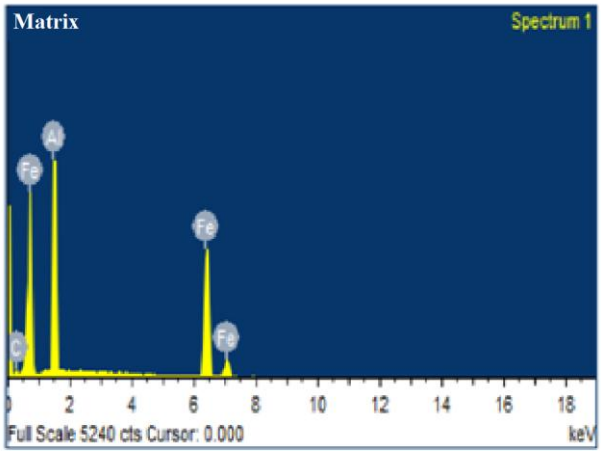
Matrix
Spectrum 1
Al
Fe
Fe
C
Fe
2 4 6 8 10 12 14 16 18
Full Scale 5240 cts Cursor: 0.000
keV

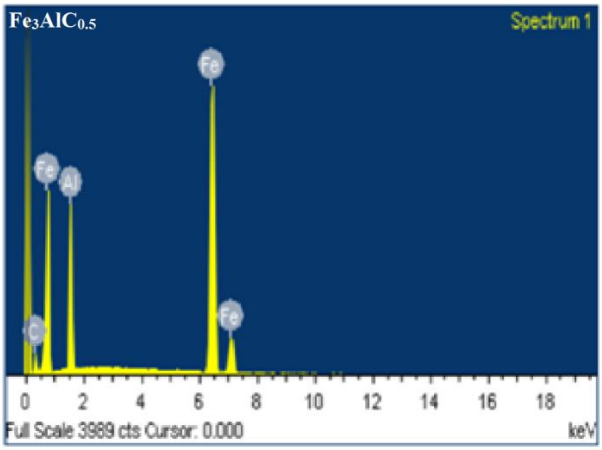
Fe3AlC0.5
Spectrum 1
Fe
Al
C
0 2 4 6 8 10 12 14 16 18
Full Scale 3989 cts Cursor: 0.000
keV

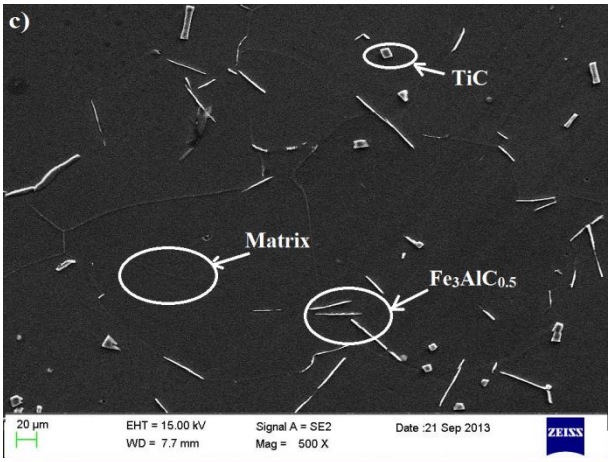
c)
TiC
Matrix
Fe3AlC0.5
20 µm
EHT = 15.00 kV
WD = 7.7 mm
Signal A = SE2
Mag = 500 X
Date :21 Sep 2013
ZEISS

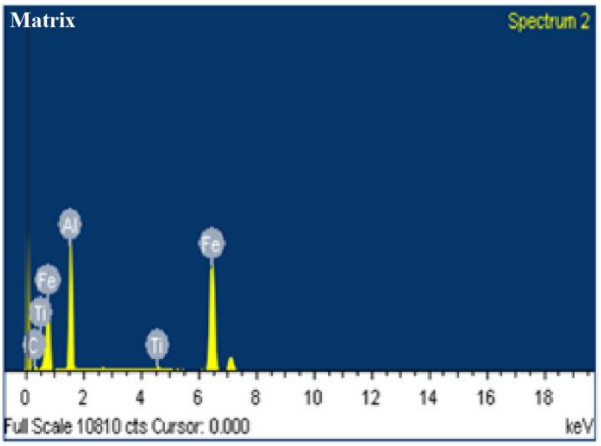
Matrix
Spectrum 2
Al
Fe
Fe
Ti
C
Ti
0 2 4 6 8 10 12 14 16 18
Full Scale 10810 cts Cursor: 0.000
keV

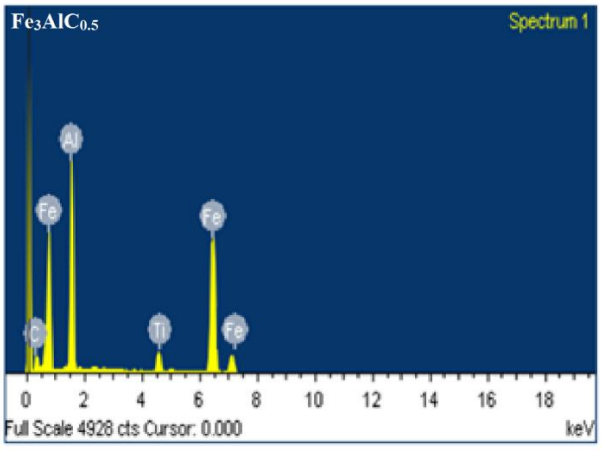
Fe3AlC0.5
Spectrum 1
Al
Fe
Fe
C
Ti
Fe
0 2 4 6 8 10 12 14 16 18
Full Scale 4928 cts Cursor: 0.000
keV

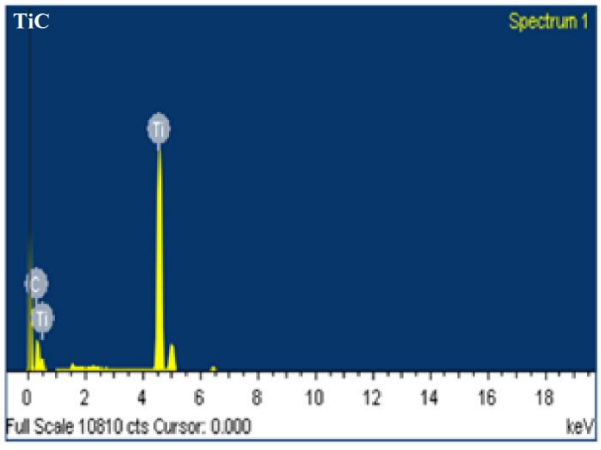
TiC
Spectrum 1
Ti
C
Ti
0 2 4 6 8 10 12 14 16 18
Full Scale 10810 cts Cursor: 0.000
keV

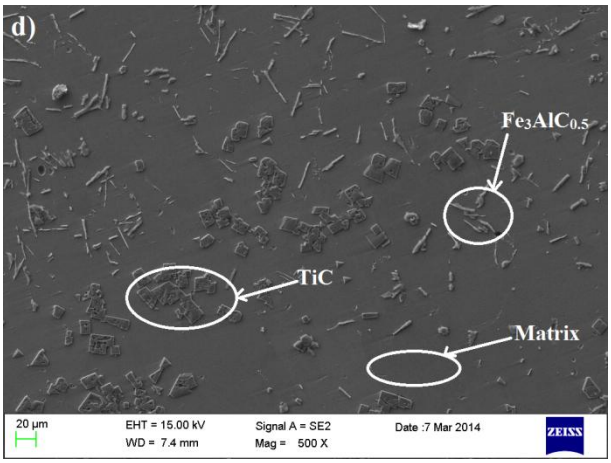
d)
$Fe_3AlC_{0.5}$
TiC
Matrix
20 µm
EHT = 15.00 kV
WD = 7.4 mm
Signal A = SE2
Mag = 500 X
Date :7 Mar 2014
ZEISS

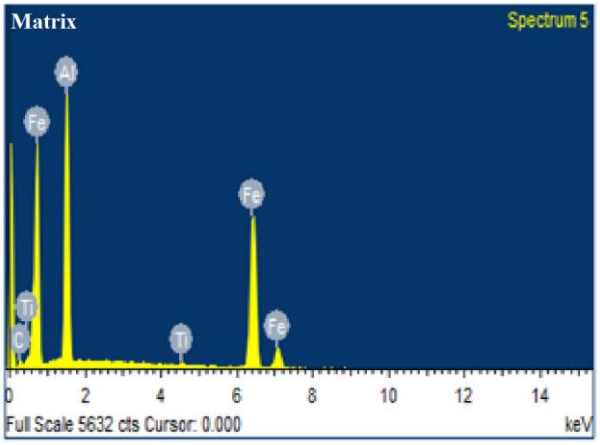
Matrix
Spectrum 5
Al
Fe
Fe
Ti
C
Ti
Fe
0 2 4 6 8 10 12 14
Full Scale 5632 cts Cursor: 0.000
keV

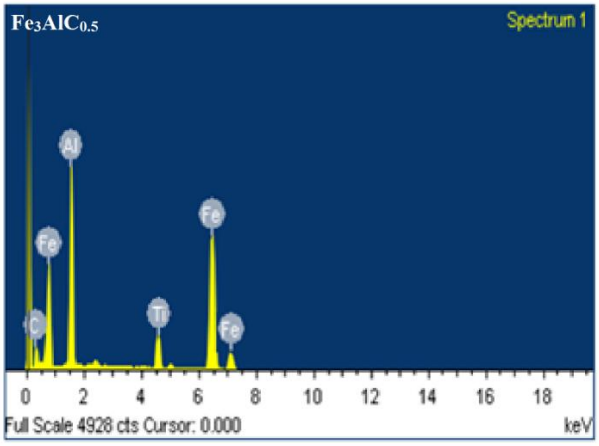
$Fe_3AlC_{0.5}$
Spectrum 1
Al
Fe
Fe
C
Ti
Fe
0 2 4 6 8 10 12 14 16 18
Full Scale 4928 cts Cursor: 0.000
keV

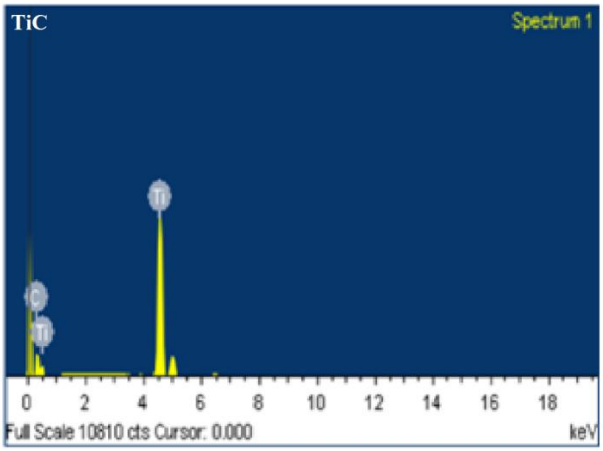
TiC
Spectrum 1
Ti
C
Ti
0 2 4 6 8 10 12 14 16 18
Full Scale 10810 cts Cursor: 0.000
keV

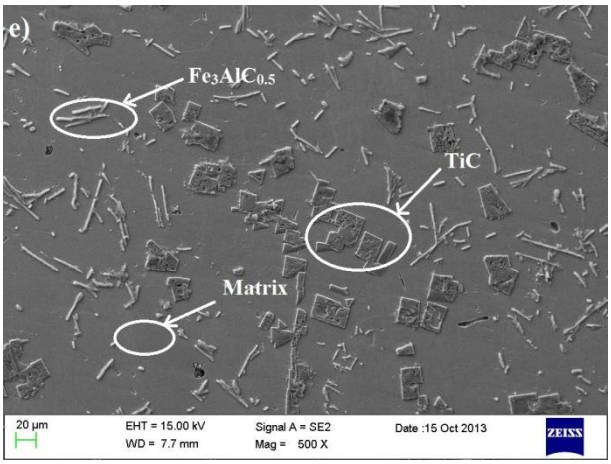
e)
$Fe_3AlC_{0.5}$
TiC
Matrix
20 µm
EHT = 15.00 kV
WD = 7.7 mm
Signal A = SE2
Mag = 500 X
Date :15 Oct 2013
ZEISS

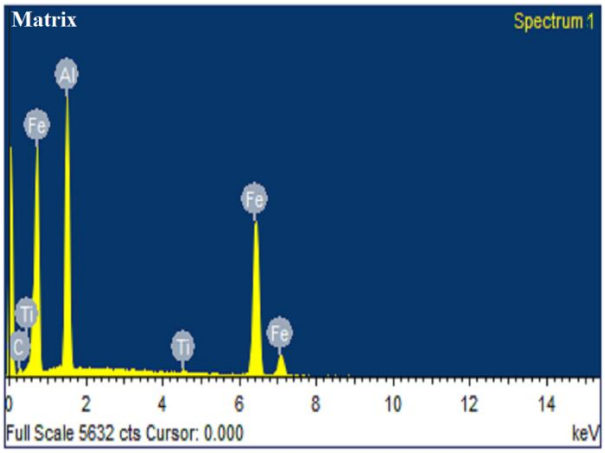
Matrix
Spectrum 1
Al
Fe
Fe
Ti
C
Ti
Fe
0 2 4 6 8 10 12 14
Full Scale 5632 cts Cursor: 0.000
keV

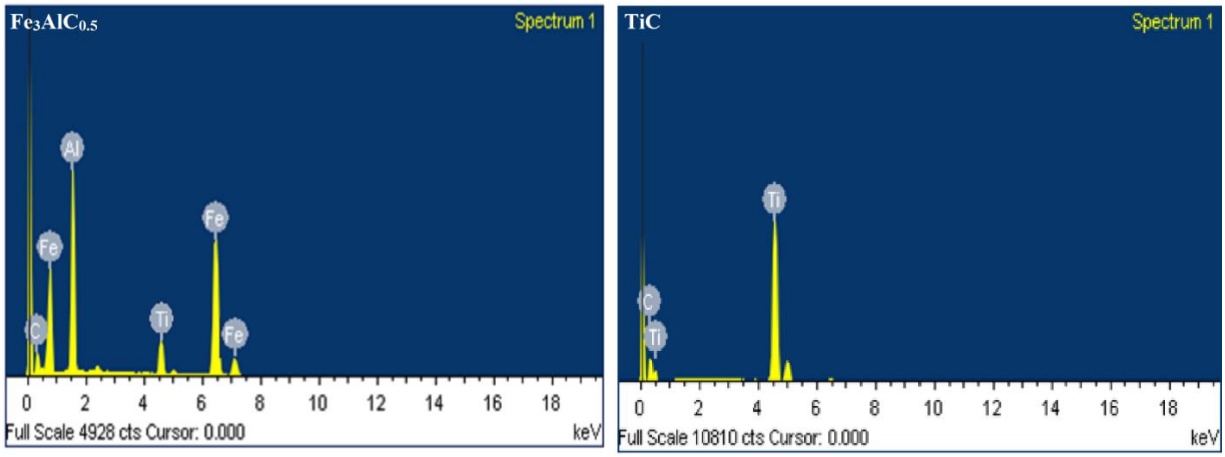

Fig. 5.2: SEM micrographs with their EDS spectrums of, (a) Alloy-1, (b) Alloy-2, (c) Alloy-3, (d) Alloy-4 and (e) Alloy-5.

5.1.3 Transmission electron microscope analysis

The bright field images under TEM of matrix, elongated and cubiod shape particles in Alloy-4 are shown in Fig. 5.4a, 5.4b and 5.4c and their corresponding Selected Area Diffraction (SAD) patterns are shown in Fig. 5.4d, 5.4f and 5.4e respectively. The SAD pattern of FeAl matrix (Fig.5.4a) is indexed with orientation$[1\bar{1}\,\bar{1}]$. Similarly the elongated and cubiod particles are indexed to be $Fe_3AlC_{0.5}$ and TiC with the orientations [011] and $[1\bar{1}2]$ respectively. The width of elongated particle is ~ 400 nm. The average edge size of cuboid is also found to be ~ 400 nm.

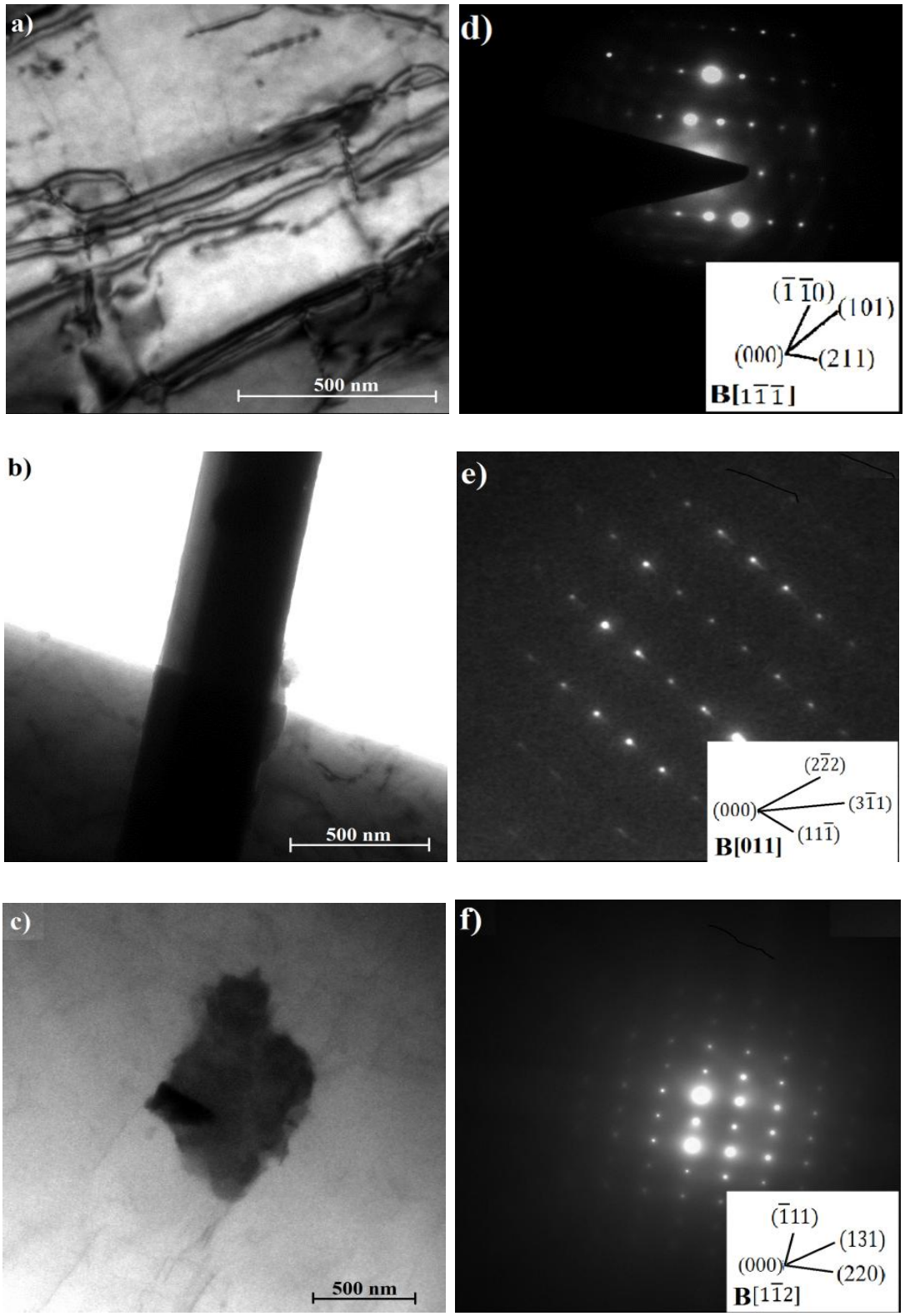

Fig. 5.3: Bright field TEM images of Alloy-4, (a) B2 matrix, (b) elongated particle ($Fe_3AlC_{0.5}$) and (c) cubiod (TiC), with (d) SAD analysis of B2 matrix, (e) SAD analysis of $Fe_3AlC_{0.5}$ and (f) SAD pattern of TiC precipitates.

5.1.4 X-ray diffraction

The X-ray diffraction studies of Alloy-1 suggests that the matrix to be of B2 lattice structure. The carbide volume fraction was very small and thus no carbide peaks were observed. In Alloy-2, the matrix has B2 lattice structure and carbides with grey colour are identified to be $Fe_3AlC_{0.5}$ (Fig. 5.2). The dark elongated particles may be that of graphite flakes and but due to their low volume fraction graphite peaks were not observed in XRD pattern. Similarly, in Alloy-3, the fraction of carbides is too low to be identified by XRD. On the other side, Alloy-4 and Alloy-5 contain large volume fraction of carbides and XRD confirms the presence of $Fe_3AlC_{0.5}$ and TiC. The types of TiC carbides obtained in the alloys is in good agreement with the precipitates reported by Ko and Handa [Ko 1999].

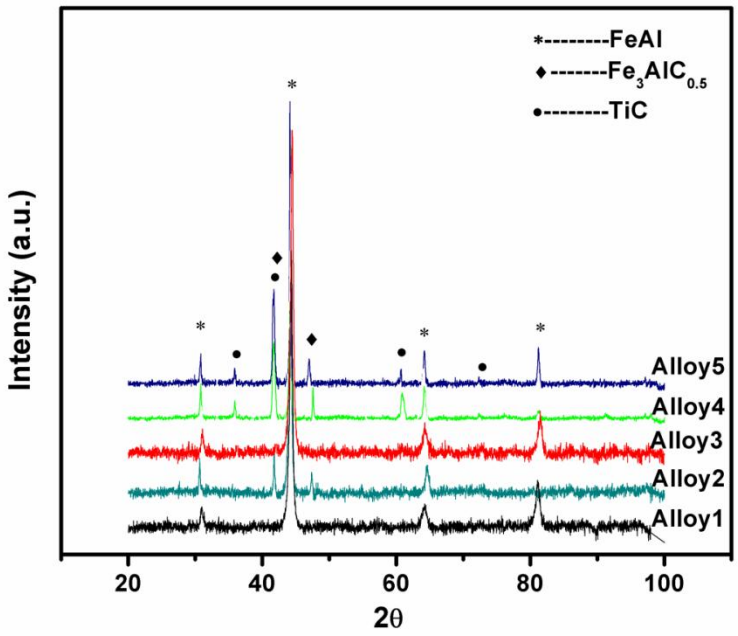

Fig. 5.4: XRD pattern of different FeAl based alloys.

5.2. Mechanical properties

5.2.1 Hardness and microhardness of phases

The hardness of FeAl based alloys were studied by Vickers hardness tester. Each data point of hardness reported here is an average of three measurements. The hardness of FeAl based alloy increased with increase in the carbon content up to certain extent. i.e. carbon has limited addition to FeAl based alloys (Table 5.2). Carbon addition to FeAl based increases the

hardness as noticed in Alloy-1 and Alloy-2. This is mainly attributed to the precipitation of carbide $Fe_3AlC_{0.5}$. But in Alloy-2, the hardness was not increased up to expected level. This is due to precipitation of soft graphite. In Ti addition, the alloys show improvement in the hardness values with same carbon additions. Alloy-3 has higher hardness than Alloy-1 having same carbon content. This improvement in the hardness is not simply attributed to the presence of few TiC carbides with $Fe_3AlC_{0.5.}$ Ti addition also causes grain refinement of matrix due to solid solution hardening and contributes to improvement of hardness of the alloy. The improvement in the matrix hardness confirms the presence of Ti in the matrix (Table 5.2). Similarly, in Alloy-2 and Alloy-4 having same carbon content shows improvement in the hardness on Ti addition. This is due to fact that no graphite precipitation was observed in Alloy-4 on Ti addition and the presence of TiC with $Fe_3AlC_{0.5}$ results in the improvement of the hardness. Alloy-5 with high carbon content exhibits highest hardness. This demonstrates that the hardness of the alloy increases with increase in the volume fraction of carbides and their fraction increase with increase in the carbon and Ti contents.

Table 5.2: Volume fraction and mirohadrness of different phases present in FeAl based alloys.

Alloys	Bulk Hardness (VHN)	Microhardness (VHN)			Volume fraction of phases (%)	
		Matrix	Carbides			
			TiC	$Fe_3AlC_{0.5}$	Graphite	Carbides
Alloy-1	365	335	---	---	---	<3.5
Alloy-2	400	350	---	600	3.5	14-17
Alloy-3	380	400	2980	610	---	06-07
Alloy-4	425	410	3000	615	---	18-21
Alloy-5	475	410	3000	615	---	22-25

5.2.2 Tensile properties

The tensile strength of Alloy-1 is superior to that reported for thermomechanically processed and heat treated alloy Fe-22.0Al alloy (Table 5.3). This strengthening arises due to solid solution strengthening by interstitial carbon as well as precipitation of hard $Fe_3AlC_{0.5}$. The increase in carbon content from 0.1 to 1.0 wt% has resulted in the increase in the room temperature strength. But this increase is not up to the expected level. This is mainly due to precipitation of soft graphite as well as $Fe_3AlC_{0.5}$ carbides. Further increase of carbon content to 1.3 wt% results reduction in the tensile strength. This reduction in strength with an increase in carbon addition from 1.0 to 1.3 wt% may be attributed to the precipitation of carbon as soft graphite.

Table 5.3: Tensile properties of FeAl based alloys.

Alloys	As cast		Annealed at 400^{o}C, 100h	
	Yield strength (MPa)	Elongation (%)	Yield strength (MPa)	Elongation (%)
Fe-22Al*	360	2.20	---	---
Alloy-1	365	2.50	320	3.10
Alloy-2	400	4.20	342	4.30
Alloy-3	385	4.0	300	4.20
Alloy-4	505	4.30	410	4.40
Alloy-5	520	4.10	440	4.30

*[Liu 1989]

Ti addition to FeAl alloy containing carbon results in the improvement of tensile strength without loss in the ductility. Alloy-3 exhibits better strength than Alloy-1. Similarly, Alloy-4 shows improved strength than Alloy-2. Alloy-5 with large volume fraction of TiC and $Fe_3AlC_{0.5}$ carbides possesses highest strength. Thus *in-situ* formation of TiC has not resulted in loss of ductility in these alloys though TiC is a hard and brittle phase. The addition of TiC to FeAl has been reported to lead to loss in ductility [Subramanian 1997] in an alloy produced by liquid phase sintering of TiC and FeAl powders. This limitation has been overcome by the *in-situ* formation of TiC in the present work. TiC carbides with $Fe_3AlC_{0.5}$ results in the increase in the strength of FeAl based alloys without loss in the ductility. The size of different carbides particles varies from few microns to nano meters. The uniform distribution of these carbide particles helps in improvement in the strength of FeAl based alloys. The addition of the Ti in Fe-Al alloys containing carbon leads to the strengthening effects on hardness and yield strength of the alloys at room temperature. The improvement in ductility may be due to the improved resistance of carbon containing alloys to hydrogen embrittlement [Prakash 2001]. At the same time Ti addition has resulted in an increase in strength.

It may be pointed out that FeAl based intermetallics showed poor ductility due to susceptibility to environmental embrittlement in the presence of moisture. Form the literature, it has been found that the carbide particles ($Fe_3AlC_{0.5}$) can acts as hydrogen traps and causes in the reduction of susceptibility to hydrogen embrittlement [Prakash 2001]. Thus, improved ductility of FeAl based alloy on Ti addition may be due to fact that the $Fe_3AlC_{0.5}$ precipitates containing Ti may acts as strong hydrogen traps and reduce the hydrogen diffusivity. It may also contributes to the improvement in the ductility of FeAl based alloys.

The ductility of FeAl based alloy is strongly depend on the amount of thermal vacancies present in the alloy. The heat treatment of FeAl alloys at 400^{o}C for 100 h cause increase in the ductility (Table 5.3). This increment is mainly attributed to removal of thermal vacancies present in the alloys. At the same time there is decrease in the strength of the alloys.

SEM fractrographs of the investigated alloys are shown in Fig. 5.5. In carbon containing alloys, Alloy-1 with low carbon percentage exhibited intergranular fracture with coarse cleavage facets (Fig 5.5a), which corresponds to their brittle nature. On the other hand, Alloy-2 with higher percentage of carbon showed change in the tensile fractured mode from intergranular to predominantly cleavage (Fig. 5.5b). The fracture surfaces of alloys with the addition of Ti (Alloy-3 and 4) are showing the change in tensile fracture mode from intergranular (Fig. 5.5c) to mixed mode (cleavage + ductile dimple) failure (Fig. 5.5d). The similar failure was observed in Alloy-5 (Fig 5.5e). The presence of carbides may provide a modified path by influencing the nature of crack propagation [Pang 2000].

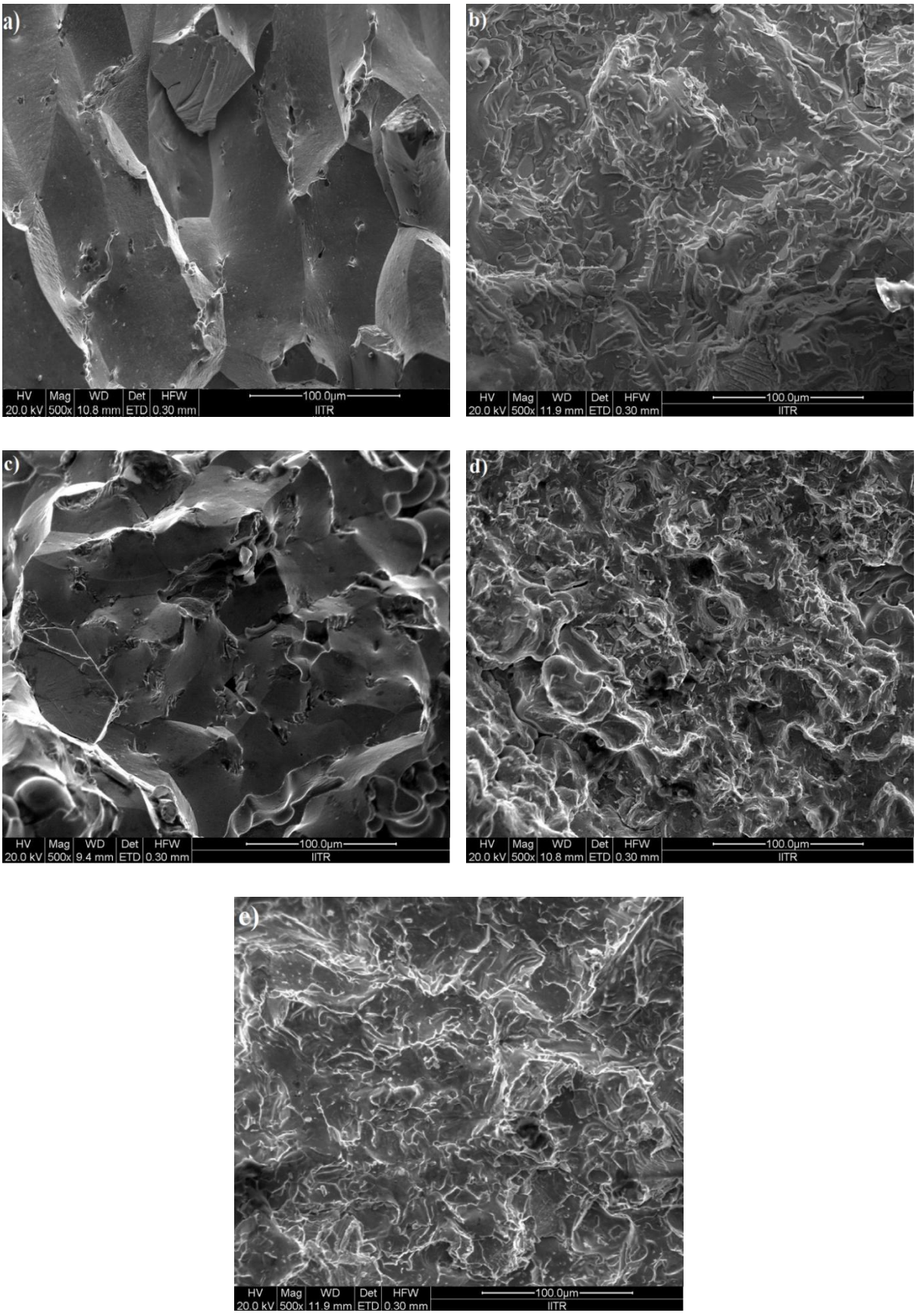

Fig. 5.5: SEM fractographs showing tensile fracture surfaces of, (a) Alloy-1, (b) Alloy-2, (c) Alloy-3, (d) Alloy-4 and (e) Alloy-5.

5.2.3 Compression properties

The compression test results are shown in Fig.5.6. The compressive yield strength of binary FeAl based alloy has been reported to be ~580 MPa [Eumann 2004]. The addition of 0.1 wt% C (Alloy-1) has resulted in significant increase in the strength. At higher (1wt.%C) carbon content (Alloy-2) only nominal increase in strength is observed which may be due to presence of graphite in the alloy. Alloy-3 and 4 containing both $Fe_3AlC_{0.5}$ and TiC carbides showed superior strength as compared to Alloy-1. Alloy-2 with larger volume fraction of carbides compared to Alloy-3 exhibited slightly higher strength at room temperature. Alloy-5 exhibits highest strength at room temperature due the large volume fraction TiC and $Fe_3AlC_{0.5}$ carbides. With increase in the temperature, the fall in the strength of alloys follow the same trend except Alloy-2. At 873K or higher, Alloy-3 exhibits higher strength than Alloy-2 as the presence of graphite in Alloy-2 leads to rapid loss in strength at high temperatures. Thus the presence of graphite is clearly undesirable. Alloy-5 with large volume fraction of TiC and $Fe_3AlC_{0.5}$ carbides exhibited highest strength at all the temperatures as shown in Fig 5.6. The high temperature stability and high melting point of TiC carbide helps in increase in the high temperature strength of FeAl based alloys.

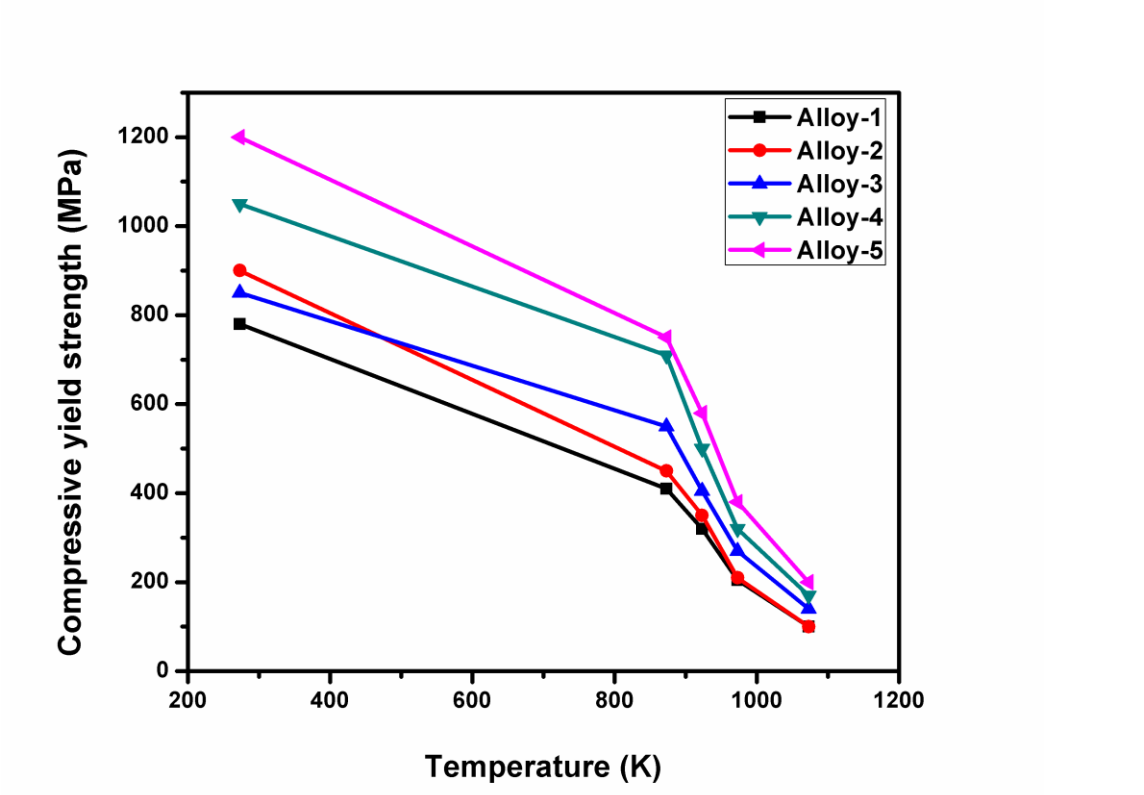

Fig. 5.6: Variation of compressive yield strength with temperature of FeAl based alloys.

The compressive yield strength decreases with increase in temperature (Fig. 5.6). The loss in strength is particularly steep above 923K due to a rapid decrease in strength of the iron aluminide matrix. At 1073K all the alloys have comparable strength. Due to the loss in strength above 923K, iron aluminides are being developed for structural applications at or below 923K [Stoloff 1998]. As can be seen from Fig. 5.6 up to 75% increase in elevated temperature yield strength can be obtained at target service temperatures with suitable carbon and Ti additions. This is accomplished without compromising on the room temperature ductility.

The increase in yield strength is due to combination of load transfer to carbide precipitates (composite strengthening) [Kolluru 1998] as well as solid solution strengthening. Efforts to improve elevated temperature strength may lead to deterioration in room temperature ductility. The present results are significant because the elevated temperature strengthening is achieved without compromising on room temperature ductility. Addition of carbon to Fe_3Al (and FeAl) is known to reduce susceptibility to environmental embrittlement [Prakash 2007]. This may offset loss in ductility due to the presence of (brittle) carbides. Carbon addition was unsuccessful due to graphite formation in FeAl which leads to loss of strength at elevated temperatures [Radhakrishna 2001]. It is successful in the present work as formation of graphite is prevented by addition of Ti.

The values of yield stresses in tension are significantly lower than those obtained in compression. In bcc crystal structure, this compression-tension asymmetry is well known. This has been related to the glide of the screw dislocations with nonplanar core structure [Koeppe 1999]. Also, in iron aluminides with ordered B2 structure (FeAl), the asymmetry in flow stress has been reported based on different compression and tensile specimens [Yoshimi 1997].

5.3. Thermal behavior of FeAl based alloys

In order to understand the phase transition in the different alloys, the alloys were subjected to heating up to 1400^{o}C in differential thermal analysis (DTA) as shown in Fig. 5.7. DTA method disclosed that transformation during heating of the alloys. Before analyzing the effect of alloying additions on the transition temperature of order-disorder transition during heating alloys, it was confirmed that matrix has B2 structure in all the alloys. Fig 5.7 shows DSC thermograms of the B2 type ordered Fe-Al alloys on heating around their melting point temperatures. Peaks appearing in an L+ α-Fe (A2) two-phase region after melting were identified as B2-A2 order-disorder phase transition temperatures. The characteristics of the DSC thermograms and values of order-disorder transition temperatures, measured as 1503K

(1230^{o}C) are consistent with the phase diagram [Frommeyer 1999] and other literature data. Ti addition to FeAl based alloy slightly decrease the order-disorder transformation. This decrease in ordering temperature was also found in FeAl based alloys [Yildirim 2012]. The solid solubility behavior of Ti addition in B2-type FeAl alloys may be ascribed to the site occupancy characteristics of the alloying element. The presence of Ti in the matrix was also confirmed by EDS analysis. Ti elements were preferentially found to be occupied Fe sublattice sites in B2 ordered structure of FeAl [Mekhrabov 1999].

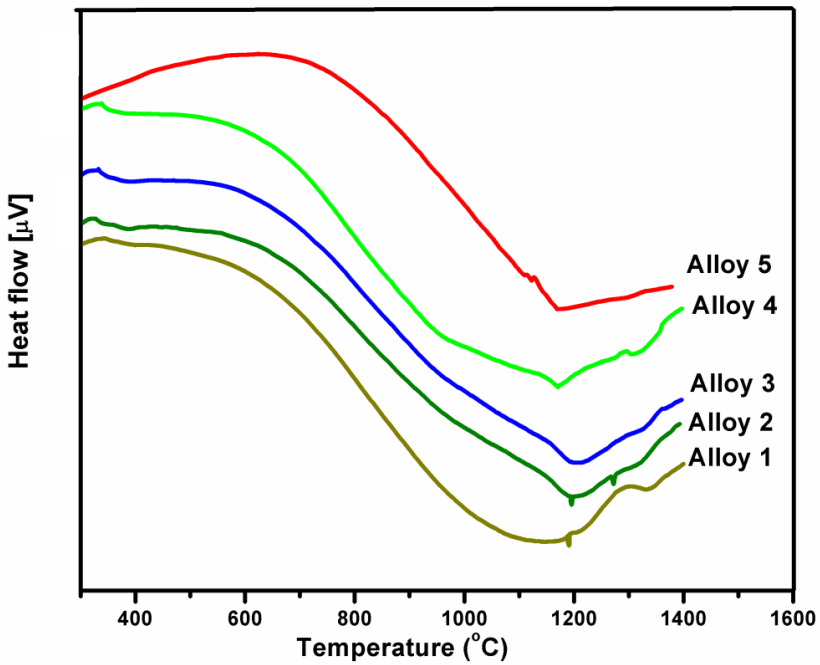

Fig. 5.7: DTA flow of FeAl based alloys.

To analyze the transformation, the different specimens were subjected to heat at different temperatures i.e. 1100^{o}C and 1300^{o}C and then followed by water quenching. These temperatures selected are above and below the transition temperature i.e. ~1200^{o}C. Fig. 5.8a shows the XRD pattern of alloys subjected to quenching from 1100^{o}C. XRD pattern confirms the presence of B2 phase. Similarly, in Fig. 5.8b shows XRD pattern of same alloys subjected to quenching from 1300^{o}C. The matrix phase indentified to be α (Fe). As mentioned earlier, the DTA analysis suggests that order-disorder transformation (B2/α) is taking place near 1200^{o}C. In both Fig. (5.8a and 5.8b), no peaks for $Fe_3AlC_{0.5}$ carbides was observed, while peaks of TiC carbide were present after both heat treatments. These results are in consistent with the thermal

stability of TiC carbides at high temperatures. On the other hand, $Fe_3AlC_{0.5}$ carbide got dissolve in the matrix due to its low melting point i.e. 950°C [Pang 1998].

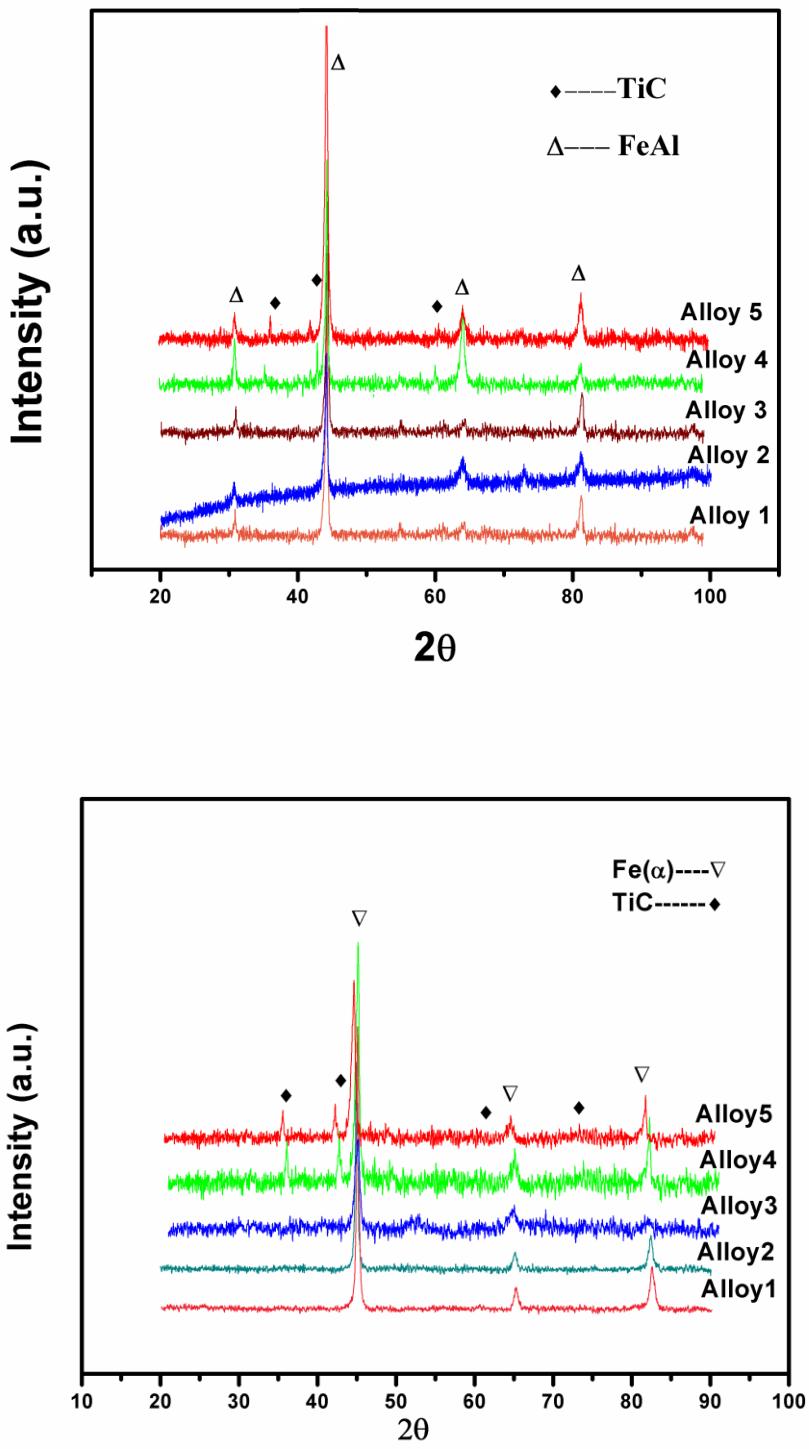

Fig. 5.8: XRD pattern of FeAl based alloys after heat treatment for 1 h (water quenched), (a) 1100°C and (b) 1300°C.

In Fig. 5.9, the plot of mean coefficient of thermal expansion (CTE) of different FeAl based alloys reinforced with carbide particles. The graph reveals the rise in CTEs with increasing temperature. Alloy-1 shows sharp increase in mean CTEs initially followed by steady state and again rises after 600^{o}C for small interval. This increase is also observed in Alloy-2 but not so sharp. This could be due to dissolution of $Fe_3AlC_{0.5}$ carbides in FeAl matrix as this carbide melts in FeAl matrix around 950^{o}C [Pang 1998]. The large volume fraction and coarser in size of $Fe_3AlC_{0.5}$ carbides in Alloy-2 result in less expansion than Alloy-1. In Alloy-3, Alloy-4 and Alloy-5, the mean CTEs increase sharply initially and then increase is slowed down. The mean CTE decreased with increase in TiC and $Fe_3AlC_{0.5}$ content in the temperature range from 50 to 1000^{o}C. In FeAl alloys, Fe-Al bond strength is intermediate between Al-Al and Fe-Fe bond strengths. Also, note that the CTEs, $\alpha_{Fe}=1.2x10^{-5}$ and $\alpha_{Al}=2.2x10^{-5}\,{}^{o}C^{-1}$ at room temperature [Ho 1998, Klemens 1986]. The thermal expansion coefficient, CTEs of α_{TiC} and α_{FeAl} are $0.74x10^{-5}$ [Pierson 1996] and $2.18x10^{-5o}C^{-1}$ [Zhang 2001] respectively in the temperature range from room temperature to 1000^{o}C. The mean CTE of Alloy-5 with large contents of TiC and $Fe_3AlC_{0.5}$ reinforcements was found to be $1.3x10^{-5o}C^{-1}$. The thermal expansion of FeAl based alloys with different reinforcement is a complicated function of elastic and thermal properties of the individual components. Thus, the presence of TiC in FeAl based alloys significantly influenced the mean CTE of FeAl based alloys.

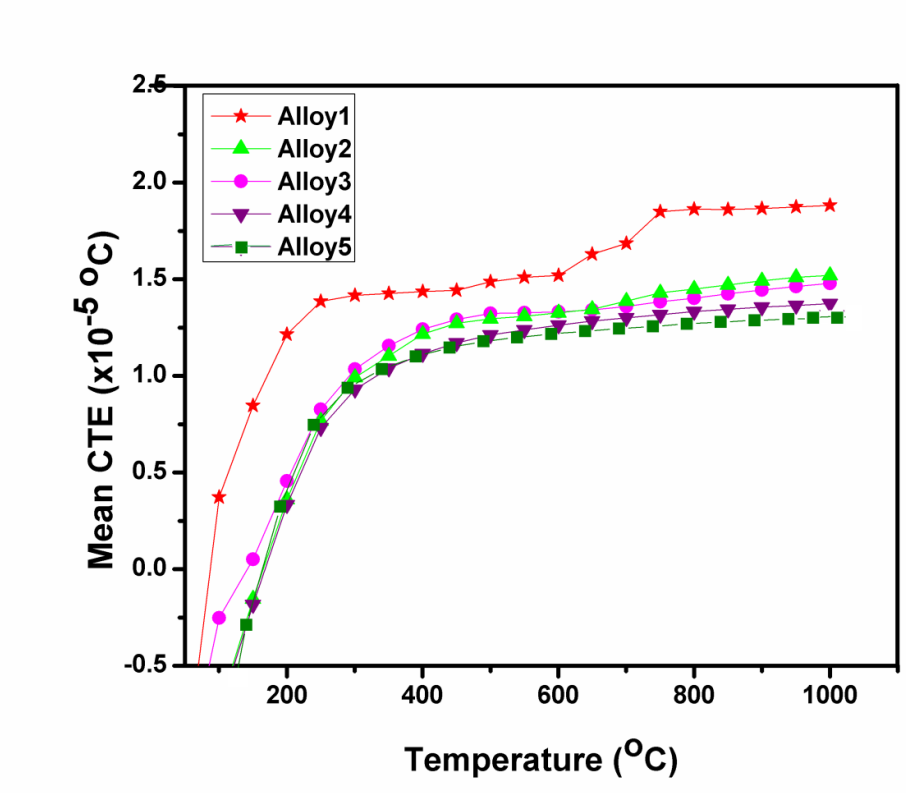

Fig. 5.9: Variation in mean CTEs of FeAl based alloys as a function of temperature.

The low solubility of precipitate phase is important parameter in ensuring resistance against coarsening at test temperature. $Fe_3AlC_{0.5}$ carbide is hardly stable at testing temperature and is readily dissolved in FeAl matrix. On the other hand, TiC carbide due to their lower solubility is hardly dissolved at testing temperature. This could bring the thermal stability to FeAl based alloys at the testing temperature.

Fig. 5.10 shows the variation in Vickers hardness of FeAl based alloys as a function of annealing time at 1123K. In initial stage, the hardness value decreased slightly due to relieving in the internal stress. At initial stage, Alloy-2 with large volume fraction of carbides than Alloy-3 exhibits higher hardness. The hardness values of Alloy-1 and Alloy-2 exhibited slight decrease with further increase in the annealing time. This could be related to decrease of $Fe_3AlC_{0.5}$ carbide content (Fig. 5.11b) due to dissolution. It was also found that $Fe_3AlC_{0.5}$ carbide dissolves in the B2 FeAl matrix at 950^{o}C [Pang 2001]. To the contrary, the addition of Ti in Alloy-3 and Alloy-4 led no significant change in hardness values with increase in the annealing time. This might be due to high melting point and thermal stability of TiC carbide particles in addition with $Fe_3AlC_{0.5}$. It was found that even after 20h annealing at 900^{o}C, the interface of TiC and FeAl matrix remain sharp (Fig. 5.11d). It indicates the thermal stability of TiC in FeAl matrix.

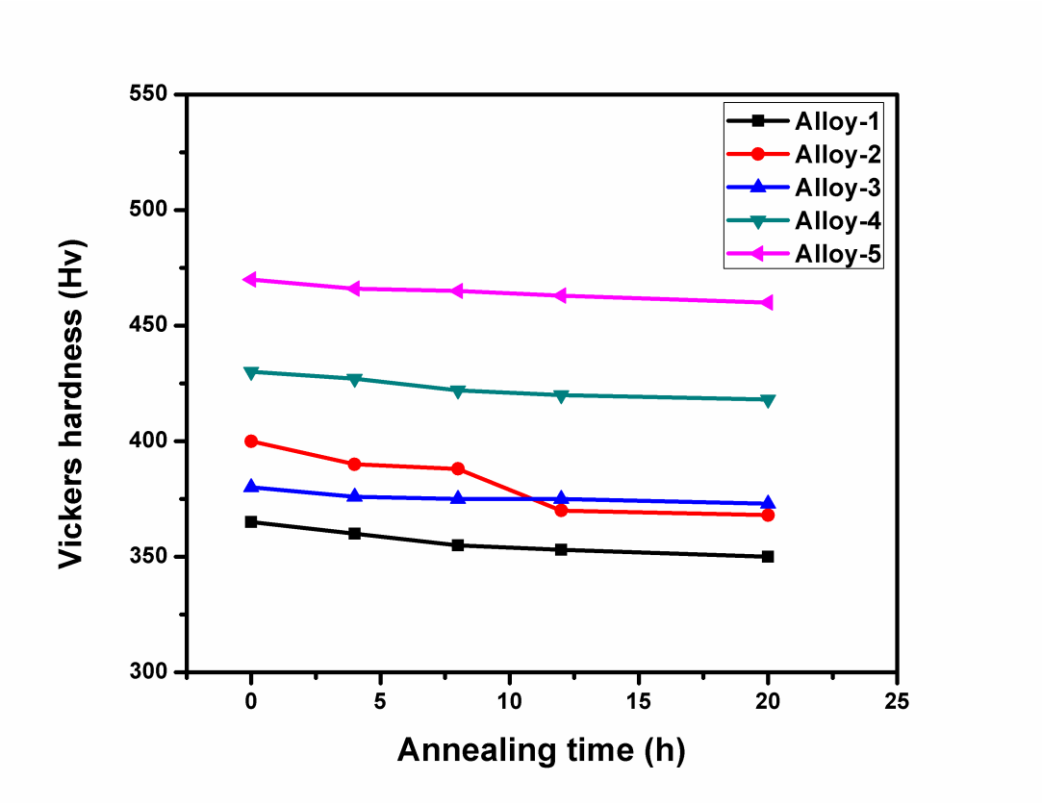

Fig. 5.10: Variation in Vickers hardness during annealing at 1173K for different hours.

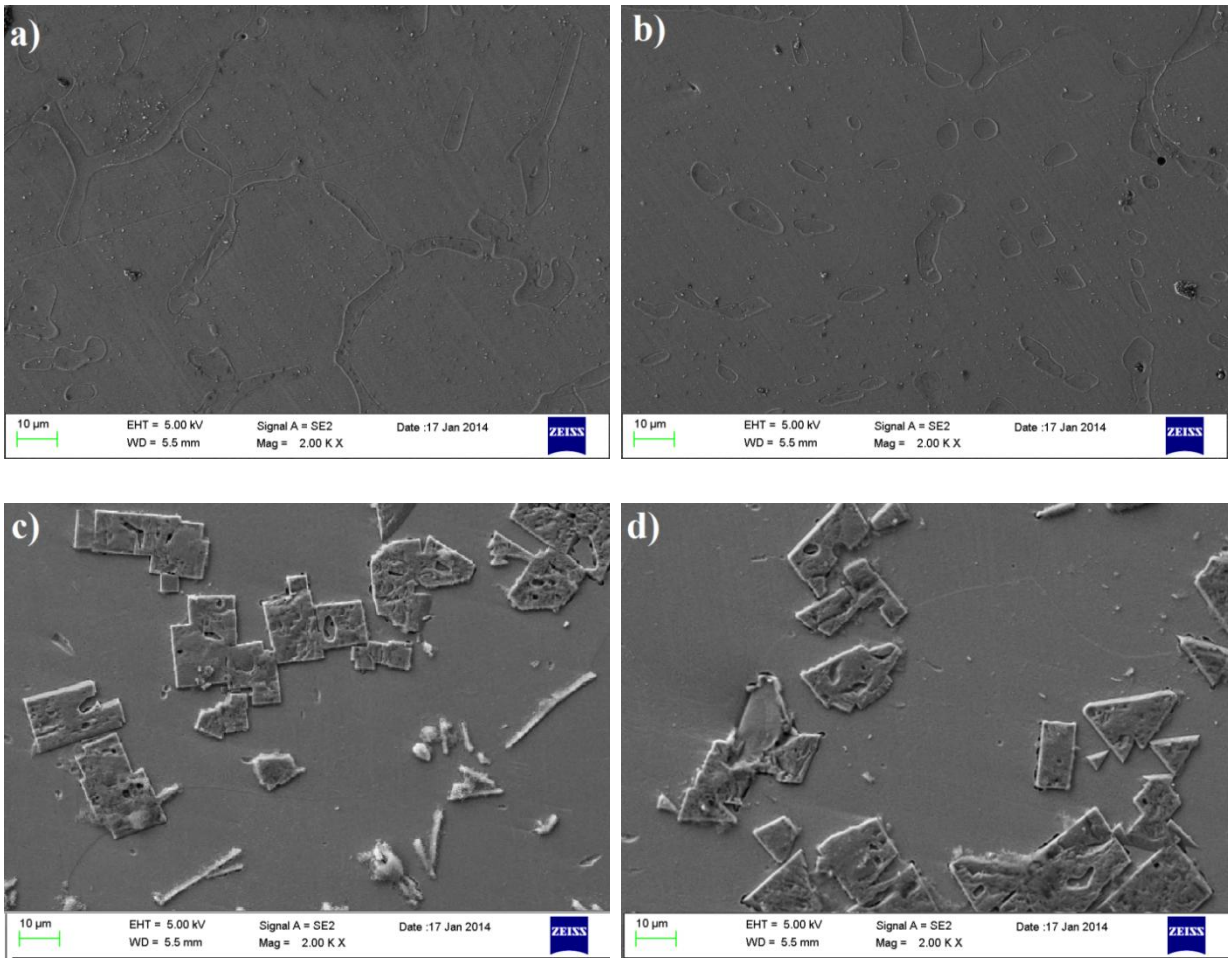

Fig. 5.11: SEM micrographs illustrating, (a) As cast sample of Alloy-2, (b) Annealed at 1173K after 12 h showing $Fe_3AlC_{0.5}$ (with nearly round shape) carbide getting dissolve in matrix of Alloy-2, (c) As cast of Alloy-4 and (d) Annealed at 1173K after 12 h showing sharp interface of TiC carbides (stable carbide) in Alloy-4.

5.4 Conclusions

- Due to graphite formation, carbon addition has not been successful for FeAl in the past. Addition of Ti to carbon containing B2 FeAl alloys prevents the formation of graphite in these alloys by forming TiC precipitates.

- Both perovskite $Fe_3AlC_{0.5}$ as well as TiC carbides were observed in the alloys investigated. The strength and hardness of B2 FeAl alloys depend on the volume fraction of different carbides which in turn depends on the levels of carbon and Ti present.

- Addition of Ti imparts strength to FeAl alloys containing carbon without loss of ductility. This can lead to successful development of carbon containing FeAl based alloys for elevated temperature structural applications.

- The order-disordered transformation of the B2 phase in FeAl based alloys have been studied. DTA studies revealed that FeAl phase to be stabilized upto ~1200 ^{o}C. Ti addition decreases the ordering temperature of FeAl based alloy slightly.

- It is found that the means of CTEs of FeAl based composites were significantly influenced by the presence of TiC in addition to $Fe_3AlC_{0.5}$ carbides. The mean CTE of FeAl with TiC (Alloy-5) was found to be $1.37x10^{-5o}C^{-1}$ in the temperature range room temperature to 1000 ^{o}C.

- Hardness seems to be dependent on the type of carbide particles. Annealing at 1173K has no significant effect on hardness in TiC reinforced alloys due to their thermal stability.

Chapter 6
Wear behavior of FeAl based alloys on carbon and titanium additions

This chapter deals with the wear behavior of FeAl based alloys. The wear resistance of iron aluminides families varies in the order of FeAl>Fe_3Al>αFe containing 11at%Al. The wear resistance of FeAl based alloys can also improved by carbon addition up to certain extent. This can be further be improved by the addition of alloying element such as Ti in FeAl based alloys containing carbon. The present chapter deals with how the wear rate of FeAl based alloys vary with carbon and Ti additions and explain the phenomenon of the wear mechanism.

Table 6.1: Nominal composition of different alloy investigated.

	Compositions (wt. %)			
S. No.	**Al**	**C**	**Ti/Zr**	**Fe**
1	22.0	0.1	---	Balance
2	22.0	1.0	---	Balance
3	22.0	0.1	1.0 (Ti)	Balance
4	22.0	1.0	5.0 (Ti)	Balance

The nominal compositions of the alloys studied are given in table 6.1. The wear tests were performed on the polished specimens using ball-on-disc testing machine. Before performing the wear test, the surface roughness of each specimen was measured using surface profiler. Fig. 6.1 shows the initial roughness of the specimens of each alloy. After performing the wear test, the depth of the wear scar was again measured by using surface profiler. The depth of wear scar of each specimen is shown in the Fig. 6.5.

The wear rate was calculated by dividing the volume of wear scar by the sliding distance and applied load according to following relation,

$$\text{Wear volume } (V) = 2\pi rdw \quad (1)$$

where V is wear volume in mm^3; r, d and w are radius, depth and width of wear scar respectively in mm.

$$\text{Wear rate } (k) = V / Ls \quad (2)$$

Where s is total sliding distance (m), L is applied normal load (N) and k is the wear rate in ($mm^3N^{-1}m^{-1}$).

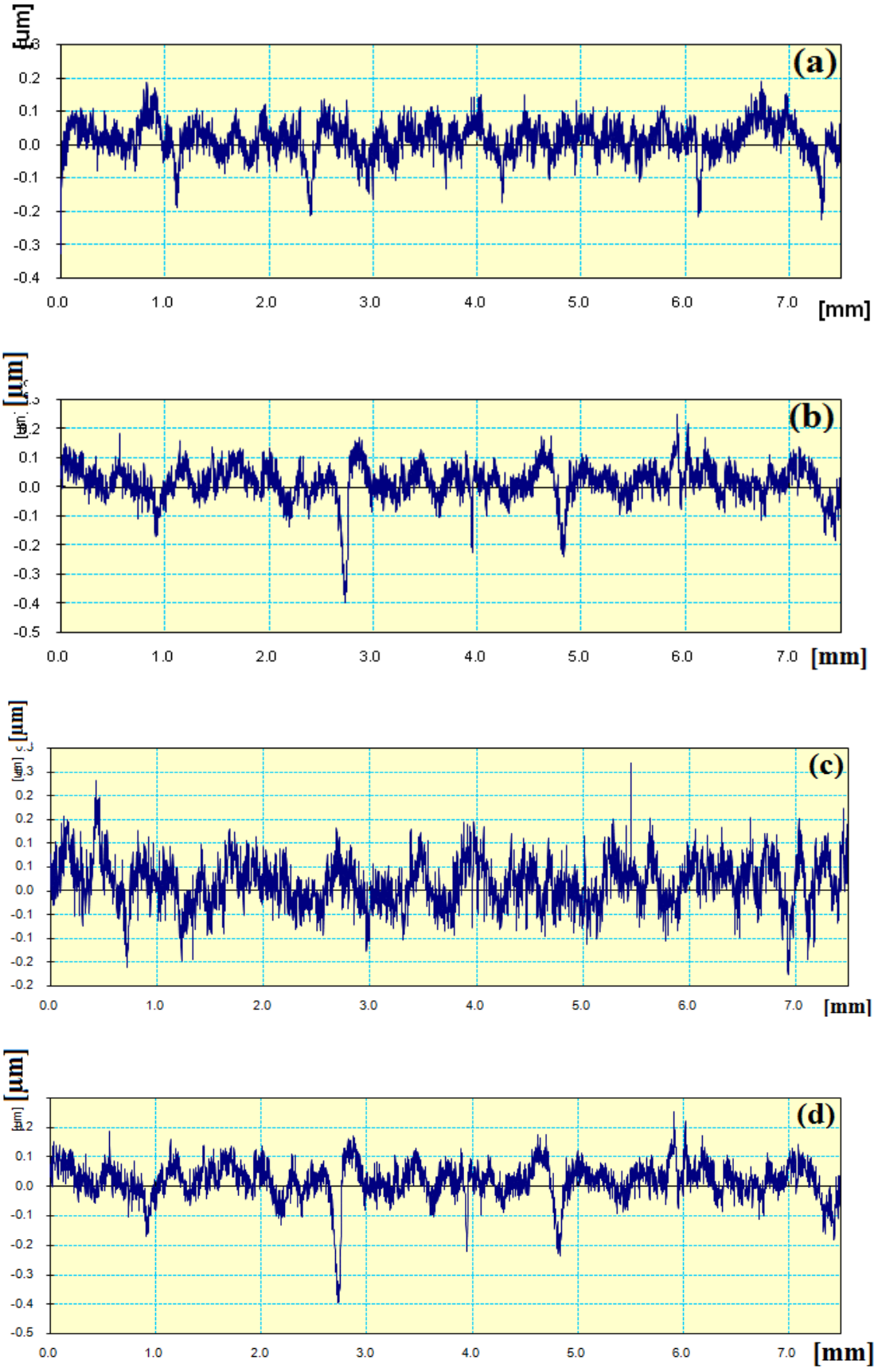

Fig. 6.1: The initial surface roughness of the specimen before performing the wear test, (a) Alloy-1, (b) Alloy-2, (c) Alloy-3 and (d) Alloy-4.

6.1 Coefficient of friction (CoF) of FeAl based alloys

Fig.6.2 shows the variation of friction coefficient of FeAl based alloys with time at constant load of 10 N with sliding speed of 0.2m/s at dry friction condition. The coefficient of friction of different FeAl based alloys lies in between 0.75 and 0.6. Generally, the coefficient of FeAl based alloys containing Ti and carbon are slightly lower than that of containing carbon only, and become steady state after initial fluctuation in all the cases. The FeAl based alloys on addition of Ti and carbon exhibit two types of carbides namely TiC and $Fe_3AlC_{0.5}$ as discussed in the previous section. This is because TiC (3000 VHN) has higher hardness as compared to $Fe_3AlC_{0.5}$ (600VHN). The high hardness of TiC causes low area in contact, which needs low energy to be sheared than that of Ti free alloys during the sliding. Also, the contact area between matrix and counterface is reduced as load is mainly shared by TiC carbides in the alloy, thus minimizing the smearing effect on the conterface surface [Liu DS 2012]. It may also be pointed out that the alloy with large volume fraction of carbides has lower friction coefficient. Thus, Alloy-1 and Alloy-2 with $Fe_3AlC_{0.5}$ having lower hardness than TiC exhibit higher fiction coefficient than alloys containing TiC carbides. Among TiC carbides containing alloys, the alloy with large fraction of carbides i.e. Alloy-4 exhibits lower friction coefficient as shown in Fig. 6.2.

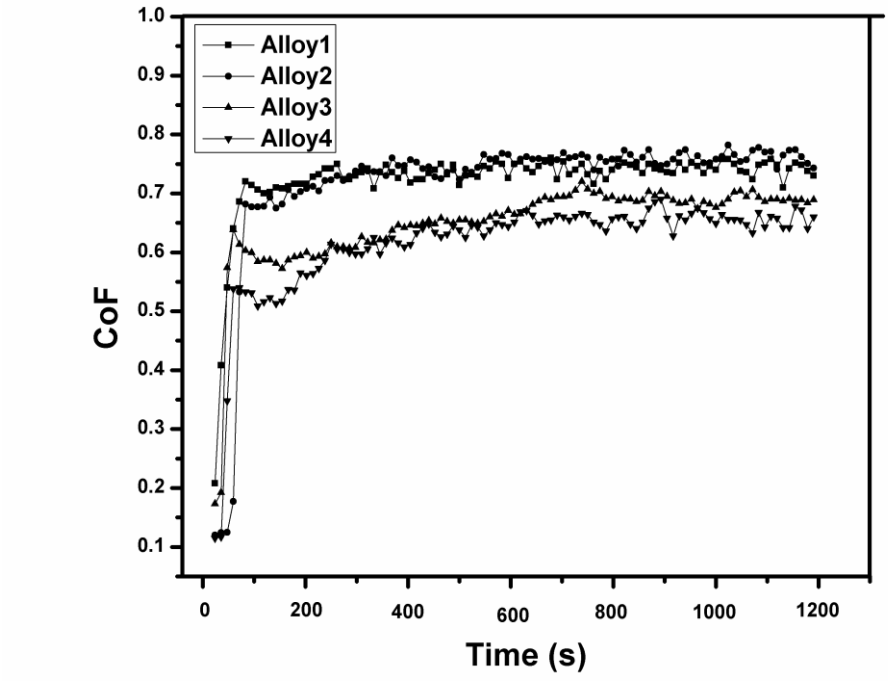

Fig. 6.2: Variation of coefficient of friction (CoF) with time of FeAl based alloys at a load of 10N and sliding speed 0.21m/s.

6.2 Effect of load on wear rate of FeAl based alloys

Fig. 6.3 shows the variation of wear rates of FeAl based alloys with applied normal loads at constant sliding speed of 0.21m/s. The wear rate of the alloys generally increases with increase in the normal load. The difference in wear rate is least when tested at lower load. Alloy-1 with low ($Fe_3AlC_{0.5}$) carbide fraction has highest wear rate. Alloy-2 has a high volume fraction of carbides than Alloy-3 but its wear rate is higher. The addition of Ti to carbon containing FeAl alloys results in the decrease in wear rate in Alloys-3 and 4. Among the alloys, Alloy-4 with large volume fraction of carbides shows the least wear rate. Contact stress on the friction surface increased with the normal load [Hogmark S 1990, Bowden EP 1954, Jahanmir S 1990], thus a few cracks would be initiated thereon in the presence of a smaller contact stress at a smaller normal load, while much more cracks would be produced and are more liable to promote propagation at higher normal load owing to the increased contact stress. Therefore wear rate of the FeAl based alloys increased with the load.

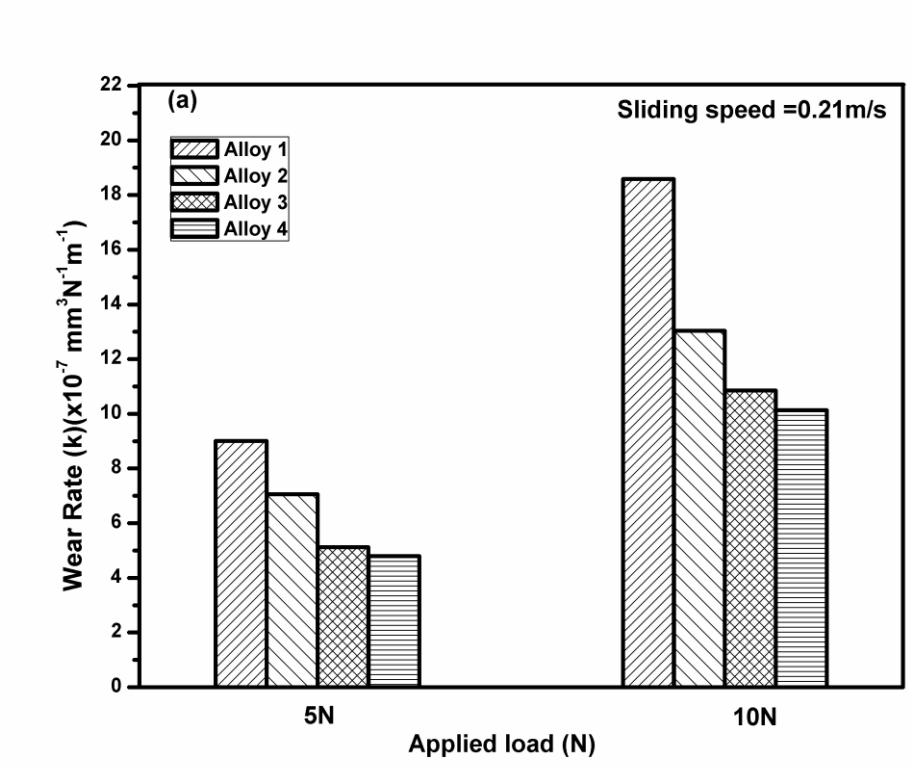

Fig. 6.3: Variation of wear rates of FeAl based alloys as function of normal loads at constant sliding speed of 0.21m/s.

The *in-situ* production of hard TiC in FeAl matrix improved the wear resistance significantly. Addition of Ti also prevents formation of graphite. The reinforcing carbide is mainly TiC in Alloy-3 and Alloy-4 as it has higher micro-hardness than $Fe_3AlC_{0.5}$. Khruschov

[Khruschov MM 1974] demonstrates that higher is the micro-hardness of the reinforcing particles, more is the wear resistance. The presence of graphite in FeAl based alloys has been reported to improve the wear resistance as graphite acts as a lubricant [Zhu SM 2002]. Alloy-2 contains large volume fraction of $Fe_3AlC_{0.5}$ carbides with few graphite flakes than TiC and $Fe_3AlC_{0.5}$ carbides in Alloy-3. Here graphite is limited to certain localized regions. These regions in Alloy-2 may be a weak center for surface removal during sliding. This overrides any effect of graphite as lubricant, thus increasing the wear rate. Also, the deformation of $Fe_3AlC_{0.5}$ carbide leads to Alloy-2 having lower wear resistance than Alloy-3 as the $Fe_3AlC_{0.5}$ carbide fraction in Alloy-3 is limited. Alloy-4 has higher volume fraction of carbides than Alloy-3 and thus shows higher wear resistance.

6.3 Effect of speed on wear rate of FeAl based alloys

Fig. 6.4 shows the variation of wear rate with sliding speed at constant load of 5N. For Alloys 1, 2 and 3 increasing speed has no significant effect on the wear rate. As the sliding speed increases, the frequency of cyclic stress increases. This may encourage initiation and propagation of flakes formation and their detachment and thus increased the wear rate. Conversely, higher sliding speed can accelerate the oxidation of worn surface which prevents the surfaces from coming into direct contact thus decreasing the wear rate. Because of these opposing factors, the effect of sliding speed at constant applied load on wear rate is not significant in the first three alloys. Alloy-4 shows increase in wear rate with increasing speed. TiC carbide in Alloy-4 has load bearing capacity due to high hardness and therefore lowers the wear rate, particularly at lower speed. At high speed the wear rate increases as the load is mainly carried by TiC and this may reduce the oxidation of matrix surface.

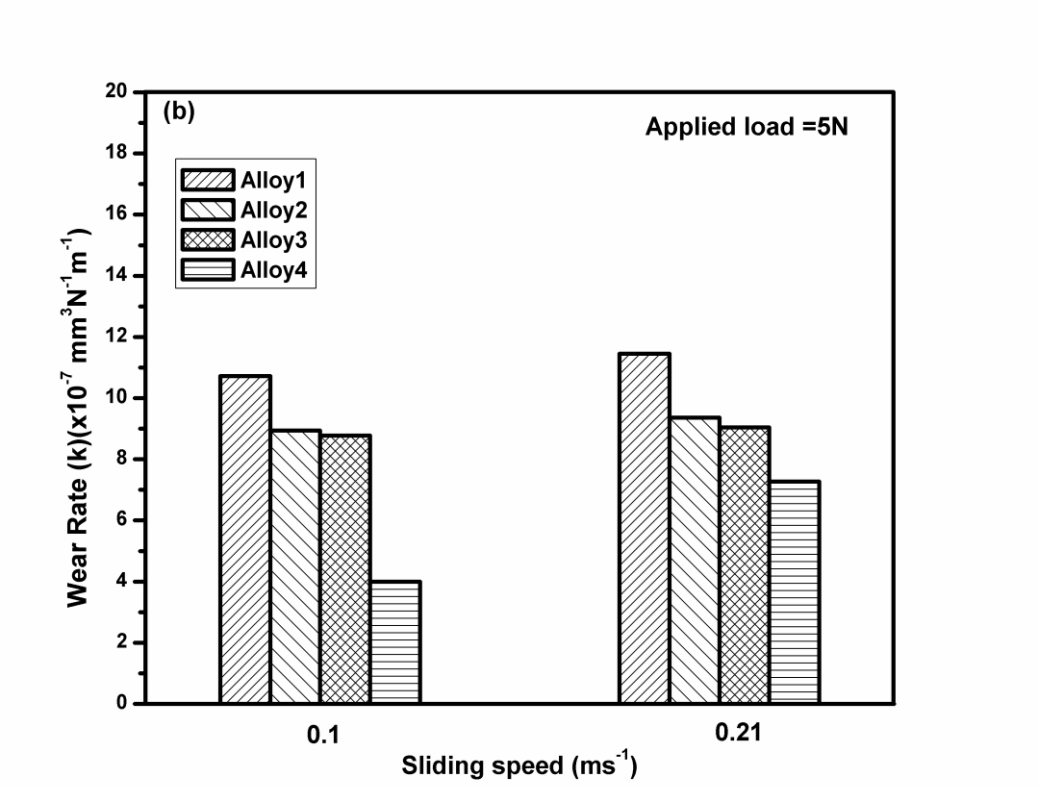

Fig. 6.4: Variation of wear rates of FeAl based alloys as function of sliding speeds at constant normal load of 5N.

Fig. 6.5 shows the profilometer traces across the wear scars on discs of the different alloys. The depths of the wear scars after sliding wear tests of different FeAl alloys are observed to be different and increased with the applied normal load. The scar on the disc of Alloy-1 after wear test is deeper than those in other alloys. Alloy-2 and Alloy-3 have comparable depth of wear scars. The depth of the wear scar after the wear test in Alloy-4 is least. These results are consistent with the wear rate of FeAl based alloys in the present investigation (Fig. 6.3). Similar trends in the depth of wear scars were also found when we measured with sliding speeds. The sliding speed has no significant effect on the depth of wear scars.

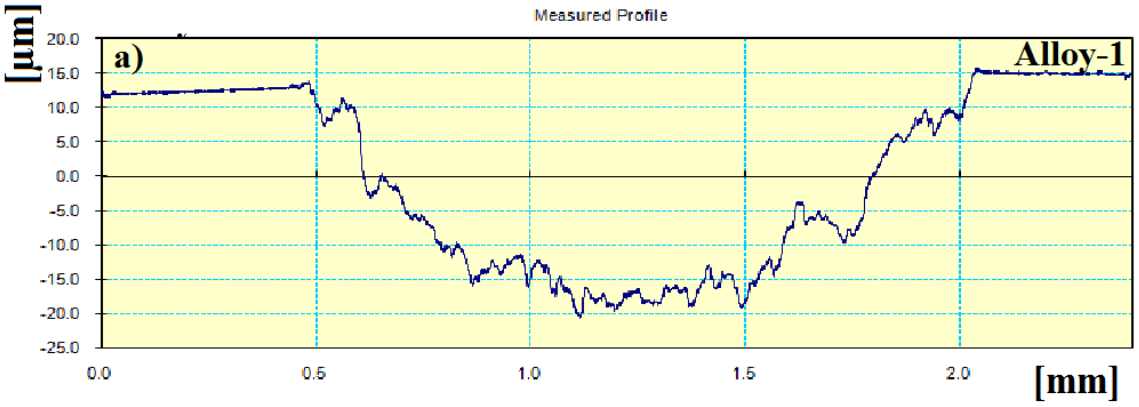
Measured Profile
a)
Alloy-1
[µm]
20.0
15.0
10.0
5.0
0.0
-5.0
-10.0
-15.0
-20.0
-25.0
0.0
0.5
1.0
1.5
2.0
[mm]

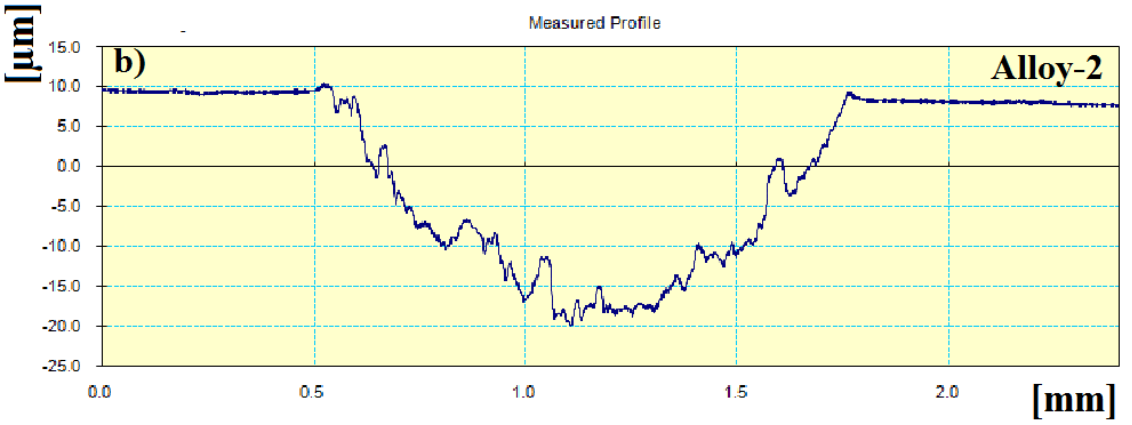
Measured Profile
b)
Alloy-2
[µm]
15.0
10.0
5.0
0.0
-5.0
-10.0
-15.0
-20.0
-25.0
0.0
0.5
1.0
1.5
2.0
[mm]

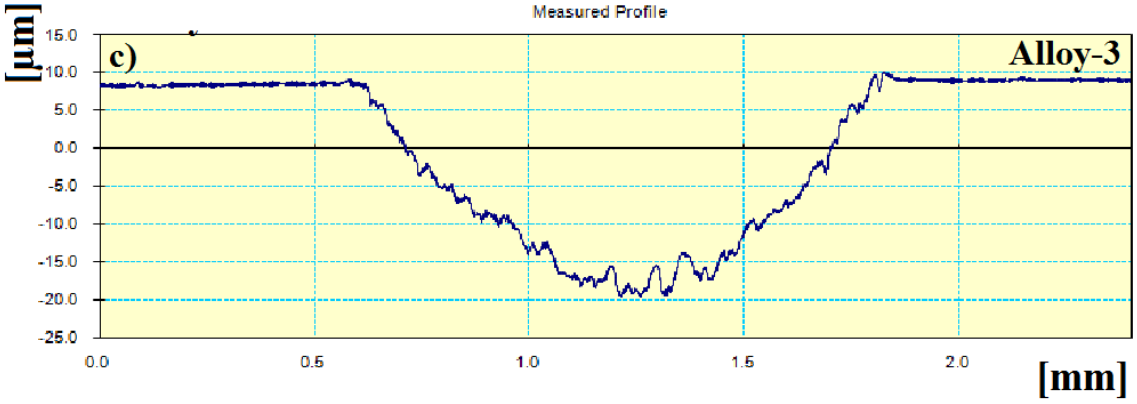
Measured Profile
c)
Alloy-3
[µm]
15.0
10.0
5.0
0.0
-5.0
-10.0
-15.0
-20.0
-25.0
0.0
0.5
1.0
1.5
2.0
[mm]

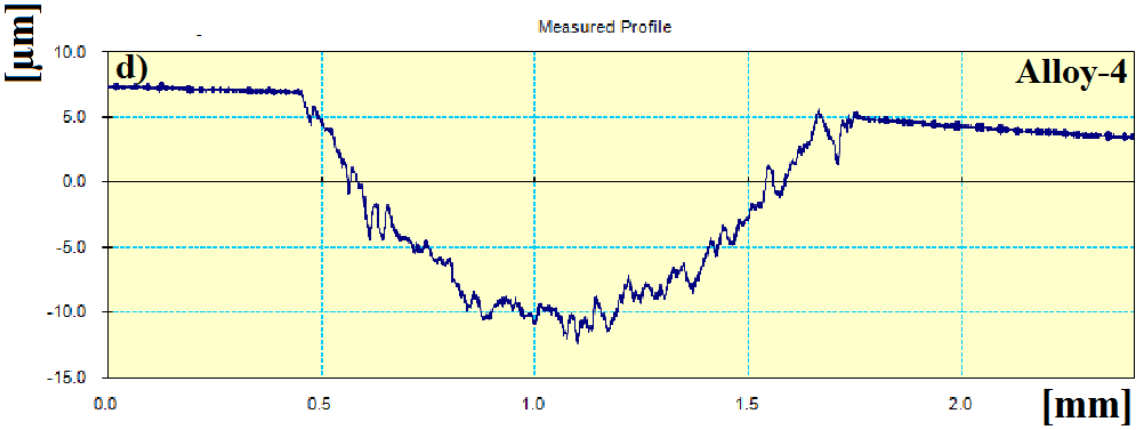
Measured Profile
d)
Alloy-4
[µm]
10.0
5.0
0.0
-5.0
-10.0
-15.0
0.0
0.5
1.0
1.5
2.0
[mm]

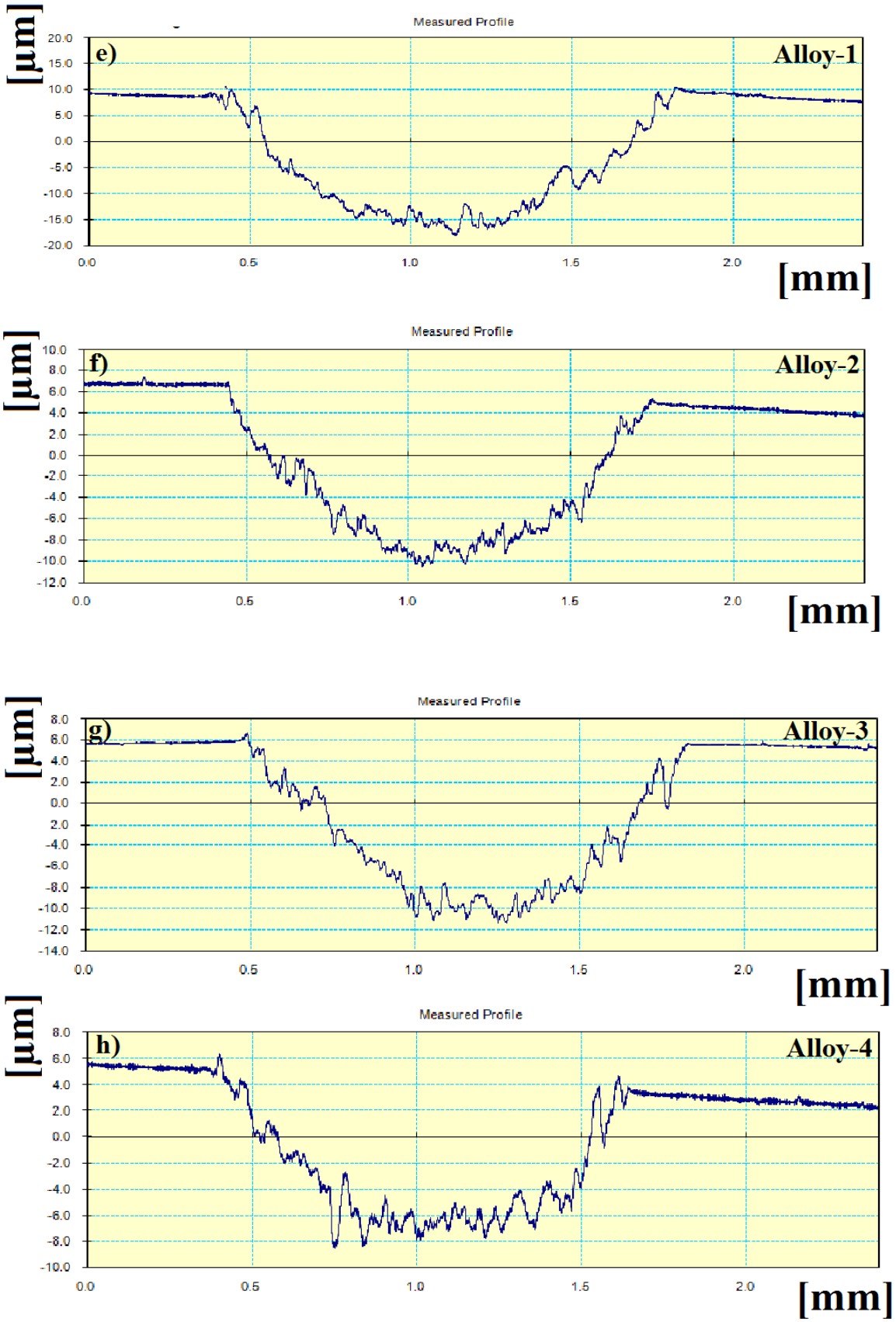

Fig. 6.5: Profilometer traces across the wear scars on the disc with sliding speed 0.1m/s at normal load of 5N, (a-d) and 10N (e-h) respectively.

6.4 Wear mechanism

Wear scars examined under SEM for all the alloys tested with applied loads of 5N and 10N at sliding speed of 0.21 m/s after sliding for 20 minutes i.e. the sliding distance 252 metres is shown in Fig. 6.6. It can be seen from the worn surfaces of all FeAl based alloys, the surfaces are covered by micro-groves and flaking pits. The worn surfaces is characterized by severe grooves at lower load which indicating that the wear mechanism is ploughing. While at higher load, the wear surfaces are characterized by micro-groves and detaching flakes suggesting that the wear mechanism is ploughing and delaminating.

The worn surfaces of Alloy-1 and Alloy-2 tested under applied normal load are extremely rough with large and deep wear grooves and adhesive wear features, as shown in Fig. 6.6a-d. The worn surface of the TiC containing alloys tested at same wear conditions is relatively smooth with few adhesive wear features (Fig. 6.6e-h). It is worth noting that the worn surface of Alloy-4 tested at same conditions is very smooth with no appreciable grooving or adhesive characteristics, as shown in Fig. 6.6g and h.

The surface deformation becomes more severe on increasing the normal load. Micro ploughing in the sliding direction was observed for all the samples at lower load. This effect was found more prominent in Alloy-1 as it contains least amount of carbides. But in Alloy-2, it contains large fraction of carbides with few graphite flakes. The graphite flakes in Alloy-2 may be a weak center for surface removal during sliding. Moreover, the lower hardness of $Fe_3AlC_{0.5}$ carbide results deformation in the sliding direction. This results in the micro ploughing in the alloy. The alloy surface is easily deformed and ploughed deeply due to lower hardness of $Fe_3AlC_{0.5}$ carbide in titanium free alloys. Therefore, large chips and their detachments can be observed (Fig 6.6a-d). As the load increases, the micro ploughing along with detachment of surface platelets was found to be the dominant mechanism (Fig. 6.6). These observations revealed that the wear occurs mainly due to plastic deformation. Similar phenomenon has been observed in Fe-28Al alloy [Guan X 2004]. In contrary to this, the alloys with titanium addition turn out to be smooth with shallow ploughing (Fig 6.6e-h). This difference is mainly occurred due to presence of TiC carbides on titanium addition. The applied load is mainly carried by hard TiC carbide in the after few seconds of the sliding. Thus, the matrix of alloys remains unaffected during the sliding. As a result, micro ploughing and deformation phenomenon become less effective in TiC containing alloys.

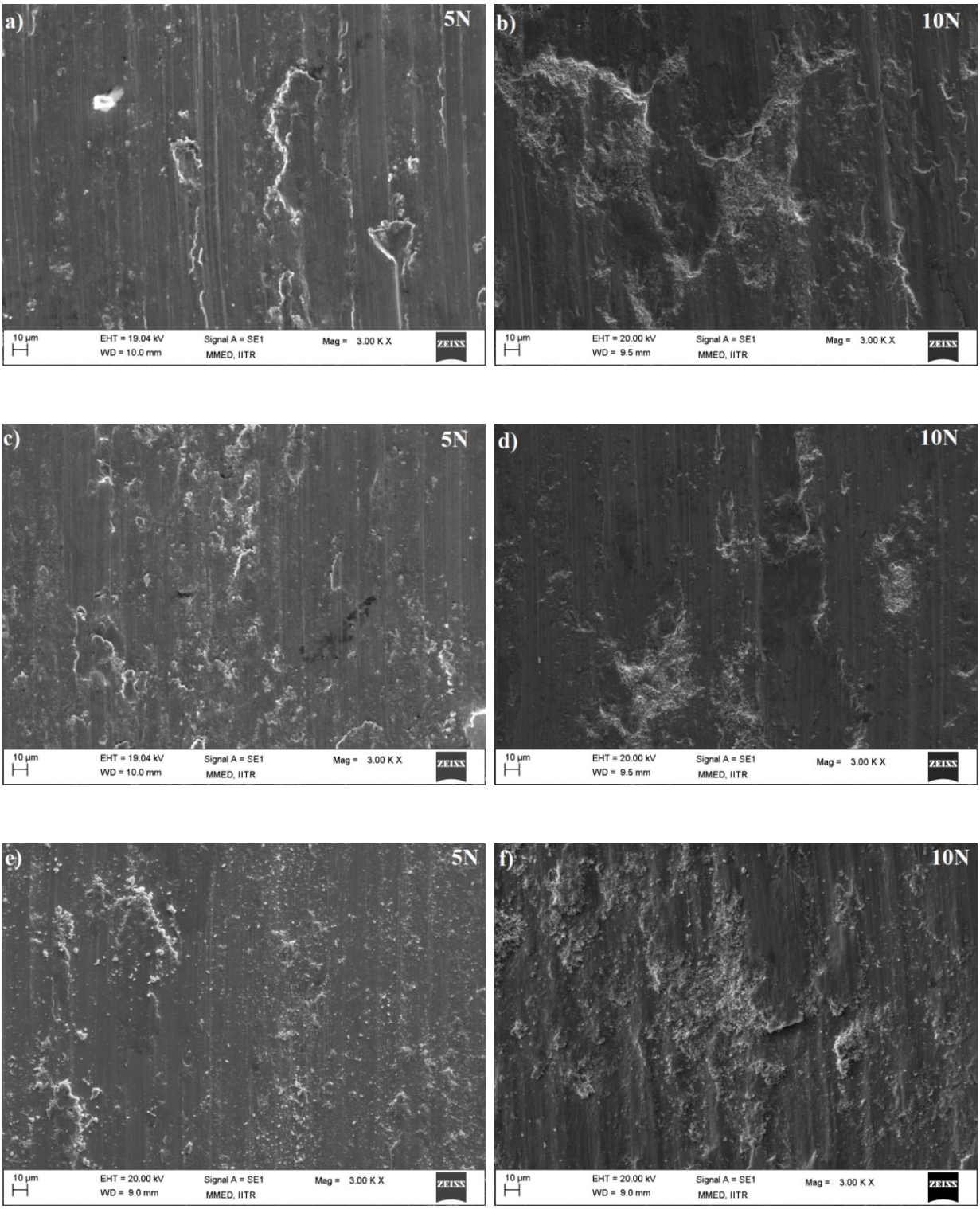
a)
5N
10 µm
EHT = 19.04 kV
WD = 10.0 mm
Signal A = SE1
MMED, IITR
Mag = 3.00 K X
ZEISS
b)
10N
10 µm
EHT = 20.00 kV
WD = 9.5 mm
Signal A = SE1
MMED, IITR
Mag = 3.00 K X
ZEISS
c)
5N
10 µm
EHT = 19.04 kV
WD = 10.0 mm
Signal A = SE1
MMED, IITR
Mag = 3.00 K X
ZEISS
d)
10N
10 µm
EHT = 20.00 kV
WD = 9.5 mm
Signal A = SE1
MMED, IITR
Mag = 3.00 K X
ZEISS
e)
5N
10 µm
EHT = 20.00 kV
WD = 9.0 mm
Signal A = SE1
MMED, IITR
Mag = 3.00 K X
ZEISS
f)
10N
10 µm
EHT = 20.00 kV
WD = 9.0 mm
Signal A = SE1
MMED, IITR
Mag = 3.00 K X
ZEISS

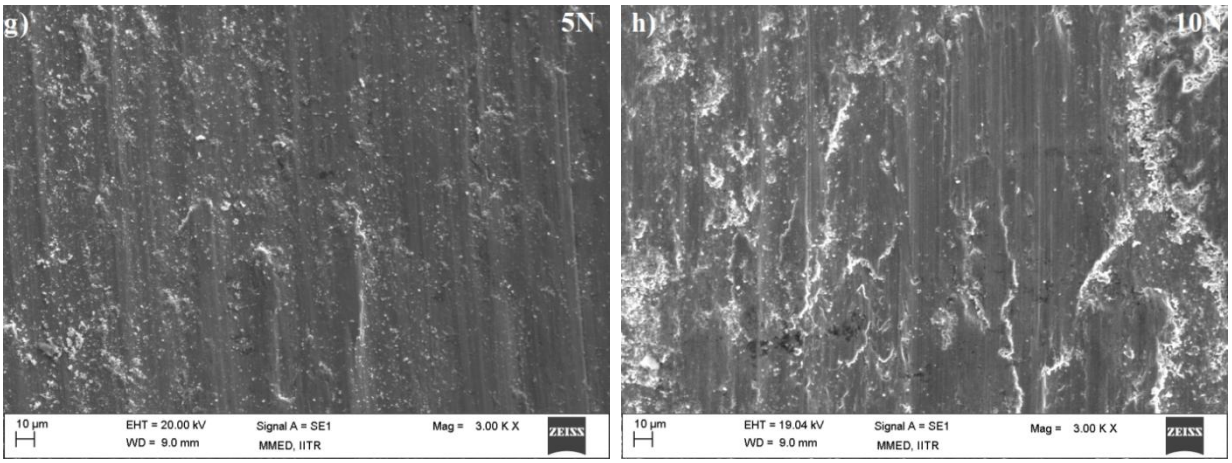

Fig. 6.6: Wear scars for alloys tested with applied loads of 5N and 10N, (a and b) Alloy-1, (c and d) Alloy-2, (e and f) Alloy-3, (g and h) and Alloy-4.

From Fig. 6.7, it is clear that the worn surfaces of Alloy-1 and Alloy-2 tested under different sliding speeds undergo deep wear grooves and adhesive wear features. The worn surface of the TiC containing alloys tested at same wear conditions is relatively smooth with few adhesive wear features (Fig. 6.7e-h). It is worth noting that the worn surface of Alloy-4 tested at same conditions has very less grooving or adhesive characteristics, as shown in Fig. 6.7g and h.

During the dry sliding wear the asperities on metallic surfaces are in contact. The hardness near these contacts quickly decreases due to local temperature increase at these contact points. Their severe plastic deformation takes place followed by detachment of material. The presence of hard TiC phase raises the capability to resist serious plastic deformation under severe conditions. Thus, during sliding the applied load is transferred to hard carbide particles thereby decreasing the material removal. The relatively smooth worn surface and lower coefficient of friction of TiC containing alloys demonstrates the strong bonding between particle and the matrix which impart excellent resistance to plastic deformation.

The carbides such as $Fe_3AlC_{0.5}$ and TiC are formed by *in-situ* process in FeAl matrix thereby promoting a strong carbide-matrix bonding. *In-situ* formation of Al_2O_3 in FeAl has been reported to improve bonding between the matrix and reinforcement [Subramanian R 1997]. The wear test results indicate that carbides support the load bearing capacity and there is a good bonding between the reinforcing carbides ($Fe_3AlC_{0.5}$ and TiC) and FeAl matrix. This can reduce the easy pull-out of the carbide particles from the matrix during sliding. The

formation of surface platelets on the wear scar is retarded by the presence of the hard TiC particles and therefore reduces the wear rate.

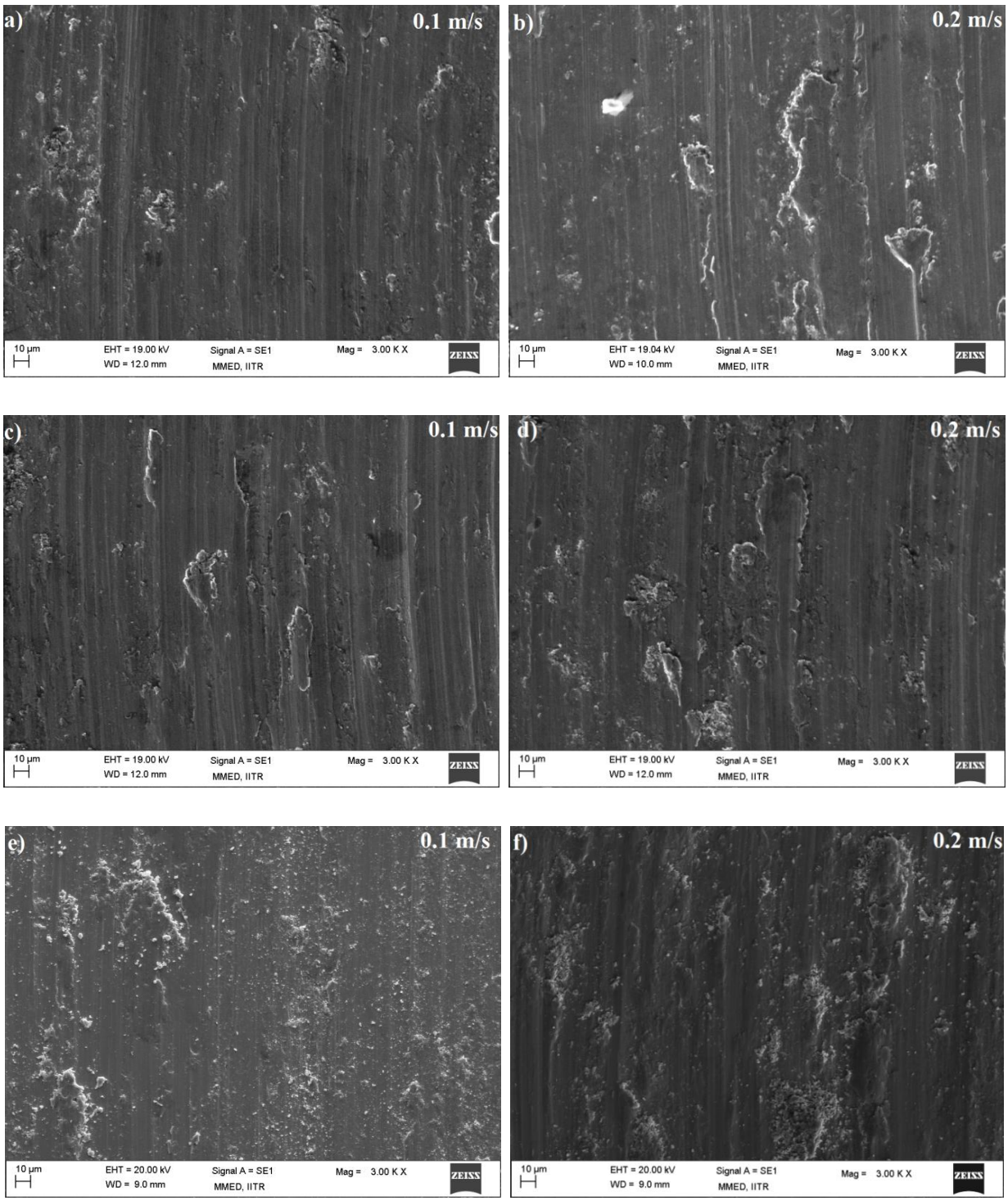

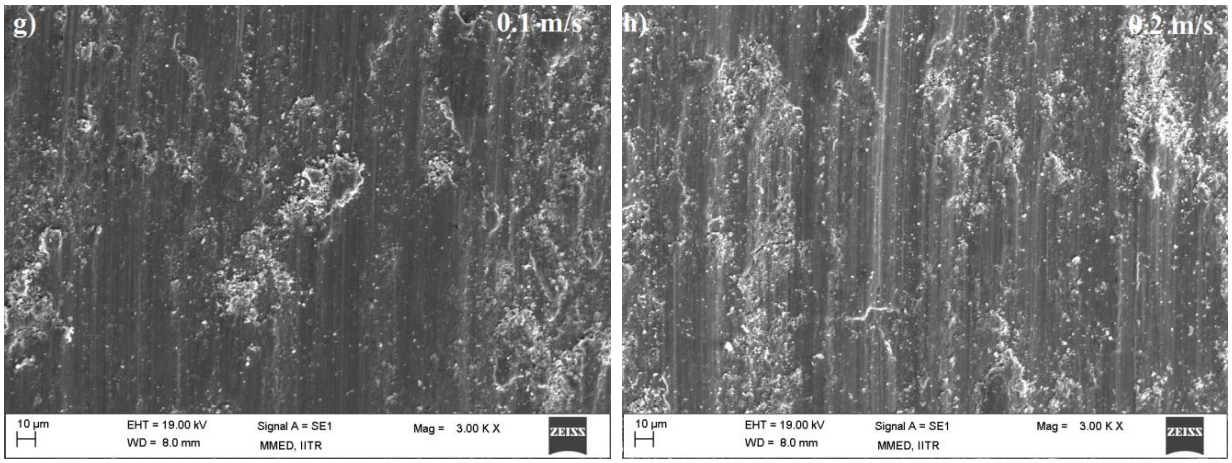

Fig. 6.7: Wear scars for alloys tested with applied loads of 0.1 and 0.21m/s, (a and b) Alloy-1, (c and d) Alloy-2, (e and f) Alloy-3 and (g and h) Alloy-4.

Figure 6.8 shows the transverse section of worn scars and confirms that the carbides are still seen embedded in the matrix phases after the sliding wear without delamination or destruction. The elongated (k-perovskite) $Fe_3AlC_{0.5}$ carbide is slightly deformed along wear direction by sliding wear at room temperature (Fig.6.8a). This deformability of $Fe_3AlC_{0.5}$ phase in Alloy-2 would bring about almost same friction coefficient as in low carbon alloy (Alloy-1) and also increases the wear rate than Alloy-3. In Alloy-4, TiC particles are embedded in the FeAl matrix after sliding wear under 10N load without any deformation (Fig. 6.8b).

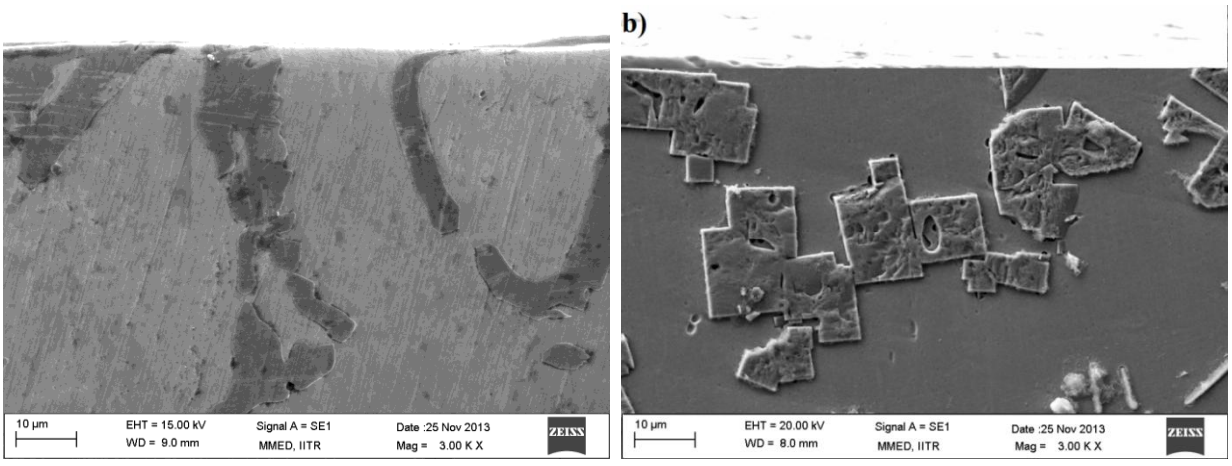

Fig. 6.8: Transverse section of worn scars of FeAl based alloys at applied load 10N, a) Alloy-2 with $Fe_3AlC_{0.5}$ and b) Alloy-4 with hard TiC.

The hardness of TiC are higher than that of $Fe_3AlC_{0.5}$ phase, therefore it is suggested that the uniform distribution of TiC particles in the FeAl matrix may work more effectively for wear resistance applications. TiC particles may inhibit the plastic deformation of surface layer to some extent and the subsequent material removal, thus enhancing the wear resistance of Alloy-3 and Alloy-4. Improvement of tribological properties of FeAl based alloys with addition of Ti can be attributed mainly due to strengthening effect of TiC precipitates. Ti addition also increases the matrix microhardness probably due to solid solution strengthening. TiC reinforced matrix are expected to combine the wear resistance and high temperature properties of ceramic phase with the engineering properties of intermetallics to perform at high temperature applications. It has been shown using phase equilibria calculations, that liquid FeAl at 1450^{o}C is compatible with TiC [Misra AK 1990, Joachim H 1999].

6.5. Effect of carbon to Fe-22Al-5Ti alloy

The nominal compositions of the alloys are given in table 6.2. Fig. 6.9 (a-c) shows the as cast microstructures of Fe-22Al-5Ti with different carbon contents. The cast alloys generally had fine grained structure, and there were new phases in the carbon added alloys. At low carbon addition (Fig.6.9a), only TiC precipitates were observed while at higher carbon contents (Fig.6.9b and Fig.6.9c), the phases identified to be TiC and $Fe_3AlC_{0.5}$.

Table 6.2: Nominal composition of different alloy investigated.

	Compositions (wt. %)			
S. No	**Al**	**C**	**Ti**	**Fe**
1	22.0	0.1	5.0	Balance
2	22.0	1.0	5.0	Balance
3	22.0	1.5	5.0	Balance

The volume fraction of precipitates was found to increase with increase in the carbon content. Addition of carbon leads the precipitation of TiC in addition with $Fe_3AlC_{0.5}$. XRD and EDAX results confirmed the presence of these carbides in chapter 5 (pages 64 and 67). From the liquid state, TiC-type carbide with high melting point and large free negative energy of formation may precipitate as primary phase from the liquid. Thus, at low carbon content (0.1wt%C) only TiC precipitates were observed. With further addition of carbon, TiC was first formed then followed by $Fe_3AlC_{0.5}$ precipitates form following solidification with decrease in temperature. Thus, these precipitates form by solid state reaction.

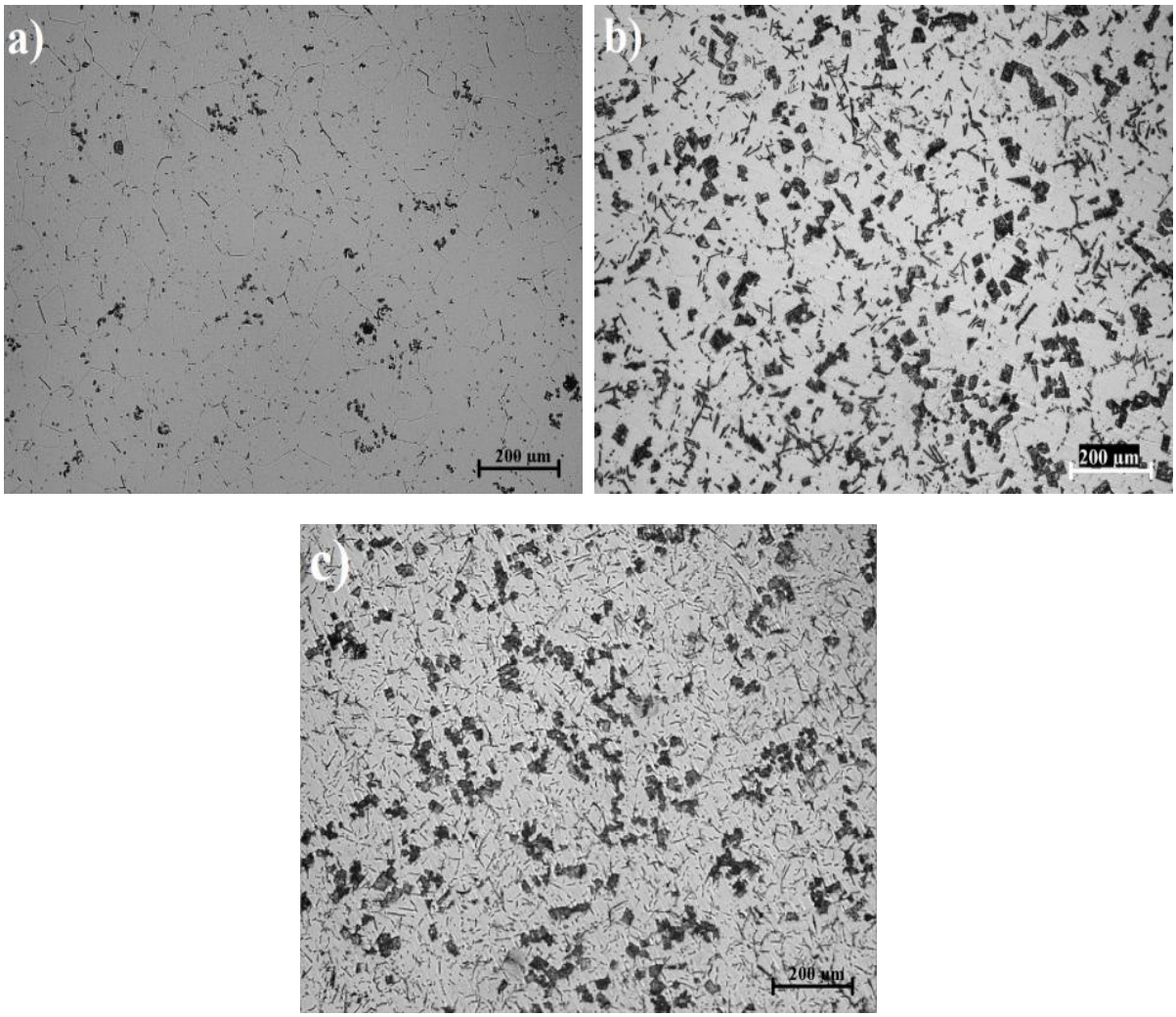

Fig.6.9: Optical micrographs of Fe-22.0Al-5.0Ti alloys showing as cast structure, (a) 0.1wt%C, (b) 1.0wt.%C and (c) 1.5wt.%C.

Table 6.2 shows the volume fraction, Vickers hardness and compressive strength of Fe-22Al-5Ti with different carbon content. The hardness exhibited the significant increase with increasing in carbon content. This could be attributed the increase in the volume fractions of TiC and $Fe_3AlC_{0.5}$ precipitates. Since both TiC and $Fe_3AlC_{0.5}$ are hard and brittle and could strengthen the matrix. The microhardness matrix has no significant effect on carbon addition. The different precipitates i.e. TiC and $Fe_3AlC_{0.5}$ have microhardness values 3000 VHN and 610VHN respectively. The compressive strength of Fe-22Al-5Ti alloy was significantly increased with increasing in the carbon content. This could also be attributed to the different precipitates namely TiC and $Fe_3AlC_{0.5}$.

Table 6.3: Bulk hardness, volume fraction and compressive strength of alloys.

Alloy	Alloy composition (wt %)	Hardness (VHN)	Volume fraction of phases (%)	Compressive Strength (MPa)
1	Fe-22.0Al-5.0Ti-0.1C	380	5-8	780
2	Fe-22.0Al-5.0Ti-1.0C	425	18-20	1050
3	Fe-22.0Al-5.0Ti-1.5C	470	24-27	1200

The wear tests were performed on the polished specimens using ball-on-disc testing machine. Before performing the wear test, the surface roughness of each specimen was measured using surface profiler. Fig. 6.9 shows the initial roughness of the specimens of each alloy.

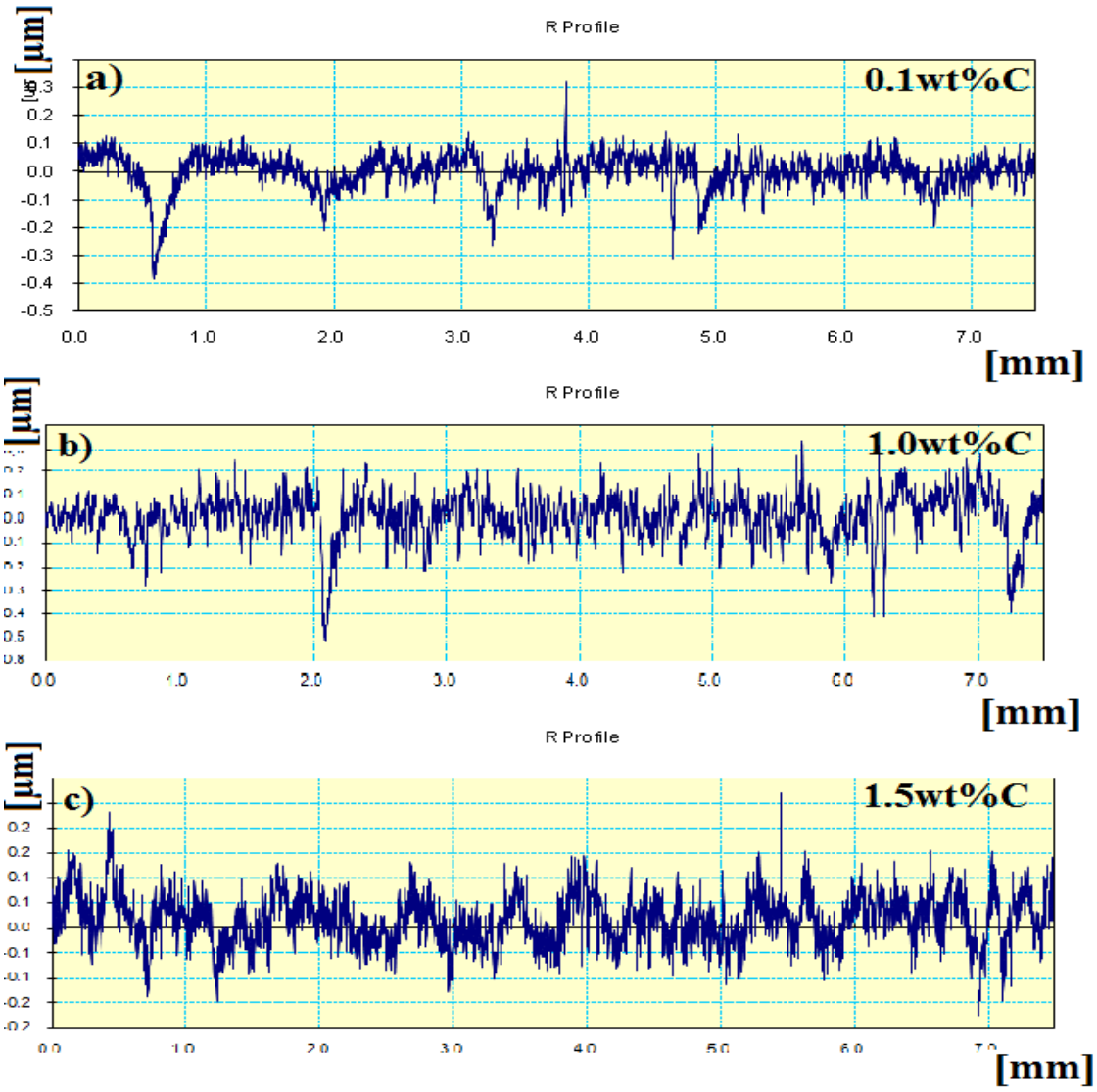

Fig.6.10: The initial surface roughness of the each specimen of Fe-22Al-5Ti alloy before performing the wear, (a) 0.1wt%C, (b) 1.0wt%C and (c) 1.5wt%C.

Figure 6.11 represents the variation of room temperature wear rate of Fe-22Al-5Ti alloys with different carbon contents at applied load. The wear rate of alloys was found to increase with applied load. With increase in the carbon contents, the wear rate decreases. It is evident that the wear resistance property of composites is not dictated by hardness alone. It also depends on microstructural parameters like size, shape, volume fraction and distribution of embedded particles and the interfacial bonding between the two phases [Pagounis 1997]. Low wear rate of high carbon based alloy may be attributed to the fact that they contain uniform distribution of $Fe_3AlC_{0.5}$ and TiC having hardness 610 and 3000 VHN respectively. Khrushov [Khrushov 1974] suggests that wear resistance of composite material increase with hardness of reinforcing particles. Thus, higher is the hardness of the reinforcing particle, better will be the wear resistance. Moreover, the large volume fraction of reinforcing particles also reduced the wear rate with identical conditions. Thus, the alloy with high volume fraction of TiC and $Fe_3AlC_{0.5}$ precipitates exhibits low wear rate.

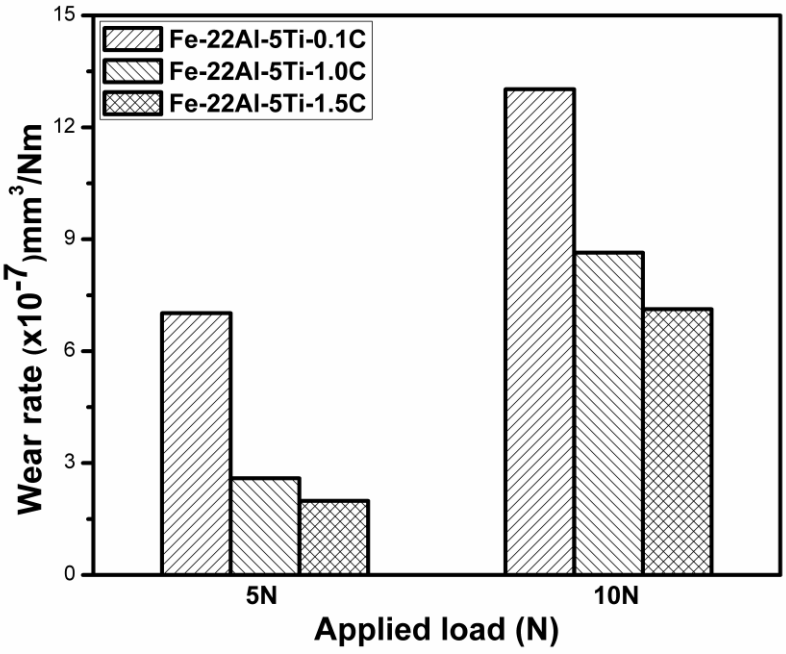

Fig. 6.11: Comparative wear rate of Fe-22Al-5Ti alloys with different carbon contents at various loads.

The micrographs show microploughing in the sliding direction tested at low load and detachment of thin surface platelets tested at high load. Few sharp lines along the sliding direction on wear scar are evident of microploughing, so that the worn surfaces show typical abrading. The behavior in all alloys during wear appears to be very similar. Generally, the

applied load increased the contact stress on the friction surface. At low applied load, the contact stress would initiate few cracks in friction surface (Fig. 6.12) and would be produced and are more liable to promote propagation under higher applied load. Therefore, the wear rate of Fe-22Al-5Ti alloys increases with the increase of applied load. The cross sectional area across the wear scar shows that the precipitates are still embedded in the matrix even after the wear without delamination (Page 97). This demonstrates that the secondary precipitates affect the wear rate of the alloy significantly.

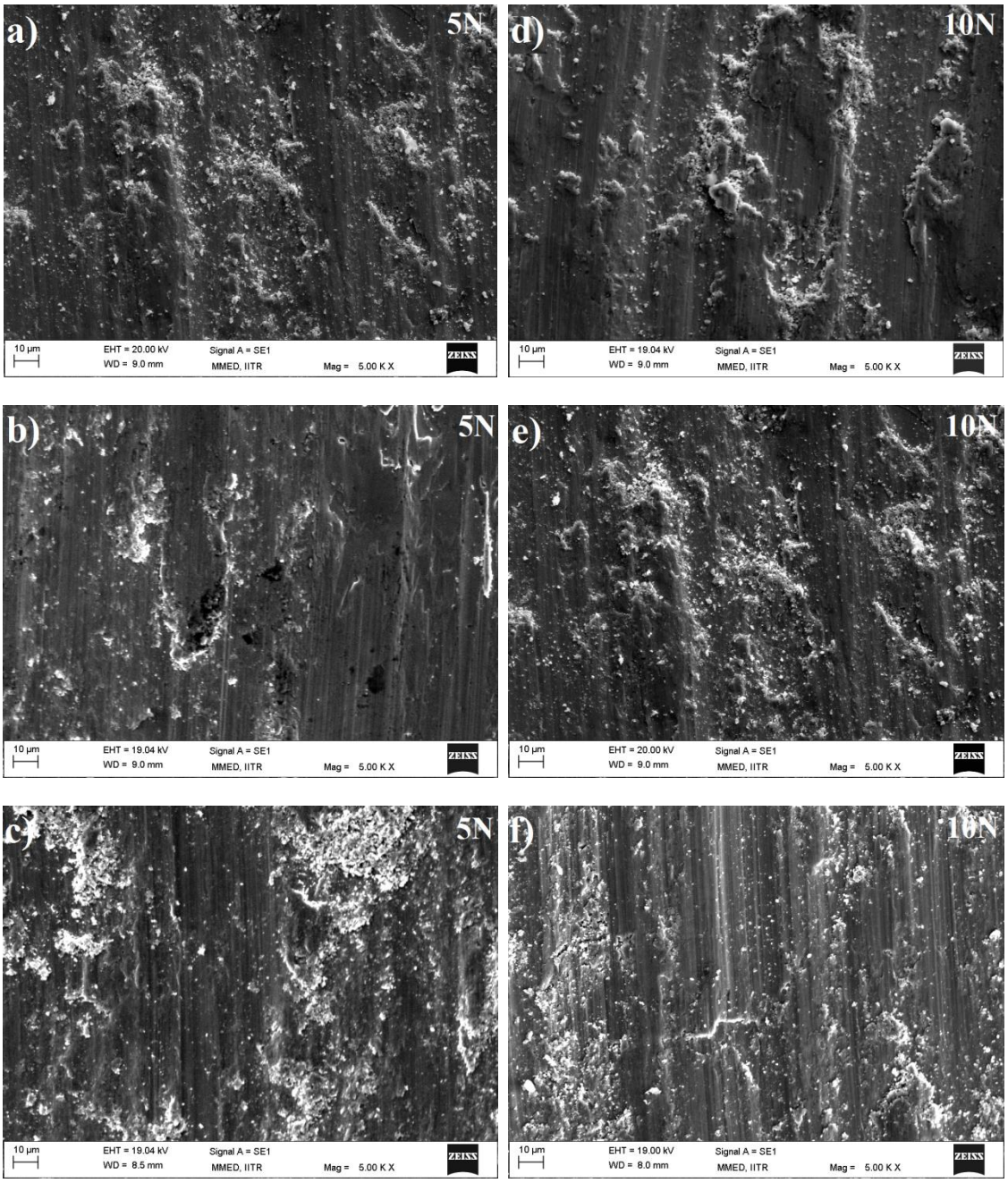

Fig. 6.12: Wear scars for Fe-22Al-5Ti alloy tested at applied loads of 5N and 10N, (a and b) 0.1wt%C, (c and d) 1.0wt.%C and (e and f) 1.5wt.%C.

6.6 Conclusions

1) Carbon addition to FeAl alloys results in formation of perovskite-type $Fe_3AlC_{0.5}$ carbide phase and graphite. Addition of Ti promotes the formation of TiC and $Fe_3AlC_{0.5}$ and prevents the formation of graphite in the alloy. The volume fraction of both carbides increases with increase in the contents of C and Ti. This significantly affects wear behaviour of these alloys.

2) The *in-situ* precipitation of TiC carbides on addition Ti results in the improvement in wear resistance of FeAl based alloys. This may be attributed to the increase in the matrix hardness due to solid solution strengthening and formation of hard TiC with $Fe_3AlC_{0.5}$ carbides. The wear resistance is also found to increase with increase in the volume fraction of TiC carbides with $Fe_3AlC_{0.5}$.

3) The coefficient of friction of FeAl alloys reinforced with TiC and $Fe_3AlC_{0.5}$ carbides is lower than FeAl alloys containing $Fe_3AlC_{0.5}$ carbides only, which may be attributed to high hardness of TiC. This results in decrease of the coefficient of friction of FeAl based alloys from 0.75 to 0.6. Further, deformation of $Fe_3AlC_{0.5}$ carbides may lead to higher coefficient of friction.

4) The *in-situ* precipitation of carbides provides the strong bonding between the FeAl matrix and carbides. The carbides are found to be embedded in the matrix without any delamination after sliding wear studies. This helps in achieving better wear resistance. This *in-situ* precipitation of carbides overrides the composites produced by powder metallurgy route which offers the direct inclusion of carbide particles and results in weak bonding between the matrix and second phase particles.

5) It is also observed that presence of graphite in localized regions reduces the wear resistance of alloy due to lower load bearing capacity.

6) At low carbon (0.1wt%C) addition to Fe-22Al-5Ti alloy, results in precipitation of TiC phase. With further higher addition of carbon (1.0 and 1.5wt%C) resulted in the precipitation of hard TiC and $Fe_3AlC_{0.5}$ phases. The volume fraction of different phases increases with increase in the carbon content. The hardness and strength of Fe-22Al-5Ti

alloy appear to be determined by the presence of the volume fraction of different phases.

7) Increase in the carbon content from 0.1 to 1.5 wt% has resulted in the reduction in the wear rate. This may be attributed to the presence of hard TiC and $Fe_3AlC_{0.5}$ phases. The wear rate Fe-22Al-5Ti alloy increase with increased in applied load.

Chapter 7
Comparative studies of FeAl based alloys on different alloying elements (titanium and zirconium) additions

From the previous chapters studies, it is concluded that Ti addition to FeAl based alloys containing carbon are helpful in improvement in the mechanical properties. The present chapter deals with Zr addition to FeAl alloys and comparative studies on microstructural and mechanical properties of FeAl based alloys containing carbon on Zr and Ti additions.

7.1 Microstructure properties and phase analysis

7.1.1 Optical

The nominal composition of the alloys used in the present investigation is given in table 7.1. The optical microstructures of FeAl based alloys on different alloying additions is shown in Fig. 7.1. As discussed in previous chapter, FeAl alloys with Ti addition (FeAl-1C-5Ti) exhibited equiaxed grains of size around 110 µm. Inside grains and on grain boundaries there were many carbon bearing second phase particles (Fig. 7.1a), corresponding to perovskite-type carbide $Fe_3AlC_{0.5}$ and TiC carbide. The FeAl based alloy with Zr addition (FeAl-1C-5Zr) exhibited grain size of around 150 µm with less second phase particles inside grains and on grain boundaries than FeAl alloy with Ti addition. A Zr-rich phase (Fig. 7.1b) is distributed along the grain boundaries of FeAl matrix as a hard skeleton. The ZrC carbide phase is also present within the grains as well as grain boundaries. No graphite precipitation was observed.

Table 7.1: Nominal composition of different alloy investigated.

	Compositions (wt. %)			
S.No.	**Al**	**C**	**Zr/Ti**	**Fe**
1	22.0	1.0	5.0 (Zr)	Balance
2	22.0	1.0	5.0 (Ti)	Balance

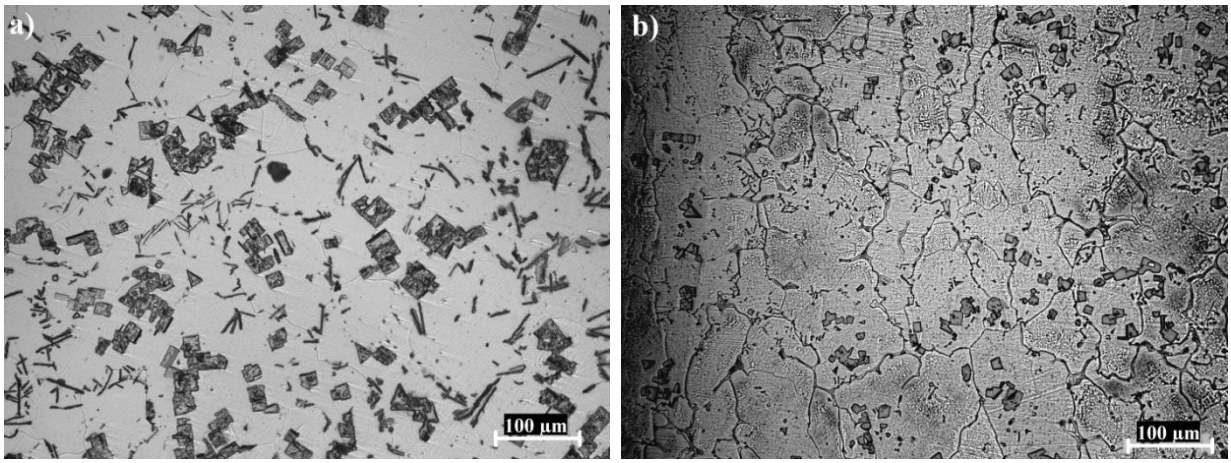

Fig. 7.1: Optical microstructure of FeAl based alloys, (a) FeAl-1C-5Ti having cuboid TiC and elongated $Fe_3AlC_{0.5}$ carbides and (b) FeAl-1C-5Zr having cuboid ZrC and $Zr(FeAl)_2$ phase along the grain boundary.

7.1.2 Scanning electron microscope equipped with EDS

EDS analysis of FeAl alloy with Ti addition revealed composition of second phase with cuboid shape particles close to TiC (Fig. 7.2). The elongated particles were rich in Al, Ti and Fe and revealed the presence of $Fe_3AlC_{0.5}$. It also confirmed that part of Ti is also present in $Fe_3AlC_{0.5}$. The EDS spectrum obtained from the matrix also reveals that small amount of Ti is present in the matrix. Similarly, FeAl alloys with Zr addition revealed that the cuboid shape particle composed of ZrC (Fig. 7.2). The grain boundary particles comprise of Zr, Al and Fe which is corresponding to Laves phase $Zr(Fe,Al)_2$ compositions. The average edge size of TiC is ~15µm while the average width and length of $Fe_3AlC_{0.5}$ carbide is found to be ~2µm and ~20µm respectively. The average edge size of ZrC carbides is found to be ~10µm.

7.1.3 X-ray diffraction

The XRD patterns of FeAl-1C-5Zr and FeAl-1C-5Ti alloys are shown in Fig 7.3. The peaks are identified by using panalytic X'Pert Highscore software which has inbuilt inorganic JCPDS (Joint Committee on Powder Diffraction Standards) X-ray diffraction data. Figure7.3 illustrates that the patterns from FeAl based alloys with different alloying additions remain cubic in nature. XRD pattern of Ti-alloyed alloy confirms the presence of the presence of TiC and $Fe_3AlC_{0.5}$ with ordered B2 FeAl matrix. While, Zr-alloyed alloy confirmed the presence of ZrC carbides, few peaks of Laves phase $Zr(Fe,Al)_2$ and ordered B2 FeAl matrix.

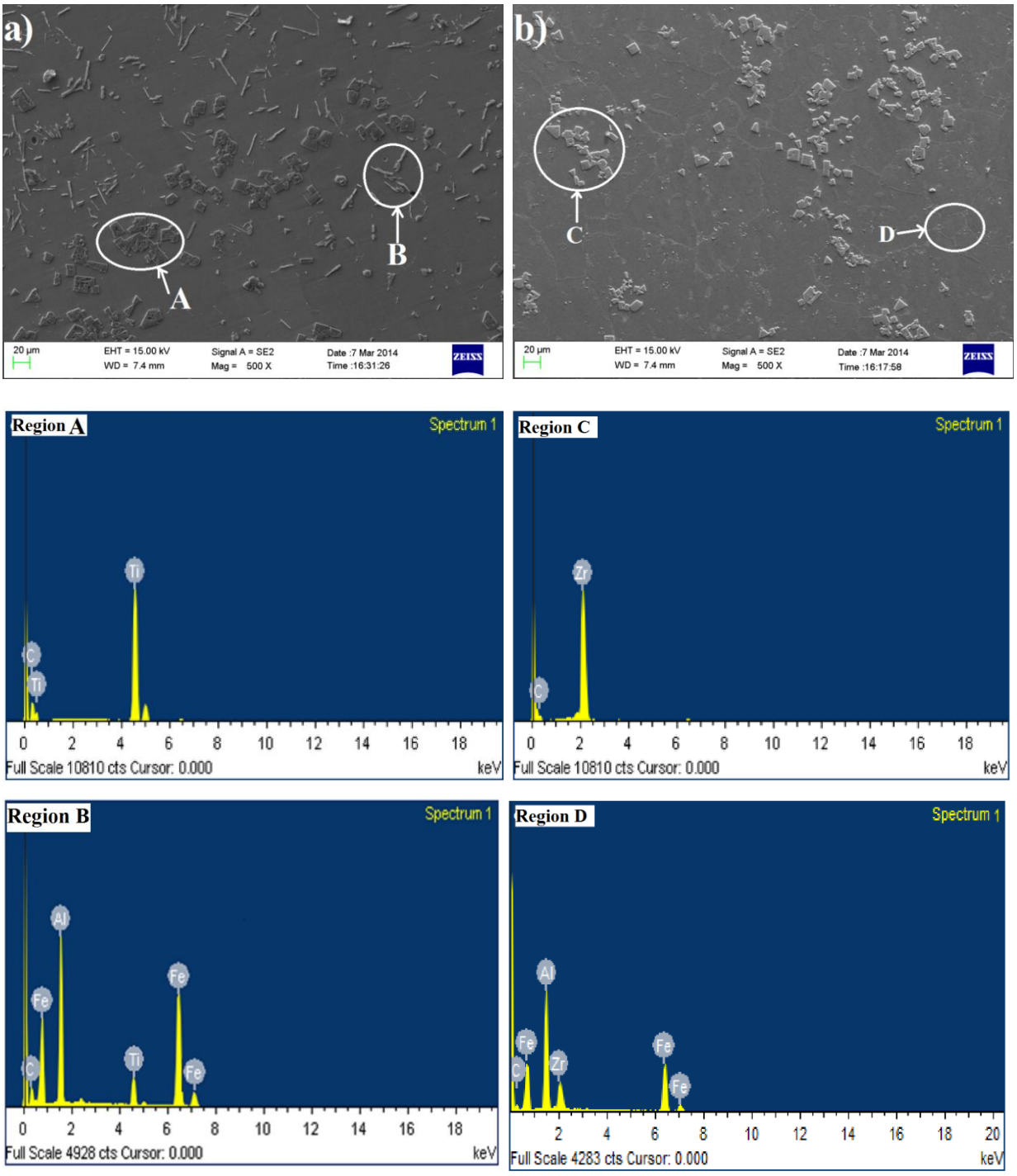

Fig. 7.2: SEM micrographs of FeAl based alloys, (a) with Ti addition showing the elemental composition of cuboid particle (Region A) and elongated particles (Region B) and (b) with Zr addition showing elemental compositions of cuboid particle (Region C) and particles along the grain boundary (Region D).

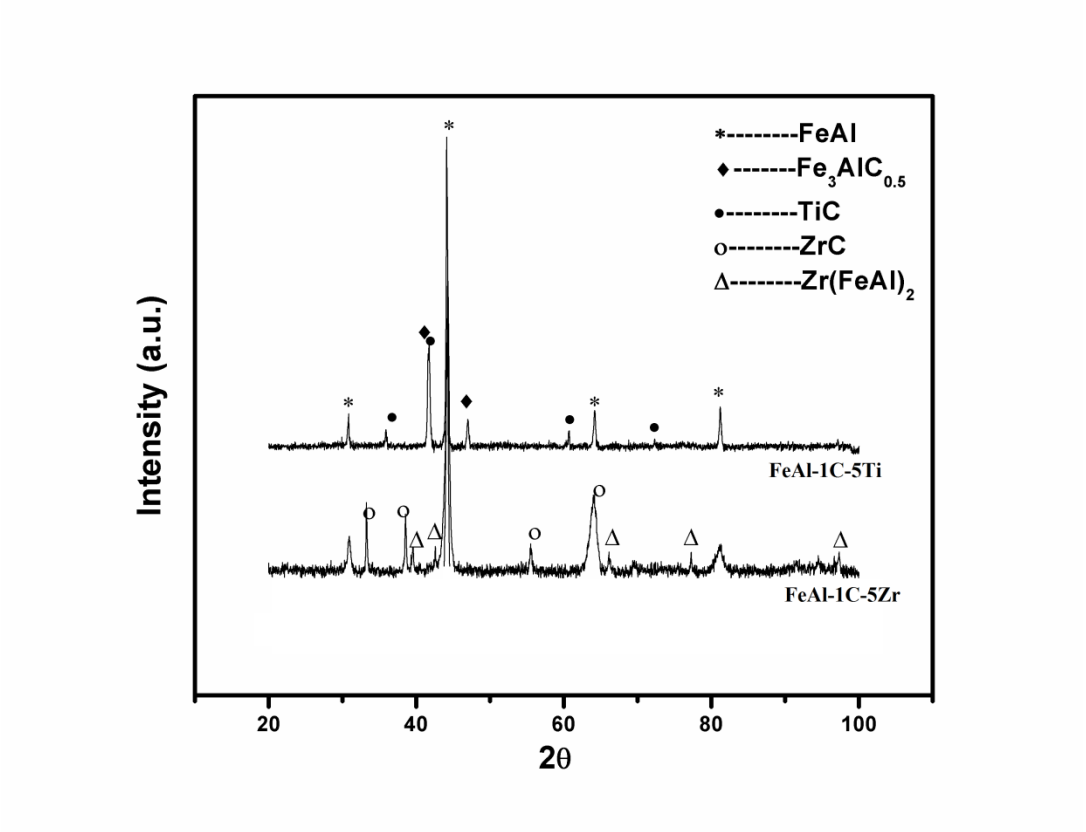

Fig. 7.3: XRD patterns obtained from FeAl based alloys with different alloying additions.

7.1.4 Transmission electron microscope analysis

In Fig.7.4, one can see the TEM images of FeAl-1C-5Zr and FeAl-1C-5Ti alloys with different alloying additions. In FeAl-1C-5Ti, cuboid shape TiC carbide is observed (Fig. 7.4a) with edge size ~400 nm with its corresponding selected area diffraction (SAD) pattern. The elongated shape particle with an average width of ~400 nm is shown in Fig.7.4b. This is illustrated by the bright field image of $Fe_3AlC_{0.5}$ and its corresponding SAD pattern. Similarly, in alloy FeAl-1C-5Zr, one can observed cuboid shape ZrC carbide (Fig 7.4c) with an edge size of ~500 nm with its corresponding SAD. In Fig. 7.4d, one can observed elongated particle with their corresponding SAD pattern of FeAl-1C-5Zr alloy.

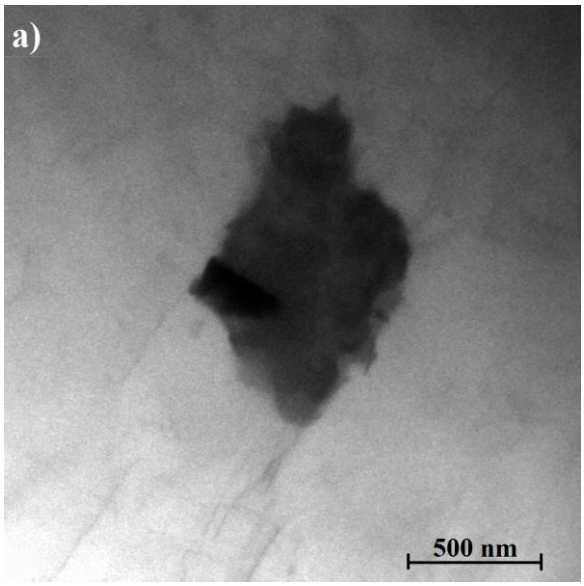
a)
500 nm

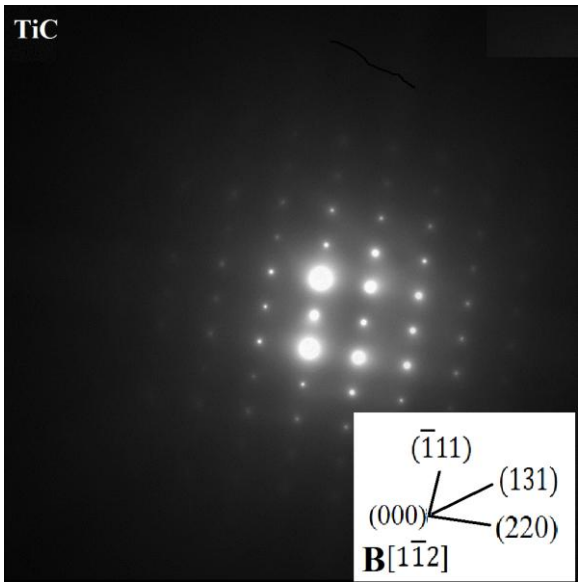
TiC
(1̄11)
(131)
(000)
(220)
B[1̄1̄2]

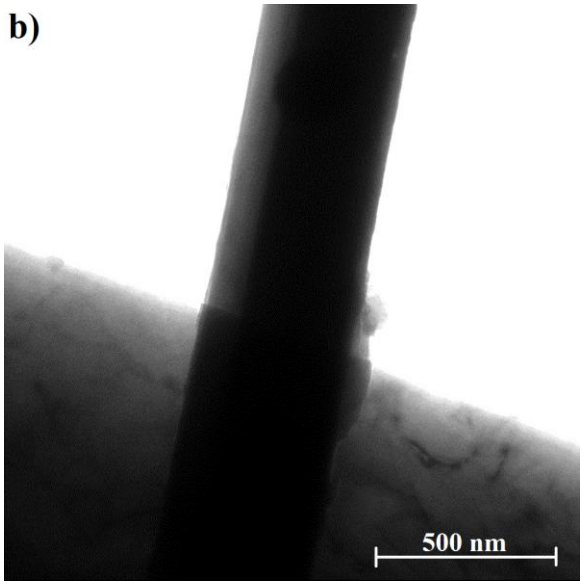
b)
500 nm

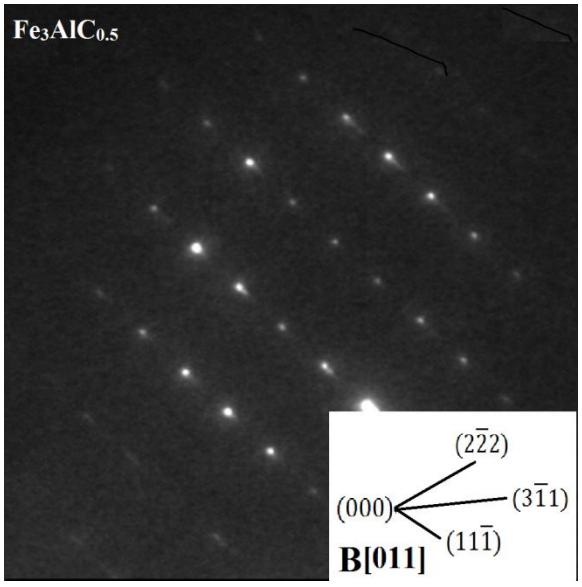
Fe3AlC0.5
(2̄2̄2)
(000)
(3̄1̄1)
(11̄1̄)
B[011]

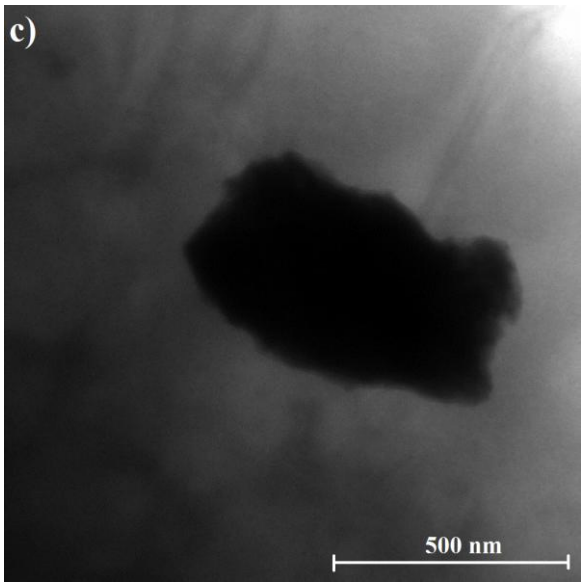
c)
500 nm

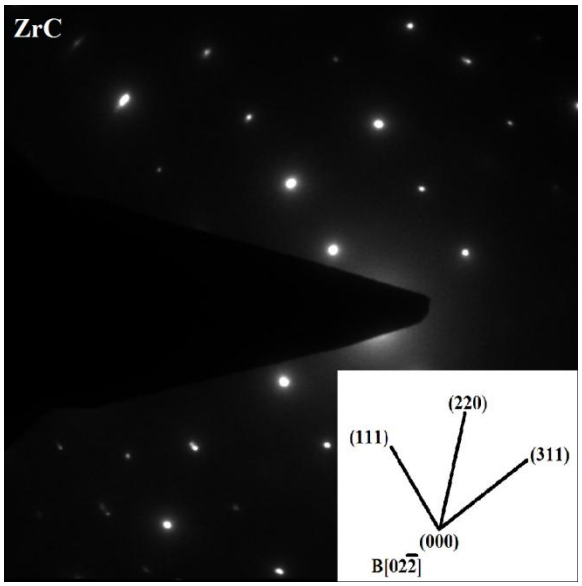
ZrC
(220)
(111)
(311)
(000)
B[02̄2̄]

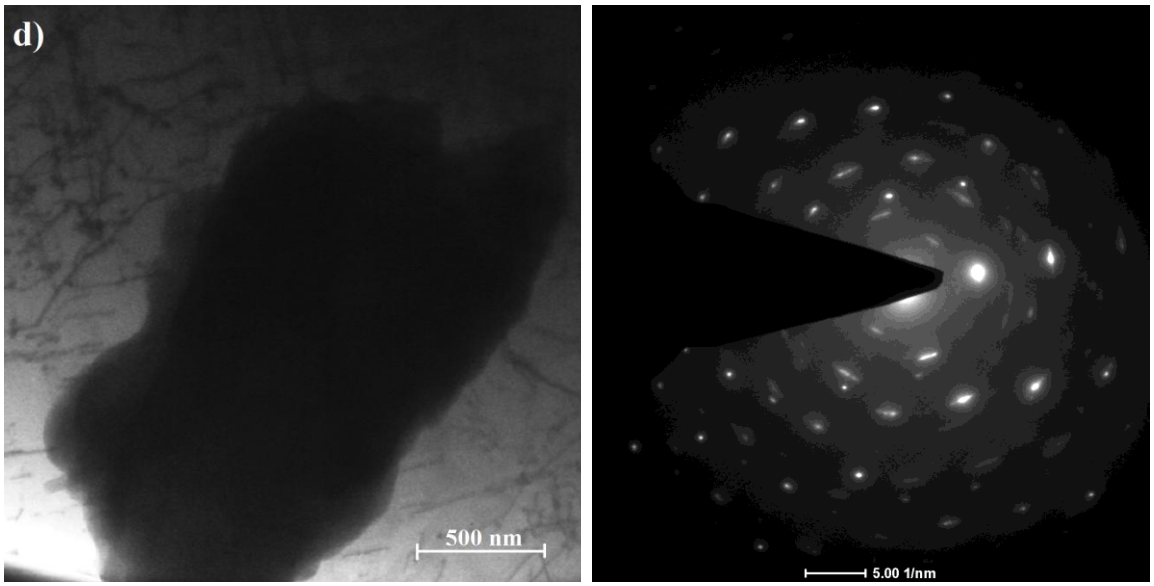

Fig. 7.4: Bright field TEM images of FeAl-1C-5Ti and FeAl-1C-5Zr alloys, (a) (TiC), with SAD pattern, (b) elongated particle ($Fe_3AlC_{0.5}$) with SAD pattern, (c) cuboid ZrC with SAD pattern and (d) Laves phase with SAD pattern.

7.2 Mechanical properties

7.2.1 Bulk hardness and microhardness

Hardness measurements (Vickers) of FeAl-1C-5Ti and FeAl-1C-5Zr specimens were carried out. Figure 7.5 illustrates the results of these measurements obtained from alloys with and without heat treatments. The figure shows that the addition of Ti or Zr to the FeAl alloy tends to increase the hardness values as compared to the values obtained from carbon containing FeAl alloy. However, the additions of Ti and Zr tend to increase the hardness values, but largest hardness increment is obtained with the Ti addition. This may be due to higher hardness of TiC in comparison to ZrC and in accordance with rule of mixture. The heat treatment of FeAl alloys at 400^{o}C for 100 h causes decrease in the hardness. This is mainly attributed to removal of thermal vacancies present in the alloys. The microhardness values of different phases were also obtained. Figure 7.6 shows the indentation marks (dark circle) on the different phases of the specimens and their values were listed in the Table 7.2.

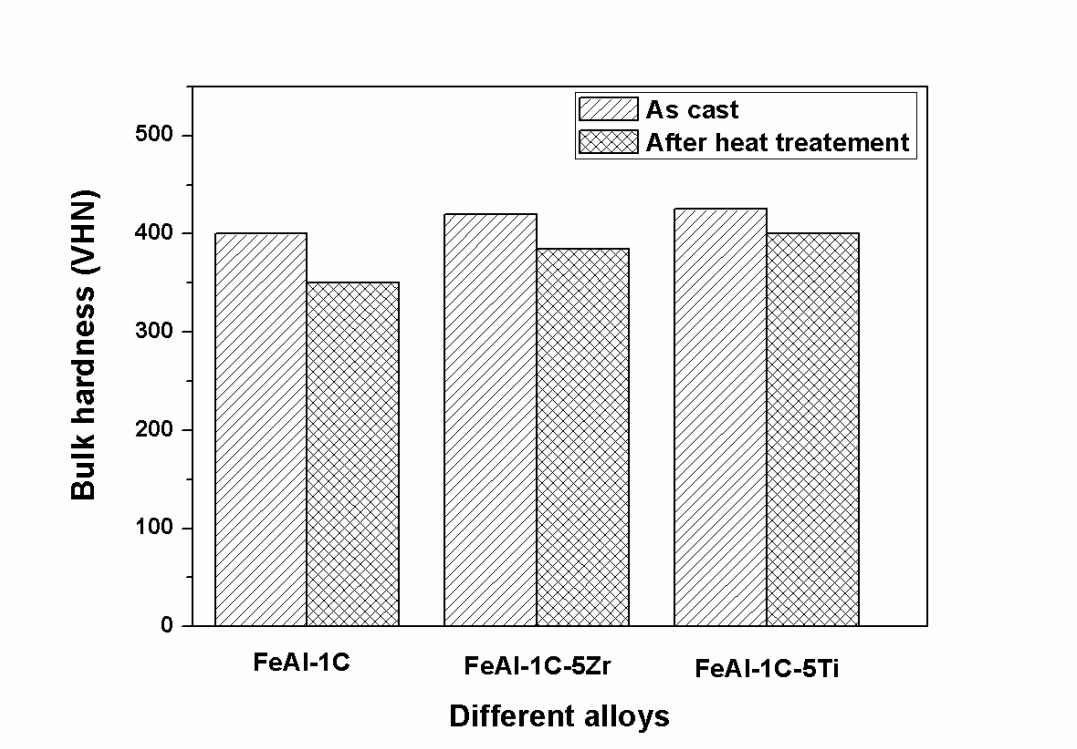

Fig. 7.5: Bulk hardness of FeAl based on different alloying addition.

Table 7.2: Bulk hardness, microhardness of FeAl based alloys.

Alloys	**Bulk Hardness (VHN)**	**Microhardness values (VHN)**		
		Matrix	**$Fe_3AlC_{0.5}$ or Laves phase**	**TiC or ZrC**
FeAl-1C-5Zr	420	380	800	2650
FeAl-1C-5Ti	425	410	610	3000

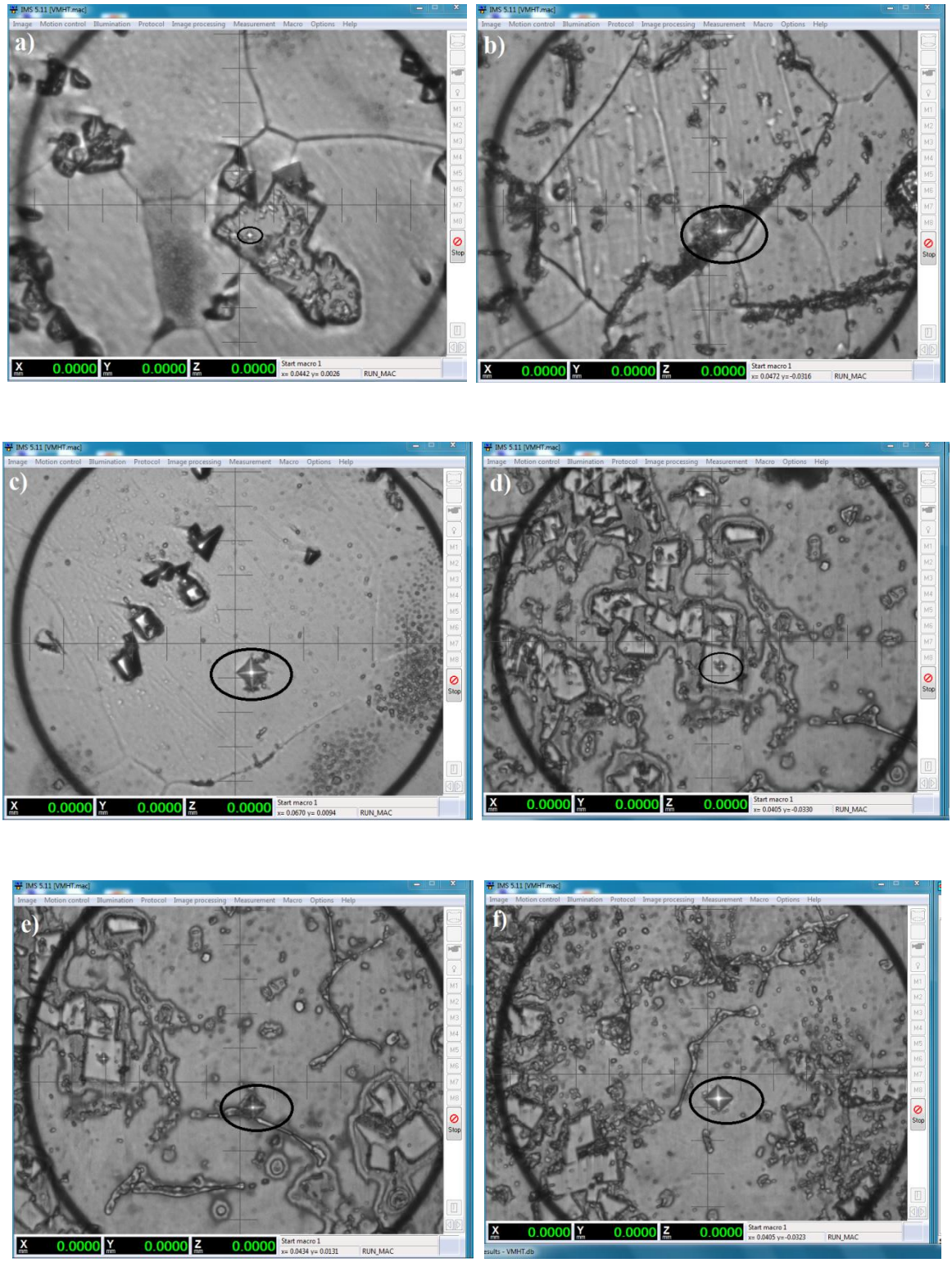

Fig. 7.6: The indentation marks on different phases, (a) TiC, (b) $Fe3AlC_{0.5}$, (c) matrix of FeAl based alloy on Ti addition and (d) ZrC, (e) $Zr(FeAl)_2$ and (f) matrix of FeAl based alloy on Zr addition.

7.2.2 Tensile properties

The tensile results of different alloys are shown in Fig 7.7. The results show that FeAl-1C-5Ti provided higher strength than FeAl-1C-5Zr and FeAl-1C alloys without compromising the ductility. Alloying with Ti produced higher strength in FeAl alloy indicating that Ti in caused strengthening due to precipitation of TiC and $Fe_3AlC_{0.5}$. The Zr addition also improved the strength but results in loss in the ductility. This increase in the strength is due to precipitation of ZrC and Laves phase and the decrease in the ductility in FeAl-1C-5Zr alloy may also be attributed to precipitation of Laves phase.

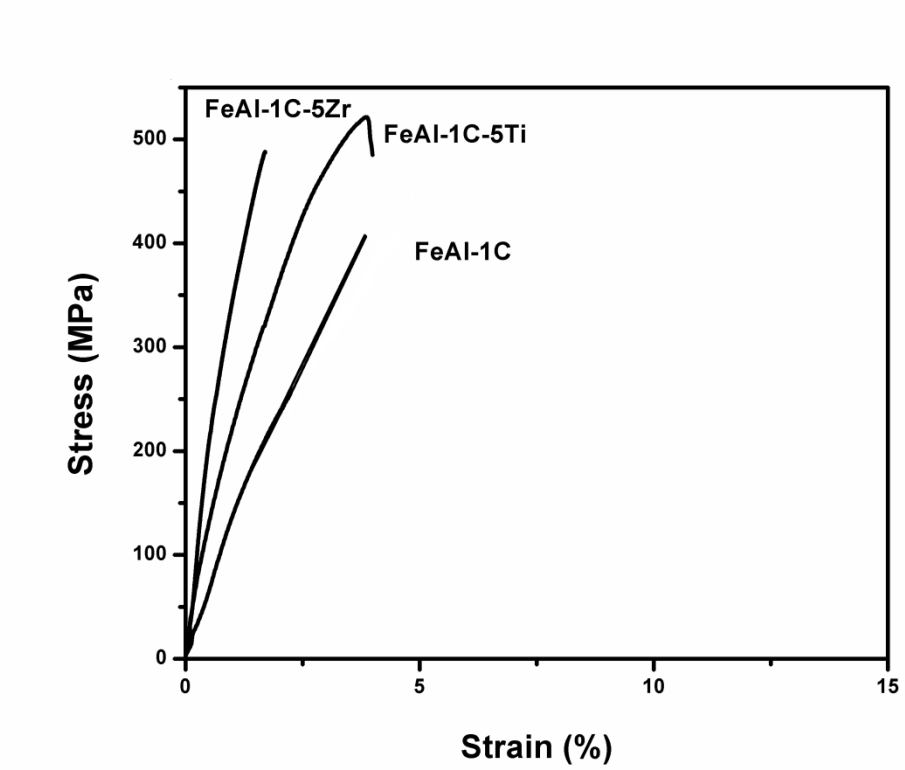

Fig. 7.7: Typical stress-strain curve of tensile testing for FeAl based alloys on different alloying additions.

7.2.3 Compression properties

At higher (1wt.%C) carbon content only nominal increase in strength is observed. The graphite precipitation may inhibit the increase in the strength. FeAl-1C-5Zr exhibits higher strength than FeAl-1C alloy. This can be attributed to the presence of hard ZrC and Laves phase along the grain boundaries (Fig 7.1b). On Ti addition, FeAl-1C-5Ti alloy exhibits superior strength than both FeAl-1C and FeAl-1C-5Zr. The precipitation of both $Fe_3AlC_{0.5}$ and TiC carbides in FeAl-1C-5Ti alloy help in the improvement in the strength at room temperature

(Fig. 7.8). Thus the presence of graphite is clearly undesirable. Among the FeAl-1C-5Zr and FeAl-1C-5Ti alloys, Ti containing alloy has ductility advantage over the alloy with Zr addition. The presence of $Fe_3AlC_{0.5}$ carbides in FeAl-1C-5Ti alloy may serve as hydrogen trap and may reduce the mobility of hydrogen [Prakash 2001]. This may help in the improvement in the ductility.

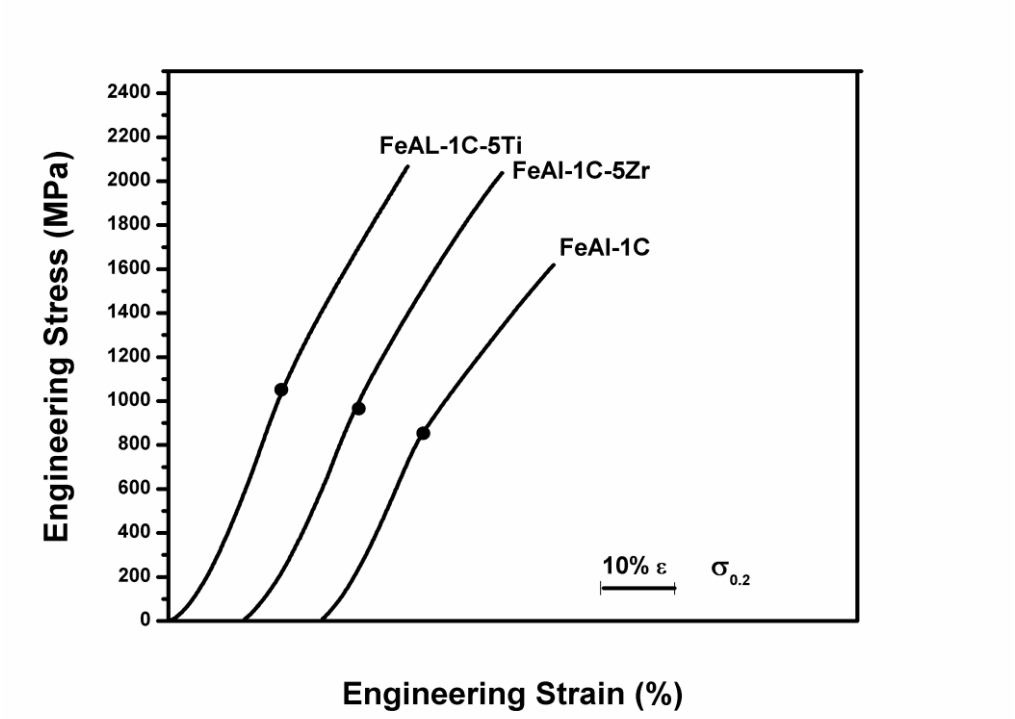

Fig. 7.8: Typical stress-strain curve for compression test of FeAl based alloys at room temperature.

Figure 7.9 shows the compressive yield stress data as a function of temperature for different alloys. With increase in temperature, the fall in the strength of alloys follow the same trend. At 873K or higher, due to the presence of graphite in FeAl-1C leads to rapid loss in strength at high temperatures. Thus the presence of graphite is clearly undesirable. FeAl-1C-5Zr and FeAl-1C-5Ti with alloy Zr and TiC alloy carbides respectively results improvement in the strength at all the temperatures as shown in Fig 7.9. The high temperature stability and high melting point of TiC and ZrC alloy carbide may cause increase in the high temperature strength of FeAl based alloys.

The compressive yield strength decreases with increase in temperature (Fig. 7.9). The loss in strength is particularly steep above 923K due to a rapid decrease in strength of the iron aluminide matrix. At 1073K all the alloys have comparable strength. Due to the loss in strength

above 923K, iron aluminides are being developed for structural applications at or below 923K. As can be seen from Fig. 7.9 up to 75% increase in elevated temperature yield strength can be obtained at target service temperatures with suitable carbon and Ti additions. This is accomplished without compromising on the room temperature ductility.

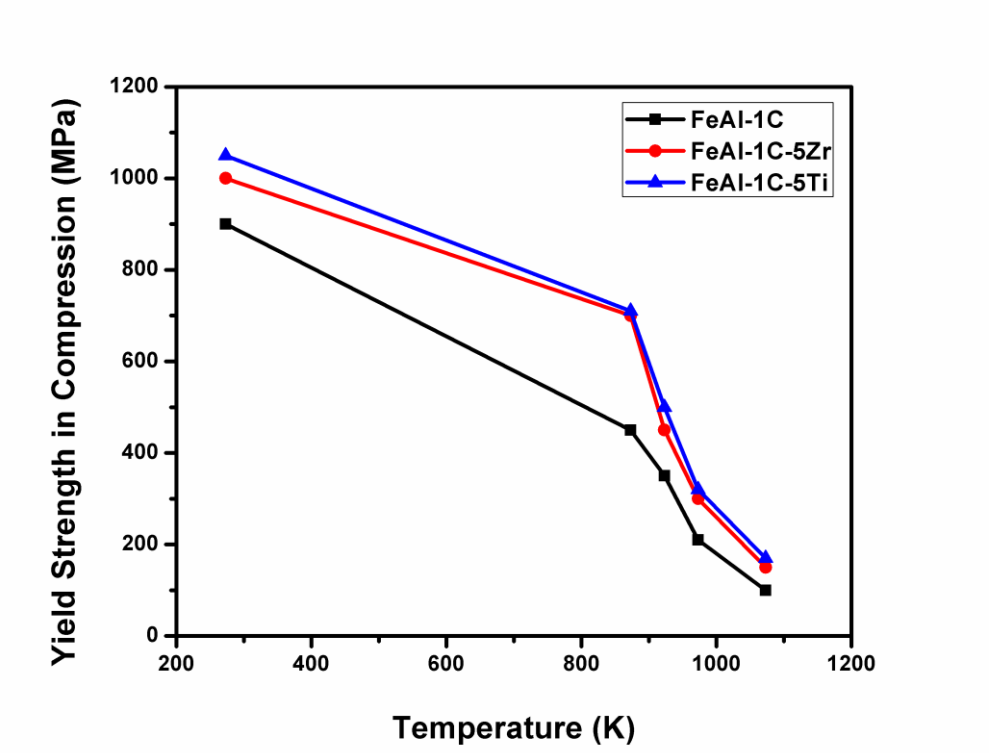

Fig. 7.9: Compression yield stress of FeAl based alloy with different alloying additions at different temperatures.

7.3 Effect of hot forging

In Fig. 7.10, the hardness values of as cast and after hot forging of different alloys are compared. The forged samples show improvement in the hardness of the alloys. This improvement in the hardness is mainly attributed to fine and homogenous distribution of second phase particles. It has been found that very heavy deformation introduced by multiple forging passes at high-temperature in orthogonal directions has led to refinement of the second-phase particles. This would tend to slight redistribution and homogenize of second phase particles throughout the material. The high level of strain imposed by forging led to a fracturing of the carbide particles present in the as-cast material, with these particles produced by solidification. Such particles are refined and narrowed by the forging strain (Fig. 7.11).

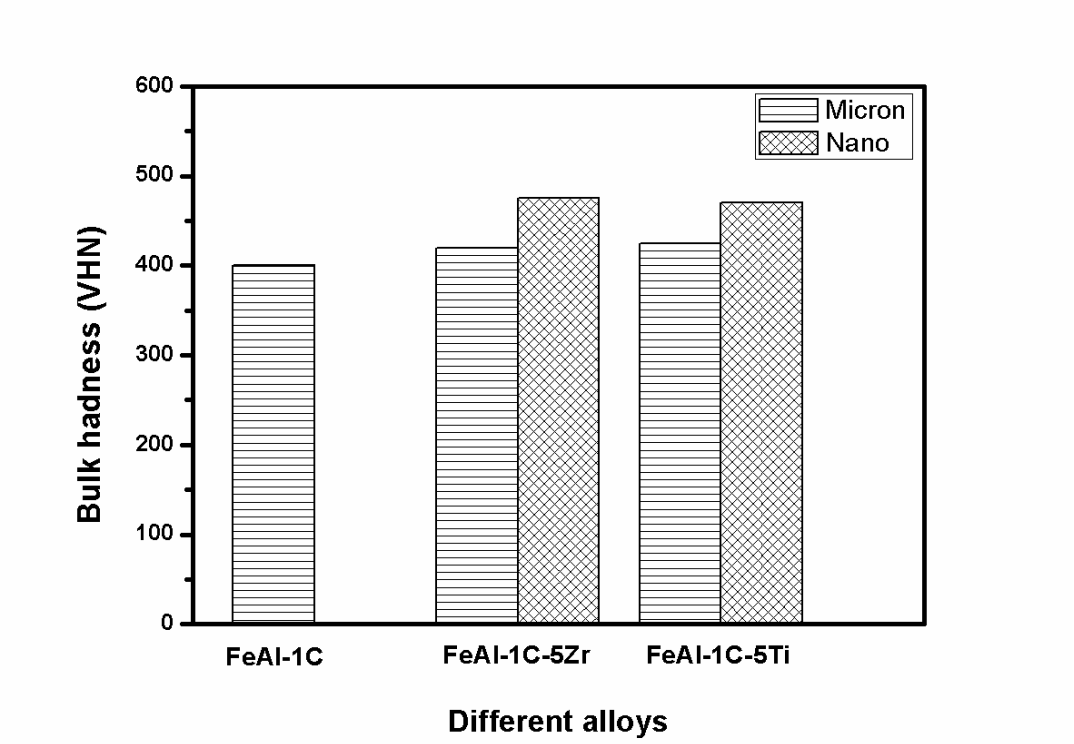

Fig. 7.10: Vickers hardness of as cast and hot forged FeAl alloys with different alloying additions.

The randomization and distribution of second-phase particles is similar to mechanical alloying of the alloys. The particles would become finer and inter particle distance in forged samples is smaller as compared to as cast sample. Some of these fine particles are shown in Fig. 7.11 and the effective size of the second phase particle is found to be ~50 nm. This leads to effective pinning of the dislocations as compared to coarse particles in as cast conditions.

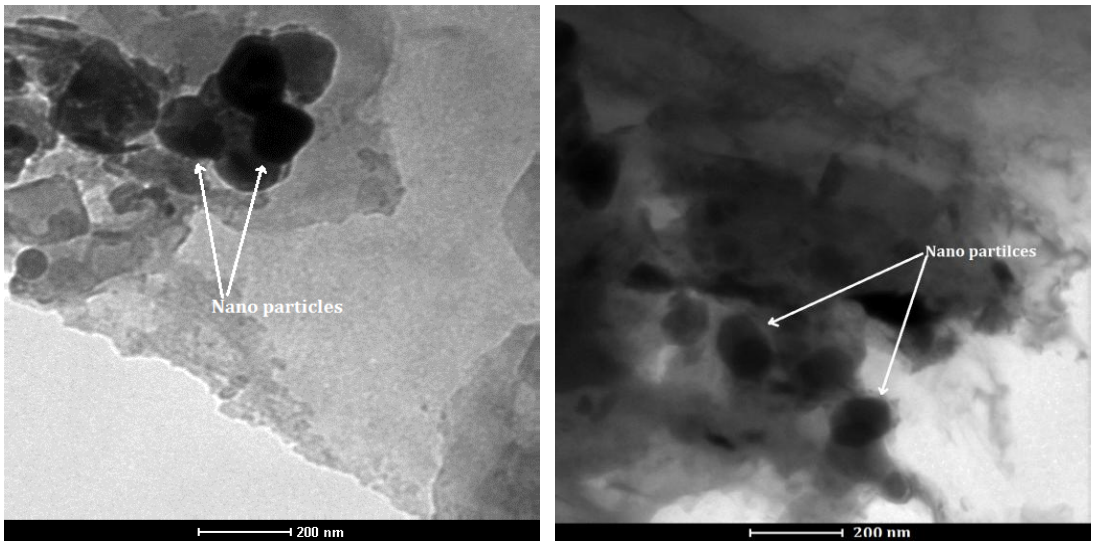

Fig. 7.11: TEM images of forged samples showing nano meter sized second phase particles in the matrix.

Figure 7.12 shows the stress strain curve of compression test for different alloys. The strength of hot forged FeAl-1C-5Ti and FeAl-1C-5Zr alloys is found to be superior to that reported in as cast alloys. This may be attributed to similar kind fine distribution of second phase particles seen after mechanical alloying [Karwan-Baczewska 2013]. In view of the redundant or partially reversed strain introduced to the material, the total strain imposed is significantly larger than the overall shape change, somewhat analogous to other methods of severe plastic deformation, such as equal channel angular pressing. Such refinement and redistribution of second-phase particles has also led to a significant improvement in the high-temperature creep strength of the material. The TiC carbide particles are distributed in cuboid shape in the as-cast material and could be somewhat refined beyond that found for the present starting material by increasing the solidification rate. However, much heavier working by forging would be required to improve further the refinement and homogenization of the carbide particles over that obtained in the present investigation.

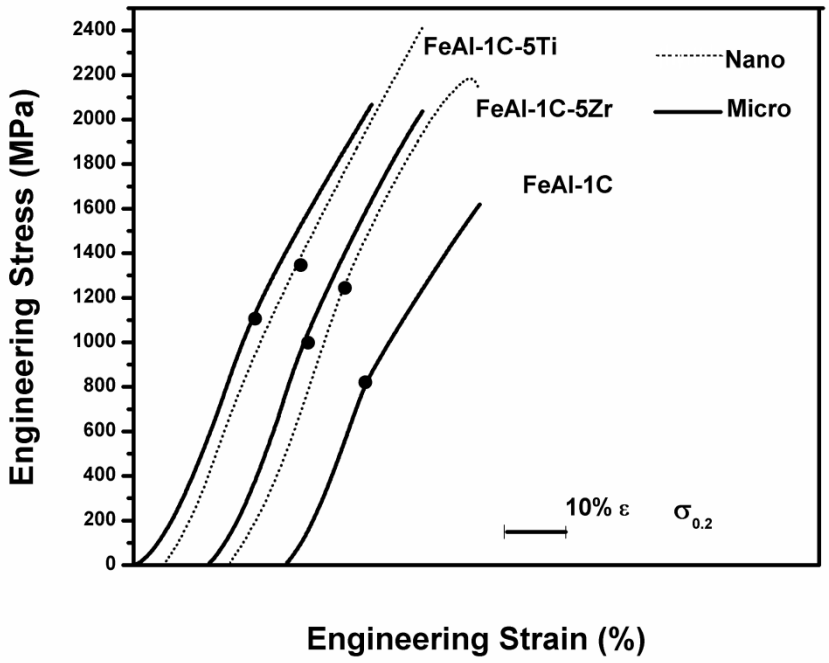

Fig. 7.12: Typical stress-strain curve for different FeAl based alloys before and after hot forging.

7.4 Thermal expansion coefficient

The alloying additions have remarkable effect on the thermal behavior of FeAl alloy as shown in Fig. 7.13. The graph reveals the rise in CTEs with increasing temperature. FeAl-1C

shows sharp increase in mean CTEs initially followed by steady state. This increase is also observed in other alloys but not so sharp. This could be due to dissolution of $Fe_3AlC_{0.5}$ carbides in FeAl matrix as this carbide melts in FeAl matrix around 950^oC [Pang 1998]. The mean CTEs increase sharply initially and then increase is slowed down in FeAl-1C-5Ti and FeAl-1C-5Zr alloys. The mean CTE decreased with increase in TiC and $Fe_3AlC_{0.5}$ content in the temperature range from 50 to 1000^oC. In FeAl alloys, Fe-Al bond strength is intermediate between Al-Al and Fe-Fe bond strengths. Also, note that the CTEs, $\alpha_{Fe}=1.2x10^{-5}$ and $\alpha_{Al}=2.2x10^{-5o}C^{-1}$ at room temperature [Ho 1998, Klemens 1986]. The thermal expansion coefficient, CTEs of α_{TiC} and α_{FeAl} are $0.74x10^{-5}$ [Pierson 1996] and $2.18x10^{-5o}C^{-1}$ [Zhang 2001] respectively in the temperature range from room temperature to 1000^oC. The mean CTE of FeAl-1C-5Ti with large contents of TiC and $Fe_3AlC_{0.5}$ reinforcements was found to be $1.3x10^{-5o}C^{-1}$. The thermal expansion of FeAl based alloys with different reinforcement is a complicated function of elastic and thermal properties of the individual components. Thus, the presence of TiC in FeAl based alloys significantly influenced the mean CTE of FeAl based alloys.

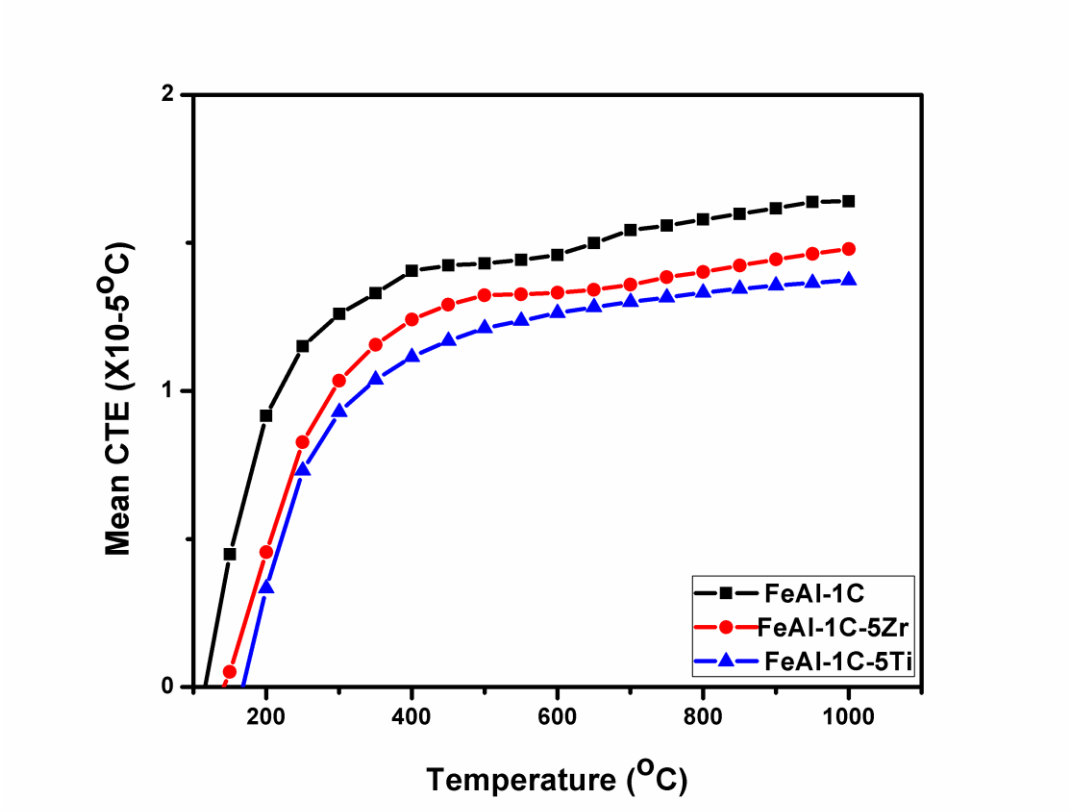

Fig. 7.13: Variation in mean CTEs of FeAl based alloys as a function of temperature.

The low solubility of precipitate phase is important parameter in ensuring resistance against coarsening at test temperature. $Fe_3AlC_{0.5}$ carbide is hardly stable at testing temperature

and is readily dissolved in FeAl matrix. On the other hand, TiC carbide due to their lower solubility is hardly dissolved at testing temperature. This could bring the thermal stability to FeAl based alloys at the testing temperature. Similar observation was also noticed with Zr addition to FeAl alloy. The precipitation of stable and hard ZrC carbide and Laves phase improved the thermal stability of FeAl alloy.

7.5 Wear behavior of FeAl alloys on titanium and zirconium additions

The wear tests were performed on the polished specimens using ball-on-disc testing machine. Before performing the wear test, the surface roughness of each specimen was measured using surface profiler. Fig. 7.14 shows the initial roughness of the specimens of each alloy. After performing the wear test, the depth of the wear scar was again measured by using surface profiler.

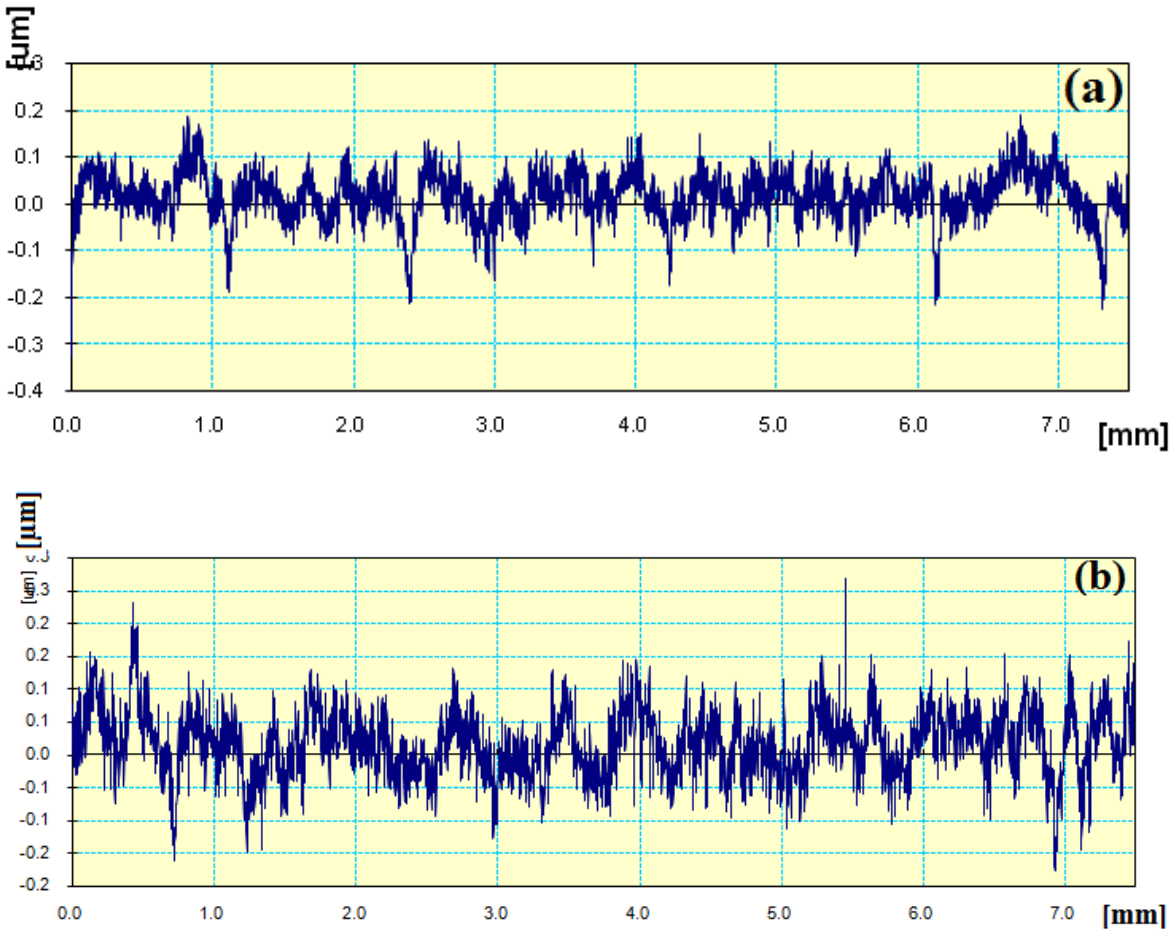

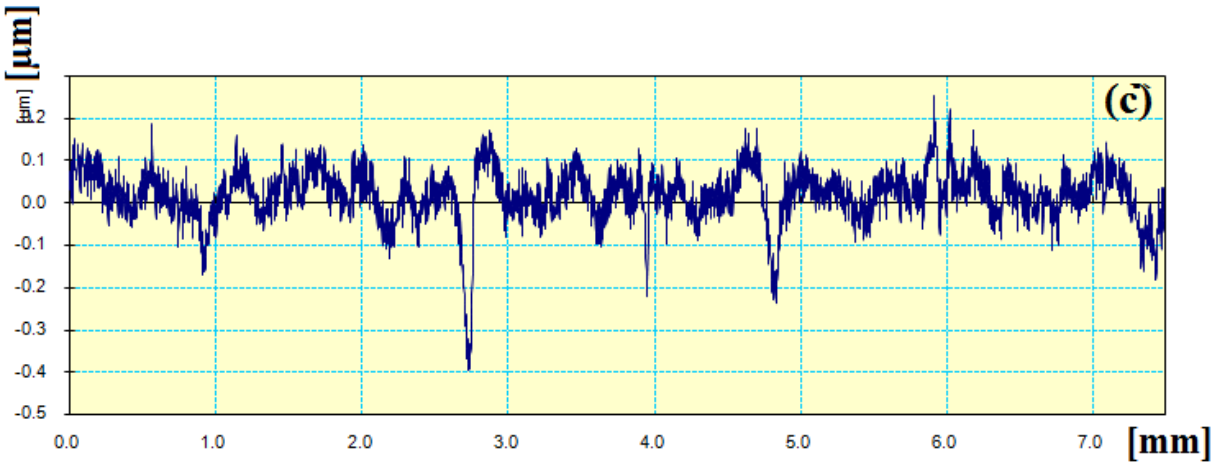

Fig. 7.14: The initial surface roughness of the specimen before performing the wear test, (a) FeAl-1C, (b) FeAl-1C-5Zr and (c) FeAl-1C-5Ti.

The wear rate was calculated by dividing the volume of wear scar by the sliding distance and applied load according to following relation,

$$\text{Wear volume } (V) = 2\pi rdw \quad (1)$$

Where, V is wear volume in mm^3; r, d and w are radius, depth and width of wear scar respectively in mm.

$$\text{Wear rate } (k) = V / Ls \quad (2)$$

Where, s is total sliding distance (m), L is applied normal load (N) and k is the wear rate in ($mm^3N^{-1}m^{-1}$).

7.5.1 Effect of load on wear rate

The wear rate of FeAl based alloys is shown to increase as applied load increases as shown in Fig 7.15. FeAl-1C shows highest wear rate among the alloys. FeAl-1C-5Zr has moderate wear rate. FeAl-1C-5Ti has least wear rate under the given tests conditions. The results obtained demonstrate that hardness, morphology and dispersion states of the precipitates affect the wear rate of FeAl based alloys at a given load. It is observed from the plot (Fig.7.15) that the wear rate increases with applied load. During the sliding, the surface of the material is removed initially and load is mainly transferred to the carbide particles. Thus, the hardness of the carbide particles plays an important role under the applied load. In the present case, the hardness of different primary carbide particles such as $Fe_3AlC_{0.5}$, ZrC and TiC in FeAl-1C,

FeAl-1C-5Zr and FeAl-1C-5Ti are 600, 2650 and 3000 VHN respectively. Thus, higher hardness causes lower removal of material and wear rate.

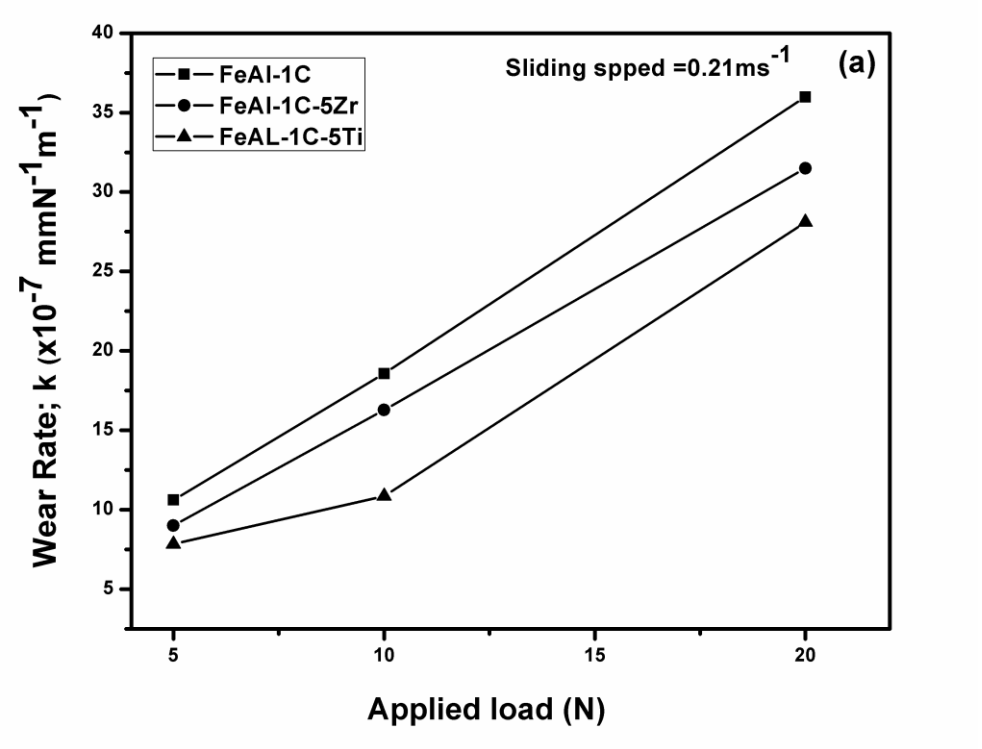

Fig. 7.15: The variation of wear rate of FeAl based alloy with applied normal loads at constant sliding speed.

7.5.2 Effect of speed on wear rate

The wear rate of FeAl based alloys is plotted as a function of the sliding speed in Fig 7.16. It can be seen from the graph that wear rate of alloys has no effect at lower speeds, but increases sharply at higher speed. FeAl-1C has highest wear rate. FeAl-1C-5Zr show almost same rate but difference becomes significant at higher speed. FeAl-1C-5Ti exhibits lowest wear rate among the alloys. This is because the higher sliding speed results increase in the frequency of cycle stress. This should have encouraged breakage of the particulates by dislocation shearing under plastic deformation. At the same time, matrix oxidation and removal of the rapidly grown oxide film, and subsurface matrix softening due to high frictional temperature conditions may also be effective. The increase of frictional energy consumed in the form of heat energy at higher sliding speeds softens the matrix. This may allow easier pullout of carbide particles due to weaker strength at the interface. The fine carbide particles may be served as third body between the two surfaces and allow more removal of the materials. Thus, the wear rate of alloys is increased as the sliding speed becomes higher.

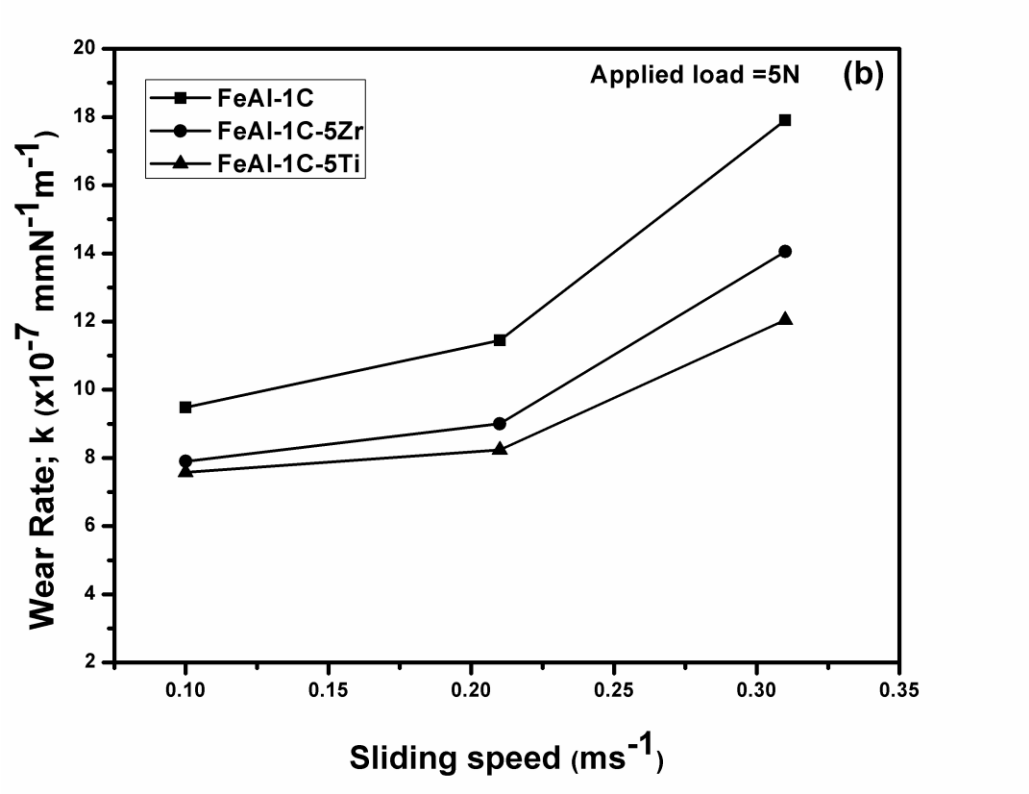

Fig. 7.16: The variation of wear rate of FeAl based alloy with sliding speeds at constant applied load.

7.5.3 Coefficient of friction (CoF)

Fig. 7.17 shows the behavior of coefficients of friction for all alloys tested at applied load of 10N with sliding speed 0.21m/s. The coefficient of friction, which increases sharply and after initial fluctuations acquires relatively steady state and prevails (Fig. 7.17). Due to the difference in the hardness and microstructures of the alloys, the coefficient of friction shows a little deviation. This indicates that hard alloy carbides (ZrC in FeAl-1C-5Zr, TiC in FeAl-1C-5Ti) in matrix lower the shear and therefore contact area is much smaller. This leads to decrease in the coefficient of friction. In short, the coefficient of friction is strongly affected by the presence of hard ZrC and TiC carbides in FeAl based alloys. It is well known that higher the friction coefficient results higher wear rate.

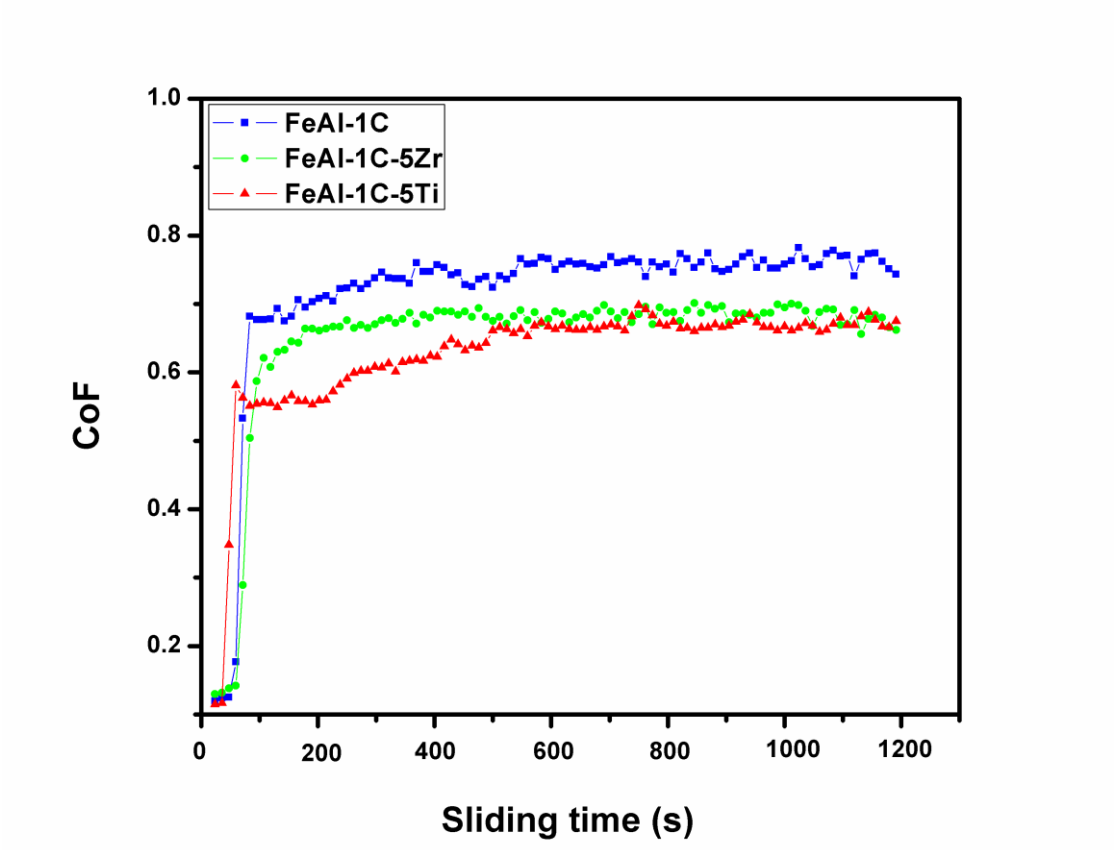

Fig. 7.17: The variation of coefficient of friction (CoF) with time for FeAl based alloys at applied load 10N with sliding speed 0.21m/s.

Wear resistance of materials strongly dependent on the hardness or bond strength and compatibility of reinforcement with matrix. Archard suggests [Archard 1953] that the wear rate (k) is normally described by modified equation, $k = d(N/H)$ where d is pre factor related to ductility, N is applied normal load and H is hardness of the material. Among the carbides, TiC is found to be high hardness value even harder than ZrC. Vickers microhardness values of TiC and ZrC are 3000 and 2650 VHN respectively which are much higher than $Fe_3AlC_{0.5}$, phase (600 VHN). Thus, FeAl-1C-5Ti with TiC precipitates obviously increased the hardness than FeAl-1C and FeAl-1C-5Zr. This would lead to decrease the wear rate.

7.6 Wear mechanism

Figure 7.18a show the deformation of $Fe_3AlC_{0.5}$ carbide in sliding wear direction. Thus, deformation of $Fe_3AlC_{0.5}$ carbide would result a higher friction coefficient of FeAl-1C than others. It may also be observed that the graphite flakes in FeAl-1C has lower load bearing capacity causes the abrasive particles to trap there and serious removal of material during

sliding. Thus, the deformation of $Fe_3AlC_{0.5}$ carbides in the sliding direction with few graphite flakes enhanced the wear rate. On the other hand, the carbides such as ZrC and TiC in FeAl-1C-5Zr and FeAl-1C-5Ti are embedded in the matrix even after sliding wear without any deformation. Fig 7.18b and 7.18c shows the cross-sectional area of the wear scars of the alloys. It reveals that the carbides mainly ZrC and TiC in FeAl-1C-5Zr and FeAl-1C-5Ti respectively, have very little effect of applied load. This strongly indicates that these carbides affect the wear rate of FeAl alloys without delamination or destruction while $Fe_3AlC_{0.5}$ carbide is started to deform in sliding direction under the applied load. This deformation of $Fe_3AlC_{0.5}$ carbides would bring the higher wear rate of FeAl-1C among the alloys.

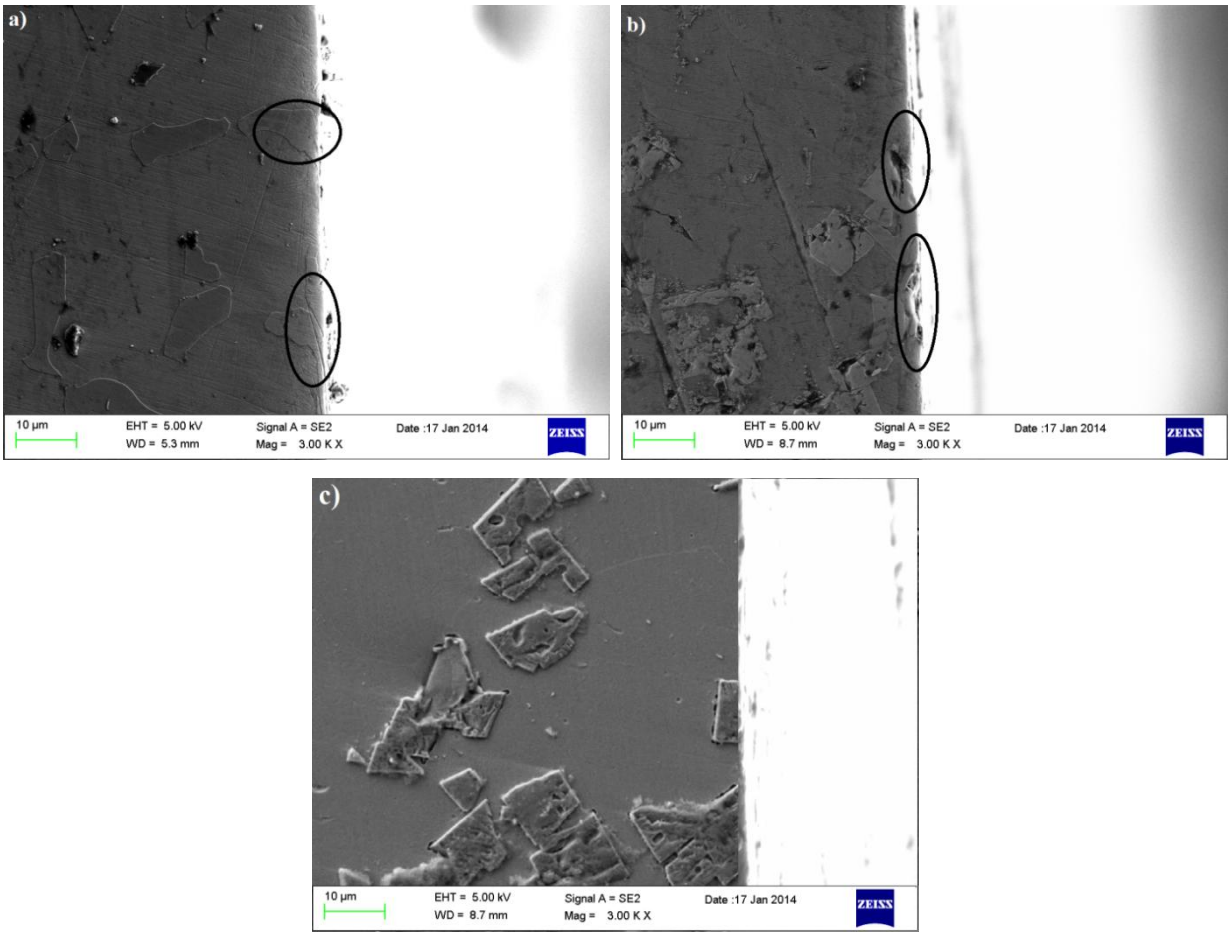

Fig. 7.18: Cross section of wear scars of, (a) FeAl-1C, (b) FeAl-1C-5Zr and (c) FeAl-1C-5Ti showing different carbides embedded in matrix after sliding wear.

Thus, the dispersion of carbides improves the wear resistance and friction coefficient of FeAl based alloys. However, as mentioned earlier, the hardness values of TiC or ZrC are extremely higher than that of $Fe_3AlC_{0.5}$ carbide. Also, no graphite precipitates are observed in these alloys (FeAl-1C-5Zr and FeAl-1C-5Ti). Therefore, the results demonstrate that uniform distribution of carbides in FeAl based alloys works more effectively for wear resistance. The

XRD of wear scars of different alloys further confirms the presence of carbide particles in the matrix. Figure 7.19 shows XRD pattern of the wear scars of alloys. The peaks of $Fe_3AlC_{0.5}$, ZrC and TiC in XRD pattern of FeAl-1C, FeAl-1C-5Zr and FeAl-1C-5Ti confirm the presence of the carbides in the matrix.

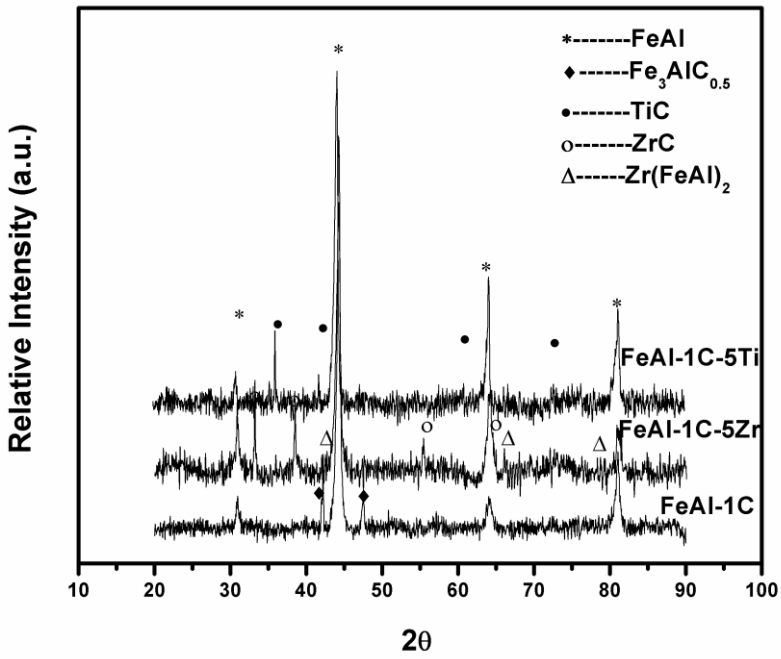

Fig. 7.19: XRD pattern of wear scars of FeAl alloys.

These results also reflect that the wear rate of FeAl based alloys decreased because different carbide particles play supporting role during the sliding wear. It is reported that the microhardness difference between TiC and ZrC is not very large, thus wear rate should be similar. The compatibility issue among the matrix and the reinforcement plays the important role. TiC is found to be more compatible with FeAl matrix in comparison to ZrC [Houska 1964]. This is due to the low CTE (coefficient of thermal expansion) mismatch between TiC and FeAl in comparison to ZrC and FeAl [Houska 1964]. From the Fig. 7.18, it is also clear that in ZrC reinforced FeAl matrix, few ZrC particles (marked as dark circle) are stubbed from the matrix during sliding wear process. As hard abrasives, the detached ZrC carbides would also act as third particles between the two surfaces, thus increased the wear rate. Comparing the wear and compression test results, it is suggested that yield strength determine the wear rate of FeAl based alloys under high load conditions. It is obvious that high yield strength would result in a low wear rate, if the wear occurs due to plastic deformation mechanism.

SEM micrographs of the wear scars for different alloys are shown in Fig. 7.20. In general, the shear stress among the contact surfaces increased with increase in the applied load. Few lines in the friction surface with very small flakes would be initiated at lower applied load (Fig. 7.20a, 7.20c, and 7.20e), while much more flakes would be produced and are more responsible to propagate at higher applied load (Fig. 7.20b, 7.20d and 7.20f). Thus, the wear rate in general of all alloys enhanced with increase in the applied load.

The micrographs were taken after the sliding wear conducted at different applied loads. In the mild testing conditions i.e. low normal load and sliding speed the surfaces show small flakes with fine debris and traces of micro-ploughing were observed as shown in Fig 7.20. However, in the severe conditions i.e. at high normal load, the surface appearance was quite different. The wear surfaces were covered with deep grooves and flaking pits. The wear scars were heavily damaged, and the platelets and a trace of their detachment from the surface were observed together with the micro-ploughing.

During the sliding wear, the strains accumulate at the contacting points between the asperities, which subsequently form the surface deformation layers with increased dislocation density. The delamination is mainly occurred due to cracking along the region of high dislocation density. The second phase particles (carbides) restrict the dislocations to accumulate at the point of contacts. Thus, removal of the material from the surface becomes difficult. This effect is more pronounced in FeAl-1C-5Zr and FeAl-1C-5Ti due to hard ZrC and TiC precipitates respectively. These observations reveals that wear in FeAl based alloys is mainly occurred due to plastic deformation and thus, hardness plays a dominant role for the sliding wear. Compared with $Fe_3AlC_{0.5}$ in carbon based alloy, the higher hardness of both ZrC and TiC in other alloys seem to play a positive role to resist the wear damage from the counterface and thus makes the process of delamination more difficult. It may be pointed out that in delamination mechanism of sliding particles wear, [Hutchings 1992] the strength of material is presumed to be a dominant parameter. A material which exhibits higher strength may allow lower wear rate. In the present study, the alloy with carbon addition does not show a significant improvement in the tribological properties. The localized graphite region in FeAl-1C alloy serve as weak zone and causes for the removal of material.

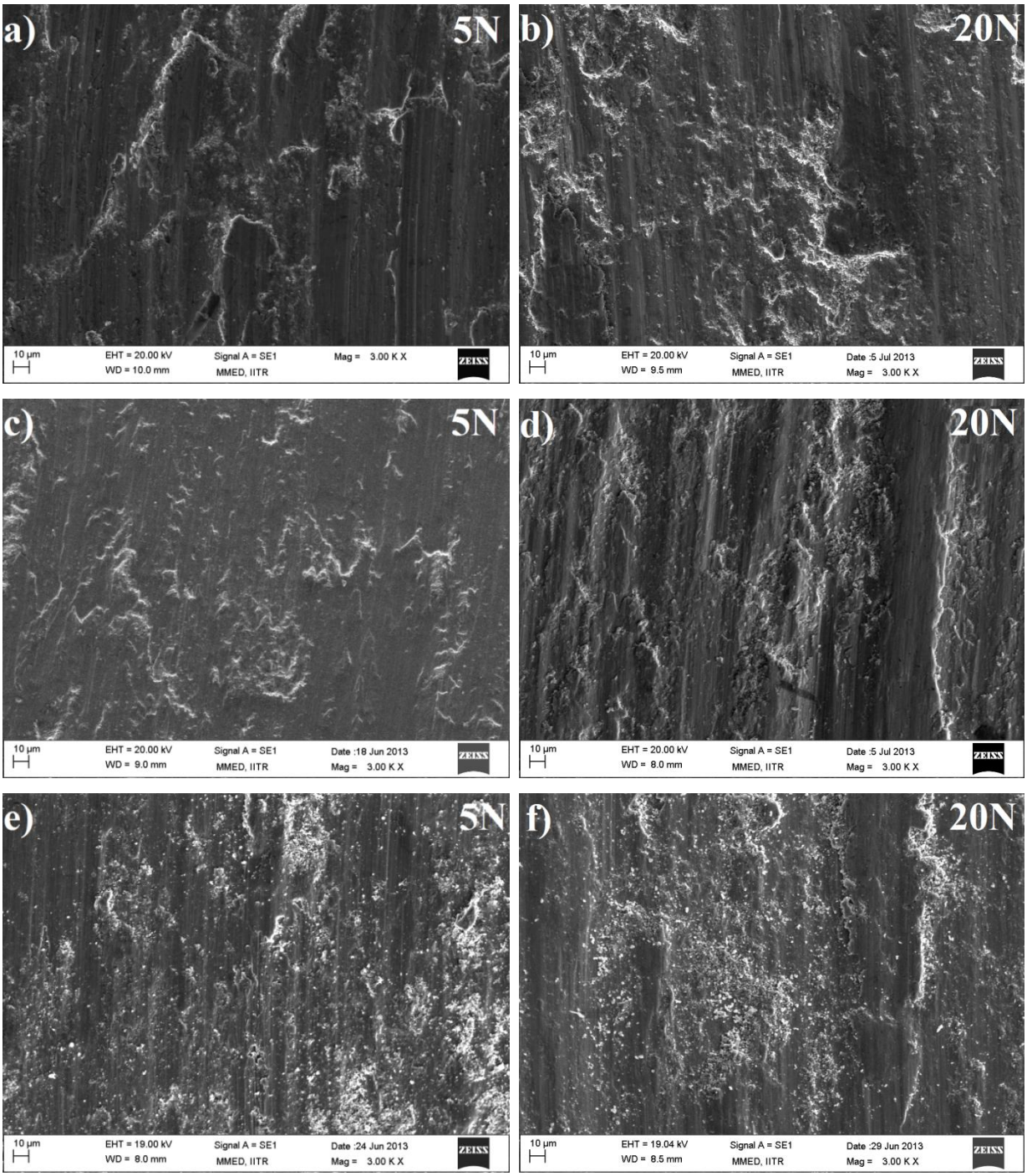

Fig. 7.20: SEM micrographs showing morphologies of wear scars obtained for different loads of (5N, 20N) with sliding speed 0.21m/s, (a, b) FeAl-1C, (c, d) FeAl-1C-5Zr, and (e, f) FeAl-1C-5Ti.

The microploughing with very fine flakes can be seen from the material surface at low speed as shown in Fig. 7.21. At higher speed, some of carbide particles are broken into fine piece and very fine particles are observed which may pull out of the surface due to rise in the temperature of the surface. These fine particles may serve as third body between the surfaces

and thus may increase the wear rate. In the case of FeAl-1C-5Zr and FeAl-1C-5Ti alloys, the improvement in tribological properties can be attributed to the strengthening effect imparted by ZrC and TiC carbides as compare to $Fe_3AlC_{0.5}$ carbides in FeAl-1C. ZrC and TiC carbides may inhibit the plastic deformation of surface layer to more extent due to higher hardness as compare to $Fe_3AlC_{0.5}$ carbide and the subsequent material removal.

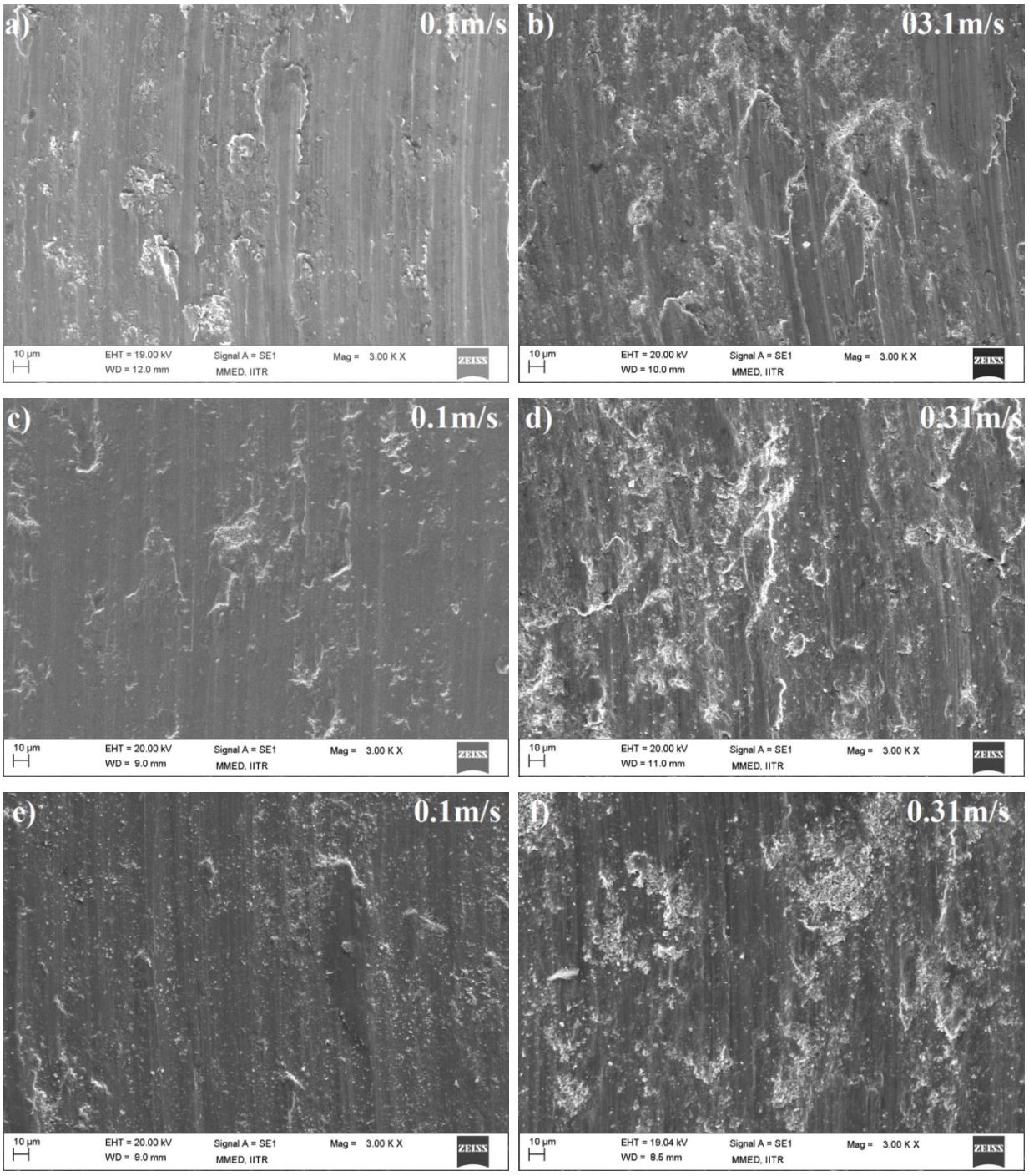

Fig. 7.21: SEM micrographs showing morphologies of wear scars obtained for different sliding speeds of (0.1, 0.31m/s) at applied load 5N, (a, b) FeAl-1C, (c, d) FeAl-1C-5Zr, and (e, f) FeAl-1C-5Ti.

7.7 Conclusions

- The addition of transition alloying elements such as Zr and Ti to FeAl based alloys containing carbon resulted in increase in the strength and hardness. This increase mainly attributed to the precipitation of hard carbides (ZrC/TiC). Zr addition results precipitation of hard ZrC and Laves phase $Zr(FeAl)_2$. On the other side, Ti addition causes precipitation of hard TiC and $Fe_3AlC_{0.5}$. No graphite precipitation was observed in FeAl based alloys on Zr and Ti addition.

- The morphology of second phase particles has been changed due to refinement during severe plastic deformations by high temperature forging. Such refinement can be understood due to transformation of tensile force to second phase particles by the matrix. Obtaining somewhat uniform distribution of fine (nano sized) particles with reduced inter-particles distance may lead to increase in the strength and hardness of FeAl alloys.

- The mean coefficients of thermal expansion (CTEs) of FeAl alloys were significantly influenced by the carbide particles. The mean CTEs of FeAl with carbon addition was found to be $1.6x\ 10^{-5}\ ^oC$ which was reduced to $1.485x\ 10^{-5}\ ^oC/1.42x10^{-5}\ ^oC$ with Zr/Ti additions respectively in the temperature range between room temperature to 1000^oC.

- Initially, the coefficients of friction (CoF) of FeAl based alloys increased with sliding speed and load sharply and then tend to constant with time. Further, the deformation of $Fe_3AlC_{0.5}$ carbide brings higher COF than other alloys. With addition of Zr and Ti, the coefficient of friction was found to be decreased from 0.76 to 0.6. This is mainly attributed to presence of ZrC (2650 VNH) and TiC (3000 VHN) having higher hardness values than $Fe_3AlC_{0.5}$ (600 VHN) carbide.

- The wear rate of FeAl based alloys were found to be increased with increase with applied loads and speeds. It has been significantly affected by the different carbide particles and found to be reduced with addition of Zr/Ti from $35x10^{-7}$ to $28x10^{-7}$ mm^3/Nm at 20N. This reduction was also attributed to hard ZrC/TiC carbides as load is mainly transferred to these particles.

- Wear mechanism of FeAl based alloys was transferred from the microploughing to microfracture and their detachment from the surface with applied load and sliding speed.

- The compatibility of alloy carbides with FeAl matrix played an important role in wear rate of FeAl based alloys. ZrC found to be less compatible with FeAl matrix than TiC and thus resulted in higher wear rate.

Chapter 8
Suggestions for future work

1. The present study has shown that in FeAl based alloys containing carbon on Ti addition there are different carbides namely $Fe_3AlC_{0.5}$ and TiC. The alloys in this investigation possess different carbon and Ti additions and limited to 1.5 wt%C with 5wt% Ti additions. The study needs to optimize the additions of carbon and Ti to achieve the desire mechanical properties. An approach in this direction to develop the phase diagram of the alloy.

2. In this investigation the alloys studied containing carbon and Ti only and one alloy with carbon and Zr. The studies can further be done by addition other carbides forming elements like Cr, W and Nb. The comparative studies on different alloying additions to FeAl alloys containing carbon can be done.

3. The investigation has revealed that the carbide mainly TiC is stabilized up to 1173K. It is well known that some mechanical properties like tensile strength, ductility and creep are strongly temperature dependent. In this study, the mechanical properties mainly tensile strength and ductility have been determined at room temperature, whereas in certain critical applications such as thermal engines, compressor stages of jet engines, coal gasification plants and the petrochemical industry, the material undergoes at elevated temperature. Hence studies need to be undertaken to investigate the mechanical properties at high temperatures.

4. The results show the excellent wear resistance of FeAl based alloys on carbon and Ti additions at room temperature. The excellent oxidation and sulfidation resistance at high temperature of FeAl based alloys motivate to investigate the high temperature wear properties of these alloys. Hence, it is necessary to find out the wear behavior of these alloys at different elevated and different environmental conditions such as in oxygen, acidic and inert atmosphere.

5. It has been found from the literature that Ti addition to iron aluminides deteriorates the oxidation and sulfidation resistance. Hence investigations need to be undertaken to study the oxidation and sufidation resistance of these allloys.

6. Best performance against ductility has been observed in FeAl alloys after grain refinement. But the present study mainly based on the coarse structure of the alloys. The secondary process such as hot forging or hot rolling or addition of grain refining elements can be done which will provide a fine grain to FeAl matrix with fine carbides. It is possible to fabricate various components by hot rolling / forging at such a high temperature. To obtain a fine grain matrix free of carbides, investigations may be undertaken on low C alloys and micro-alloyed with grain refining elements like B.

References

1) Alexander D.J., Maziasz P.J., Wright J.L., "Processing and alloying effects on tensile and impact properties of FeAl alloys", Materials Science and Engineering A, 258, 276-284, (1998).
2) Agarwala V., Karwan-Baczewska J., "Thermo Mechanical Treatment of Nickel and Titanium Aluminides", Defect and Diffusion Forum, 237-240, 653-658, (2005).
3) Alman D.E., Hawk J.A., Tylczak J.H., Dogan C.P., Wilson R.D., "Wear of iron-aluminide intermetallic-based alloys and composites by hard particles", Wear, 251, 875-884, (2001).
4) Axen N., "Abrasive Wear of Metal Matrix Composites", Ph.D. Thesis, Uppsala University, Uppsala, (1993).
5) Axen N., Jacobson S., "A model for the abrasive wear resistance of multiphase materials" Wear, 174, 187-199, (1994).
6) Badisch E., Katsich C., Winkelmann H., Franek F., Roy M., "Wear behaviour of hardfaced Fe-Cr-C alloy and austenitic steel under 2-body and 3-body conditions at elevated temperature", Tribology International, 43, 1234–1244, (2010).
7) Baker I. and Gaydosh D.J., "Flow and fracture of Fe-Al" Mater. Sci. Eng,. 96, 147, (1987).
8) Baker I., Munroe P.R., Improving Intermetallic Ductility and Toughness, JOM, 28-31, (1988).
9) Baker I., Munroe P.R., "Mechanical properties of FeAl", Int Mater Rev, 42,181–205, (1997).
10) Balasubramaniam R., "On the role of chromium in minimizing room temperature hydrogen embrittlement in iron aluminides", Scr. Mater., 34, 127–133, (1996).
11) Baligidad R.G., Prakash U., Rao V.R., Rao P.K., Ballal N.B., "Electroslag remelting of an Fe-28at%Al intermetallic alloy", Iron Making and Steel Making, 24, 321-330, (1994).
12) Baligidad R.G., Ph.D. Thesis, Indian Institute of Technology Bombay, (1996).
13) Baligidad R.G., Prakash U., Rao V.R., Rao P.K., Ballal N.B., "Effect of hot working on room temperature mechanical properties and stress rupture behaviour of ESR processed Fe-16wt%Al intermetallic alloys", ISIJ Internat., 36, 1215-1221, (1996a).

14) Baligidad R.G., Prakash U., Rao V.R., Rao P.K.,Ballal N.B., "Processing of Fe_3Al-based intermetallic alloys through electroslag remelting", ISIJ Internat., 36, 1448-1452, (1996b).

15) Baligidad R.G., Prakash U., Rao V.R., Rao P.K., Ballal N.B., "Effect of carbon content on high temperature tensile properties of Fe_3Al based intermetallic alloys", Scripta Mater., 36, 105-109, (1997a).

16) Baligidad R.G., Prakash U., Radhakrishna A., "High temperature tensile and creep properties of a cast AIM and ESR intermetallic alloy based on Fe_3Al", Mater. Sci Engg., A231, 206-210, (1997b).

17) Baligidad R.G., Prakash U., Rao V.R., Rao P.K.,; Ballal N.B., "Effect of carbides on embrittlement of Fe_3Al-based intermetallic alloys", Scripta Mater., 36, 667-671, (1997c).

18) Baligidad R.G., Prakash U., Radhakrishna A., "Processing of high carbon Fe_3Al-based intermetallic alloy", Intermetallics, 6, 765-769, (1998a).

19) Baligidad R.G., Prakash U., Radhakrishna A., "Mechanical properties of high carbon Fe_3Al-based intermetallic alloys", Mater. Sci. Engg., A257, 235-239, (1998b).

20) Baligidad R.G., Prakash U., Radhakrishna A., "Effect of carbon addition on structure and mechanical properties of electroslag remelted Fe–20 wt.% Al alloy" Mater. Sci. Eng. A, 249, 97-102, (1998).

21) Baligidad R.G., Prakash U., Radhakrishna A., "Effect of Al-content on creep and stress rupture properties of high carbon Fe-Al alloys", Mater Sci. Engg A, 269, 125-128, (1999).

22) Baligidad R.G., Radhakrishna A., "Effect of alloying additions on structure and mechanical properties of high carbon Fe-16wt%Al alloy", Mater. Sci. Eng. A, 287, 17-24, (2000).

23) Baligidad R.G., Radhakrishna A., Dutta A., Rama Rao V.V., "Effect of Mo addition on structure and properties of high carbon Fe-16wt%Al alloy", Mater. Sci. Eng. A,. 313, 117-122, (2001).

24) Baligidad R.G., Radhakrishna A., Sarma D.S., "Effect of carbon on mechanical properties of Fe-23wt%Al alloy", J. Mater. Sci. 40, 5537-5539, (2005).

25) Baligidad R.G., Prakash U., Radhakrishna A., "An air induction melting process for preparation of intermetallic alloy", India Patent No. 242438, (2010).

26) Baker I., Gaydosh D.J., “Flow and fracture of Fe-Al”, Mater. Sci. Eng. 96, 14-21, (1987).

27) Baker I., Munroe P.R., “Improving Intermetallic Ductility and Toughness”, JOM, 28-31, (1988).

28) Blickensderfer R., Laird G., “A Pin-on-Drum Abrasive Wear Test and Comparison with Other Pin Tests” J. Test Eval, 16, 516-523, (1988).

29) Bordeau R. D., “Development of iron aluminides”, Technical report no. AFWAL-TR-87-4009, Materials Laboratory, Air Force Wright Aeronautical Laboratories, Wright-Patterson air force base, Ohio, USA, (1987).

30) Brajpuriya R., Sharma P., Jani S., Kaimal S., Shripathi T., Lakshmi N., Venugopalan K., “Correlation between microstructure, magnetic and electronic properties of Fe1−*x*Al*x* ($0.2 \leq x \leq 0.6$) alloys produced by arc melting”, Appl. Surf. Sci., 257, 10–16, (2010).

31) Bowden E.P., Tabor D., “The friction and lubrication of solids”, part 2. Oxford: Oxford University Press; (1954).

32) Burdett J. K. Chemical Bonds, a Dialog (New York: Wiley), (1997).

33) Cahn R.W., Haassen P.P., Physical Metallurgy Ed. North Holand, (1996).

34) Cantor B., Fionn .P.E Dunne, Ian C., “Metal and Ceramic Matrix Composites”, chapter 14, (2003).

35) Chaudhary S., Khaple S., Satya Prasad V.V., Rao A.S., Baligidad R.G., “Effect of Titanium and Carbon on Microstructure and Mechanical Properties of Disordered Solid Solution Fe–7wt%Al Alloy,” Trans Indian Inst Met., DOI 10.1007/s12666-015-0514-z, (2015).

36) Chen Y., Wang H.M., “Microstructure and wear resistance of laser clad TiC reinforced FeAl intermetallic matrix composite coatings”, Surf. Coat. Technol., 168, 30–36, (2003).

37) Chen Y., Wang H.M., “High-temperature wear resistance of a laser clad TiC reinforced FeAl in situ composite coating”, Surf. Coat. Technol., 179, 252–256, (2004).

38) Chen Y., Wang H.M., “Peritectic solidification of under cooled Fe–Co alloys”, Journal of Alloys and Compounds, 49, 391-395, (2005).

39) Cohron J. W., Lin Y, Zee R.H., George E.P., “Room-temperature mechanical behavior of FeAl: effects of stoichiometry, environment, and boron addition”, Acta Mater, 46, 6245–6256, (1998).

40) Collins G.S., Peng J.S., Nuovo I., Cimento 18d, 329, (1996).

41) Crimp M.A., Vedula K., "Effect of boron on the tensile properties of B2 FeAl", Mater. Sci. Eng., 78, 193-197, (1986).

42) Darolia R., Lahrman D., Field R., "The effect of iron, gallium and molybdenum on the room temperature tensile ductility of NiAl", Scr. Metall. Mater. 26, 1007–1012, (1992).

43) Das D., Balasubramanian R., Mungole M.N., "Hot corrosion of carbon-alloyed Fe3Al-based iron aluminides", Mater. Sci. Eng. A, 338, 24-32, (2003).

44) D'Angelo L., D'Onofrio L., Gonzalez G., "Nanophase intermetallic FeAl obtained by sintering after mechanical alloying, J. Alloys Compd.", 483, 154-158, (2009).

45) Deevi S.C., Sikka V.K., Liu C.T., "Processing, properties, and applications of nickel and iron aluminides", Materials Science, 42. 177-192, (1991).

46) Deevi S.C. and Sikka, V.K., "Nickel and iron aluminides: an overview on processing, properties and applications", Intermetallics, 357-375, (1996).

47) Deevi S.C., Sikka V.K., Liu C.T. "Processing, properties and applications of nickel and iorn Aluminides", Progress of material Science, 42, 177-192, (1997).

48) Dey G.K., Tewari R., Roa P., Wadekar S.L., Mukhopadhyay P., "Precipitation hardening in nickel copper alloy monel K500". Metall. Trans. A, 24, 2709–2719, (1993).

49) Dey G.K., Sekhar J.A., "Micropyretic synthesis of tough NiAl alloys", Metall. Mater. Trans. B, 28, 905-911, (1997).

50) Diehm R.S., Mikkola D.E., Stoloff N.S., Koch C.C., Liu C.T., Izumi O., "High-Temperature Ordered, Intermetallic Alloy II", MRS Symposium Proceedings 81, MRS, Pittsburgh 329-333, (1987).

51) Dobes F., Kratochvil P., "The effect of Zr addition on creep of Fe-30 at.% Al alloys", Intermetallics, 43, 142-146, (2013).

52) Doucakis T., Kumar K.S., "Formation and stability of refractory metal diborides in an Fe_3Al matrix", Intermetallics 7, 765-777, (1999).

53) Eumann M, Palm M., Sauthoff G., "Alloys based on Fe_3Al and FeAl with strengthening Mo_3Al precipitates", Intermetallics, 12, 625-633, (2004).

54) Falat L., Schneider H., Sauthoff G., Frommeyer G, "Mechanical Properties of Fe-Al-M-C (M = Ti, V, Nb, Ta) alloys with strengthening carbides and Laves phases", Intermetallics, 13, 1256-1262, (2005).

55) Field R.D., Lahrman D.F., Darolia R., "The effect of alloying on slip systems in h001i oriented NiAl single crystals" Acta. Metall. Mater. 39, 2961–2969, (1991).

56) Foster C.N., Shockley W. "Order-disorder transformations in the Alloys", Review of Modern Physics, 10, 1-15, (1938).

57) Frommeyer G., Drewes E.J. Engl B., "Subject of a presentation at the ATS" International Steelmaking Conference, Paris, December 8-9, 4, (1999).

58) Gao M.X., Oliveira F.J, Pan Y.,Yang L., Baptista J.L., Vieira J.M., "Strength improvement and fracture mechanism in Fe40Al/TiC composites with high content of TiC", Intermetallics, 13, 460-466,(2005).

59) Gao, M.X., Pan, Y., Oliveira, F.J., Baptista, J.L., Vieira, J.M. "High strength TiC matrix Fe28Al toughened composites prepared by spontaneous melt infiltration", J. Eur. Ceram. Soc. 26, 3853–3859, (2006).

60) Garcia Oca C., Munoz-Morris M. A., Morris D. G., "High temperature structural coarsening of an ODS FeAl intermetallic", Intermetallics, 11, 425-434, (2003).

61) Gaydosh D.J., Draper S.L., Nathal M.V., "Microstructure and tensile properties of Fe-40 At. pct Al alloys with C, Zr, Hf, and B additions", Metall. Trans. A, 20A, 1701-1714, (1989).

62) George E.P., Yamaguichi M., Kumar K.S., Liu C.T., "Ordered intermetallics", Annual Review in Materials Science, 24, 409-415, (1994).

63) Gleiter H, "Materials with ultrafine microstructures: Retrospectives and perspectives", Nano Struct. Mater. 1, 1–19, (1992).

64) Gupta R.K., Pant B., Sinha P.P, "Theory and Practice of $\gamma+\alpha_2$ Ti Aluminide: A Review", Trans Indian Inst Met., 67, 143–165, (2014).

65) Gupta R.K., Pant B., Agarwala V., Sinha P.P, "Differential scanning calorimetry and reaction kinetics studies of $\gamma+\alpha_2$Ti aluminide", Materials Chemistry and Physics, 137, 483-492, (2012).

66) Gupta R.K., Pant B., Agarwala V., Agarwala R.C., Sinha P.P, "Effect of Pressure and Temperature on Phase Transformation and Properties of Titanium Aluminide Obtained through Reaction Synthesis", J. Mater. Sci. Technol., 26, 693-704, (2010).

67) Gupta R.K., Pant B., Agarwala V., Ramkumar P., Sinha P.P., "Development of TiB_2 reinforced in-situ Ti aluminide matrix composite through reaction synthesis," Trans Indian Inst Met., 63, 715-718, (2010).

68) Gutierrez-Urrutia I., Muñoz-Morris M.A., Morris D.G., "The effect of coarse second-phase particles and fine precipitates on microstructure refinement and mechanical properties of severely deformed Al alloy", Mater Sci Eng A, 394, 399-410, (2005).

69) Gutierrez-Urrutia I., Muñoz-Morris M.A., Morris D.G., "Contribution of microstructural parameters to strengthening in an ultrafine-grained Al–7% Si alloy processed by severe deformation", Acta Mater 55, 1319-30, (2007).

70) Guan X., Zhu S.M, Shibata K., Iwasakin K., "Effect of carbon on tensile properties and wear behaviour of P/M FeAl alloy", Materials Trans., J. Inst. of Metals, 1325-1331, (2002).

71) Guan X., Iwasaki K., Kishi K., Yamamoto M., Tanaka R., "Dry sliding wear behavior of Fe-28Al and Fe-28Al-10Ti alloys", Mater. Sci. Eng.A, 366, 127–134, (2004).

72) Hanada S., Watanabe S., Sato T., Izumi O. "Deformation of Fe_3Al single crystals at high temperatures", Script Metall, 15, 1345-1453, (1981)

73) Hausild P., Siegl J., Malek P., Sima V., "Effect of C, Ti, Zr and B alloying on fracture mechanisms in hot-rolled Fe–40 (at.%)Al", Intermetallics, 17, 680–687, (2009).

74) Hawk J.A., Alman D.E., Wilson R.D., "Abrasive Wear of Intermetallics" Mater. Res. Soc. Sympo. Proc., 364, 243, (1994).

75) Herbert M.A., Maiti R., Mitra R., Chakraborty M., "Wear behaviour of cast and mushy state rolled Al–4.5Cu alloy and in-situ Al4.5Cu–5TiB_2 composite", Wear, 265, 1606-1618, (2008).

76) Herbert M.A., Maiti R., Mitra R., Chakraborty M., "Microstructural evolution and Wear properties of In-situ Al-4.5Cu-5TiB_2 Composite Processed in Mushy State", Solid State Phenomena, 116, 217-220, (2006).

77) Ho C.Y. Thermal expansion of solids, CINDAS Data Series on Material Properties, Vols. I-4, ASM International (1998).

78) Hogmark S, Jacobson S, Vingsbo O. Metals handbook. 10th ed. Metals Park (OH): ASM; p. 176, (1990).

79) Hotar A., Palm M., Kratochvil P., Vodickova V., Danis S., "High-temperature oxidation behaviour of Zr alloyed Fe_3Al-type iron aluminide", Corr. Sci., 63, 71-81, (2012).

80) Huang S C, and Chesnutt J C, in Intermetallic Compounds, (vol 2), (eds) Westbrook J H, and Fleisher R L, Wiley, New York, 73, (1994).

81) Hutchings I.M., Tribology, "Friction and Wear of Engineering Materials", Bodmin, Cornwall, 22-35, (1992).

82) Inoue M., Nagao H., Suganuma K., Nihara K., "Fracture properties of Fe-40at%Al matrix composites reinforced with oxide particles and fibres", Mater. Sci. Eng. A, 258, 298-305, (1998).

83) Inoue M., Sugunama K., Nihara K., "Mechanical properties of aluminide matrix composites fabricated by reactive hot processing in several environments", Intermetallics, 8, 1025-1042, (2000).

84) Itoi T., Mineta S., Kimura H., Yoshimi K., Hirohashi M., "Fabrication and wear properties of Fe_3Al-based composites", Intermetallics, 18, 2169-2177, (2010).

85) Jahanmir S. "Friction and wear of ceramics", New York (NY): Marcel Dekker; (1990).

86) Jasim K.M., Dwarakadasa E.S., "Wear in Al-Si alloys under dry sliding conditions", Wear, 119, 119–130, (1987).

87) Ji G., Grosdidier T., Bernard F., Paris S., Gaffet E., Launois S., "Bulk FeAl nanostructured materials obtained by spray forming and spark plasma sintering" J. Alloys Compd., 434–435, 358-361, (2007).

88) Joachim H, Schneibel J.H., Becher P.F., "Iron and Nickel aluminide composites", J Chin Inst Eng, 22, 1–12, (1999).

89) Józwiak S., Karczewski K.. "Influence of aluminum oxides on abrasive wear resistance of Fe-50 at.% Al intermetallic sinters" Journal of Alloys and Compounds, 482, 405-11, (2009).

90) Jung I., Sauthoff G., "High-Temperature Deformation Behavior of the different phases Fe_3AlC and Ni_3AlC", Metallkd Z., 80, 490, (1989).

91) Kai W., Haung R.T., "The corrosion behavior of Fe-Al alloys in $H_2/H_2S/H_2O$ atmospheres at 700–900°C", Oxid. Met., 48, 59-86, (1997).

92) Kambakas K., Tsakiropoulos P., "Sedimentation casting of wear resistant metal matrix composites", Mater Sci and Engg A, 435-436, 187-192, (2006).

93) Karwan-Baczewska J., Rosso M., "Effect of boron on microstructure and mechanical properties of PM sintered and nitrided steels", Powder Metallurgy, 44, 221-227, (2001).

94) Karwan-Baczewska J., Gotman I., Gutmanas E.Y., Shapiro M, "Structure Investigation of Ball Milled Composite Powder Based on $AlSi5Cu_2$ Alloy Chips Modified by Sic Particles", Archives of Metallurgy and Materials, 58, 437-441, (2013).

95) Kanth V.K., Pramila Bai B.N., Biswas S.K., "Wear mechanisms in a hypereutectic aluminium silicon alloy sliding against steel", Scr. Metall. Mater., 24, 267–271, (1990).

96) Kerr W R, "Fracture of Fe_3Al", Metall. Trans. A, 17, 2298-2300, (1986).

97) Khaple S., Baligidad R.G., Sankar M., Satya Prasad V.V, "Structure and properties of Fe–(3–7wt.%) Al–0.5wt.%C alloys", Mater Sci and Eng A, 527, 7452-7456, (2010).

98) Khodaei M., Enayati M. H., Karimzadeh F., "Mechanochemical behaviour of Fe_2O_3-Al-Fe powder mixtures to produce Fe_3Al-Al_2O_3 nanocomposite powder", J. Mater. Sci, 43, 132-138, (2008).

99) Khruschov M.M., "Principles of abrasive wear" Wear 28, 69. (1974).

100) Kim Y.S., Kim Y.H., "Sliding wear behavior of Fe_3Al-based alloys", Mater. Sci. Eng. A, 258, 319–324, (1998).

101) Klemens P.G., Williams R.K., "Thermal conductivity of metals and alloys" Int Met Rev, 31, 197-215, (1986).

102) Ko S.H., Hanada S., "In-situ production and microstructures of iron aluminide/TiC composites", Intermetallics, 7, 947, (1997).

103) Koeppe M., Hartig C., Mecking H., "Anomalies of the plastic yield stress in the intermetallic compound Fe–30 at.% Al" Intermetallics, 7, 415–22, (1999).

104) Kolluru D.V., Pollock T.M., "Numerical modeling of the creep behavior of unidirectional eutectic composites", Acta Mater., 46, 2859-2876, (1998).

105) Ko S.H., Park B.G., Hashimoto H., Abe T., Park Y.H., "Effect of MA on microstructure and synthesis path of in-situ TiC reinforced Fe–28at.% Al intermetallic composites", Mater. Sci. Eng. A, 329-331, 78-83, (2002).

106) Koch C. C., "Intermetallic matrix composites produced by mechanical alloying-a review", Mater. Sc. Eng., A244, 39-48, (1998).

107) Kogachi M., Haraguchi T., "Quenched-in vacancies in B2-structured intermetallic compound FeAl", Mater. Sci. Eng. A, 124, 124-131, (1997).

108) Kok, M., Ozdin, K., "Wear resistance of aluminium alloy and its composites reinforced by Al_2O_3 particles" J. Mater. Process. Technol. 183, 301–309, (2007).

109) Kratochvil P., Dobes F., Pesick J., Malek P., Bursik J., Vodickova V. Hanus P., "Microstructure and high temperature mechanical properties of Zr-alloyed Fe3Al-type aluminides: The effect of carbon", Mater Sci and Eng. A, 548, 175-182, (2012).

110) Krasnowski M., Kulik T., "Nanocrystalline FeAl intermetallic produced by mechanical alloying followed by hot-pressing consolidation", Intermetallics, 15, 201-205, (2007).

111) Krasnowski M., Witek A., Kulik T., "The FeAl–30%TiC nanocomposite produced by mechanical alloying and hot-pressing consolidation" Intermetallics, 10, 371–376, (2002).

112) Kumar K. S., Bao G., "Intermetallic matrix composites: an overview, Compos. Sci Tech.", 52, 127-150, (1994).

113) Kumar K.S., Pang L., "Effect of temperature and strain rate on the mechanical properties of Fe–40Al–0.6C", Mater Sci and Eng A, 258, 153-160, (1998).

114) Kupka M., Stępien K., Kulak K., "Effect of hydrogen on room-temperature plasticity of B2 iron aluminides", Corr. Sci., 53, 1209-1213, (2011).

115) Lahrman D.F., Field R.D., Darolia R., "The effect of strain rate on the mechanical properties of single NiAl, in high temperature ordered intermetallic alloys IV", Mater. Res. Symp. Proc. 213, 603, (1991).

116) Lapin J., Tieberghein D., Delannay F., "On the parameters affecting formation of iron aluminides during pressure assisted infiltration of aluminium into a perform of steel fibres", Intermetallics, 8, 1429-1438, (2000).

117) Lejcek P., Fraczkiewicz A., "Boron segregation in intermetallics: on the possible origins of a low-level intergranular segregation" Intermetallics, 11, 1053–63. (2003).

118) Lesch C., Lvarez P.A., Bleck W., Gil Sevillano J., "Rapid Transformation Annealing: a Novel Method for Grain Refinement of Cold-Rolled Low-Carbon Steels", Metallurgical and Materials Trans. A, 38A, 1882-90, (2007).

119) Levit V.I., Bul I.A., Hu J., Kaufmann M.J., "High tensile elongation of β-NiAl single crystals at 293 K", Scr. Mater. 34, 1925-1930, (1996).

120) Liu C.T., George E.P.. "Environmental embrittlement in boron-free and boron doped FeAl (40 at.% Al) alloys", Scr Metall Mater, 24, 1285-1290, (1990).

121) Liu C.T., Lee E.H., McKamey C.G., "An environmental effect as the major cause for room-temperature embrittlement in FeAl", Scripta metall. 23, 875-880, (1989).

122) Liu C.T., Stiegler J.O. “Oredered intermetallic. Properties and selection: nonferrous alloys and special purpose materials”, Metals Handbook, ASM international. tenth edition , vol 2, Properties and selection: nonferrous alloys and special purpose materials, (1990).

123) Liu C.T., Yang J. Suo Z., Evans A.G., Hecht R., Mehrabian R., “Matrix cracking in intermetallic composites caused by thermal expansion mismatch”, Acta Metall. Mater., 39, 1883-1890, (1991).

124) Liu C.T., Sikka V.K., McKamey C.G., “Alloy Development of FeAl Aluminide Alloys for Structural Use in Corrosive Environments”, Oak Ridge National Laboratory Report, ORNLrTM-12199, (1993).

125) Liu C.T., Stringer J.O., Mundy J.N., Horton L.L., Angelini P., Ordered intermetallic alloys: an assessment, Intermetallics 5, 579-96, (1997).

126) Liu C.T., George E.P., Maziasz P.J., Schneibel J.H., “Recent advances in B2 iron aluminide alloys: deformation, fracture and alloy design”, Mater. Sci. Eng.A, 258, 84-98, (1998).

127) Liu D.S., Liu R.P., Wei Y.H., Qiu Y., Pan P., Zhu K., Gao W.L., “Comparative behaviour of cobalt and iron base hardfacing alloys”, Surf. Eng., 28, 338–44, (2012).

128) Liu Z.Y., Gao W., Wang F.H., “Oxidation behaviour of FeAl intermetallic coatings produced by magnetron sputter deposition”, Scripta Mater., 39, 1497-1502, (1998).

129) Maerky C., Guillou M.O., Henshall J.L., Hooper R.M.,“Indentation hardness and fracture toughness in single crystal TiC0.96”, Mater. Sci. Eng. A, 209, 329-336, (1996).

130) Malek P., Kratochvil P., Pesicka J., Hanus P., Sediva I., The nature of high temperature deformation of the Fe-30Al-4Cr iron aluminide modified by TiB_2, Intermetallics, 10, 985-992, (2002).

131) Martinez M., Viguier B., Maugis P., Lacaze J., “Relation between omposition, microstructure and oxidation in iron aluminides”, Intermetallics, 14, 1214-1220, (2006).

132) Massalski T. B. ed., “Binary alloy phase diagrams”, Vol.1, Amer. Soc. Met., p112 (1986).

133) Matsushita T., Chapman L., Brooks R., Egry I., Seetharaman S., “Thermal Diffusivity of TiAlNb and AlNi alloys - the European IMPRESS Project”, Defect and Diffusion Forum, 273-276, 375-380, (2008).

134) Maupin H.E., Wilson R.D., Hawk J.A., "Wear deformation of ordered Fe-Al intermetallic alloys", Wear, 162-164, 432-440, (1993).

135) Maziasz P.J., Goodwin G.M., Alexander D.J., Viswanathan S., Deevi S.C., (Eds.), "Proceedings of the International Symposium on Nickel and Iron Aluminides: Processing, Properties and Applications", ASM International, Cleveland, OH, , 157, (1996).

136) McKamey C.G., Liu C.T., "Chromium addition and environmental embrittlement in Fe_3Al", Scr. Metall. Mater., 24, 2119-2122, (1990).

137) McKamey C.G., DeVan J.H., Tortorelli P.E., Sikka V.K., "A review of recent developments in Fe_3Al-based alloys" J. Mater. Res. 6, 1779-1805, (1991).

138) Mckamey C.G., "Physical Metallurgy and Processing of Intermetallic Compounds", eds. Stoloff N.S., Sikka V.K., Chapman and Hall London, 351-355, (1996).

139) McKamey C.G., Horton J.A., "The effect of molybdenum addition on properties of iron aluminides", Metall. Trans., 20A, 751-757, (1989).

140) McKamey C.G., Horton J.A., Liu C.T., "Effect of chromium on room temperature ductility and fracture mode in Fe_3Al", Scripta Metallurgica, 22, 1679-1681, (1988).

141) McKamey C.G., Maziasz P.J., Jones J.W., "Effect of addition of molybdenum or niobium on creep-rupture properties of Fe_3Al", J. Mater. Res., 7, 2089-2106, (1992).

142) Mekhrabov A.O., Akdeniz M.V., "Effect of ternary alloying elements addition on atomic ordering characteristics of Fe–Al intermetallics", Acta Mater., 47, 2067-2075 (1999).

143) Mendiratta M.G., Ehlers S.K., Dimiduk D.M, Kerr W.R., Mazdiyasni S., Lipsitt H.A., "A Review of Recent Developments in Iron Aluminides" Mater. Res. Soc. Symp. Proc., 81, 393, (1987).

144) Mendiratta M.G., Ehlers S.K., Dimiduk D.M., Kerr W.R., Baker I., Darolia R., Wittenberger J. Yoo M. (Eds.) "High-Temperature Ordered Intermetallic Alloys V", MRS Symposium Proceedings, MRS, Pittsburgh, 288, 885, (1993).

145) Mendritta M.G., Lipsit H.A., Koch C.C., Liu C.T., Stoloff N.S. (Eds.), "High-Temperature Ordered Intermetallic Alloys I", MRS, Symposium Proceedings MRS, Pittsburgh, 39155, (1985).

146) Misra A. K., "Identification of thermodynamically stable reinforcement materials for iron aluminide matrices", Metall. Trans. 21A, 441-446, (1990).

147) Morales R., Seetharaman S., Agarwala V., "Mechanical and structural characterization of uniaxially cold-pressed Fe_2Mo powders", J. Mater. Res., 17, 154-1959, (2002).

148) Morris D.G., "Possibilities for high-temperature strengthening in iron aluminides", Intermetallics, 6, 753-758, (1998).

149) Morris D.G., Peugiron D. Nazmy M., "Yield stress and stress anomaly in an Fe_3Al alloy" Philos. Mag. A, 71, 441-463, (1995).

150) Morris D.G., Gunther S., "Strength and ductility of Fe-40Al alloy prepared by mechanical alloying", Mater. Sci. Engg., A208, 7-19, (1996).

151) Morris D.G., Gutierrez-Urrutia I., Muniz-Morris M.A., "The high temperature creep behaviour of an Fe-Al-Zr alloy strengthened by intermetallic precipitates", Scripta Mater., 57, 449-452, (2007).

152) Morris D.G., Gutierrez-Urrutia I., Muniz-Morris M.A., "High temperature creep behaviour of an FeAl intermetallic strengthened by nanoscale oxide particles", Int. J. Plasticity, 24, 1205-1223, (2008).

153) Morris D.G., Morris M.A., "Mechanical properties of FeAl-ZrB_2 alloys prepared by rapid solidification", Acta Mater., 39, 1771-1779, (1991).

154) Morris D.G., Munoz-Morris M.A., "High temperature mechanical properties of iron aluminides", Revista De Metalurgia, 37, 230-239, (2001).

155) Morris D.G., Munoz-Morris M.A, Baudin C., "The high temperature strength of some Fe_3Al alloys", Acta Materialia, 52, 2827-2836, (2004).

156) Morris D.G., Munoz-Morris M.A. "Intermetallics: past, present and future" Rev. Meted, Madrid Vol Extr. 498-501, (2005).

157) Morris D.G., Munoz-Morris M.A., Requejo L.M., "New iron-aluminum alloy with thermally stable coherent intermetallic nanoprepicitates for enhanced high temperature creep strength", Acta Mater., 54, 2335-2341, (2006).

158) Morris D.G., Munoz-Morris M.A. "Refinement of second phase dispersions in iron aluminide intermetallics by high-temperature severe plastic deformation", Intermetallics, 23, 1-8, (2012).

159) Morris M.A., Morris D.G., "Dispersoid additions and their effect on high temperature deformation of Fe-Al", Acta Metall. Mater., 38, 551-559, (1990).

160) Morris M.A., Morris D.G., “Mechanical alloying of Fe-Al with oxide and carbide dispersoids”, Mater. Sci. Eng. A, 125, 97-106, (1990).

161) Morris-Munoz M.A., “Creep deformation of oxide-dispersion-strengthened Fe-40Al intermetallic: thermal and athermal contributions”, Intermetallics, 7, 653-661, (1999).

162) Morris M.A., Garcia Oca C., Morris D.G., “An analysis of strengthening mechanisms in a mechanically alloyed oxide dispersion strengthened iron aluminide intermetallic”, Acta Mater., 50, 2825-2836, (2002).

163) Morris M,A,, Morris D,G,, “Microstructure control during severe plastic deformation of Al–Cu–Li and the influence on strength and ductility”, Mater Sci Eng A, 528, 3445-54, (2011).

164) Mosbah A.Y., Wexler D., Calka A., “Abrasive wear of WC–FeAl composites”, Wear, 258, 1337-1341, (2005).

165) Mosecker L., Göttmann A., Saeed-Akbari A., Bleck W., Bambach M., Hirt G., “Deformation mechanisms of Ti6Al4V sheet material during the incremental sheet forming with laser heating”, Key Engineering Materials 549, 372-380, (2013).

166) Munroe P.R., Kong C.H., “The effect of ternary additions on vacancy hardening in near stoichiometric FeAl”, Intermetallics, 4, 403-15, (1996).

167) Musalek R., Kovark O., Skiba T., Hausild P., Karlk M., Colmenares-Angulo J., “Fatigue properties of Fe–Al intermetallic coatings prepared by plasma spraying”, Intermetallics, 18, 1415-1418, (2010).

168) Nigam A.K., Balasubramaniam R., Bhargava S., Baligidad R.G., “Electrochemical impedance spectroscopy and cyclic voltammetry study of carbon-alloyed iron aluminides in sulfuric acid”, Corr. Sci., 48, 1666-1678, (2006).

169) Noebe R.D., Bowman R.R., Nathal M.V., “Review of the physical and mechanical properties of the B2 compound NiAl”, Int. Mater. Rev. 38, 193–232, (1993).

170) Nourbakhsh S., Margolin H., “Processing of continuous ceramic fibre reinforced intermetallic composites by pressure casting composites”, Mater. Sci. Engg., A144, 133-141, (1991).

171) Obara Y., Kudoh M., Matsuura K., “Pseudo-HIP combustion synthesis of Fe_3Al-TiB_2 composites”, Mater. Trans., 49, 1168-1174, (2008).

172) Oleszak D., Krasnowski M., “Mechanically alloyed nanocrystalline intermetallic matrix composites reinforced with alumina”, Mater. Sci. For., 260-262, 235-240, (2001).

173) Palm M., Inden G., “Experimental determination of phase equilibria in the Fe-Al-C system”, Intermetallics, 3, 443-454, (1995).

174) Palm M, Sauthoff G., “Deformation behaviour and oxidation resistance of single-phase and two-phase $L2_1$-ordered Fe–Al–Ti alloys”, Intermetallics 12, 1345-59, (2004).

175) Pang L., Kumar K.S., “Mechanical behavior of an Fe–40Al–0.6C alloy”, Acta Mater., 46, 4017-4028, (1998).

176) Pang L,, Kumar K,S,, “Effect of heat treatment on the microstructure of an Fe-40Al-0.7C-0.5B alloy”, Mater Sci Eng A, 258, 161-166, (1998).

177) Pang L., Kumar K.S., “Tensile ductility of an Fe–40Al–0.6C alloy”, Intermetallics, 8, 693-698, (2000).

178) Pang L., Kumar K.S., “On the impact toughness of Fe-40Al-based B2 aluminides”, Intermetallics, 8, 157-163, (2000).

179) Pang L., Zhing D., Zhang A., Xu J., Zhang J., Fan R, “Carbon nanotube reinforced intermetallic”, Adv. Compos. Mater., 19, 261-267, (2010).

180) Pant M., Bleck W., “Continuous impact wear resistance of duplex surface-modified hot work tool steel H10,” Wear 259, 377–382, (2005).

181) Park B. G., Ko S.H., Park Y.H., Lee J.H., “Mechanical properties of in situ Fe_3Al based metal matrix composites fabricated by MA-PDS process”, Intermetallics, 14, 660-665, (2006).

182) Parvathavarthini N., Prakash U., Dayal R.K., “Effect of carbon addition on hydrogen permeation in an Fe_3Al- based intermetallic alloy”, Intermetallics, 10, 329-332, (2002).

183) Parvathavarthini N., Prakash U., Dayal R.K., “Effect of carbon addition on hydrogen permeation in an Fe_3Al-based intermetallic alloy”, Intermetallics, 10, 329-332, (2002).

184) Pather R., Mitten W.A., Holdway P., Ubhi H.S., Wisbey A., Bzooks J.W., “The effect of high temperature exposure on the tensile properties of γ TiAl alloys”, Intermetallics, 11, 1015, (2003).

185) Pauschitz A., Roy M., Franek F., “Mechanisms of sliding wear of metals and alloys at elevated temperatures”, Tribology International, 41, 584-602, (2008).

186) Peng L.M., Li H., Wng J.H., Gong M., “High strength and high fracture toughness ceramic-iron aluminide (Fe_3Al) composites”, Materials Letters, 60, 883-887, (2006).

187) Pierson H.O, "Handbook of Refractory Carbides and Nitrides: Properties, Characteristics, Processing and Applications", Noyes Publications, New Jersey, (1996).

188) Pike L.M., Chang Y.A., Liu C.T., "in: Schneibel J H and Crimp M A (Eds.), Processing and Properties and Applications of Iron Aluminides", TMS, Warrendale, 217, (1994).

189) Porter D.A., Easterling K.E., Phase transformations of metals and alloys Ed. Van Nostrand Reinhold (1981).

190) Prakash U., "Development of iron aluminides containing carbon", Trans. Ind. Inst. Met., 61, 193-199. (2008).

191) Prakash U., Buckley R.A., Jones H., Sellars C.M., "Structure and properties of intermetallics based on the Fe-Al system", ISIJ International, 31, 1113-1126, (1991).

192) Prakash U., Buckley R.A., Jones H., Sellars C.M., "Structure and Properties of Ordered Intermetallics Based on the Fe-Al System", ISIJ International, 31, 1113-1126, (1991).

193) Prakash U., Parvathavarthini N., Dayal R.K., "Effect of composition on hydrogen permeation in Fe–Al alloys", Intermetallics, 15, 17-19, (2007).

194) Prakash U., Sauthoff G., "Machinable iron aluminides containing carbon", Scripta Mater., 44, 73-78, (2001).

195) Prakash U., Sauthoff G., "Structure and properties of Fe–Al–Ti intermetallic alloys", Intermetallics, 9, 107-112, (2001).

196) Prescott R., Graham M.J., "The formation of aluminum oxide scales on high-temperature alloys", Oxidation of Metals, 38,233-254, (1992).

197) Rabin B.H., Wright R.N., "Synthesis of iron aluminides from elemental powders", Metall Trans., 22A, 277-286, (1991).

198) Rabin B.H., Wright R.N., Nibloe J.R., Raman R.V., Rale S.V., "Reaction processing of iron aluminides", Mater Sci. Engg, A153, 706-711, (1992).

199) Radhakrishna A., Baligidad R.G., Sarma D.S., "Effect of carbon on structure and properties of FeAl based intermetallic alloy", Scr Mater, 45, 1077-1082, (2001).

200) Rafiei M., Enayati M.H., Karimzadeh F., "Mechanochemical synthesis of (Fe, $Ti)_3Al$- Al_2O_3 nanocomposite", J. Alloys Comp., 488, 144-147, (2010).

201) Pandey B., Suwas S., Verma H.C., "Phase transformations in $Fe_{72-x}Al_{28}Ti_x$ (x= 0, 2, 6, 9) alloys induced by severe plastic deformation", Journal of Magnetism and Magnetic Materials 246, 151-161, (2002).

202) Rao V.S., Raja V.S., Baligidad R G., "Effect of Carbon on the Long-Term Oxidation Behavior of Fe_3Al Iron Aluminides", Oxidation of Metals 57 5, 449-471, (2002).

203) Rao V.S., Baligidad R.G., Raja V.S., "Effect of carbon on corrosion behaviour of Fe_3Al intermetallics in 0.5 N sulphuric acid", Corr. Sci., 44, 521-533, (2002).

204) Rao V.S., "High temperature oxidation behaviour of Fe–Al–C alloys: an overview", Mater Sci. Eng. A, 364, 232-239, (2004).

205) Rao V.S., Baligidad R.G., Raja V.S., "Effect of composition on hydrogen permeation in Fe–Al alloys", Intermetallics, 10, 73-84, (2002).

206) Rao V.S., Norell M., Raja V.S., "Scanning Auger electron spectroscopy study of the oxide film formed on dendritic and interdendritic regions of C containing Fe_3Al intermetallic", Corr. Sci., 45, 2717-2728, (2003).

207) Rao V.S., Raja V.S., "Long-term sulfidation behaviour of Fe_3Al-$Fe_3AlC_{0.69}$ iron aluminides", Intermetallics, 11, 119-128, (2003).

208) Rao. V.S., Kwon H.S., "AFM study of the oxide film formed on dual phase Fe_3Al–Fe_3AlC intermetallics", Intermetallics, 13, 23-36, (2005).

209) Ray R., Panchanathan V., Isserow S., "Microcrystalline Iron-Base Alloys Made Using a Rapid Solidification Technology", JOM, 35, 30-36, (1983).

210) Risanti D.D., Sauthoff G., "Microstructures and mechanical properties of Fe–Al–Ta alloys with strengthening Laves phase", Intermetallics, 19, 1727-36, (2011).

211) Roy M., Venkataraman B., Bhanuprasad V.V., Mahajan Y.R., Sundararajan G., "The effect of participate reinforcement on the sliding wear behavior of aluminum matrix composites", Metallurgical Transactions A, 23, 2833-2847, (1992).

212) Roy D., Singh S.S., Basu B., Lojkowski W., Mitra R., Manna I., "Studies on wear behavior of nano-intermetallic reinforced Al-base amorphous/nanocrystalline matrix in situ composite", Wear, 266, 1113-1118, (2009).

213) Russell A.M., "Ductility in intermetallic compounds". Adv Eng Mater, 5, 629-39, (2003).

214) Tetsui T., “Effects of high niobium addition on the mechanical properties and high-temperature deformability of gamma TiAl alloy”, Intermetallics, 10, 239-245, (2002).

215) Tetsui T., “Development of a TiAl turbocharger for passenger vehicles”, Mater Sci Eng A, 329, 582-589, (2002).

216) Sanders W., Sauthoff G., “Deformation behaviour of the perovskite type phases in the system Fe-NiAl-C: I Strength and ductility of Ni_3Al_X and Fe_3Al_X alloys with various microstructures”, Intermetallics 5, 361-375, (1997a).

217) Sanders W., Sauthoff G., “Deformation behaviour of the perovskite type phases in the system Fe-NiAl-C: II Deformation behaviour of a two phase $Fe_3Al_{0.45}$ alloy”, Intermetallics 5, 377-385, (1997b).

218) Sauthoff G., “Analysis of relationships between cohesive energy, elastic moduli and lattice parameter of some high temperature intermetallics”, Intermetallics, 3, 137-140, (1995).

219) Satya Prasad V.V., Khaple S., Baligidad R.G., “Melting, Processing, and Properties of Disordered Fe-Al and Fe-Al-C Based Alloys” JOM, 66, 1785-1793, (2014).

220) Sauthoff G., “Multiphase intermetallic alloys for structural applications”, Intermetallics, 8-9, 11, 1101-1109, (2000).

221) Schniebel J.H., Becher P.F., “Iron and nickel aluminide composites”, J. Chinese Inst. Engrs, 22, 1-12, (1999).

222) Schniebel J.H., Carmichael C.H., Specht E.D., Subramanian R., “Liquid-phase sintered iron aluminide-ceramic composites”, Intermetallics, 5, 61-68, (1997).

223) Schniebel J.H., Deevi S.C., “Processing and properties of iron aluminide composites containing oxide particles”, Mater. Sci. Engg., A364, 166-170, (2004).

224) Schniebel J.H., Grahle P., Rosler J., “Mechanical alloying of FeAl with Y_2O_3”, Mater, Sci. Engg., A153, 684-690, (1992).

225) Schniebel J.H., Subramanian R., Alexaxender K.B., Becher P.F., “Processing and Properties of FeAl-bonded composites, International Symposium on nickel and iron aluminides”, eds. S. C.. Deevi and Sikka V. K., ASM, 329-37, (1997).

226) Schnieder A., Falat L., Sauthoff G., Frommeyer G., “Microstructures and mechanical properties of Fe_3Al-based Fe-Al-C alloys”, Intermetallics, 13, 1322-1331, (2005).

227) Schneider A., Sauthoff G., “New chemical structures by microfluidic Steel”, Research International, 126, 5858-5861, (2014).

228) Sen M., Balasubramaniam R., "Hydrogen trapping at carbide-matrix interfaces in Fe_3Al-C intermetallics", Scripta Mater, 44, 619-623, (2001).

229) Senderowski C., Bojar Z., Wo1czynski W., Paw1owski A., "Microstructure characterization of D-gun sprayed Fe–Al intermetallic coatings", Intermetallics, 18, 1405-1409, (2010).

230) Sharma G., Limaye P.K., Ramanujan R.V., Sundararaman M., Prabhu N., "Dry sliding wear studies of Fe_3Al-ordered intermetallic alloy", Mater. Sci. Eng. A, 386, 408-414, (2004).

231) Sharma G., Limaye P.K., Sundararaman M., Soni N.L., "Wear resistance of Fe-28Al-3Cr intermetallic alloy under wet conditions", Mater. Lett., 61, 3345-3348, (2007).

232) Shao G., Tsakiropoulos P., "On the structural evolution of Fe-A1 laminates obtained by physical vapour deposition", Philosophical Magazine, 80, 693-710, (2000).

233) Shih D.S., Scar G.K., "in Mater Res Soc Symp Proc High Temp Ordered Intermetallic Alloys IV", (vol 213), 727, (1991).

234) Singh A.P., Balasubramanian R., Baligidad R.G., "High temperature environmental interactions in carbon-alloyed iron aluminide of low Al content", Mater. Sci. Eng. A, 368, 48-55, (2004).

235) Sikka V.K., Blue C.A., Sklad S.P., Deevi S.C., Shih H.R., "Fabric cutting application of FeAl-based alloys", Mater. Sci. Eng. A, 258, 325–330, (1998).

236) Sikka V.K., Wilkening D., Liebetrau J., Mackey B., "Wear of iron–aluminide intermetallic-based alloys and composites by hard particles", Mater. Sci. Eng. A, 258, 229–235 (1998).

237) Sikka V.K., Wilkening D., Liebetrau J., Mackey B, "Melting and casting of FeAl-based cast alloy", Mater. Sci. Eng. A, 258, 229-235 (1998).

238) Sriram S., Balasubramaniam R., Mungole M.N, Bhargava S., Baligidad R.G., "Effect of cerium addition on the corrosion behaviour of carbon-alloyed iron aluminides", Corr. Sci., 48, 1059-1074, (2006).

239) Stein F., Schneider A., Frommeyer G., "Flow stress anomaly and order–disorder transitions in Fe_3Al-based Fe–Al–Ti–X alloys with X=V, Cr, Nb, or Mo", Intermetallics 11, 71- 82, (2003).

240) Stoloff N.S., Liu C.T., "Environmental embrittlement of iron aluminides", Intermetallics, 2, 75-87, (1994).

241) Stoloff N.S., “Iron aluminides: present status and future prospects”, Mater. Sci. Eng. A, 258, 1-14, (1998).

242) Stoloff N.S., Liu C.T., Deevi S.C., “Emerging applications of intermetallics”, Intermetallics 8, 1313-20, (2000).

243) Subramanian R., Schneibel J.H., Alexander K.B., Plucknett K.P., “Iron aluminide-titanium carbide composites by pressureless melt infiltration - Microstructure and mechanical properties”, Scr. Mater., 35, 583-588, (1996).

244) Subramanian R., McKamey C.G., Buck L.R., Schneibel J.H., “Synthesis of iron aluminide Al_2O_3 Composites by in-situ displacement reactions”, Mater. Sci. Eng. A 239-240, 640-46, (1997a).

245) Subramanian R., Schneibel J., “Processing iron-aluminides composites containing carbides or borides, JOM, 49, 50-56, (1997b).

246) Subramanian R., Schneibel J.H., “FeAl-TiC cermets—melt infiltration processing and mechanical properties”, Mater. Sci. Eng. A, A239–240, 633–639, (1997c).

247) Subramanian R., Schneibel J.H., “Intermetallic bonded WC-based cermets by pressureless melt infiltration”, Intermetallics, 5, 401-408, (1997d).

248) Subramanian R., Mckamey C.G., Schniebel J.H., Buck J.R., Menchhofer P.A., “Iron aluminide-Al_2O_3 composites by in-situ displacement reaction: processing and mechanical properties”, Mater. Sci. Eng., A254, 119-128, (1998a).

249) Subramanian R., Schneibel J.H., “The ductile–brittle size transition of iron aluminide ligaments in an FeAl/TiC composite”, Acta. Mater., 46, 4733-4741 (1998b).

250) Subramanian R., Schneibel J.H., “FeAl–TiC and FeAl–WC composites—melt infiltration processing, microstructure and mechanical properties” Mater. Sci. Eng. A 244, 03-112, (1998c).

251) Suryanarayana C., Froes F.H., “The structure and mechanical properties of metallic nanocrystals”, Metall. Trans. A 23, 1071-1081, (1992).

252) Sun, K., Li, A., Cui, X., Yin, Y., Li, P., “Sintering technology research of Fe_3Al/Al_2O_3 ceramic composites” J. Mater. Process. Technol. 113, 482–485, (2001).

253) Sundar R.S., Deevi S.C., “Effect of carbon addition on the strength and creep resistance of FeAl alloys”, Metall. Mater. Trans., 34A, 2233-2246, (1994).

254) Sundar R.S., Baligidad R.G, Prasad Y.V.R.K., Sastry D.H, “Processing of iron aluminides” Mater. Sci. Eng. A 258, 219, (1998).

255) Suwas S., Bhargava S., Sangal S., “Morphology of the boride phase in a cast iron-aluminide matrix Composite”, Journal of Materials Science letters, 15, 1216-1218, (1996).

256) Suwas S., Bhargava S., Sangal S., “The Effect of Deformation Processing on Microstructural Evolution in a Boron Containing Fe-25Al Intermetallic Alloy”, High Temperature Materials and Processes, 16, 29–38, (1997).

257) Syahrila, Rawlings R.D., “Effect of thermomechanical treatment on the properties of Fe-11Al and Fe-14Al alloys”, Journal of Material Science, 37, 1823-1830, (2002).

258) Teng L., Nakatomi D., Seetharaman S., “Oxidation Behavior of TiAl-8Nb Turbine Blade Alloy”, Metallurgical and Materials Transactions B, 38B, 477-484, (2007).

259) Tieberghein D., Lapin J., Ryelandt S, Delannay F., “On the control of residual porosity in iron aluminides processed by reactive squeeze filtration of aluminium into a perform of steel fibres”, Mater. Sci. Eng., A323, 427-435, (2002).

260) Tortorelli P.F., Natesan K., “Critical factors affecting the high-temperature corrosion performance of iron aluminides”, Mater. Sci. Eng. A, 258, 115-125, (1998).

261) Tsakiropoulos P., Shao G., “Phase selection in non-equilibrium processed TM–Al intermetallic alloys”, Materials Science and Engineering A 375–377, 201–206, (2004).

262) Tu J.P., Liu M.S., “Wet abrasive wear of ordered Fe_3Al alloys”, Wear, 209, 31–36, (1997).

263) Tu J.P., Meng L., Liu M.S., “Friction and wear behavior of Cu-Fe_3Al powder metallurgical composites in dry sliding”, Wear, 220, 72-79, (1998).

264) Tylczak J.H., “Evaluation of the planar array field wear tests under abrasion”, presented at The International Conference on Wear of Materials, ASM, 126-130, (1978).

265) Umakoshi Y., Yamaguchi M., “Deformation of FeAl single crystals at high temperature” Phil. Mag. A 41, 573, (1980).

266) Vedula K.V., Stephens J.R., “Indentation creep studies of iron aluminide intermetallic alloy”, Mater. Res. Soc. Symp. Proc., 81, 381-390, (1987).

267) Vedula K. In: Westbrook J.H., Fleischer R.L., editors. Intermetallic compounds: principles and practice, vol 2. Chichester (UK): Wiley; p. 199, (1994).

268) Vedula K., "Intermetallic Compounds: Principles and Practise" eds. Westbrook J.H. Fleischer R.L., John Wiley and Sons, Chichester, 2, (1999).

269) Verma H.C., Suwas S., "Mossbauer studies of phase stability in mechanically stressed Fe-28 at% Al alloy", Journal of Magnetism and Magnetic Materials, 212, 361-367, (2000).

270) Wang J., Xing J.D., Cao, Su V., Gao Y.M., "Dry sliding wear behavior of Fe_3Al alloys prepared by mechanical alloying and plasma activated sintering", Wear, 268, 473–480, (2010).

271) Ward-Close C.M., Minor R., Doorbar P.J., "Intermetallic-matrix composites: a review", Intermetallics, 4, 217-229, (1996).

272) Wasilkowska A., Bartsch M., Stein F., Palm M., Sztwiertnia K., Sauthoff G., Messerschmidt U., "Plastic deformation of Fe–Al polycrystals strengthened with Zr-containing Laves phases I. Microstructure of undeformed materials", Materials Science and Engineering A 380, 9-19, (2004).

273) Welsch G., Desai P.D. (Eds.), Oxidation and Corrosion of Intermetallic Alloys, Metals Information and Analysis Center, Center for Information and Numerical Data Analysis and Synthesis, Purdue University, West Lafayette, IN, (1996).

274) Wolski K., Therenot F., Coze J.L., "Effect of nanometric oxide dispersion on creep resistance of ODS-FeAl prepared by mechanical alloying", Intermetallics, 4, 299-307, (1996).

275) Wright R.N., Anderson W.T., Wright J.K., "Microstructure and Properties of an oxide dispersion strengthened iron aluminide", Mater. Sci. Engg., A258, 285-290, (1998).

276) Wu X, "Review of alloy and process development of TiAl alloys",Intermetallics 14, 1114, (2006).

277) Wunnicke-Sanders W., Dr. Ing. Thesis, RWTH, Aachen, Germany, (1993).

278) Wurschum R., Grupp C., Eschaefer H., "Characterization of radiation-induced lattice vacancies in intermetallic compounds by means of positron-lifetime studies", Phys. Rev. B, 54, 849-856, (1996).

279) Xiao C., Chen W., "Sulfidation resistance of CeO_2-modified HVOF sprayed FeAl coatings at 700°C", Surf. Coat. Technol., 201, 3625-3632, (2006).

280) Xiao H., Baker I., "The relationship between point defects and mechanical properties in Fe-Al at room temperature", Acta Metall. Mater., 43, 391-396, (1995).

281) Yang J., La P., Liu W., Hao Y. "Microstructure and properties of Fe_3Al-$Fe_3AlC_{0.5}$ composites prepared by self-propagating high temperature synthesis casting", Mater. Sci. Eng. A, 382, 8-14, (2004).

282) Yang J., La P., Liu W., Ma J., Xue Q., "Tribological properties of Fe_3Al-$Fe_3AlC_{0.5}$ composites under dry sliding", Intermetallics, 13, 1184-1189, (2005).

283) Yang Y., Baker I., "The influence of vacancy concentration on the mechanical behavior of Fe-40Al", Intermetallics, 6, 167-175, (1998).

284) Yildirim M., Akdeniz M.V., Mekhrabov A.O. "Effect of Ternary Alloying Elements Addition on the Order-Disorder Transformation Temperatures of B2-Type Ordered Fe-Al-X Intermetallics" Met. and Mat. Trans. 43A, 1809, (2012).

285) Yoshimi K., Hanada S., Yoo M.H. In: Koch C.C., Liu C.T., Stoloff N.S., Wanner A., editors. High-temperature ordered intermetallic alloys VII. MRS Symp Proc 460, Pittsburgh, PA, 313, (1997).

286) Zhang W. J., Sundar R. S., Deevi S. C., "Improvement of the creep resistance of FeAl-based alloys", Intermetallics, 12, 893-897, (2004).

287) Zhang X., Ma J., Yang J., Bi Q., Liu W, "Dry-sliding tribological behavior of Fe-28Al-5Cr/TiC composites", Wear, 271, 88-888, (2011).

288) Zhang Y.G., Han Y.F., Chen G.L., Guo J.T., Wan X.J., Feng D., Intermetallic Structural Materials, National Defense Industry Press, Beijing, (2001).

289) Zhang Z.R., Zhu W.X., "Mechanical properties of Fe_3Al-based alloys with addition of carbon, niobium and titanium", Mater. Sci. Eng. A 423, 343-349, (2006).

290) Zhao J,C,, Westbrook J.H, "Ultrahigh-temp mater for jet engines and westbrook", MRS Bull, 622, (2003).

291) Zhu S,M,, Guan X,S., Shibata K., Iwasaki K., "Microstructure and mechanical and tribological properties of properties of high carbon Fe_3Al and FeAl intermetallic alloy", Mater. Trans., 43, 36-41, (2002).

292) Zhu S.M., Guan X.S., Shibata K., Iwasaki K., "Effect of high temperature deformation and different cooling rates on microstructure and mechanical properties of Fe–Al alloys", Mater. Trans., 43, 36, (2002).

293) Zhu S.M., Tamura M., Sakamoto K., Wasaki K., "Characterization of Fe_3Al-based intermetallic alloys fabricated by mechanical alloying and HIP consolidation", Mater. Sci. Eng. A, 292, 83–89, (2000).

294) Zum G.K.H., "Microstructure and Wear of Materials", Tribology Series, Elsevier, Amsterdam, Volume 10, Pages ii-vi, 1-560, (1987).